NTNU – Trondheim
Norwegian University of
Science and Technology

Measurement and Calculation of Surface Tension of Oil, Gas and Glycol

Henrik Norgaard
Lars Nygaard

Master of Energy and Environmental Engineering
Submission date: June 2014
Supervisor: Even Solbraa, EPT

Norwegian University of Science and Technology
Department of Energy and Process Engineering

NTNU

Norwegian University
of Science and Technology

Department of Energy
and Process Engineering

EPT-M-2014-77

MASTER THESIS

for

Students Henrik Norgaard and Lars Nygaard

Spring 2014

Measurement and calculation of surface tension of gas, oil and glycol

Eksperimentell måling og beregning av overflatespenning for olje, gass og glykol

Background and objective

Process simulation software and multiphase flow simulators involve the use of a number of thermodynamic and physical property models. Correct thermodynamic and physical property prediction is of high importance to get optimal design of pipelines and process equipment. Simulation tools such as OLGA, HYSYS and PROII requires input of thermodynamic properties as well as transport properties such as surface tension. Normally the thermodynamic properties are calculated using classic equations of state such as SRK and PR, while transport properties are calculated with relatively simple and computational effective methods.

During recent years, a number of more advanced thermodynamic and transport property models have been developed. An example of a modern model for calculation of interfacial tension is the gradient theory.

A number of techniques have been presented in literature for experimental measurement of surface tension between a gas and liquid. The pendant drop method is a popular method used for such measurements. In this work a high pressure pendant drop experimental equipment will be used to measure surface tension in gas and oil/glycol systems. Finally theoretical models will be evaluated for their accuracy of predicting surface tension.

The following tasks are to be considered:

1. Review of experimental techniques used for measurement of surface tension
2. Collection of experimental data for surface tension for gas and oil/glycol systems
3. Experimental measurement of interfacial tension of selected fluids (gas/oil/glycol)
4. Evaluation of models and software for calculation of interfacial tension

Within 14 days of receiving the written text on the master thesis, the candidate shall submit a research plan for his project to the department.

When the thesis is evaluated, emphasis is put on processing of the results, and that they are presented in tabular and/or graphic form in a clear manner, and that they are analyzed carefully.

The thesis should be formulated as a research report with summary both in English and Norwegian, conclusion, literature references, table of contents etc. During the preparation of the text, the candidate should make an effort to produce a well-structured and easily readable report. In order to ease the evaluation of the thesis, it is important that the cross-references are correct. In the making of the report, strong emphasis should be placed on both a thorough discussion of the results and an orderly presentation.

The candidate is requested to initiate and keep close contact with his/her academic supervisor(s) throughout the working period. The candidate must follow the rules and regulations of NTNU as well as passive directions given by the Department of Energy and Process Engineering.

Risk assessment of the candidate's work shall be carried out according to the department's procedures. The risk assessment must be documented and included as part of the final report. Events related to the candidate's work adversely affecting the health, safety or security, must be documented and included as part of the final report. If the documentation on risk assessment represents a large number of pages, the full version is to be submitted electronically to the supervisor and an excerpt is included in the report.

Pursuant to "Regulations concerning the supplementary provisions to the technology study program/Master of Science" at NTNU §20, the Department reserves the permission to utilize all the results and data for teaching and research purposes as well as in future publications.

The final report is to be submitted digitally in DAIM. An executive summary of the thesis including title, student's name, supervisor's name, year, department name, and NTNU's logo and name, shall be submitted to the department as a separate pdf file. Based on an agreement with the supervisor, the final report and other material and documents may be given to the supervisor in digital format.

☐ Work to be done in lab (Water power lab, Fluids engineering lab, Thermal engineering lab)
☐ Field work

Department of Energy and Process Engineering, 14. January 2014

Even Solbraa

Olav Bolland
Department Head

Even Solbraa
Academic Supervisor

Research Advisors:
Ole Johan Berg, Oddbjørn Rekaa Nilssen

Preface

This master thesis was written at the department of Energy and Process Engineering at the Norwegian University of Science and Technology. The experimental work was conducted at Statoil research center at Rotvoll, Trondheim.

The workload of this thesis has been quite large due to the lab work, but we have fortunately not experienced any major issues with the experimental setup. The collaboration between the two of us has also worked out well.

We would like to thank our supervisor Dr. Even Solbraa for guidance and help during the work on this master thesis. We would like to extend a special thanks to Mr. Ole Johan Berg for all the help he has provided us with regard to the experimental work. Finally we want to thank Miss Line Nygaard Kristensen and Dr. Hui Nie Nilssen for proofreading the report.

Trondheim, 06 June 2014

Henrik Norgaard Lars Nygaard

Henrik Norgaard Lars Nygaard

Abstract

The importance of surface tension in separation design was evaluated in this report. Surface tension was found to have importance when calculating essential design parameters, like droplet size, which is is fundamental in several vessel design operations. Other impacts of surface tension in separation are the ability to sustain a liquid film and avoid droplet re-entrainment into the gas flow, both being discussed in the report. Miscalculation of surface tension could lead to incorrect sizing of separation equipment, subsequently causing expensive fault in operation and decreased separation effect.

The main objective of this thesis was to experimentally measure surface tension with the pendant drop technique. Although surface tension was the main task, density and solubility data were also collected and evaluated, as they too are important parameters in separator design. The measurements were carried out on MEG/water systems because of low availability of such data in the literature. The deviation of the surface tension measurements was calculated on the basis of recommendations from the International Organization for Standardization (ISO), and the total average deviation for all mixtures was stated to be 2.00%.

The second objective was to evaluate models for the calculation of surface tension in process simulation software. The simulation tools PRO/II, HYSYS, PVTSim and NeqSim were used for calculation. PRO/II and HYSYS use simple models that are based on pure component values. PVTsim utilizes the well-known parachor method when simulating hydrocarbon systems, while for MEG/water systems it uses a model based on the corresponding state theory. NeqSim uses the most complicated and computational demanding model, the gradient theory, which is based on thermodynamics. Some of the software have additional models implemented, but in this thesis the default models have been used.

The mono ethylene glycol (MEG)/water and hydrocarbon systems were simulated in the software, and thereafter compared against the experimental data.

The results of the comparison regarding hydrocarbon systems showed two distinct tendencies. Firstly, the performance of PRO/II and HYSYS was not adequate. They both were, with a few exceptions, overestimating the surface tension for all mixtures. Second, even though the performance of both PVTsim and NeqSim could be termed satisfactory, NeqSim was superior to the estimations of PVTsim throughout most of the experimental data. The only exception was for the ternary systems, on which the base of surface tension data was rather insufficient.

The results of the comparison regarding glycol systems showed that all software overestimate the surface tension. NeqSim was once again the software with the best accuracy, and the CPA equation of state was the overall preferred choice. In contrast to hydrocarbon mixtures PVTsim now has a large discrepancy throughout. However, the accuracy improved drastically for the 50 wt% MEG/50 wt% water mixture. PRO/II and HYSYS performed better than they did on hydrocarbon mixtures, especially for the 100wt%MEG mixture. However, as water was added to the composition, PRO/II's deviation increased substantially.

Sammendrag

I denne rapporten har betydningen av overflatespenning ved design av separasjonsinstrumenter blitt studert. Det ble konkludert med at overflatespenning spiller inn ved beregning av essensielle parametere, som dråpestørrelse, som er fundamentale ved design av separatorer til olje- og gass-separasjon. Overflatespenning påvirker også andre egenskaper som er viktig i separasjon, som evnen til å holde faser separert og å unngå at dråper tilbakeføres til gassfasen. Feilberegning av overflatespenning kan føre til feildimensjonering av separasjonsutstyr, som igjen kan forårsake kostbar nedetid for operasjonen og lavere separasjonseffekt.

Det primære arbeidet i denne avhandlingen besto i eksperimentelle målinger av overflatespenning ved bruk av 'pendant drop' teknikk. Som en konsekvens av disse målingene, ble også data på tetthet og løselighet bokført, da dette også er viktige egenskaper for design av separasjonsenheter. Målingene ble utført på MEG/vann-systemer grunnet lav tilgjengelighet på data for slike systemer i litteraturen. Avviket for overflatespenningsmålingene ble beregnet på bakgrunn av anbefalinger fra ISO, og det totale avviket ble 2.00%.

Et annet formål med avhandlingen var å evaluere modeller for beregning av overflatespenning i simuleringsprogramvare. Simuleringsverktøyene PRO/II, HYSYS, PVTSim og NeqSim ble benyttet. PRO/II og HYSYS bruker enkle modeller som er basert på rene komponenter. PVTsim benytter den kjente parachor-metoden i simulering av hydrokarboner, mens for systemer av MEG og vann benyttes en modell basert på prinsippet om korresponderende tilstander. NeqSim bruker gradient teorien, som er basert på termodynamikk, og er den mest avanserte modellen som ble evaluert. Noen av programvarene har mange modeller implementert, men i denne avhandlingen har standard modeller blitt brukt.

MEG/vann- og hydrokarbonsystemene har blitt simulert i de ulike programvarene, og deretter sammenliknet mot eksperimentell data.

Resultatene fra sammenligningen vedrørende hydrokarbonsystemer viste to tydelige trender. For det første var resultatene for PRO/II og HYSYS ikke tilfredsstillende. De overestimerte overflatespenningen for alle blandingene, med enkelte unntak. Dernest viste det seg at selv om både PVTsim og NeqSim gav gode estimater, så er NeqSim overlegen PVTsim for stort sett alle datasett. Det eneste unntaket var for ternære systemer, hvor datagrunnlaget var heller tynt.

Resultatene fra sammenlikningen vedrørende glykolsystemer viste at alle programvarene overestimerte overflatespenningen. NeqSim var nok en gang det mest nøyaktige verktøyet, med tilstandslikningen CPA som den mest foretrukne. I kontrast til hydrokarbonblandinger produserte nå PVTsim resultater med store avvik til de eksperimentelle data. Nøyaktigheten ble derimot drastisk forbedret for 50 vekt% MEG/50 vekt% vann blandingen. PRO/II og HYSYS gav bedre resultater enn for hydrokarbonblandingene, og det gjaldt spesielt for 100 vekt% MEG blandingen. Da vann ble tilført systemet, økte derimot avviket vesentlig.

List of Abbreviations

Abbreviation	Designation
ISO	International Organization for Standardization
MEG	Mono Ethylene Glycol
NORSOK	Norsk Sokkels Konkurranseposisjon
SI	International System of Units
SRK	Soave-Redlich-Kwong
CPA	Cubic Plus Association
PR	Peng-Robinson
EoS	Equation of State
HSS	Hakim-Steinberg-Stiel
API	American Petroleum Institute
GT	Gradient Theory
LGT	Linear Gradient Theory
NTNU	Norwegian University of Science and Technology
GC	Gas Chromatograph
TDC	Thermal Conductivity Detector
ROLSI	Rapid Online Sampler-Injector

Contents

1 Introduction 1
1.1 Study Background . . . 1
1.2 Scope and Objectives . . . 1
1.3 Limitation of Scope . . . 2
1.4 Organization . . . 2

2 Review of Design Methods of Gas Separation Equipment 4
2.1 Separation . . . 4
  2.1.1 Removal Mechanisms . . . 4
  2.1.2 Separator Components . . . 6
2.2 Surface Tension in Separation Design . . . 11
  2.2.1 Droplet Size . . . 11
  2.2.2 Vessel Diameter . . . 12
  2.2.3 Liquid Entrainment . . . 15
  2.2.4 Wire Mesh . . . 16
  2.2.5 Centrifugal Elements . . . 17
  2.2.6 Scaling Rules . . . 17

3 Theoretical Concepts 18
3.1 Fundamental Concepts . . . 18
  3.1.1 Surface Tension . . . 18
  3.1.2 The Law of Corresponding States . . . 20
  3.1.3 Equation of State . . . 20
3.2 Models for Calculating Surface Tension . . . 22
  3.2.1 Corresponding State Theory . . . 22
  3.2.2 Parachor Method . . . 25
  3.2.3 Thermodynamic Models . . . 25
  3.2.4 Guidelines Regarding Choice of Models . . . 27

4 Software 28
4.1 Process Simulation Programs . . . 28
  4.1.1 SIMSCI PRO/II (version 9.1) . . . 28
  4.1.2 AspenTech HYSYS (version 8.0) . . . 29
  4.1.3 Calsep PVTsim (version 20.1.0) . . . 29
  4.1.4 NTNU/Statoil NeqSim . . . 29

5 Experimental Techniques 31
5.1 Selection of Data . . . 31
5.2 Measurment methods . . . 32
  5.2.1 Laser Light Scattering . . . 32
  5.2.2 Capillary Rise Method . . . 32

5.2.3 The Wilhelmy Plate Method 34
5.2.4 The Du Noüy Ring Method 34
5.2.5 Jaeger's Method 35
5.2.6 Pendant Drop and Sessile Drop Methods 35
5.2.7 Drop Weight or Volume Method 35
5.2.8 Spinning Drop Method 36

6 Experimental Apparatus and Setup 37
6.1 Introduction 37
6.2 Schematic Overview 38
6.3 Experimental procedure 41
6.4 Fluid specification 42

7 Measurement Results 44
7.1 Surface Tension 44
7.2 Density 45
7.3 Solubility 46
7.4 Uncertainty analysis 48

8 Discussion 51
8.1 Surface Tension 51
8.1.1 Hydrocarbon systems 51
8.1.2 Glycol systems 78
8.1.3 Comparison of Models 89
8.1.4 Importance of Surface Tension 93
8.2 Density and Solubility 94
8.2.1 Density 94
8.2.2 Solubility 98

9 Conclusion 106

10 Further Work 108

A Appendix 113
A.1 Experimental Data 113
A.2 Tables 116

List of Figures

2.1 Horizontal Separator Schematic Showing the Four Major Sections . 6
2.2 Half Open Pipe Inlet Device 7
2.3 FMC Technologies CDS Inlet Cyclone 8
2.4 Inlet Vane Distributor 8
2.5 Wire Mesh Mist Extractor 10
2.6 Horizontal Gas Flow in Vane Packs 10
2.7 Cyclone Mist Extractors 11

3.1 Mechanics of Curved Surfaces 19
3.2 Pendant Drop With Characteristic Dimensions 20
3.3 Surface Tension of Petroleum Fractions 24

5.1 Laser Light Scattering Method Schematic Overview 33
5.2 Capillary Rise Method 33
5.3 The Wilhelmy Plate Method 34
5.4 The Du Noüy Ring Method 34
5.5 Jaeger's Method 35
5.6 Spinning Drop Method 36

6.1 Temperature Test Chamber 37
6.2 SRI TOGA Gas Chromatograph 39
6.3 Schematic Overview of Gas Chromatograph 39
6.4 Rapid Online Sampler-Injector 40
6.5 Flow sheet of High Pressure Surface Tension Rig 41

8.1 Methane + Propane 52
8.2 Methane + Propane 53
8.3 Methane + Propane 54
8.4 Methane + Propane Using Laser Light Scattering Method 54
8.5 Methane + Propane Using Capillary Rise Method 55
8.6 Methane + Propane Using Drop Volume Method 55
8.7 Methane + n-Pentane 57
8.8 Methane + n-Butane 58
8.9 Methane + n-Pentane 59
8.10 Surface Tensions at High Temperatures 60
8.11 Surface Tensions at High Temperatures 60
8.12 Methane + n-Hexane 61
8.13 Methane + n-Heptane: Comparison of Two Works 63
8.14 Methane + n-Heptane 64
8.15 Methane + n-Nonane 65
8.16 Sub-zero Temperature Surface Tension Comparison 66
8.17 Methane + n-Decane 67

8.18 Ethane + n-Pentane 68
8.19 Methane + Ethane + n-Pentane 70
8.20 Methane + Propane + n-Decane 71
8.21 Surface Tension for Danesh Fluid A @ 40°C 73
8.22 Surface Tension for Danesh Fluid B @ 35°C 74
8.23 NeqSim Phase Envelope for Fluid B @ 35°C and 276.6 bar 75
8.24 Surface Tension for Danesh Fluid C @ 65.5°C 75
8.25 Surface Tension for GPA Wet Gas @ 10°C 76
8.26 Surface Tension for GPA Associate Gas @ 10°C 77
8.27 Surface Tension for GPA Associate Gas 93.3°C 77
8.28 100wt% MEG + Methane 79
8.29 100wt% MEG + Methane/Ethane 80
8.30 100wt% MEG + Methane 81
8.31 100wt% MEG + Methane/Ethane 81
8.32 100wt% MEG + Methane/Ethane 82
8.33 80wt% MEG/20wt% Water + Methane 83
8.34 80wt% MEG/20wt% Water + Methane/Ethane 84
8.35 80wt% MEG/20wt% Water + Methane 84
8.36 80wt% MEG/20wt% Water + Methane/Ethane 85
8.37 80wt% MEG/20wt% Water + Methane/Ethane 85
8.38 50wt% MEG/50wt% Water + Methane 86
8.39 50wt% MEG/50wt% Water + Methane/Ethane 87
8.40 50wt% MEG/50wt% Water + Methane 88
8.41 50wt% MEG/50wt% Water + Methane/Ethane 88
8.42 50wt% MEG/50wt% Water + Methane 89
8.43 50wt% MEG/50wt% Water + Methane/Ethane 89
8.44 Methane + Propane 90
8.45 Methane + n-Butane 90
8.46 Methane + n-Heptane 91
8.47 Wet Gas 92
8.48 100wt% MEG + Methane/Ethane 92
8.49 80wt% MEG/20wt% Water + Methane/Ethane 93
8.50 50wt% MEG/50wt% Water + Methane/Ethane 93
8.51 Liquid Density of 50wt% MEG/50 wt% Water + Methane/Ethane @ 20°C 95
8.52 Liquid Density of 50wt% MEG/50 wt% Water + Methane @ 20°C . 95
8.53 Vapor Density of 50wt% MEG/50 wt% water + Methane/Ethane @ 20°C 97
8.54 Vapor Density of 50wt% MEG/50 wt% Water + Methane @ 20°C . 97
8.55 Methane Liquid Phase Composition of 50wt% MEG/50wt% Water + Methane @ 5°C 99
8.56 Methane Liquid Phase Composition of 50wt% MEG/50wt% Water + Methane @ 20°C 99
8.57 Methane Liquid Phase Composition of 50wt% MEG/50wt% Water + Methane/Ethane @ 20°C 101
8.58 Methane Liquid Phase Composition of 80wt% MEG/20wt% Water + Methane/Ethane @ 20°C 101
8.59 Ethane Liquid Phase Composition of 100wt% MEG + Methane/Ethane @ 20°C 102

8.60 Ethane Liquid Phase Composition of 80wt% MEG/20wt% Water + Methane/Ethane @ 5°C 102
8.61 Ethane Liquid Phase Composition of 50wt% MEG/50wt% Water + Methane/Ethane @ 5°C 103
8.62 MEG Liquid Phase Composition of 80wt% MEG/20wt% Water + Methane/Ethane @ 20°C 104
8.63 Water Liquid Phase Composition of 80wt% MEG/20wt% Water + Methane/Ethane @ 20°C 104

List of Tables

6.1 Response Factors for the Applied Components 41
6.2 Composition of MEG/Water Mixtures 43
6.3 Apparatus Technical Information 43

7.1 Experimental Phase Densities 45
7.2 Experimental Results 47
7.3 Experimental Results 48
7.4 Uncertainty in Measuring Equipment 48
7.5 Input Parameters to Equation 7.2 (e_2) 49
7.6 Experimental Surface Tension and Deviation for the 100wt% MEG + Methane/Ethane Mixture at 20°C 49
7.7 Total Average Uncertainty 50

8.1 Deviation in mN/m to Experimental Data 53
8.2 Results Using Laser Light Scattering Method versus Software 56
8.3 Results Using Capillary Rise Method versus Software 56
8.4 Results Using Drop Volume Method versus Software 56
8.5 Deviation from Experimental Data on Methane/n-Hexane at 26.9°C 62
8.6 Deviation from Experimental Data on Methane/n-Hexane at 76.9°C 62
8.7 Deviation from Experimental Data on Methane/n-Heptane at 71.1°C 62
8.8 Deviation from Experimental Data on Methane/n-Heptane at 137.8°C 63
8.9 Deviation from Experimental Data on Methane/Propane at -15°C . 65
8.10 Deviation from Experimental Data on Methane/n-Nonane at -1.1°C 65
8.11 Deviation from Experimental Data on Methane/n-Decane 67
8.12 Deviation from Experimental Data on Methane/n-Decane 68
8.13 Deviation from Experimental Data on Ethane/n-Pentane 69
8.14 Deviation from Experimental Data on Methane/Ethane/n-Pentane 70
8.15 Composition of the Two Samples Given in Mole Fractions 70
8.16 Deviation of Methane + Propane + n-Decane Sample 2 to Experimental Data @ 21°C 71
8.17 Deviation of Methane + Propane + n-Decane Sample 1 to Experimental Data @ 20°C 72
8.18 Composition of Fluid A and B 72
8.19 Composition of Fluid C 73
8.20 Deviation to Experimental Surface Tension for Danesh Fluid A @ 40°C 74
8.21 Deviation to Experimental Surface Tension for Danesh Fluid B @ 35°C 74
8.22 Composition of Wet and Associate Gas 76
8.23 Deviation to Experimental Surface Tension for GPA Wet Gas @ 10°C 76

8.24 Deviation to Experimental Surface Tension for GPA Associate Gas @ 10°C 78
8.25 Deviation to Experimental Surface Tension for GPA Associate Gas @ 93.3°C 78
8.26 Deviation of the 100wt% MEG + Methane Mixture 80
8.27 Deviation of the 100wt% MEG + Methane/Ethane Mixture 80
8.28 Deviation of the 100wt% MEG + Methane/Ethane Mixture 82
8.29 Deviation of the 80wt% MEG/20wt% Water + Methane Mixture . 83
8.30 Deviation of the 80wt% MEG/20wt% Water + Methane/Ethane Mixture 83
8.31 Deviation of the 80wt% MEG/20wt% Water + Methane/Ethane Mixture 85
8.32 Deviation of the 50wt% MEG/50wt% Water + Methane Mixture . 87
8.33 Deviation of the 50wt% MEG/50wt% Water + Methane/Ethane Mixture 87
8.34 Deviation to Experimental Data for Liquid Density 96
8.35 Change in Deviation to Experimental Data as Ethane is Added . . 96
8.36 Deviation to Experimental Data for Vapor Density 98
8.37 Deviation to Experimental Data for Methane Liquid Phase Composition 100
8.38 Deviation to Experimental Data for Ethane Liquid Phase Composition 103
8.39 Deviation to Experimental Data for MEG Liquid Phase Composition 105
8.40 Deviation to Experimental Data for Water Liquid Phase Composition 105

A.1 Experimental Data on Binary and Ternary Systems 114
A.2 Experimental Data on Reservoir Fluids 115
A.3 Methane + Propane 117
A.4 Methane + Propane 118
A.5 Methane + Propane 119
A.6 Methane + n-Butane 120
A.7 Methane + n-Pentane 121
A.8 Methane + n-Hexane 122
A.9 Methane + n-Heptane 122
A.10 Methane + n-Heptane 123
A.11 Methane + n-Nonane 124
A.12 Methane + n-Decane 125
A.13 Methane + n-Decane 126
A.14 Ethane + n-Pentane 126
A.15 Methane + Ethane + n-Pentane 127
A.16 Methane + Propane + n-Decane 128
A.17 Methane + Propane + n-Decane 129
A.18 Gas Condensate 130
A.19 Gas Condensate 130
A.20 Gas Condensate 131
A.21 Associate Gas 131
A.22 Wet Gas 132
A.23 100wt% MEG + Methane 132
A.24 80wt% MEG/20wt% Water + Methane 133
A.25 50wt% MEG/50wt% Water + Methane 133
A.26 100wt% MEG + Methane/Ethane 134

A.27 80wt% MEG/20wt% Water + Methane/Ethane 134
A.28 50wt% MEG/50wt% Water + Methane/Ethane 134

Chapter 1

Introduction

1.1 Study Background

Process simulation software and multiphase flow simulators involve the use of a number of thermodynamic and physical property models. Correct thermodynamic and physical property prediction is of high importance to achieve optimal design of pipelines and process equipment, such as separators. The design of separators is influenced by multiple parameters. One parameter, which recently has received increased focus, is the droplet diameter. The droplet diameter, in addition to the gas/liquid interface, can be related to surface tension.

Simulation tools such as OLGA, HYSYS and PRO/II require input of thermodynamic properties as well as transport properties, such as surface tension. Normally the thermodynamic properties are calculated using classic equations of state such as Soave-Redlich-Kwong (SRK) and Peng-Robinson (PR), while transport properties are calculated with relatively simple and computational effective methods. During recent years, a number of more advanced thermodynamic and transport property models have been developed. An example of a modern model for calculation of surface tension is the gradient theory.

A number of techniques have been presented in literature for experimental measurements of surface tension between a gas and liquid. The pendant drop method is a frequently used method for such measurements. In this work high pressure pendant drop experimental equipment will be used to measure surface tension in gas and glycol systems. Moreover, theoretical models will be evaluated for their accuracy in predicting surface tension.

1.2 Scope and Objectives

Experimental measurements is in this study conducted with the pendant drop technique and carried out at Statoil research center at Rotvoll. The measurement of surface tension is the primary focus but as experimental testing yields more data than surface tension only, phase densities and liquid phase compositions are also measured. Different MEG/water mixtures combined with methane and ethane gas are examined in the lab in this study.

The second part of this study will be to evaluate surface tension models implemented in process simulation software. The simulation tools NeqSim, PVTsim, PRO/II and HYSYS will be used for calculating properties. Evaluation of the different software will be done by comparing their performance against experimental data obtained in the lab and collected from literature. It is of particular interest to assess the performance of NeqSim against the other software, as it utilizes more modern and advanced models. The SRK, PR and cubic plus association (CPA) equation of state are utilized to compute the surface tension.

The following objectives are to be covered:

1. Review of experimental techniques used for measurements of surface tension
2. Collection of experimental data for surface tension for gas and oil/glycol systems
3. Experimental measurement of surface tension of selected fluids (gas/oil/glycol)
4. Evaluation of models and software for calculation of surface tension tension

1.3 Limitation of Scope

- When simulating glycol mixtures in NeqSim the linear gradient theory is used because the full gradient theory is not yet fully implemented. As data is produced through this thesis, they will be used to tune the full gradient theory to match glycol mixtures as well.
- This thesis focuses on mixtures containing hydrocarbon and MEG/water relations. Systems which contains water without the presence of MEG will not be taken into consideration. That is also the case for streams dominated by carbondioxide and nitrogen.
- The experimental work in this study focuses solely on MEG/water mixtures. Due to limited time it was not possible to examine further glycol mixtures or more complex hydrocarbon fluids in the lab.
- The models selected for analysis in this thesis are the default options in each software. Some of the software (PRO/II, HYSYS) have several models implemented, and better results will be obtained by changing them. It would be too time consuming to simulate all mixtures with every model, and it is also our view that users of these software apply the default models. However, a section in chapter 8 is devoted to this subject.

1.4 Organization

Chapter 2 Review of separators, why they are important, what type of components they consist of and finally how surface tension influence the design.

Chapter 3 Deals with fundamental concepts from theory. It starts by defining concepts such as surface tension, law of corresponding states and equation of state. The focus is then shifted towards theoretical models used to calculate surface tension.

Chapter 4 Gives an introduction to the software used in this report, more specifically the application area. The chapter further describes which models for calculating surface tension that are implemented in each software.

Chapter 5 Starts by showing an outline of the experimental data used in this thesis. Surface tension data is collected for binary, ternary and reservoir fluid mixtures. It further describes different techniques used to measure surface tension.

Chapter 6 Gives a full description of the experimental setup used in this study. The procedure used when conducting the experiment is also explained.

Chapter 7 Shows the results from the experimental work. The results are divided into density, composition and surface tension. An uncertainty analysis concerning the measurements of the surface tension is given at the end of the chapter.

Chapter 8 Illustrates the results from the simulation work. The results from the different mixtures are given as graphs and tables, and it shows the simulated values against the experimental values over a large temperature and pressure range.

Chapter 9 Summarizes the results and findings and presents the conclusions.

Chapter 10 Suggests further work on this report.

Appendix A All additional information is given in this chapter. Part A.1 displays the complete set of experimental data for hydrocarbon mixtures collected in this study. Part A.2 displays all the data from the simulations in tabular form.

Chapter 2

Review of Design Methods of Gas Separation Equipment

2.1 Separation

The purpose of the separation equipment is to separate liquid and gas. This is done for a number of reasons. The most important being:

- Controlling air pollutants
- Protecting rotating equipment. Liquid droplets in compressors, turbines, and expanders can cause great damage
- To prevent foaming in gas dryers and CO2 removal units
- To prevent hydrate formation in equipment downstream of the separator
- Be able to control dew point for sales and transport specifications

Separators can generally be divided into two different types: the vertical separator and the horizontal separator. The former is normally used for gas dominated service where liquid quantity is low. This kind of separator is usually called a scrubber. The latter is more applicable in cases where the liquid is the dominating fraction and the gas flow rate is low, i.e. crude oil systems. The horizontal separator typically has a higher surface area, which makes it better for three-phase separation and foaming fluids.

There are huge costs associated with dysfunctional separation equipment. Premature replacement of compressors or expanders, cleaning of foam or hydrate formation, or not meeting air pollution standards and requirements demand expensive measures. Hence, the design of separators and scrubbers is of utmost importance.

2.1.1 Removal Mechanisms

Before giving a brief introduction to some of the standard separation equipment used, an understanding of the different mechanisms for removal of gas from liquid should be present. Separation equipment employs one or more of the following mechanisms:

1. Gravity settling
2. Centrifugal force

3. Impingement
4. Electrostatic precipitation
5. Sonic precipitation
6. Filtration
7. Adhesive separation
8. Adsorption
9. Thermal

The primary mechanisms in oil and gas separation are gravity settling, centrifugal force and impingement [10].

Gravity Settling

The gravitational settling mechanism may be the easiest and the more implicit one. The multiphase flow hits the separator at high velocity. This kinetic energy is broken down by some inlet device, as will be described in section 2.1.2, and a bulk of liquid is already separated at this instant. However, some liquid is entrained within the gas as droplets. As the gravitational force exceeds that of drag from the flow, separation of gas and liquid occurs. That is, the weight of the droplets is forcing the liquid to fall despite the drag force from the flowing gas.

Equation 2.1 shows the correlation between terminal velocity and separation parameters and fluid properties. The terminal velocity is the gas velocity where the liquid droplet is suspended in the gas flow, moving neither up nor down.

$$v_t = \sqrt{\frac{4gd}{3C_d}(\frac{\rho_L - \rho_g}{\rho_g})} \tag{2.1}$$

v_t = terminal velocity

g = gravitational constant

d = droplet diameter

C_d = drag coefficient

ρ_l = fluid density

ρ_g = gas density

C_d is a function of particle diameter, shape, terminal velocity, gas density and viscosity.

One approach is to evaluate C_d for three separate flow regimes - laminar (Stoke's Law), intermediate and turbulent (Newton's Law). This approach assumes that the plot of drag coefficient versus Reynold's number can be approximated by three straight lines. This does not result in a serious loss of accuracy at typical oil and gas separator conditions.

Centrifugal Force

The centrifugal force is the force that acts on a rotating body, pulling it away from the center of rotation. This force is strongly linked to gravity, but can be several times stronger. It is thus a more effective way of separation.

Impingement

Lastly, there is the impaction force. It occurs when a gas passes through a network, such as fibers and impingement barriers. In this case the gas follows a tortuous path around these obstacles while the liquid droplets tend to go into straighter paths, impacting these obstacles. Once this occurs the droplet loses velocity, coalesces and eventually falls to the bottom of the vessel or remains trapped in the fiber. Surface tension is essential for impingement to work properly, as to low surface tension could result in break up of the liquid film created on the surface and re-entrainment of liquid into the bypassing gas flow.

2.1.2 Separator Components

Efficient removal of contaminants (i.e. liquids, solids) from a gas stream can prevent costly problems and downtime in equipment like compressors, turbines, and burners. There are several internal components available for separation of liquids and solids from gas. For the scope of this thesis a few will briefly be presented:

- Inlet device
- Liquid collection section
- Gravity settling section
- Mist extractor

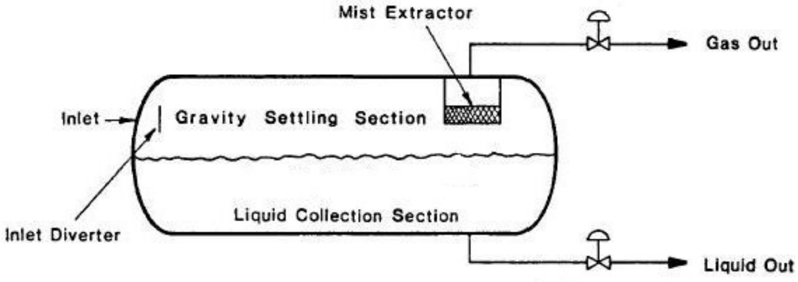

Figure 2.1: Horizontal Separator Schematic Showing the Four Major Sections

In addition, the separator can be equipped with several other internal components and control devices as well such as liquid level controller, pressure control valve, wave breaker, de-foaming plates, vortex breaker, stilling well, sand handling systems etc. They are not discussed in further detail in this thesis.

Inlet Devices

As the flow enters the separator it has a high kinetic energy. Its velocities can reach 6-10 m/s [10] and this energy needs to be dissipated before the flow can enter the gravity separation section. This can be done in several ways, the easiest one being to place a simple solid plate in the fluid path downstream of the inlet, called a diverter or baffle plate. Its shape could be that of a flat plate, a dish, cone or basically anything that induce a rapid change in flow direction and velocity, causing separation of the two phases. It is cheap and simple but not very effective at higher velocities, as very small droplets are then created which are more difficult to separate.

Another widely used inlet device is the half-open inlet device as seen in figure 2.2 [5]. The flow enters the separator through a pipe where the bottom is left open. It has a simple design, but sends both gas and liquid downward into the separator and some gas may be entrained into the liquid. With this device the initial separation is quicker because it entails a smoother transaction. However, like the inlet plate device the half open pipe is not very well suited for high inlet velocities.

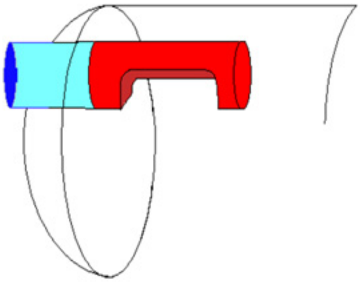

Figure 2.2: Half Open Pipe Inlet Device

The inlet device that often performs best is the inlet cyclone. Accordingly, it is the one with the most complex structure. Figure 2.3 shows the CDS Inlet Cyclone from FMC Technologies. It operates at both high and low gas oil ratios without the risk of gas blow and excessive liquid re-entrainment into the gas phase. The feed stream is brought into rotation by a spin device. The resulting centrifugal forces move the liquid (and solids if present) to the wall of the cyclone where it is drained out at the bottom into the liquid compartment of the separator vessel. The inlet device can consist of either one large cyclone or several smaller ones where the flow is distributed equally to each cyclone.

Lastly, the inlet vane distributor is another complex option, shown in figure 2.4. They are used when the gas load is high compared to liquid, therefore this is the most commonly used inlet device in scrubbers. This can be used where foaming is predicted and also for streams containing solids. An inlet vane gradually releases the gas and liquid into the separator and distributes the phases at a low pressure drop.

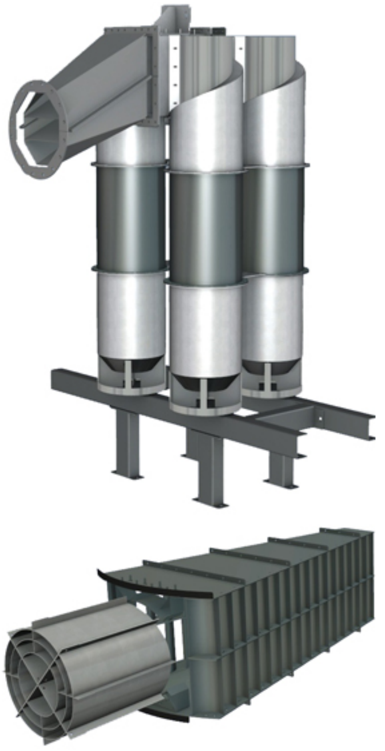

Figure 2.3: FMC Technologies CDS Inlet Cyclone

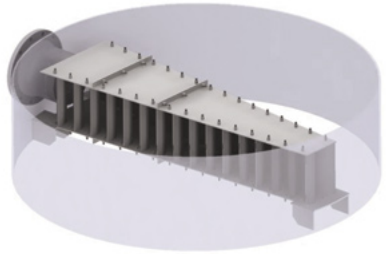

Figure 2.4: Inlet Vane Distributor

Liquid Collection Section

In the liquid collection section the entrained gas in the liquid escapes to the gravity settling section. The separator needs to be designed so that it provides the required retention time to let gas evolve out of the oil and reach equilibrium state. This is where the critical part of the degassing of the oil occurs. Retention time is defined as the volume of liquid divided by the liquid flow rate and is therefore directly affected by the amount of liquid the vessel can hold and the rate at which the fluid enters the vessel. The liquid collection section also provides a surge volume to handle intermittent slugs.

Gravity Settling Section

Smaller liquid drops entrained in the gas are separated out in the gravity settling section as the gas velocity is reduced substantially. Very fine drops of liquid following the gas stream are removed in the mist extractor. The gas flows through elements which causes it to make several changes in direction. The liquid droplets cannot follow because of their greater mass, thus they fall out due ti impingement.

Mist Extractors

The gas drag force cause small liquid particles to follow the gas stream. Mist extractors must therefore somehow intervene the natural balance between gravitational and the drag forces. This can be accomplished by reducing the gas velocity (hence reduce drag), introduce additional forces by use of cyclones or increase gravitational forces by boosting the droplet size (impingement). The selection of mist extractor is based on evaluation of:

- Droplet sizes that must be removed
- Tolerated pressure drops
- Presence of solids and the probability or risk of plugging because of this
- Liquid handling in the separator

The rate of droplets following the gas stream is governed by simple laws of fluid mechanics. As gas flows upward, two opposing forces are acting on a liquid droplet namely a gravitational force (accelerates the droplet down) and a drag force (slows down the droplet's rate of fall). An increase in gas velocity will increase the drag and when the drag force equals the gravitational force the droplet will settle at the terminal velocity. Further increase in the gas velocity causes the droplet to move upwards and then follow the gas stream out of the separator.

Mist extractors' operation is usually based on a design velocity given by:

$$V = K\sqrt{\frac{\rho_l - \rho_g}{\rho_g}} \tag{2.2}$$

V = gas velocity

K = souders-Brown coefficient

ρ_l = fluid density

ρ_g = gas density

In other words it is the K-factor that determines the operating gas velocity, where a too low factor can cause the droplets to remain in the gas streamlines and pass through the device uncollected while a too high value can cause re-entrainment because of droplet breakup.

Common types of mist extractors are:

- Wire mesh
- Vane packs
- Cyclones

The most common impingement type mist extractor are the wire mesh type, figure 2.5. A large surface area is obtained by knitting wire together to a pad. The mesh pad is mounted close to the gas outlet of the separator, as shown in figure 2.1. As the gas flows through, the inertia of the entrained droplets makes them contact the wire surfaces and coalesce. Because of the dense structure of the pad it is best suited for low viscosity, non-congealing liquids with no solids present. Otherwise it may get clogged.

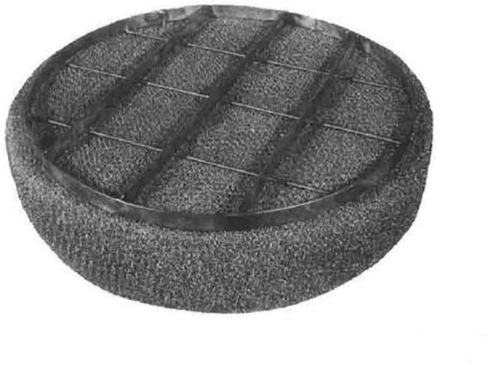

Figure 2.5: Wire Mesh Mist Extractor

The operating principle for a vane pack is that the feed stream passes through parallel vane plates and is forced to change direction several times. The droplet impinge and collect at the surface of the plates and create a liquid film which is drained through slits into a liquid sump and then further to the liquid compartment of the vessel. Figure 2.6 shows a double pocket design. Here the collected liquid is guided into separate channels that move the liquid away from the gas. Because the liquid is isolated from the gas the chance for re-entrainment of liquid into the gas again is reduced. Simpler single pocket designs are also common, but here the liquid is drained with the gas flowing by, increasing the chance of re-entrainment of liquid. Hence, gas velocity can be much higher for double pockets.

Vane mist extractors normally remove liquid droplets with a diameter larger than 10 - 40 μm, but with special designs such as the one in figure 2.6, droplets with a diameter down to 8 μm can be removed [48].

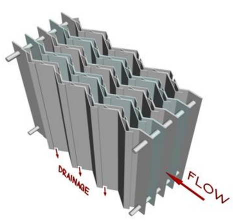

Figure 2.6: Horizontal Gas Flow in Vane Packs

In a cyclonic demisting device multiple cyclone tubes are mounted on a deck or into a housing. Cyclone demisters can handle high gas capacities combined with efficient droplet removal, and are more efficient than mist extractors and vanes and less susceptible to clogging. Figure 2.7 shows a principle sketch of a cyclone mist extractor. Gas and mist enters the cyclone and goes through a swirl element. This induces high centrifugal forces causing the liquid droplets to move outwards and coalesce to a liquid film on the cylinder wall. The liquid is purged through slits in the wall together with some gas into a chamber where the phases are separated. The purge gas, with some remaining mist is led to a low pressure zone of the cyclone where the remaining entrainment is removed. The main gas flow is discharged at the top of the cyclone while the liquid is drained at the bottom.

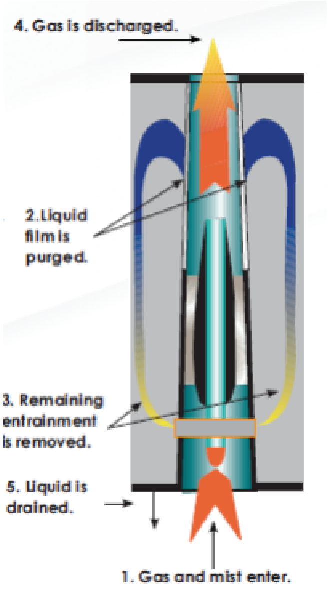

Figure 2.7: Cyclone Mist Extractors

Cyclones can be configured both horizontally and vertically, often corresponding to the orientation of the gravitational separator. Cyclonic mist extractors can remove droplets down to 5 μm in diameter [48]. As for inlet devices the cyclone alternative is the most difficult to design, are quite expensive and have larger pressure drop than the other devices. It is also sensitive to changes in the flow. On the other hand, by installing a cyclonic device costs can be saved elsewhere by minimizing the size of the total separator.

2.2 Surface Tension in Separation Design

Traditionally there is a lot of focus on the geometry of separators when it comes to design. Details on the effects of variations in physical fluid properties like surface tension are less known. In a design phase the available parameters are usually the fluid properties and the minimum and maximum gas and liquid rates. There is a whole range of parameters used to describe multiphase flow. Although, in order to apply correlations/expressions one must be able to relate them to the available design parameters in combination with geometrical parameters.

This chapter will seek to give an overview of how the fluid property of surface tension is related to gas separation design. The theory is based on data from Norsk Sokkels Konkurranseposisjon (NORSOK) [38] and the doctoral thesis by Trond Austrheim [4].

2.2.1 Droplet Size

The droplet size is a parameter used in several expressions and for several reasons. If the droplet size is to be used in calculating the separation design, then there is a need of expressions that can calculate the droplet size based on the available design parameters. A correlation between surface tension and droplet size is described by the Young-Laplace equation:

$$\triangle p = \sigma(\frac{1}{R_1} + \frac{1}{R_2}) \tag{2.3}$$

$\triangle p$ = pressure difference across the fluid interface

σ = surface tension

R_i = principal radii of curvature

The Young-Laplace equation is a nonlinear partial differential equation that describes the capillary pressure difference sustained across the interface between two static fluids due to surface tension. It relates the pressure difference to the shape of the surface, and in the case of a spherical droplet ($R_1 = R_2$), the equation reduces to:

$$\triangle p = \frac{2\sigma}{R} \tag{2.4}$$

From equation 2.4 the droplet diameter is then easily calculated.

This is a very simplified version of the correlation between surface tension and droplet diameter, assuming static fluids and spherical droplets. However, the pendant drop method is based on this equation, and most surface tension measuring methods are correlating the surface tension and droplet diameter.

2.2.2 Vessel Diameter

The geometry of the separator is often limited by practical parameters like weight and footprint. This is especially the case for offshore units, where low weight and little available area are the main concerns. However, when these factors are indecisive, the vessel diameter is often calculated using the K-value. The K-value is decided by the Souders-Brown equation.

Souders-Brown Equation

The most used expression for sizing of gas separators is the Souders-Brown equation, developed in 1934. It was designed for sizing of fractionation columns. This equation contains an empirical factor known as the Souders-Brown value, or the K-value. The basis of the equation is the force balance performed on a droplet in an upwards flowing gas field. The gravitation force on the droplet adjusted for buoyancy when resolved in vertical direction is:

$$G_d = \frac{\pi}{6} d^3 (\rho_i - \rho_g) \tag{2.5}$$

d = droplet diameter

ρ_l = fluid density

ρ_g = gas density

The resistance of a droplet in a moving fluid resolved in the vertical direction can be expressed:

$$F_r = K\mu_g \frac{\sqrt{\pi}}{2} du_g + C_d A_d \frac{1}{2} \rho_g u_g^2 \tag{2.6}$$

K = K-value

μ_g = gas viscosity

u_g = gas velocity

A_d = cross-sectional area of drum

Souders and Brown argued that the viscosity of the gas phase was very small so that the viscous term could be neglected. The vapor viscosity they sketched for a fractionating column was in the range of 0.01 to 0.001 cP. This leaves only the drag force as the relevant force acting upwards on the droplet. Assuming that the droplet has the shape of a sphere, the drag force can be expressed as:

$$F_d = C_d A_d \frac{1}{2} \rho_g u_g^2 = C_d \frac{\pi}{4} d^2 \frac{1}{2} \rho_g u_g^2 \tag{2.7}$$

The terminal settling velocity is found when the drag force equals the gravitation. By equating the right-hand-sides of equation 2.5 and 2.7 the settling velocity becomes:

$$u_{g,set} \sqrt{\frac{\rho_g}{\rho_l - \rho_g}} = \sqrt{\frac{4gd}{3C_d}} \tag{2.8}$$

If the droplet size and drag force coefficient is constant the right hand side of the expression is also a constant and this is the definition of the K-value:

$$K = \sqrt{\frac{4gd}{3C_d}} \tag{2.9}$$

C_d is the drag coefficient which is dependent on the Reynolds number for the droplet. The classical result of Stoke is that the drag coefficient is related to the Reynolds number as:

$$C_d = \frac{24}{Re_r} \tag{2.10}$$

where Re_r is the Reynolds number based on the relative velocity. This result, however, is only valid for Stokes flow i.e. $Re_r < 1$. In the settling section of a scrubber the Reynolds number is generally larger than this. Putnam [43] developed this correlation for larger Reynolds numbers:

$$C_d = \frac{24}{Re_r}(1 + \frac{Re_r^{\frac{2}{3}}}{6}) \tag{2.11}$$

This correlation is valid for $Re_r < 1000$, which is sufficient for most cases of droplet in a settling section of a scrubber.

Calculation of Vessel Diameter

In order to calculate the vessel diameter, the maximum velocity is calculated based on the critical K-value. The critical K-value is the K-value where the gas velocity equals the terminal velocity of the mean droplet size. As the K-value is proportional to the superficial gas velocity, the velocity can be calculated using this correlation:

$$u_{s,g} = K\sqrt{\frac{\rho_l - \rho_g}{\rho_g}} \tag{2.12}$$

Then, using the actual gas volume rate, $\dot{Q}_g$, the vessel diameter can be decided:

$$D = \sqrt{\frac{4\dot{Q}_g}{\pi u_{s,g}}} = \sqrt{\frac{4\dot{Q}_g}{\pi K\sqrt{\frac{\rho_l-\rho_g}{\rho_g}}}} \tag{2.13}$$

Empirical data and experience from vessels with comparable fluid properties are important parameters when choosing the K-value. It could also be chosen based on the expected or required droplet size. However, a limitation for equation 2.12 is that because it uses superficial velocity and not the actual velocity, it is not working well when applied to larger liquid flows. If the liquid flow rate is increased, the cross sectional flow area for the gas is decreased and thus raises the mean velocity.

For low pressure applications, when designing a column to avoid that the upward velocity entrains droplets, the recommended K-value is K $<$ 0.1 m/s. When pressure is increased the critical K-value has been known to decline. This makes sense, as an increase in pressure in oil and gas application is normally equivalent to a decrease in surface tension and thus a decrease in droplet size. This increases the risk of re-entrainment of separated liquid. However, all separators experience re-entrainment or carryover. Even the separators with the highest efficiency have a carryover of 2-3% [10]. A carryover, however, is not necessarily intolerable. Liquid entrainment from primary production separators may not be a major operating problem if secondary separation is provided downstream. However, in critical separation applications, the cost of the problems created by the entrainment often far exceeds the incremental cost of a properly sized vessel. More on entrainment in section 2.2.3.

The K-value also serve as a benchmark parameter when describing the compactness of a gas separator. NORSOK [38] recommends that separators with demisting internals should operate below K = 0.15 m/s. A K-value larger than 0.1 m/s therefore means that there is need for another instrument downstream to separate the liquid that has not been separated in the inlet or mesh section. This could be a cyclone or vane packs.

Use of Mass flow rate

Another parameter often used for sizing purposes is the mass flow rate. Often done when sizing fractionators and absorbers, the mass velocity, w, is linked to the linear velocity by the equation

$$w = 3600 u_{s,g} p_g \tag{2.14}$$

Substituted into equation 2.12, the result is

$$w = 3600K\sqrt{\frac{\rho_l - \rho_g}{\rho_g}} \tag{2.15}$$

Then, knowing that

$$w = \frac{\dot{m}}{A} = \frac{4\dot{m}}{\pi D^2 F_g} \tag{2.16}$$

and combining equations 2.15 and 2.16 enables one to solve for the internal vessel diameter

$$D = \frac{0.0188\sqrt{(\frac{\dot{m}}{F_g K})}}{(\frac{\rho_l - \rho_g}{\rho_g})^{0.25}} \tag{2.17}$$

The value of $\dot{m}$ is related to standard volume rate of flow as follows:

$$\dot{m} = (1762)(\frac{10^6 stdm^3}{d})(MWgas) = (51060)(\frac{10^6 stdm^3}{d})(\gamma_{gas}) \tag{2.18}$$

Using flow rate to calculate the internal vessel diameter is again dependent on the K-value.

Also, when calculations of the vessel diameter is based on the flow rate, one has to be aware that these flow rates are reservoir engineering estimates. As multiphase flows are complex physics, surges and slugs will be encountered. Thus, normal practice is to apply a design factor to adjust upwards the expected average flow. Typical design factors range from 1.2 to 1.5 depending on the location and nature of the inlet stream.

2.2.3 Liquid Entrainment

Entrainment may be defined as the entrapment of one substance by another substance, for instance liquid droplets in a gas flow. This occurs when the relative velocity between the gas and the liquid phase exceeds a critical limit. This limit is highly dependent on physical properties of the fluid. As Viles [60] concludes in his paper; re-entrainment becomes more likely at higher operating pressures. This tendency is a result of increased gas density and reduced surface tension.

There are a number of ways in which entrainment can occur, depending on flow situation. The report of Ishii and Grolmes [28] summarizes the basic entrainment mechanisms. They are roll wave, wave undercut, liquid impingement, bubble bursting and liquid bulge disintegration. The former one, the roll wave type of mechanism dominates the other types and contributes most to the entrainment of liquids. This is also the mechanism where surface tension is most apparent. Thus, this will be the evaluated mechanism in this theoretical part.

Roll Wave Entrainment

In roll wave entrainment, the drag force acting on the wave tops deforms the interface against the retaining force of the liquid surface tension. Then the tops of the roll waves are sheared off from the wave crest by the gas flow and then broken into small droplets. A criterion for the onset of re-entrainment can be derived by considering the force balance between the drag force F_d from the high shear flow of gas acting on the liquid wave crest, and the retaining force of the surface tension, F_σ. Ishii and Grolmes assumed that roll wave entrainment was possible when the drag forces exceeded the retaining force of the surface tension:

$$F_d \geq F_\sigma \tag{2.19}$$

Furthermore, they derived one criterion for the inception of entrainment in the transition regime, and one criterion for the rough turbulent regime.

For the transition regime the criteria were

$$\frac{\mu_l \mu_{g,s}}{\sigma}\sqrt{\frac{\rho_g}{\rho_l}} \geq 11.78 N_\mu^{0.8} Re_l^{-1/3} \tag{2.20}$$

for $N_\mu \leq \frac{1}{15}$

and

$$\frac{\mu_l \mu_{g,s}}{\sigma}\sqrt{\frac{\rho_g}{\rho_l}} \geq 1.35 Re_l^{-1/3} \tag{2.21}$$

for $N_\mu \geq \frac{1}{15}$

Now, N_μ is the viscosity number which originally was used by Hinze [23] to analyze the problem of droplets disintegration in a gas flow. The group measured the viscous force induced by an internal flow to the surface tension force. When it is used for droplet entrainment it is defined as

$$N_\sigma = \frac{\mu_l}{\sqrt{\rho_l \sigma \sqrt{\frac{\sigma}{g \delta \rho}}}} \tag{2.22}$$

2.2.4 Wire Mesh

Wire mesh is historically the most common type of mist extractor for vertical separators. It is made up of wire knitted into a pad with as much as 97-98% [10] void in-between them. It can be installed in a scrubber to catch smaller droplets, which do not settle in the gravity settling section, and coalesce them to larger droplets that do settle out. Alternatively, it can be used as a preconditioner to increase the average droplet size prior to the final demisting stage.

The main mechanism of separation in the wire mesh is impingement. The gas flowing through the pad is forced to change direction a number of times, and in connection with the wet surfaces of the wire, droplets coalesce.

A liquid particle striking the metal surface which it does not wet, flows downward where adjacent wires provide some capillary space. At these points, liquid collects and continues to flow downward. Surface tension tends to hold these drops on the lower face of the pad until they are large enough for the downward force of gravity to exceed that of the upward gas velocity and surface tension.

The diameter of the wire mesh is normally based on the K-value. A maximum value of K = 0.107 is generally satisfactory for non-viscous liquids and assuming the gravity settling section has removed the bulk of the liquids.

A caution regarding the use of wire mesh is the possibility of flooding. Flooding can occur when upstream gas velocity exceeds a certain limit. The coalesced droplets can no longer be drained efficiently by gravity and therefore liquid start to build up in the mesh.

2.2.5 Centrifugal Elements

Standard oil and gas separators may have an inlet that utilizes centrifugal force to separate larger drops. Some mist extractor elements use the same principles, the only difference being that higher velocities are needed in order to separate the smaller droplets. The required velocity is a function of particle diameter, particle and gas densities and also the gas velocity.

Typical centrifugal elements are the reverse flow cyclone, the axial-flow cyclone and the recycle axial cyclone.

2.2.6 Scaling Rules

When designing separators, efficiencies of internals are often found in low-pressure tests. When designing for high pressure operations, this can cause a problem because test conditions will deviate considerably from real life conditions. Thus, a way to scale the test results to match real life conditions is needed. In most cases vendors of scrubber internals try to take into account the effect of one or more of the changing physical properties. It is common to decrease the superficial gas velocities with increasing pressure.

One common way of doing scaling is to keep the gas dynamic pressure constant. Another approach is to scale the superficial gas velocity by use of the K-value. Keeping the K-value constant in a cyclone means that the ratio of the total cyclone area to the vessel diameter is kept constant.

It is sometimes a goal to keep the cut size of the cyclone constant. In that case the gas and liquid density and the gas viscosity should be taken into account.

Chapter 3

Theoretical Concepts

3.1 Fundamental Concepts

3.1.1 Surface Tension

Surface tension is the boundary between a liquid phase and a vapor phase, and has properties distinct from the two phases. A definition is given by Poling et al. [42] “Surface tension is the force exerted in the plane of the surface per unit length”.

There is an imbalance of intermolecular attractive forces between molecules in the bulk liquid and gas. This causes the surface to be in tension, and results in an excess free energy per unit area. Consider a reversible process where the area A of the surface is changing. The reversible work is σdA, which corresponds to the increase in surface free energy. The surface tension is therefore equivalent to the surface free energy per unit of area. The concept of surface energy is important to understand the shape of liquid droplets. A system at equilibrium is in a state of minimum surface energy, and because it is proportional to the surface area, the area is also minimized.

The mechanics of fluid surfaces is important when investigating surface tension. There are forces acting upon the curved surfaces in the droplet as illustrated in figure 3.1 [57]. In the left picture surface tension forces pull the surface toward the concave side, thus the pressure must be greater on the concave side of the surface. In the picture to the right the surface tension forces oppose each other, thus reducing the pressure difference across the surface. The mean curvature of a two-dimensional surface is specified in terms of the two principal radii R_1 and R_1. A mechanical analysis shows that the pressure change across the surface is directly proportional to the surface tension, and to the mean curvature of the surface. This relationship is known as the Young-Laplace equation, which was mentioned in section 2.2. The pressure change across the interface is named the Laplace pressure [57] [36].

$$P_A - P_B = \sigma(\frac{1}{R_1} + \frac{1}{R_2}) \tag{3.1}$$

The Young-Laplace equation can be written as coupled first-order differential equations in terms of the coordinates of the surface:

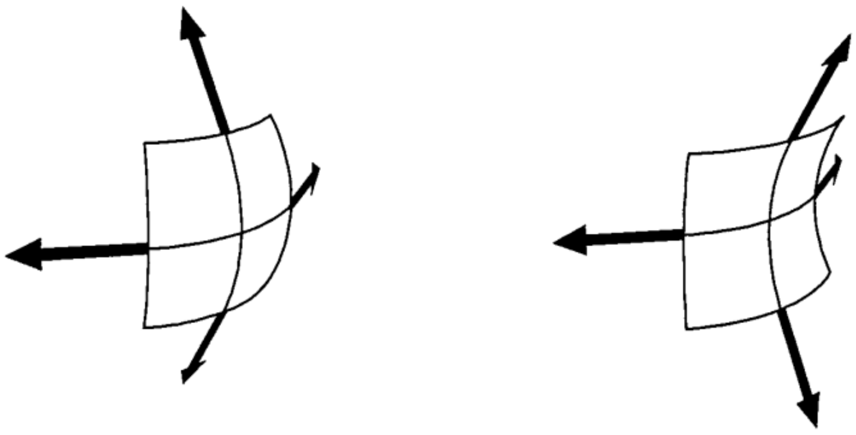

Figure 3.1: Mechanics of Curved Surfaces

$$\frac{dx}{ds} = cos\phi \tag{3.2}$$

$$\frac{dz}{ds} = sin\phi \tag{3.3}$$

$$\frac{d\phi}{ds} = \frac{2}{R_0} + \left(\frac{\triangle\rho g}{\sigma}\right)z - \frac{sin\phi}{x} \tag{3.4}$$

$\triangle\rho$ = density difference

x, z = horizontal and vertical coordinate

ϕ = angle between the surface tangent and the horizontal plane

s = arc length

R_0 = radius of curvature at the drop apex

g = gravity

Figure 3.2 shows a pendant drop with the same coordinates as the Young-Laplace equation [36]. The drop has a neck at the top, which means the two principal radii have opposite signs. At the bottom of the drop the two radii have the same sign, which gives a larger mean curvature. The parameters in the Young-Laplace equation can be made dimensionless, thus the resulting equation (3.5) contains only one parameter, namely the Bond number (also called shape factor). This parameter describes the shape of the drop.

$$\beta = \triangle\rho g R_0^2/\sigma \tag{3.5}$$

Interfacial tension is the boundary between two immiscible liquid phases. Surface tension and interfacial tension is used interchangeably in the literature [42]. The surface tension and interfacial tension are usually expressed in *dyn/cm* which is equivalent to *mN/m* in SI units.

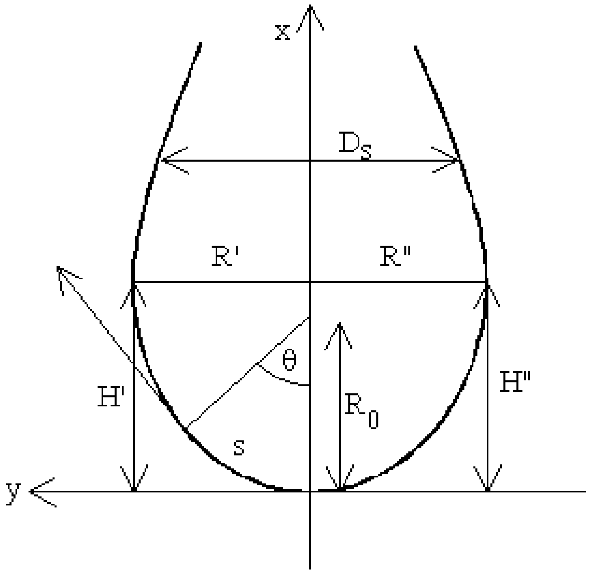

Figure 3.2: Pendant Drop With Characteristic Dimensions

3.1.2 The Law of Corresponding States

The law of corresponding states was first proposed by van der Waals, and describes how equilibrium properties are related to critical properties [42]. The relation of pressure to volume at constant temperatures varies for different substances. The law of corresponding states claims if pressure, temperature and volume are divided by the corresponding critical properties, they have approximately the same compressibility factor. The law applies to fluids containing simple molecules and for fluids where molecular orientation is not important (e.g. CH4). The reduced properties are: $P_r = \frac{P}{P_c}$, $T_r = \frac{T}{T_c}$, $V_r = \frac{V}{V_c}$.

3.1.3 Equation of State

An equation of state is a relation between state variables, such as temperature, pressure and volume. It is used to calculate properties, such as densities of liquids and gases. In this section the SRK and the PR cubic EoS are studied.

Soave-Redlich-Kwong

The SRK EoS is based on the Van der Waals EoS from 1873. It is also a modification of the Redlich-Kwong EoS [46]. The Soave modification of RK replaces the a(T) term [53]. The general equation is:

$$P = \frac{RT}{v-b} - \frac{a(T)}{v(v+b)} \tag{3.6}$$

At the critical point a, b becomes:

$$a(T_c) = 0.42747\frac{R^2T_c^2}{P_c}, \quad b = 0.08664\frac{RT_c}{P_c} \tag{3.7}$$

At temperatures other than the critical, the value of a(T) becomes:

$$a(T) = a_c \alpha(T) \tag{3.8}$$

$$\alpha^{0.5} = 1 + m(1 - T_r^{0.5}) \tag{3.9}$$

$$m = 0.480 + 1.57\omega - 0.176\omega^2 \tag{3.10}$$

The term a(T) can now be calculated at any temperature knowing only the critical constants and the acentric factor ω.

The mixing rules for the SRK are:

$$a = \left(\sum_i x_i a_i^0 .5 \right)^2 \tag{3.11}$$

$$b = \sum_i x_i b_i \tag{3.12}$$

Cubic Plus Association

The CPA EoS [30] utilizes the physical term from the SRK EoS and the association term from the SAFT EoS [25]. The general equation is:

$$P = \frac{RT}{v-b} - \frac{a(T)}{v(v+b)} + \frac{RT}{v} \rho \sum_A \left[\frac{1}{X^A} - \frac{1}{2} \right] \frac{\partial X^A}{\partial \rho} \tag{3.13}$$

The mole fraction X^A of molecules not bonded at site A can be defined as:

$$X^A = (1 + \rho \sum_B X^B \Delta^{AB})^{-1} \tag{3.14}$$

Δ^{AB} = association strength

Peng-Robinson

The SRK EoS can satisfactory calculate the vapor density, but the liquid density is not as accurate. The PR gives more accurate liquid densities [40]. As for SRK the pressure consists of two terms, namely a repulsion pressure and an attraction pressure:

$$P = P_R + P_A \tag{3.15}$$

The repulsion pressure term is the same as for SRK EoS, but the attraction pressure term is different:

$$P = \frac{RT}{v-b} - \frac{a(T)}{v(v+b) + b(v-b)} \tag{3.16}$$

At the critical point a, b becomes:

$$a(T_c) = 0.45724 \frac{R^2 T_c^2}{P_c}, \quad b = 0.07780 \frac{RT_c}{P_c}, \quad Z_c = 0.307 \tag{3.17}$$

At temperatures other than the critical, the value of a(T) becomes:

$$a(T) = a_c\alpha(T) \tag{3.18}$$

$$\alpha^{0.5} = 1 + \kappa(1 - T_r^{0.5}) \tag{3.19}$$

$$\kappa = 0.37464 + 1.54226\omega - 26992\omega^2 \tag{3.20}$$

The mixing rules for the PR are:

$$a = (\sum_i \sum_j x_i x_j a_{ij}) \tag{3.21}$$

$$b = \sum_i x_i b_i \tag{3.22}$$

Peneloux

Peneloux et al. [39] proposed a simple correction for calculation of volumes in SRK EoS. The volumes in the SRK may be considered as pseudo volumes:

$$P = \frac{RT}{\tilde{v} - \tilde{b}} - \frac{a(T)}{\tilde{v}(\tilde{v} + \tilde{b})} \tag{3.23}$$

These values can be improved by a translation along the volume axis:

$$v = \tilde{v} - \sum_{i=1}^{P} c_i x_i \tag{3.24}$$

It is then possible to apply this correction without changing the vapor-liquid equilibrium conditions in the SRK equation. This correction was later implemented with PR as well.

3.2 Models for Calculating Surface Tension

The models selected are the ones implemented in each software described in chapter 4. The selection of different models described in the literature is vast, and the reader is referred to the book by Poling et al. [42] for a thorough description. The reader is also referred to section 3.1 for a description of theoretical concepts used in this section.

The majority of the models used to calculate surface tension are based upon the corresponding states principle or the parachor. These models are empirical, but more advanced models based on thermodynamics are also used.

3.2.1 Corresponding State Theory

Hakim-Steinberg-Stiel The Hakim-Steinberg-Stiel (HSS) equation is used to calculate pure component surface tension for both polar and nonpolar fluids [20]. As seen from equation 3.25 critical pressure, critical temperature, reduced temperature, ω and χ must be supplied to solve it. The expression for polar fluids is given below:

$$\sigma = P_C^{2/3} T_C^{1/3} \sigma_R \left(\frac{1 - T_R}{0.4} \right)^m \tag{3.25}$$

$$\sigma_R = 0.1574 + 0.359\omega - 1.769\chi - 13.69\chi^2 - 0.510\omega^2 + 1.298\omega\chi$$
$$m = 1.210 + 0.5385\omega - 14.61\chi - 32.07\chi^2 - 1.656\omega^2 + 22.03\omega\chi$$

P_C = Critical pressure

T_C = Critical temperature

T_R = Reduced temperature ($T_R = 0.6$)

ω = Acentric factor

χ = Fourth parameter

For nonpolar fluids better results are obtained by eliminating ω^2 and setting $\chi = 0$ [20].

A general weighted average model can be used to find the mixture surface tension. The pure component surface tension can be obtained from e.g. 3.25. This equation is only used to approximate the surface tension for the mixture. The equation for a surface tension mixture is shown below:

$$\sigma_m^r = \sum_{i=1}^{n} x_i \sigma_i^r \tag{3.26}$$

x_i = Mole fraction
r = Exponent (r = 1 for most cases)

API The American Petroleum Institute (API) has issued several editions of the Technical Data Book. The procedure 10A3.1, which is reviewed here, is taken from the third edition and used to calculate surface tension of petroleum fractions [26]. This method cannot be used for reduced temperatures greater than 0.9.

The procedure consists of four steps:

1. Obtain the critical temperatures
2. Obtain the normal boiling points
3. Calculate the Watson characterization factors, K
4. Calculate the surface tension from figure 3.3, σK

The Watson factor is an approximate index of paraffinicity. Factors for pure components are easily accessible in the literature (e.g $K_{methane} = 19.54$). It is defined as:

$$K = \frac{(MeABP)^{1/3}}{spgr, 60F/60F} \tag{3.27}$$

$MeABP$ = mean average boiling point
spgr = specific gravity

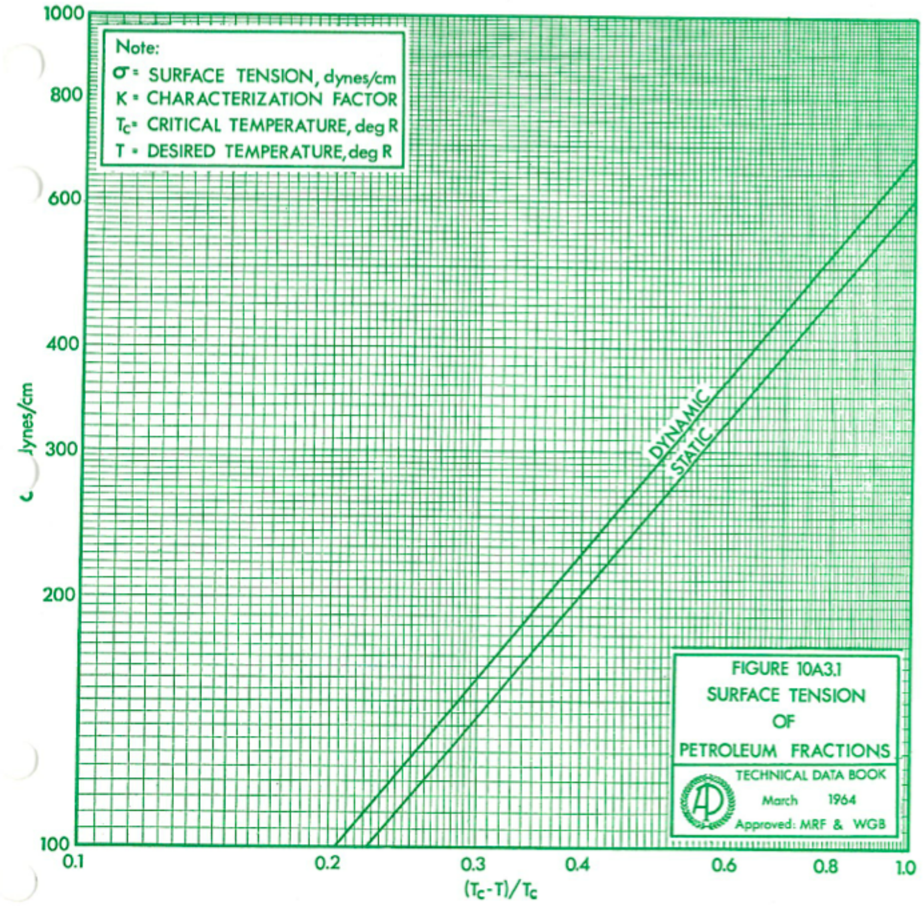

Figure 3.3: Surface Tension of Petroleum Fractions

An alternate version of this model, which is named 10A3.2, is described in the fourth edition of the Technical Data Book, and stated in equation 3.28 [27]. The Watson factor K is the same as in equation 3.27.

$$\sigma = 673.7[(T_c - T)/T_c]^{1.232}/K \tag{3.28}$$

Firoozabadi and Ramney The model by Firoozabadi and Ramney [16] is used to calculate the surface tension between a water and a hydrocarbon phase. The constants a_1 and b_1 are determined by the value of $\Delta\rho = \rho_w - \rho_{HC}$.

$$\sigma^{1/4} = \frac{a_1 \Delta\rho^{(1-b1)}}{T_r^{0.3125}} \tag{3.29}$$

$\Delta\rho = \rho_w - \rho_{HC}$

ρ_w = density of water phase

ρ_{HC} = density of hydrocarbon phase

T_r = pseudo-reduced temperature for the hydrocarbon phase

a_1, b_1 = constants which depend on the $\Delta\rho$ value

3.2.2 Parachor Method

The most famous parachor method is the one suggested by Weinaug and Katz [64]. It was first introduced for pure components by Sugden [64]. As seen from equation 3.30 the surface tension is strongly dependent on the liquid density and the parachor value. The composition of heavy petroleum fractions ($C7+$) is in some software determined as cuts rather than pure compounds. In PVTsim [9] the parachor of $C7+$ components is calculated by the following formula: $P_i = 59.3 + 2.34M_i$. The parachor values are computed from surface tension data, equilibrium densities and molecular weights. Parachors of familiar components are easily accessible from literature (e.g. $P_{Methane} = 77$) [64].

$$\sigma^{1/4} = \sum_{i=1}^{N} P_i \left(\frac{\rho_l}{M_l} x_i - \frac{\rho_v}{M_v} y_i \right) \tag{3.30}$$

P_i = parachor value

M_v = molecular weight of vapor phase

M_l = molecular weight of liquid phase

ρ_l = liquid density

ρ_v = gas density

x_i = mole fraction of constituent i in the liquid phase

y_i = mole fraction of constituent i in the gas phase

3.2.3 Thermodynamic Models

Gradient Theory The gradient theory (GT) is a thermodynamic model. It was first introduced by van der Waal in 1894 [47], and later reviewed by Cahn-Hilliard [8]. The theory has been reviewed by numerous authors up to the present day. It consists of two contributions: the local value of the property (homogeneous fluids) and the gradient value of the property. The gradient value contains information about the molecular structures of the interface, which determines the density gradient response to local deviation of the chemical potential. The gradient value can be related to the local value by applying the influence parameters [36]. Total Helmholtz free energy, chemical potential and grand thermodynamic potential is shown below, respectively:

$$F = \int_V [f_0[\eta] + \frac{1}{2} \sum_{\alpha=1}^{N} \sum_{\beta=1}^{N} c_{\alpha\beta}(\eta) \nabla\eta_\alpha \nabla\eta_\beta] d^3r \tag{3.31}$$

$$\mu_\alpha = \left(\frac{\partial F}{\partial \eta_\alpha} \right)_{T,V,N} \tag{3.32}$$

$$\omega = f^0(\eta) - \sum_{\alpha=1}^{N} \eta_\alpha \mu_\alpha \tag{3.33}$$

$f^0(\eta)$ = local Helmholtz free energy density of homogenous fluid at composition η

η_α, η_β = local density of component α and β

$c_{\alpha\beta}$ = influence parameter

Considering a planar interface between two bulk phases, the GT states that the surface tension of a mixture is:

$$\sigma = \int_{-\infty}^{+\infty} \sum_\alpha \sum_\beta c_{\alpha\beta} \frac{d\eta_\alpha}{d\eta_z} \frac{d\eta_\beta}{d\eta_z} d\eta_z \tag{3.34}$$

By using a set of mathematical operations, 3.34 can be written as:

$$\sigma = \int_{-\infty}^{+\infty} 2[f^0(\eta) - \sum_\alpha \eta_\alpha \mu_{\alpha s} + p_s] dz \tag{3.35}$$

The variable z can be eliminated by using the chain rule of differentiation:

$$\frac{d\eta_\alpha}{dz} = \frac{d\eta_\alpha}{d\eta_{ref}} \frac{d\eta_{ref}}{dz} \tag{3.36}$$

The density profile in the interface can then be written as:

$$dz = \sqrt{\frac{\sum_\alpha \sum_\beta \frac{1}{2} c_{\alpha\beta} \frac{d\eta_\alpha}{d\eta_{ref}} \frac{d\eta_\beta}{d\eta_{ref}}}{\triangle\omega(\eta_1, \dots \eta_N)}} d\eta_{ref} \tag{3.37}$$

Finally, the surface tension of a planar interface of a mixture of N components between liquid (L) and vapor (V) phases is given by:

$$\sigma = \int_{\eta_{ref}^V}^{\eta_{ref}^L} \sqrt{2 \triangle \omega(\eta_1, \dots \eta_N) \sum_\alpha \sum_\beta c_{\alpha\beta} \frac{d\eta_\alpha}{d\eta_{ref}} \frac{d\eta_\beta}{d\eta_{ref}}} d\eta_{ref} \tag{3.38}$$

To solve these related equations, first you have to solve a set of algebraic equations. The reader is referred to [36] for further discussions on the matter.

The influence parameter is important because it is essential for the accuracy of the model. The following expression was derived by Bongiorno et al.: [7]

$$c_{\alpha\beta}(n) = \frac{kT}{6} \int_V s^2 C_0^{\alpha\beta}(s; n) d^3 s \tag{3.39}$$

$C_0^{\alpha\beta}(s; n)$ = molecular interaction at the interface

The solution to this equation has been suggested by many authors, and Miqueu et al. [33] suggested the following solution:

$$\frac{c}{ab^{2/3}} = A(1 - \frac{T}{T_c}) + B \tag{3.40}$$

The same expression as above is used in this paper, but the A and B parameters are taken from [36]. The values of the parameters for SRK and PR EoS, respectively, are:

$$A = \frac{-10^{-16}}{-0.7708 + 0.4991\omega}, \; B = \frac{-10^{-16}}{0.8645 - 0.3510\omega - 0.1612\omega^2} \tag{3.41}$$

$$A = \frac{-10^{-16}}{1.3192 + 1.6606\omega}, \quad B = \frac{-10^{-16}}{1.1173 + 0.8443\omega} \tag{3.42}$$

Linear Gradient Theory The linear gradient theory (LGT) was developed by Zuo and Stenby in 1996 [68]. The method is a simpler version of the gradient theory, which does not solve the algebraic density profile equations, hence reduces the computational time significantly. The LGT uses the same set of equations as the GT (see equations 3.31, 3.32, 3.33, 3.38), but assumes linear behavior of the density $\eta_\alpha(z)$ of component α at position z across the interface:

$$\frac{d\eta_\alpha(z)}{dz} = D_\alpha, \quad D_\alpha = \frac{\eta_{\alpha L} - \eta_{\alpha V}}{h} \tag{3.43}$$

h = the interfacial width

D_α = constant for component α

3.2.4 Guidelines Regarding Choice of Models

The guidelines are obtained from Poling et al. [42]. For the calculation of surface tension of mixtures an equation based on thermodynamics, like the GT or LGT, is recommended. However, near the critical point the parachor method is assumed to give the best results. The general weighted average model should only be used when an approximation of surface tension is adequate. The most common model used in the oil and gas industry today is the concept of parachors.

Chapter 4

Software

4.1 Process Simulation Programs

There are a number of different process simulation programs out there. Some concerning batch processes, like Batch Plus and SuperPro Designer, while others are developed to describe steady state processes. Examples can be Aspen Plus, ChemCad, HYSYS, and PRO/II. In the scope of this project the two latter will be reviewed. Together with NeqSim and PVTSim they will make out the simulation tools that the comparison of data will be based on. The models referred to in this chapter are explained in section 3.2.

As for most simulation programs, the purposes of HYSYS and PRO/II are:

- To solve material and energy balances
- To allow for graphical user design of processes and connections
- To govern how data is applied
- To iterate to solution and allow for optimization
- To allow for data output in the form of PDF files

4.1.1 SIMSCI PRO/II (version 9.1)

From SimSci's homepage PRO/II is described as a steady-state simulator enabling improved process design and operational analysis. It is designed to perform rigorous heat and material balance calculations for a wide range of chemical processes.

PRO/II is spanning widely, offering a work tool for chemical, petroleum, natural gas, solids processing and polymer industries. Some key capabilities for the oil and gas-processing sector are:

- Heavy oil processing
- Crude preheating and distillation
- Naphtha splitter and stripper, sour water stripper
- Amine sweetening
- Cascade refrigeration and compressor trains
- Deethanizer and demethanizer

- Gas dehydration
- Hydrate formation/inhibition

Models

In PRO/II there are a few possibilities for calculating surface tension. It is possible to choose among PURE, PETROLEUM or TACITE option. The PURE option is a weighted average of pure-component values, where the pure-component value is obtained from the built in component library. The PETROLEUM option uses the API method (10A3.1) for calculation of petroleum fractions [26], and for surface tension between an aqueous and a hydrocarbon phase the following formula is used: $\sigma_{wet} = x_{aq}\sigma_{aq} + x_{HC}\sigma_{HC}$. The Tacite option calculates surface tension by using the Parachor method [64]. The PURE option is used as default in PRO/II [51].

4.1.2 AspenTech HYSYS (version 8.0)

Aspen HYSYS is a powerful software initially developed by Hyprotech for simulation of chemical plants and oil refineries. It includes tools for estimating physical properties and liquid-vapor phase equilibria, heat and material balances, and simulation of many types of chemical engineering equipment.

Models

The calculation of surface tension can be done in two ways in HYSYS [3]. The option is between HYSYS method and API method (10A3.2) [27]. The HYSYS method is a weighted average of pure-components, where the Hakim-Steinberg-Stiel model is used to calculate the pure component values [20]. This is also the default option used for calculation of surface tension.

4.1.3 Calsep PVTsim (version 20.1.0)

PVTsim is a versatile PVT simulation program developed for reservoir engineers, flow assurance specialists, PVT lab engineers and process engineers. Based on an extensive data material collected over a period of more than 25 years, PVTsim carries the information from experimental PVT studies into simulation software in a consistent manner and without losing valuable information on the way.

Models

The method for calculating surface tension of a hydrocarbon mixture in PVTsim is the Parachor method by Weinaug and Katz [64]. The method for calculating surface tension between a water phase and a hydrocarbon is with the model by Firoozabadi and Ramney [16]. PVTsim is the only software where the Peneloux volume correction can be chosen, but this option is not applicable to glycol systems [9].

4.1.4 NTNU/Statoil NeqSim

NeqSim has been developed at the Department of Refrigeration and Air Conditioning, at the Norwegian University of Science and Technology (NTNU). It is a dynamic process simulator especially designed to handle non-equilibrium situations. Common non-equilibrium processes include absorption, distillation and multiphase flow in pipelines, drying processes, hydrate formation and heat exchange. NeqSim also handles traditional equilibrium process calculations (equilibrium separators, equilibrium streams).

Models

In NeqSim [54] the gradient theory [47][8][36] is used as default for calculating surface tension for hydrocarbon mixtures. The SRK and PR EoS parameters used in the gradient theory are described in [36]. When glycol and water are simulated the default method is the linear gradient theory, and the preferred EoS is CPA. It is also possible to choose the Parachor method [64] to calculate surface tension in NeqSim.

Chapter 5

Experimental Techniques

5.1 Selection of Data

The availability of experimental data on surface tension is vast and thus there is a need to narrow down the scope of this thesis. The priority will be gas-oil relations and MEG/water streams. Systems that contain water without the presence of MEG will not be taken into consideration. That goes for streams dominated by carbon dioxide and nitrogen as well.

Through comparison of results from the different simulation tools against experimental data over a wide range of pressures and temperatures, it should be possible to validate whether NeqSim is comparable to, or even better, than conventional programs.

The lists below show which mixtures that were simulated in this work. The whole spectrum from light components to heavier components and reservoir fluids are simulated to give a good basis for comparison. Some hydrocarbon systems are, for various reasons, not possible to simulate in the software, and will not be included here. For a complete overview of collected data see appendix A.1. Experimental data on glycol systems at high pressure are scarce, thus the data is from this experimental work. It is presented in chapter 7.

Hydrocarbon systems

- Binary system
    - methane+propane
    - methane+n-butane
    - methane+n-hexane
    - methane+n-heptane
    - methane+n-nonane
    - methane+n-decane
    - ethane+n-pentane
- Ternary system

    - methane+ethane+n-Pentane
    - methane+propane+n-decane
- Reservoir fluid systems
    - Synthetic mixtures
        - associate gas
        - gas condensate
        - wet gas

Glycol systems

- 100wt% MEG+methane
- 80wt% MEG/20wt% water+methane
- 50wt% MEG/500wt% water+methane
- 100wt% MEG+methane/ethane
- 80wt% MEG/20wt% water+methane/ethane
- 50wt% MEG/50wt% water+methane/ethane

5.2 Measurment methods

A short introduction to some standard methods for measuring surface tension is given in this section.

5.2.1 Laser Light Scattering

Laser light scattering utilizes a laser beam to the surface of the liquid in question. As the laser is applied with an angle, the reflected beam will appear on a distant wall. A speaker is connected to a function generator. Then waves of a known frequency are created by a pointed stiff wire connected to the speaker via a rod touching the liquid surface. The set up is illustrated in figure 5.1, which is the apparatus schematic overview from an experiment on distilled water performed by Myat Tun [58].

By varying known parameters, the angle θ can be measured. Together with angle r, θ gives the wave vector q, which in turn can be used to determine A. From A, the surface tension can be calculated as A equals the square root of surface tension over density.

5.2.2 Capillary Rise Method

The end of a tube is immersed into the liquid solution as shown in figure 5.2 which is obtained from [6]. The surface tension draws the liquid into the tube due to the Laplace pressure, P, which is the pressure difference between the inside and outside of a curved surface [57].

The height at which the solution reaches in the tube is related to the surface tension:

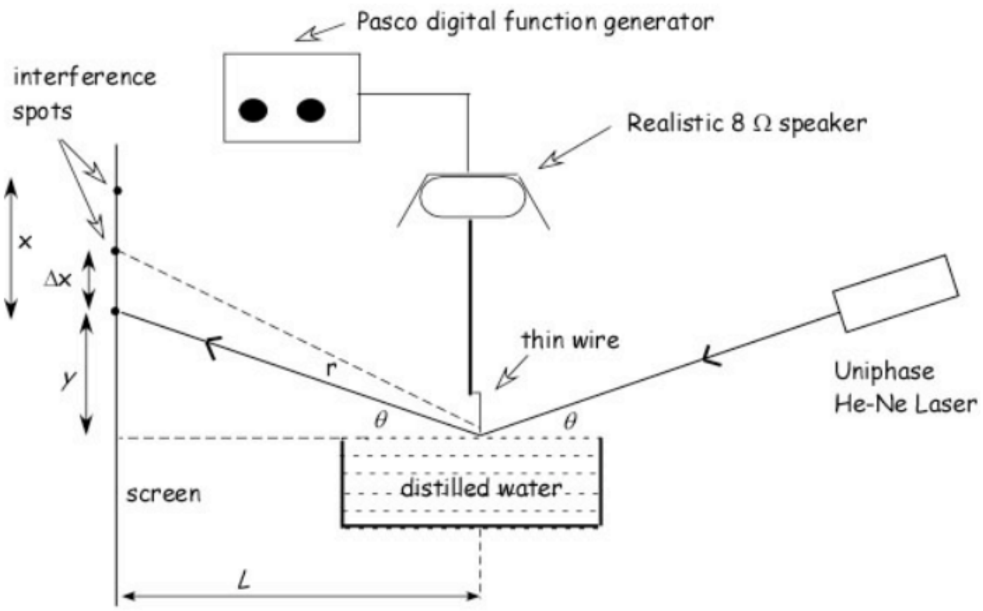
Pasco digital function generator
interference spots
Realistic 8 Ω speaker
x
Δx
y
r
thin wire
θ
θ
Uniphase He-Ne Laser
screen
distilled water
L

Figure 5.1: Laser Light Scattering Method Schematic Overview

$$h = \frac{2\sigma \cos\theta}{(\rho_L - \rho_V)gb} \tag{5.1}$$

σ = surface tension

θ = angle of contact between the surfaces

b = radius of curvature

ρ_L = density of liquid

ρ_V = density of vapor

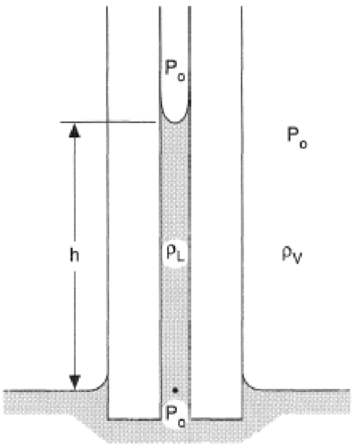
P_o
P_o
h
ρ_L
ρ_V
P_o

Figure 5.2: Capillary Rise Method

5.2.3 The Wilhelmy Plate Method

A thin plate dipping in a fluid is raised and the pull at the detachment is measured. The surface tension force draws the plate down into the liquid. A force is then applied to the plate from above to bring the plate level with the liquid surface [57]. This is shown in figure 5.3 which is obtained from [6].

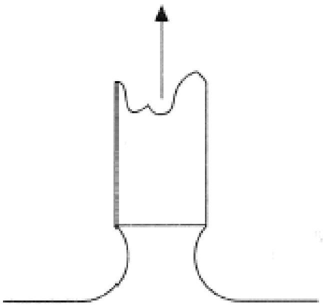

Figure 5.3: The Wilhelmy Plate Method

The pulling force, F, is related to the surface tension as shown below:

$$F \cos\theta = 2\sigma(l + t) \tag{5.2}$$

l = length of plate

t = thickness of plate

5.2.4 The Du Noüy Ring Method

Surface tension might be determined by evaluating the force needed to detach an object of known shape from a liquid surface. This method is known as the Du Noüy Ring Method [6]. A standard setup is illustrated in figure 5.4 which is obtained from [6]. As the object is exposed to a force and then separated from the liquid, a film of fluid is lifted with it. At a certain height this film becomes unstable and eventually breaks off. Some error will be associated with the value of R as some liquid inevitably will stick to the object and distort its shape. This error is balanced by a correction factor, F, so that:

$$4\pi R\sigma = mgF \tag{5.3}$$

The maximum force required to detach the object is measured together with the density of the liquid and the radii of the ring and wire.

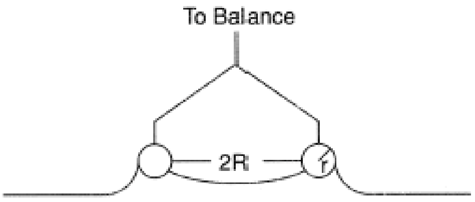

Figure 5.4: The Du Noüy Ring Method

5.2.5 Jaeger's Method

This method is also called the maximum bubble pressure method because the surface tension is related to the pressure in a bubble. A tube is immersed in a liquid, and gas is injected into the tube to form a bubble at the tip of the tube [57]. This is shown in figure 5.5 which is obtained from [6].

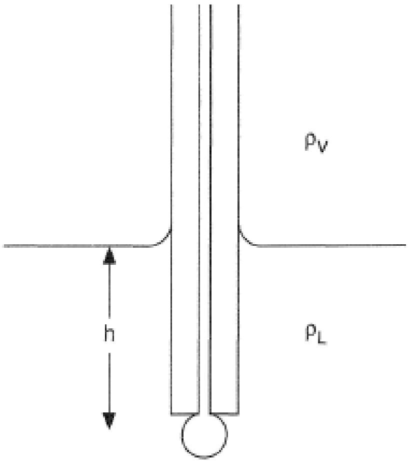

Figure 5.5: Jaeger's Method

The maximum pressure is given as the sum of hydrostatic pressure, P_o, and Laplace pressure, P:

$$P_o + P = h(\rho_L - \rho_V)g + \frac{2\sigma}{b} \tag{5.4}$$

5.2.6 Pendant Drop and Sessile Drop Methods

These two methods are based on the same principles. Whereas a sessile drop sits on a solid surface and can be used to measure contact angle and surface tension, the pendant drop is hanging from a needle. The shape of the axisymmetrical pendant or sessile drop depends only on a single parameter, namely the Bond number. The Bond number is a measure of the relative importance of gravity to surface tension in determining the shape of the drop. A droplet that is dominated by gravity, thus becoming significantly deformed, possess a high Bond number. Droplets dominated by surface tension are more spherical and have a low Bond number. Basically, both the pendant drop and sessile drop methods comprise of obtaining pictures of the droplets, capturing their shape and size, and compare them to theoretical profiles [57].

5.2.7 Drop Weight or Volume Method

When a drop gets too large it will detach from its support. The weight of the detached portion of the drop can be related to the surface tension of the fluid by [57]:

$$\sigma = (\frac{mg}{r})[F(\frac{r}{V^{(\frac{1}{3})}})] \tag{5.5}$$

where mg is the weight of the detached drop, r is the radius of the tip from which the drop hangs, and V is the volume of the detached drop. The F represents an empirical correction factor which is a function of the radius, r, and the volume of the drop detached, V. To determine the volume of the droplet, liquid density must be known in advance.

The measurement is typically done by using an average weight per drop. This average value is obtained by weighing the accumulated liquid from a large number of droplets.

Another method used is based on measuring the volumetric flow rate to the tip whilst counting the drops. The density of the fluid must be known in order to determine the drop weight. This method allows for automation of measurements [1].

5.2.8 Spinning Drop Method

The spinning drop method, or rotating drop method, is similar to the sessile and pendant drop methods in that it is a shape measurement technique. It is typically used for two immiscible fluids. Measurements are done in a rotating horizontal tube sealed at both ends. As the rotation of the tube create a gravitational force working on the wall inside the tube, the droplet deforms into an elongated shape. As the forces from the surface tension equals the centrifugal force, the elongation stops. This point is called the equilibrium point, and is where the surface tension can be derived from the shape of the elongated droplet. Three such droplets are shown in figure 5.6 which is obtained from [6].

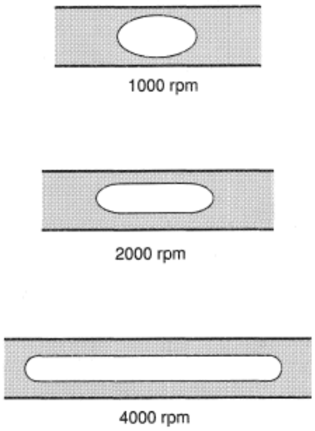

Figure 5.6: Spinning Drop Method

Measurement of the maximum drop diameter, $2r_{max}$, and length, $2h_{max}$, together with the angular velocity of rotation, Ω, allows for calculation of the surface tension according to:

$$\sigma = \frac{1}{2}(\frac{r_{max}}{r^*_{max}})^3 \Delta\rho\Omega^2 \tag{5.6}$$

where r^*_{max} is correlated to the aspect ratio r_{max}/h_{max} [52]. The spinning drop method is usually preferred for accurate measurements of surface tensions below 10^{-2} mN/m.

Chapter 6

Experimental Apparatus and Setup

6.1 Introduction

For the measurement of high pressure surface tensions a temperature test chamber from Vötsch Industrietechnik has been used (figure 6.1) [61]. This is not the exact same model, but serves as an illustration. The specific model used is a VT^3 7150. This temperature test chamber is used to set the environmental conditions in terms of temperature. Containing large parts of the pendant drop cycle, the test chamber allows the temperature to be set and kept constant whilst performing experimental measurements.

Figure 6.1: Temperature Test Chamber

6.2 Schematic Overview

A schematic overview of the apparatus vapor and liquid circulation path is provided in figure 6.5. The dotted blue line illustrates what is contained within the temperature chamber. The most important instruments have been enumerated and will be explained in further detail below. Additional data for the instruments is listed in table 6.3.

1. Pendant Drop Cell

The pendant drop cell is the key apparatus as this is where the measurements take place. This high pressure cell, with a volume of 41.5cm^3, is where the droplets are produced and studied. Inside the cell, there is an inlet port designed so that there is no physical contact between liquid and gas. At the end there is a needle producing pendant droplets. The cell has a window at this point, enabling a camera to capture and record the droplet size and shape, which in turn is used to determine the surface tension.

2. Circulation Pump

In figure 6.5 the thin line represents the fluid circulation path. The liquid is circulated from the bottom of the pendant drop cell to the top again by the help of the high pressure liquid pump. Design flow rates, temperature and pressure ranges are listed in table 6.3.

3. Densitometer

Liquid and vapor densities are determined in two Anton Paar DMH HPM units based on the vibrating U-tube method. The apparatus measures the oscillating period of the U-tube filled with sample that is automatically converted to phase density after proper calibration. The densitometers are adjusted to a wide range of density, temperature and pressure measurements. Provider information, temperature, pressure and density ranges are found in table 6.3.

4. Pressure Sensors

There are two pressure sensors, one in the vapor and one in the liquid circulation path. They both utilize passive temperature compensation. That is, sections of the accuracy curve of the pressure sensors are measured at different temperatures during the manufacturing process. Then, the previously determined temperature errors are compensated by passive elements (resistors) within the electronics of the sensor.

5. Safety Valve

There is one safety valve, situated in the liquid circulation path. This valve is directly connected to the ventilation system in the laboratory in case of an unwanted pressure build-up. More info on the safety valve is provided in table 6.3.

6. Online Gas Chromatograph Sampling System

In a binary system surface tension is not a function of composition, rather a function of temperature and pressure. However, for multicomponent systems, such as ternary (i.e. MEG, water and methane) and quaternary (i.e. MEG, water, methane and ethane) systems, surface tension is also a function of composition. The composition of the fluid examined in this thesis is determined using an online gas chromatograph (GC) system. Figure 6.2 shows the model used in the experimental work on this thesis.

Figure 6.2: SRI TOGA Gas Chromatograph

The GC consists of several parts. The most important are shown in figure 6.3.

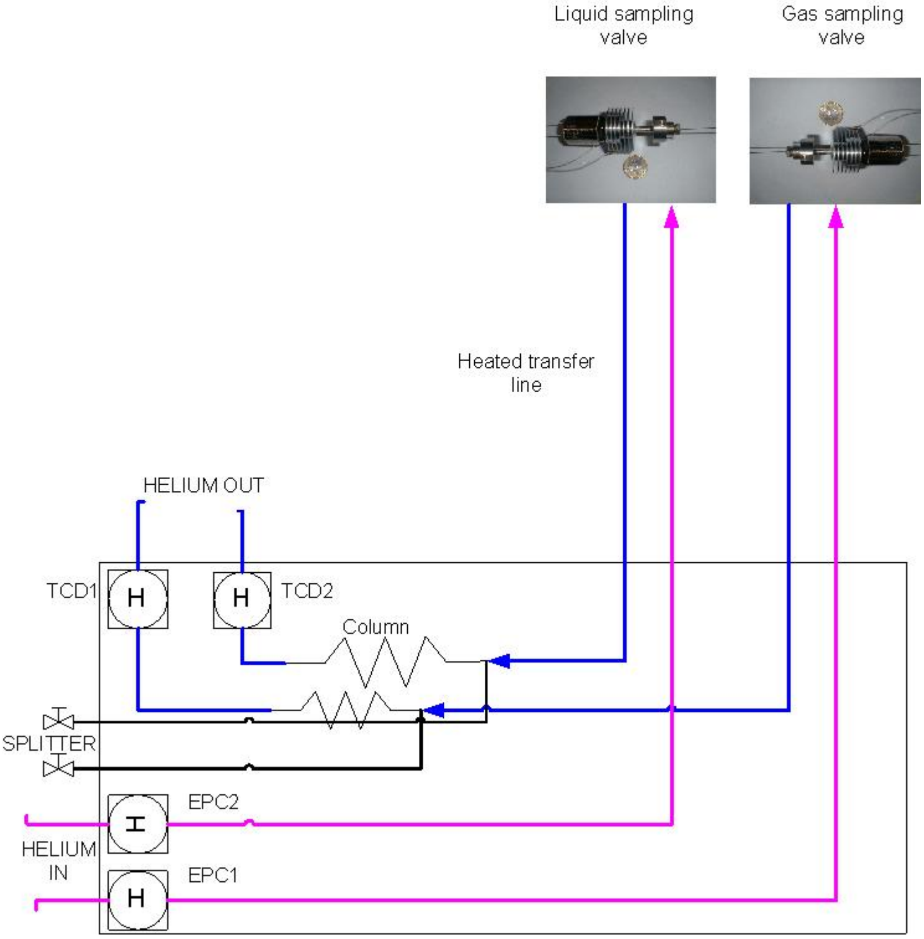
Liquid sampling valve
Gas sampling valve
Heated transfer line
HELIUM OUT
TCD1
H
H
TCD2
Column
SPLITTER
EPC2
H
HELIUM IN
EPC1
H

Figure 6.3: Schematic Overview of Gas Chromatograph

Essential to the GC is the carrier gas. This inert gas facilitates transport of the injected sample to the column for separation of components of the mixture. Desirable features in a carrier gas are inertness towards the sample and that it does not have a response on the detector. Due to its high thermal conductivity and safety, helium carrier is normally used. Helium is also used in this experimental setup even though other gases such as nitrogen, argon or hydrogen might be applied as well.

The Thermal Conductivity Detector (TDC) measures the difference in thermal conductivity in the carrier gas flow and the analyte peaks. Every compound possesses some degree of thermal conductivity, and may therefore be measured using a TDC. Depending on the compound, the TDC responds with a detection range of 0.01% to 100%. The TDC consists of four filaments housed in a stainless steel detector. Two of the filaments are exposed to the sample-laden carrier gas flow and provide the actual chromatographic signal. The other two filaments are provided with clean carrier flow, enabling them to be used as a baseline reference signal. When the effluent from the column flows over the two sample stream filaments, the bridge current is unbalanced with respect to the reference signal. The deflection is translated into an analog signal, which is sent to the data system for analysis.

The Rapid Online Sampler-Injector (ROLSI), figure 6.4, has a capillary with a free side connected to the sampling site and receives a continual flow of vector gas from the GC. The seal of the capillary is secured by a moving part, which has one end in contact with the capillary consisting of a polymer part and the other end consisting of a soft iron core pushed in the direction of the polymer part by a helical spring.

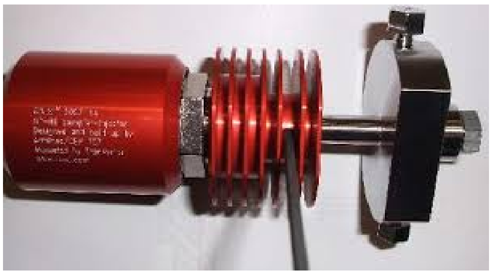

Figure 6.4: Rapid Online Sampler-Injector

Sampling is provided by prompting the electromagnet, which attracts the moving parts by moving it away from the capillary and generates a break in the seal between the fixed capillary and the moving part. The size of the samples taken, under the given pressure and temperature conditions, is directly proportional to the seal-breaking time. This time is controllable, as is the duration between two samplings by way of a timer coupled with the electromagnets power supply.

When the gas chromatograph sampling is done, the response factors of the unique components are used to calculate the respective quantities. The response factor is the ratio between a signal produced by an analyte, and the quantity of analyte that produces the signal.

One of the main reasons to use response factors is to compensate for the irreproducibility of injections into a GC. Injections volumes can be 1 mL or smaller and are hard to reproduce. Differences in the volume of injection analyte leads to differences in the areas of the peaks in the chromatograph and any quantitative results are suspect.

To compensate for this error, a known amount of an internal standard (a second compound that does not interfere with the analysis of the primary analyte) is added to all solutions. This way, if the injection volumes differ slightly, the ratio of the areas of the analyte and the internal standard will remain constant from one run to another.

Component	Response Factor
Methane	0.009984047
Ethane	0.016652253
MEG	0.013883703
Water	0.00551825

Table 6.1: Response Factors for the Applied Components

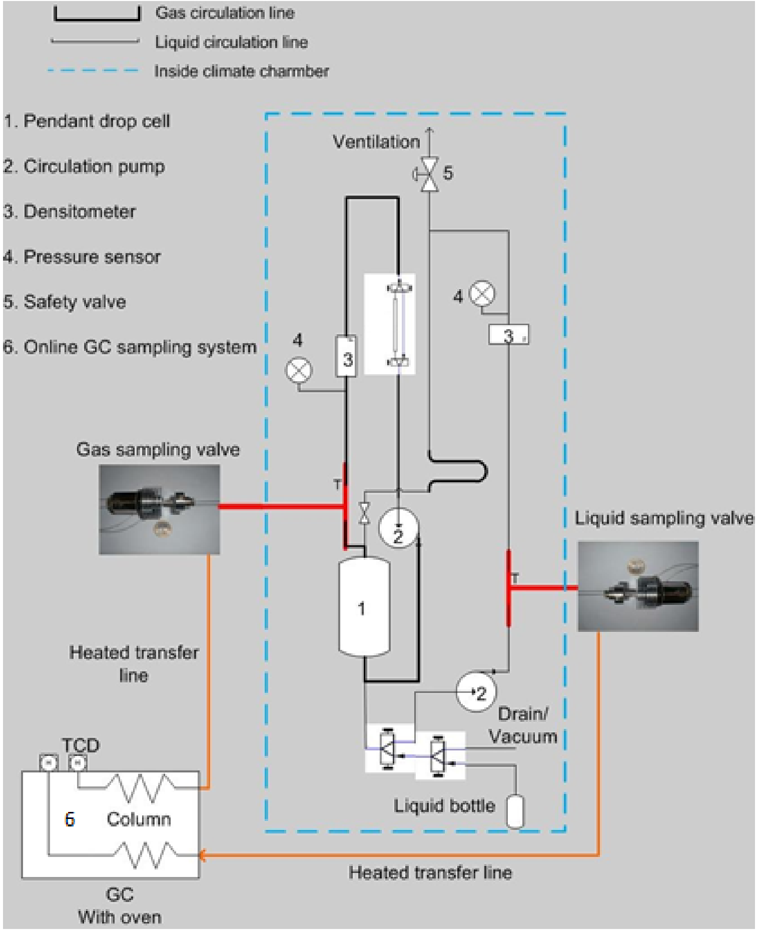
Gas circulation line
Liquid circulation line
Inside climate charmber
1. Pendant drop cell
2. Circulation pump
3. Densitometer
4. Pressure sensor
5. Safety valve
6. Online GC sampling system
Ventilation
5
4
3
4
3
Gas sampling valve
T
2
1
Liquid sampling valve
T
Heated transfer line
2
Drain/ Vacuum
TCD
6
Column
Liquid bottle
Heated transfer line
GC
With oven

Figure 6.5: Flow sheet of High Pressure Surface Tension Rig

6.3 Experimental procedure

The experimental procedure consists of three steps: filling, measurement and cleaning.

Filling The gas mixture is filled into the system via a small container and through the two valves situated at the bottom of figure 6.5. The amount of gas is determined by the desired pressure in the system. The gas mixture then follows the gas circulation path through the system. The gas container is weighted before and after the filling process to determine the gas volume. Filling of the MEG/Water liquid mixture is done via the liquid bottle shown in figure 6.5. The liquid bottle is connected to a volume displacement pump outside the climate chamber. The liquid volume is read in the filling process, and has to be at least 25 ml to flood the system. The circulation pump is then turned on and the liquid follows the liquid circulation path.

Measurement When equilibrium between the gas and liquid is reached, the surface tension measurement can commence. Firstly the temperature, pressure, density and period of the gas and liquid are written down. Droplets with appropriate volume are then created in the pendant drop cell. The droplets hang from a needle inside the cell whilst the camera takes pictures of it. These pictures are analyzed and compared with a theoretical drop shape in the software "Drop Image", where the surface tension is calculated. For each pressure level ten drops are created and analyzed, and the final value is given as an average.

After the measurement of surface tension is completed a compositional analysis is initiated. This is done with the GC described in section 6.2.

Cleaning After the measurement is done the system needs to be cleaned before a new filling can be initialized. First the system is emptied for both gas and liquid through the drain valve shown in figure 6.5. After the liquid is drained from the system distilled water is flushed several times through the system. When the water is drained the same procedure is applied with both iso-propanol and acetone. The system is now cleaned, and the next step is to connect a vacuum pump to the vacuum valve shown in figure 6.5. This is done to dry the system. When the density of both gas and liquid, and the pressure is zero, a new filling at a different pressure can begin.

6.4 Fluid specification

The gas mixture with 85.00 mol% methane and 15.00 mol% ethane was supplied by Air Liquide Norway AS with certificate no.: 27786. The gas mixture containing pure methane is also supplied from Air Liquide.

The MEG used with the methane mixture has a VWR Batch number: 10R170506.

The MEG used with the methane/ethane mixture is supplied from two bottles. The first bottle has a Product number: 24041.320 and Batch number: 12D180502. The second bottle has a Lot number: 1085894 and Code number: 295530025. They both have the CAS number: 107-21-1.

The exact mixing ratio of the different MEG/water mixtures is given in table 6.2. Two different mixtures were used for the 50wt% MEG/50wt% water + methane.

Mixture	MEG [g]	Water [g]
80wt% MEG/20wt% water + methane	320.02	80.01
50wt% MEG/50wt% water + methane	133.85	133.72
50wt% MEG/50wt% water + methane	147.93	147.97
80wt% MEG/20wt% water + methane/ethane	403.66	106.97
50wt% MEG/50wt% water + methane/ethane	250.52	250.05

Table 6.2: Composition of MEG/Water Mixtures

Name	Description
Temperature test chamber	Provider: Vötsch Industrietechnik Type: VT^3 7150 Temperature range: -75 - 180 $°C$ Max pressure: 150 bar
Pendant drop cell	Provider: Temco Inc. Type: IFT - 2 Pressure range: 0 - 690 bar Max temperature: 177 $°C$
Video camera	Provider: Ramé-Hart Instrument Co. Lens: Cosmicar Television lens; 50mm, 1:1.8 Software: Drop image
Liquid circulation pump	Provider: Eldex laboratories, Inc. Type: B - 100 - S - 2CE Flow rate: 0.2 - 8 ml/min Temperature range: 5 - 35 $°C$ Pressure range: 0 - 345 bar
Densitometer	Provider: Anton Paar GmbH Evaluation unit: mPDS 2000V3 External measuring cell: DMA HPM Temperature range: -10 - 200 $°C$ Pressure range: 0 - 1400 bar Density range: 0 - 3 g/cm^3
Pressure sensor	Provider: Paroscientific, Inc. Type: Digiquartz 410KR-HHT-101 Absolute pressure transducer Pressure range: 0 - 689 bar Temperature range: 0 - 177 $°C$
Light system	Light source: BODSON GBE 75
Safety valve	Provider: Swagelok Fluid System Technologies Type: SS-4R3A5 Pressure range: 275 - 344 bar
Gas Chromatograph	Provider: SRI Instruments Software: PeakSimple Column temperature: 160 $°C$ Carrier gas: Helium (He); 18 psi Injector time: 0.3 - 4 sec Injector temperature: 150 $°C$ TCD temperature: 160 $°C$

Table 6.3: Apparatus Technical Information

Chapter 7

Measurement Results

This chapter displays the results from the experimental lab work. Two different gas mixtures were used: 100 mol% methane and 85 mol% methane/15 mol% ethane. Three different liquid mixtures were used: 100 wt% MEG, 80 wt% MEG/20 wt% water and 50 wt% MEG/50 wt% water. The three liquid mixtures were used for both gas mixtures. Two temperature levels and four to six pressure points are measured for each mixture. The complete experimental matrices for both gas mixtures are shown in table 7.2 and 7.3. The 100 wt% MEG and 80 wt% MEG/20 wt% water mixtures in table 7.2 were completed by Mr. Ole Johan Berg at Statoil prior to our work. It was conducted with the exact same equipment and technique as the other mixtures. The results are divided into three sections: surface tension, density and solubility.

7.1 Surface Tension

The surface tension measurement is done by the pendant drop method described in sections 5.2.6 and 6.2. This method is believed to give reliable results, and we have experienced few issues with the configuration in this experiment. An uncertainty analysis of the surface tension measurements will be given in section 7.4.

The most obvious trend from tables 7.2 and 7.3 is that the surface tension is declining with increasing pressure. This trend is valid for all mixtures except for two cases. The 50wt% MEG/50wt% water + methane/ethane mixture at $20°C$ has a larger surface tension at 32.07 bar then at 16.36 bar. The surface tensions at these points are 49.8 mN/m and 49.3 mN/m. The surface tension measurement at 32.07 is therefore considered false. There is also one case for the 80wt% MEG/20wt% water + methane at $20°C$ where the surface tension does not decline, namely at 123.10 bar. The surface tension value is larger than at 117.65 bar, but this could be because the pressure difference between the two is very small. Regardless, the measurement at 123.10 bar is considered false.

The second trend is related to how the surface tension changes with variation in temperature. The general observation is that the surface tension values are larger at $20°C$ compared to $5°C$ at high pressures. Considering for instance the 80wt% MEG/20wt% water + methane mixture at the different temperatures. At $5°C$ and 92.82 bar the surface tension is 36.9 mN/m, while at $20°C$ and 91.47 bar the value is 37.9 mN/m. This relationship is however not valid at low pressures. It seems the surface tensions at pressures below 50 bars have the opposite trend, namely the values being larger at $5°C$ compared to $20°C$. This relationship is difficult to observe in table 7.3 because the lowest pressures at the different temperatures do not match, but it can be seen in the 50wt% MEG/50wt% water mixture.

The most noticeable effect for the measurements is from the amount of water present in the liquid mixture. If we compare the surface tension values in the 100wt% MEG mixture against the 80wt% MEG/20wt% water mixture and thereafter against the 50wt% MEG/50wt% water mixture, it is evident that the surface tension is increasing with a larger amount of water present. Finally table 7.2 and 7.3 are compared to investigate how the surface tension changes with the introduction of ethane in the mixture. The answer is that the surface tension decreases when ethane is used in the gas mixture. The 100wt% MEG mixture at $5°C$ is selected to show this correlation. Looking at pressures 24.37 and 89.08 bar in table 7.2, the surface tension values are 44.2 and 32.5 mN/m respectively. While looking at pressures 21.91 and 90.53 bar in table 7.3 the values are 41.8 and 30.0 mN/m.

7.2 Density

The experimental phase densities are as mentioned in chapter 6 measured with the Anton Paar DMA HPM densitometer with an uncertainty of $4.2472 * 10^{-5} g/cm^{-3}$ for the liquid, and $4.252 * 10^{-5} g/cm^{-3}$ for the gas. To validate the results a more advanced densitometer, the Anton Paar DMA 4500 with an error of $1*10^{-5} g/cm^{-5}$, is used to measure the liquid density of the three MEG/water mixtures used with the methane/ethane gas mixture. The mixtures are measured at atmospheric pressure and $20°C$ in the DMA 4500, while in the DMA HPM the mixtures are measured at $20°C$ and the lowest pressure point in each mixture. This has a small impact because the density does not vary much with increasing pressure. Table 7.1 shows this relationship. The DMA HPM generally produces larger results than that of the DMA 4500, but the deviation is very small. The largest deviation is as small as 0.38 % and occurs in the 80wt% MEG/20wt% water mixture.

Liquid mixture	Experimental liquid density		Deviation
	DMA HPM $[g/cm^3]$	DMA 4500 $[g/cm^3]$	[%]
100wt% MEG	1.1145	1.1133	0.11
80wt% MEG/20wt% water	1.0984	1.0942	0.38
50wt% MEG/50wt% water	1.0667	1.0656	0.10

Table 7.1: Experimental Phase Densities

As seen from tables 7.2 and 7.3 the change in liquid density is small with variation in pressure, and can be considered as constant. It also seems that the liquid density does not follow a pattern, but rather fluctuates randomly. The change in liquid density with temperature is however more distinct, and is declining with increasing temperature. This relationship is valid for all mixtures. The change in vapor density with variation in pressure is much larger than for liquid density. The vapor density is increasing with increasing pressure for all the mixtures. Looking at table 7.2 and the 100wt% MEG at $5°C$ the density is 0.0187 $[g/cm^3]$ at 24.37 bar and 0.1216 $[g/cm^3]$ at 132.58 bar. The vapor density is declining with increasing temperature, as was the case for liquid density.

When comparing the three different liquid mixtures in both table 7.2 and 7.3, it is found that the liquid density is decreasing when more water is present. This is expected because the density of MEG is larger than that of water. The vapor density seems quite consistent amongst the three mixtures and the amount of gas in the system is the main contribution. The vapor density for the 85 mol% methane/15 mol% ethane and the three liquid mixtures at 20°C are 0.0586, 0.0582 and 0.0588 $[g/cm^3]$ at respectively 64.15, 64.00 and 64.60 bar.

Finally table 7.2 and 7.3 are compared to investigate how the densities are changing with the introduction of ethane in the mixture. The liquid density does not change, which is expected, because very little ethane dissolves in the MEG/water. For the vapor density, at low pressures the mixtures produce similar results, but as the pressure is increased the mixture containing ethane gives larger densities. Looking at for instance 100 wt% MEG and 5°C, the vapor densities at 89.08 bar and 90.53 are 0.0769 and 0.08604 $[g/cm^3]$, respectively.

7.3 Solubility

The composition analysis is done with the GC as described in section 6.2. Only the liquid phase composition is analyzed because the vapor phase composition is too small to be detected by the GC. For the 100wt% MEG + methane mixture the GC was not used because it is not needed to find the composition as there are only two components. For the 100wt% MEG + methane/ethane mixture the GC did not provide results when the temperature was 5°C. The liquid mixture was probably too viscous at this temperature and was causing problems for the GC. Another reason could have been that something was physically stuck in the capillary tube, and it was therefore changed. The GC was also having problems at the highest pressure at 20°C. Additionally, at the lowest pressure for the 80 wt% MEG/20 wt% water + methane/ethane mixture at 5°C the GC did not yield any result.

The general trend for methane and ethane solubility seen from tables 7.2 and 7.3, is that the compositions are increasing with rising pressure. This means that more methane and ethane gas is dissolved in the aqueous phase when the pressure is high. The amounts of methane and ethane dissolved in the liquid phase are quite small. Looking at for instance 80 wt% MEG/20 wt% water + methane/ethane at 5°C, the liquid composition for methane varies from 0.18 - 0.40 mol%, and ethane varies from 0.07 - 0.10 mol%. However, this relationship does not apply for the ethane composition in the 80 wt% MEG/20 wt% water + methane/ethane mixture at 5°C. The ethane composition is at this mixture decreasing with rising pressure, hence this measurement is considered false.

The changes in MEG and water composition are small with varying pressure and have no clear trend. When for instance the MEG composition is increasing, the water composition decreases, and vice versa. Another point worth noticing is how the compositions change with increased wt% water in the mixture. The composition of water is obviously increasing when more water is present. For the 80wt% MEG/20wt% water mixture the phase composition for MEG is slightly larger than for water. For the 50wt% MEG/50wt% water liquid mixture the phase composition for water has increased to almost 80 mol%. For methane and ethane the trend is that less gas is dissolved in the aqueous mixture when the amount of water is increased.

Finally table 7.2 and 7.3 are compared to investigate how the compositions are changing with the introduction of ethane in the mixture. The only change of note is that less methane is dissolved in the liquid when the mixture contains ethane. The total amount of gas, however, is quite similar in the two cases.

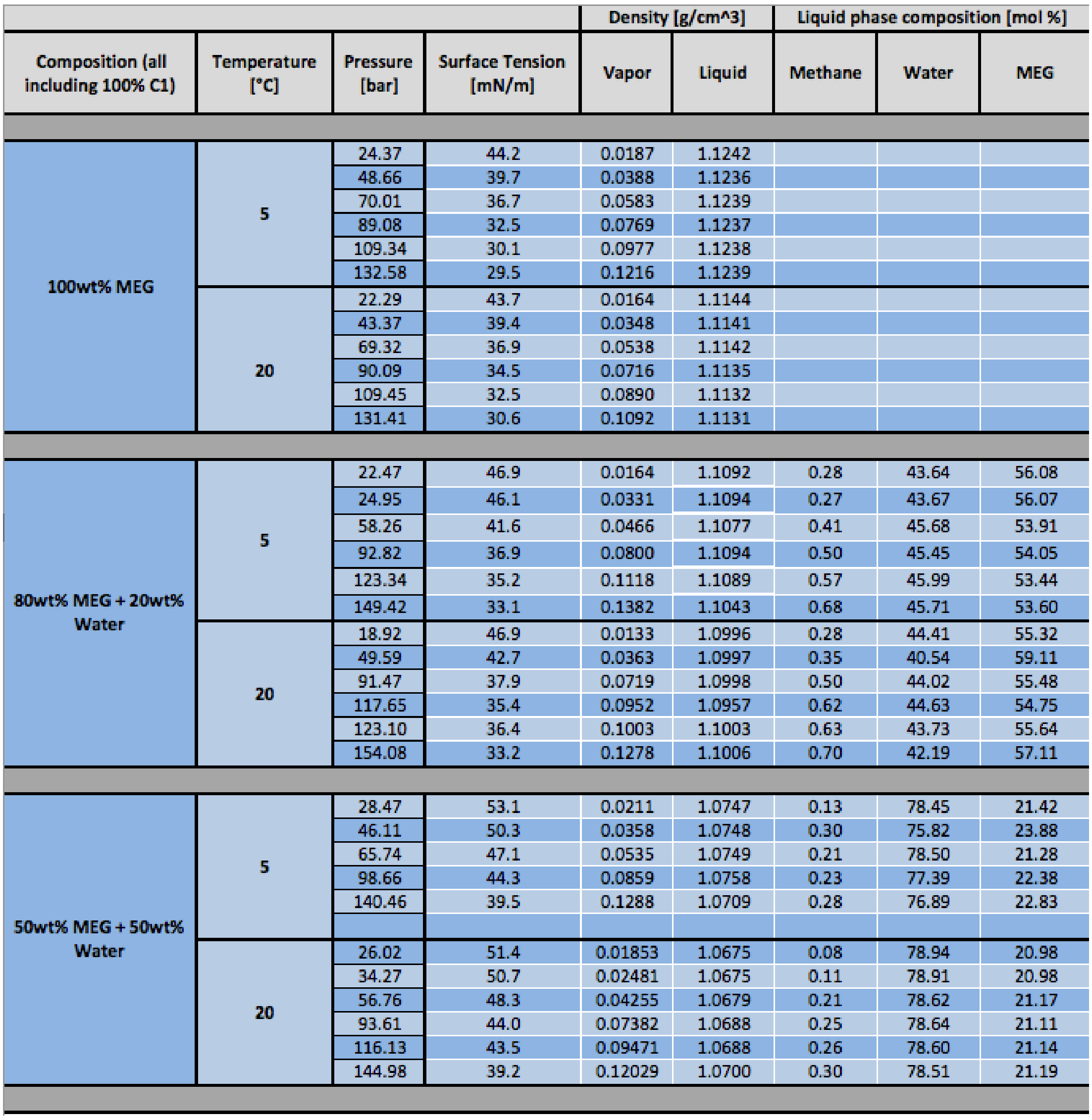

				Density [g/cm^3]		Liquid phase composition [mol %]		
Composition (all including 100% C1)	Temperature [°C]	Pressure [bar]	Surface Tension [mN/m]	Vapor	Liquid	Methane	Water	MEG
100wt% MEG	5	24.37	44.2	0.0187	1.1242			
		48.66	39.7	0.0388	1.1236			
		70.01	36.7	0.0583	1.1239			
		89.08	32.5	0.0769	1.1237			
		109.34	30.1	0.0977	1.1238			
		132.58	29.5	0.1216	1.1239			
	20	22.29	43.7	0.0164	1.1144			
		43.37	39.4	0.0348	1.1141			
		69.32	36.9	0.0538	1.1142			
		90.09	34.5	0.0716	1.1135			
		109.45	32.5	0.0890	1.1132			
		131.41	30.6	0.1092	1.1131			
80wt% MEG + 20wt% Water	5	22.47	46.9	0.0164	1.1092	0.28	43.64	56.08
		24.95	46.1	0.0331	1.1094	0.27	43.67	56.07
		58.26	41.6	0.0466	1.1077	0.41	45.68	53.91
		92.82	36.9	0.0800	1.1094	0.50	45.45	54.05
		123.34	35.2	0.1118	1.1089	0.57	45.99	53.44
		149.42	33.1	0.1382	1.1043	0.68	45.71	53.60
	20	18.92	46.9	0.0133	1.0996	0.28	44.41	55.32
		49.59	42.7	0.0363	1.0997	0.35	40.54	59.11
		91.47	37.9	0.0719	1.0998	0.50	44.02	55.48
		117.65	35.4	0.0952	1.0957	0.62	44.63	54.75
		123.10	36.4	0.1003	1.1003	0.63	43.73	55.64
		154.08	33.2	0.1278	1.1006	0.70	42.19	57.11
50wt% MEG + 50wt% Water	5	28.47	53.1	0.0211	1.0747	0.13	78.45	21.42
		46.11	50.3	0.0358	1.0748	0.30	75.82	23.88
		65.74	47.1	0.0535	1.0749	0.21	78.50	21.28
		98.66	44.3	0.0859	1.0758	0.23	77.39	22.38
		140.46	39.5	0.1288	1.0709	0.28	76.89	22.83
	20	26.02	51.4	0.01853	1.0675	0.08	78.94	20.98
		34.27	50.7	0.02481	1.0675	0.11	78.91	20.98
		56.76	48.3	0.04255	1.0679	0.21	78.62	21.17
		93.61	44.0	0.07382	1.0688	0.25	78.64	21.11
		116.13	43.5	0.09471	1.0688	0.26	78.60	21.14
		144.98	39.2	0.12029	1.0700	0.30	78.51	21.19

Table 7.2: Experimental Results

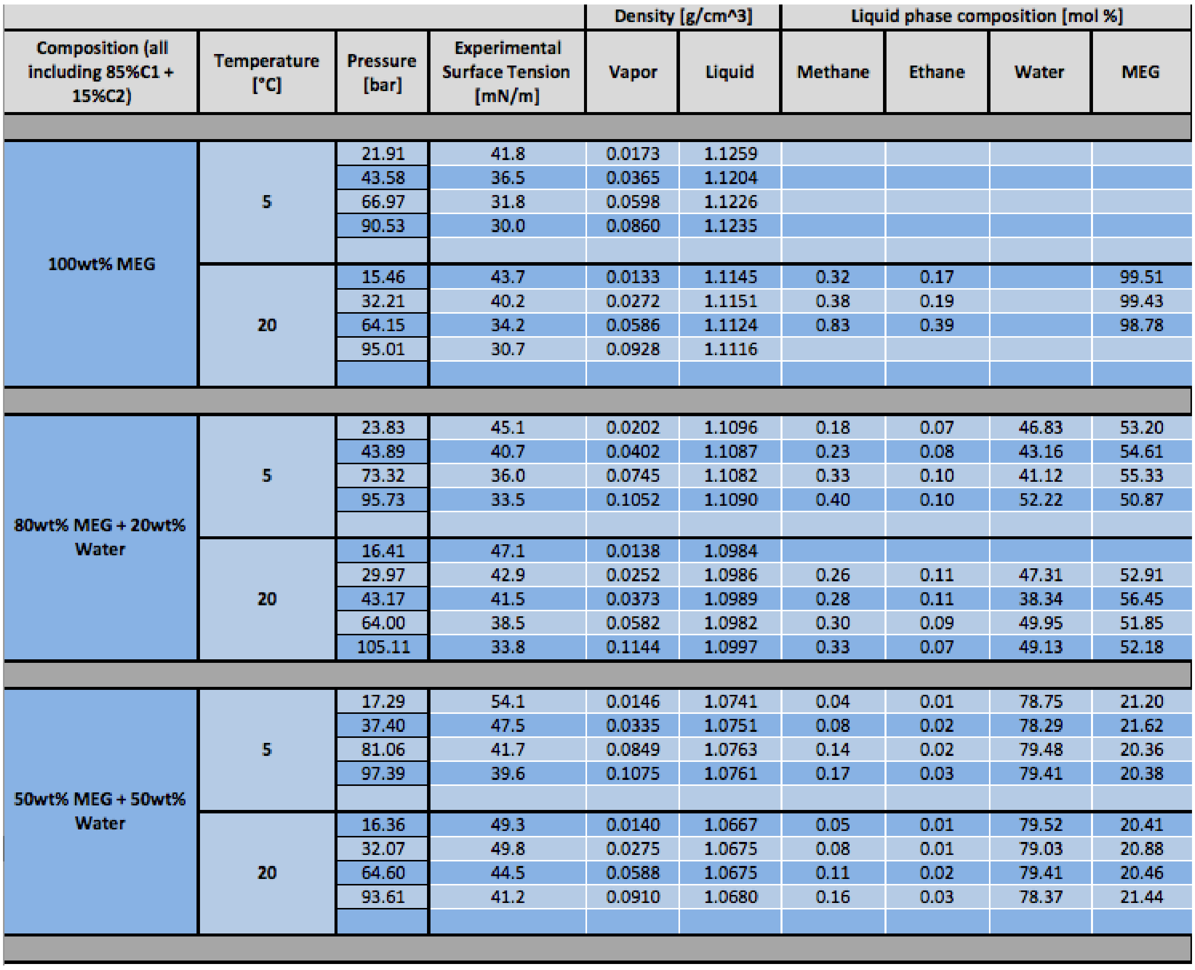

				Density [g/cm^3]		Liquid phase composition [mol %]			
Composition (all including 85%C1 + 15%C2)	Temperature [°C]	Pressure [bar]	Experimental Surface Tension [mN/m]	Vapor	Liquid	Methane	Ethane	Water	MEG
100wt% MEG	5	21.91	41.8	0.0173	1.1259				
		43.58	36.5	0.0365	1.1204				
		66.97	31.8	0.0598	1.1226				
		90.53	30.0	0.0860	1.1235				
	20	15.46	43.7	0.0133	1.1145	0.32	0.17		99.51
		32.21	40.2	0.0272	1.1151	0.38	0.19		99.43
		64.15	34.2	0.0586	1.1124	0.83	0.39		98.78
		95.01	30.7	0.0928	1.1116				
80wt% MEG + 20wt% Water	5	23.83	45.1	0.0202	1.1096	0.18	0.07	46.83	53.20
		43.89	40.7	0.0402	1.1087	0.23	0.08	43.16	54.61
		73.32	36.0	0.0745	1.1082	0.33	0.10	41.12	55.33
		95.73	33.5	0.1052	1.1090	0.40	0.10	52.22	50.87
	20	16.41	47.1	0.0138	1.0984				
		29.97	42.9	0.0252	1.0986	0.26	0.11	47.31	52.91
		43.17	41.5	0.0373	1.0989	0.28	0.11	38.34	56.45
		64.00	38.5	0.0582	1.0982	0.30	0.09	49.95	51.85
		105.11	33.8	0.1144	1.0997	0.33	0.07	49.13	52.18
50wt% MEG + 50wt% Water	5	17.29	54.1	0.0146	1.0741	0.04	0.01	78.75	21.20
		37.40	47.5	0.0335	1.0751	0.08	0.02	78.29	21.62
		81.06	41.7	0.0849	1.0763	0.14	0.02	79.48	20.36
		97.39	39.6	0.1075	1.0761	0.17	0.03	79.41	20.38
	20	16.36	49.3	0.0140	1.0667	0.05	0.01	79.52	20.41
		32.07	49.8	0.0275	1.0675	0.08	0.01	79.03	20.88
		64.60	44.5	0.0588	1.0675	0.11	0.02	79.41	20.46
		93.61	41.2	0.0910	1.0680	0.16	0.03	78.37	21.44

Table 7.3: Experimental Results

7.4 Uncertainty analysis

When working with experimental data it is important to consider the total uncertainty in the measurements. The total uncertainty is made up of two parts, the drop shape analysis and uncertainty related to the measured variables. The 100wt% MEG + methane/ethane mixture at 20°C will be used as an example to show how the computation is performed. The total uncertainty for all mixtures will be given at the end of this chapter. The uncertainties of the density measurements, together with the other measuring equipment, are given in table 7.4.

Variable	Error
Temperature	$\pm 0.1°C$
Pressure	0.01% [bar]
Liquid density	$\pm 4.2472 * 10^{-3} g/cm^3$
Vapor density	$\pm 4.252 * 10^{-3} g/cm^3$
Ethane composition	±2% relative

Table 7.4: Uncertainty in Measuring Equipment

The uncertainty in the drop shape is related to equation 7.1. e_1 is the average deviation for one droplet, where N is the total number of pictures taken at every experimental condition. This deviation is related to the camera and software used in the measurements.

$$e_1(\sigma) = \sqrt{\frac{1}{N}\sum_{i=1}^{N}(\sigma_i - \overline{\sigma})^2} \tag{7.1}$$

The uncertainty associated with the measured variables is shown in equation 7.2. This is ISO‘s recommendation concerning the combined standard uncertainty calculation of the measured surface tension [59]. e_2 consists of the measured densities, the shape factor (β), the apex radius (R_0) and their uncertainties (e(ρ_{liq}), e(ρ_{Vap}), e(β), e(R_0)). The input variables for the 100wt% MEG + methane/ethane mixture at $20°C$ are listed in table 7.5.

$$e_2(\sigma) = \sqrt{\left[\frac{\partial\sigma}{\partial\rho_{Liq}}e(\rho_{Liq})\right]^2 + \left[\frac{\partial\sigma}{\partial\rho_{Vap}}e(\rho_{Vap})\right]^2 + \left[\frac{\partial\sigma}{\partial\beta}e(\beta)\right]^2 + \left[\frac{\partial\sigma}{\partial R_0}e(R_0)\right]^2} \tag{7.2}$$

Pressure [bar]	ρ_{Liq}	ρ_{Vap}	β	e(β)	R_0	e(R_0)
15.46	1.1145	0.0133	0.52	0.00959	1.45	0.01262
32.21	1.1151	0.0272	0.54	0.00388	1.43	0.00447
64.15	1.1124	0.0586	0.58	0.00198	1.38	0.00116
95.01	1.1116	0.0928	0.60	0.00658	1.35	0.00830

Table 7.5: Input Parameters to Equation 7.2 (e_2)

The results of the total uncertainty analysis are given in table 7.6. The total uncertainty is calculated by summing up the contribution from e_1 and e_2, and dividing it by the surface tension value at the given pressure.

Pressure [bar]	Surface tension [mN/m]	e_1 [mN/m]	e_2 [mN/m]	e_{Tot} [%]
15.46	43.7	0.08	1.135	2.78
32.21	40.2	0.05	0.445	1.23
64.15	34.2	0.09	0.238	0.99
95.01	30.7	0.149	0.539	2.24
Average				**1.81**

Table 7.6: Experimental Surface Tension and Deviation for the 100wt% MEG + Methane/Ethane Mixture at $20°C$

The total average uncertainty for all mixtures is given in table 7.7. There are two obvious trends in the results. Firstly the experimental uncertainty is increasing as the amount of water in the mixture increases. The uncertainty for the 100wt% MEG + methane mixture is 1.65% while for the 80wt% MEG/20wt% water +

methane mixture the deviation is 2.52%. This relationship is not maintained when going from 80wt% MEG/20wt% water to 50wt% MEG/50wt% water. The deviation is however way larger than the 100wt% MEG mixture. The second trend is that the mixtures containing ethane have a lower uncertainty than those with pure methane. The deviations for the 50wt% MEG/50wt% water liquid mixtures for pure methane and methane/ethane mixtures respectively are 2.49% and 2.24%.

Mixture	e_{Tot} [%]
100wt% MEG + Methane	1.65
80wt% MEG/20wt% Water + Methane	2.52
50wt% MEG/50wt% Water + Methane	2.49
100wt% MEG + Methane/Ethane	1.49
80wt% MEG/20wt% Water + Methane/Ethane	1.63
50wt% MEG/50wt% Water + Methane/Ethane	2.24
Average	**2.00**

Table 7.7: Total Average Uncertainty

Chapter 8

Discussion

The discussions are based on graphs showing the performances of the software compared to the experimental data. Not all available are included in the report, except for the ones that show the general tendencies and important deviations. For the complete set of data it is referred to section A.2.

8.1 Surface Tension

8.1.1 Hydrocarbon systems

When analyzing the software performance on hydrocarbons systems, some specific points of interest are weighted:

- Are some of the software not giving results?
- How does NeqSim perform compared to the other software?
- Internally in NeqSim, which of the Equations of State (SRK and PR) gives the best results?
- General tendencies with change in temperature, pressure and composition
- Are there any ranges where certain software do not yield results?
- Comparison to lighter/heavier compositions

In addition, it should be mentioned that when analysing the performances of the software, the basis of the simulation is taken in the default mode. For evaluation on the optional methods, see section 8.1.3.

Binary Systems

Quite a few experiments have been executed on binary systems. With respect to amount of data and temperature and pressure range the mixtures will be divided into five subgroups:

- Methane + propane
- Methane + n-butane/n-pentane/n-hexane/n-heptane
- Methane + n-nonane
- Methane + n-decane
- Ethane + n-pentane

Methane/propane The experimental database on methane/propane is rather extensive, and comprises three different reports. Haniff and Pearce [21] used the laser light scattering technique to obtain surface tension data in the temperature range of 29.6 - 39.2°C and a pressure range of 69 - 94 bar. The relatively high temperature combined with the high pressure produces low surface tensions, ranging from 0 - 0.93 mN/m. The other two reports are by Weinaug and Katz [64]. In the first one they applied the capillary rise method. This is the research that spans the biggest temperature and pressure range. Temperatures are ranging from -15 - 65°C and the pressure is ranging from 3 - 85 bar. This provides for a large variation in surface tension, ranging from 0.2 - 12.0 mN/m. The second report utilizes the drop volume method. The temperature and pressure range is somewhat decreased, with temperatures from 10 - 45°C and pressures from 6 - 63 bar. Accordingly, the experimental surface tension now ranges from 2.1 - 9.1 mN/. The different use of measurement techniques represents a chance to examine how they perform compared to the software.

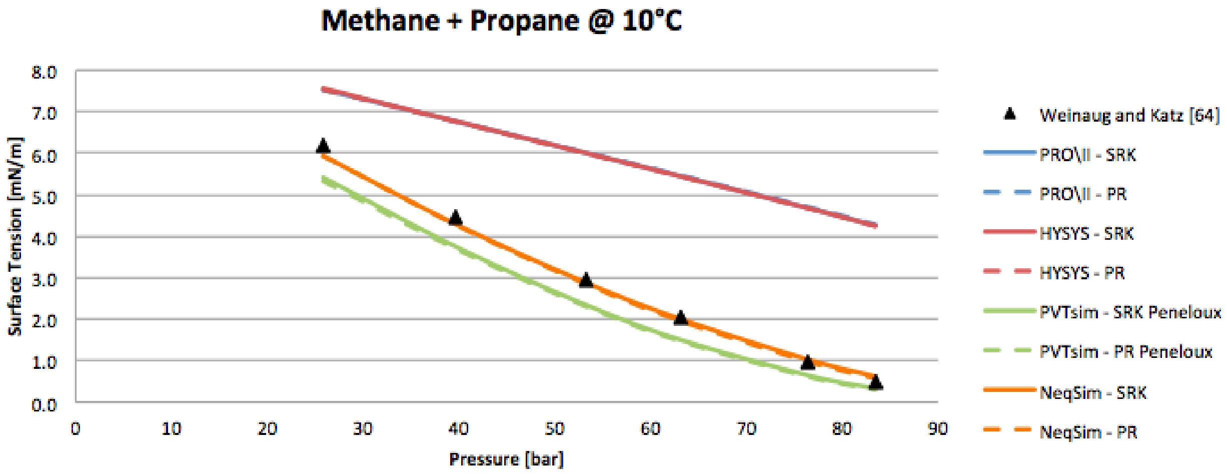

Figure 8.1: Methane + Propane

Figure 8.1 shows the general tendency as to how the software perform on the binary system of methane/propane. All the software are providing results. However, HYSYS and PRO/II are showing an equally high discrepancy compared to the experimental results. This overestimation can be attributed to the fact that in default mode these two software apply a weighted average pure-components model to calculate the surface tension (see section 4.1.1 and 4.1.2).

When analysing the performances of PVTsim and NeqSim, it is found that they match the experimental data to a higher degree. Figure 8.2 shows the same graph as figure 8.1, only PRO/II and HYSYS are excluded. The recurrent theme is quite clearly shown here. PVTsim simulations tend to underestimate the surface tension throughout the pressure range, whereas NeqSim is performing well over the same range.

Figure 8.3 shows results yielded at the lowest and highest temperature, -15°C and 65°C, respectively. For more temperature points, it is referred to appendix A.2. It is obvious that at lower temperatures and higher surface tensions both PVTsim and NeqSim are providing good results. As temperature is increased there is a tendency, however, that PVTsim is underestimating the surface tension to a higher extent than what is the case for NeqSim. It is worth noticing that the surface tension is substantially lower at 65°C, with experimental results at 1.87 mN/ at its highest (33.1 bar), compared to the surface tensions at -15°C. Thus, the graphs do not tell the whole truth. As can be observed in table 8.1, there is a consistent underestimation by both software. However, neither ever drops under 1 mN/ of the experimental data. Even though the margins are small, NeqSim is producing the best results at both extremes of the temperature range, giving an average underestimation of -0.249 mN/m and -0.263 mN/m at -15°C for SRK and PR, respectively, and similarly -0.176 mN/m and -0.184 mN/m at 65°C. In comparison, PVTsim produces an average deviation of -0.428 mN/m and -0.668 mN/m for SRK Peneloux and PR Peneloux at -15°C and -0.531 mN/m and -0.493 mN/m at 65°C. With the notion that NeqSim is performing slightly better for methane/propane, it is fair to say that both software are producing satisfactory results.

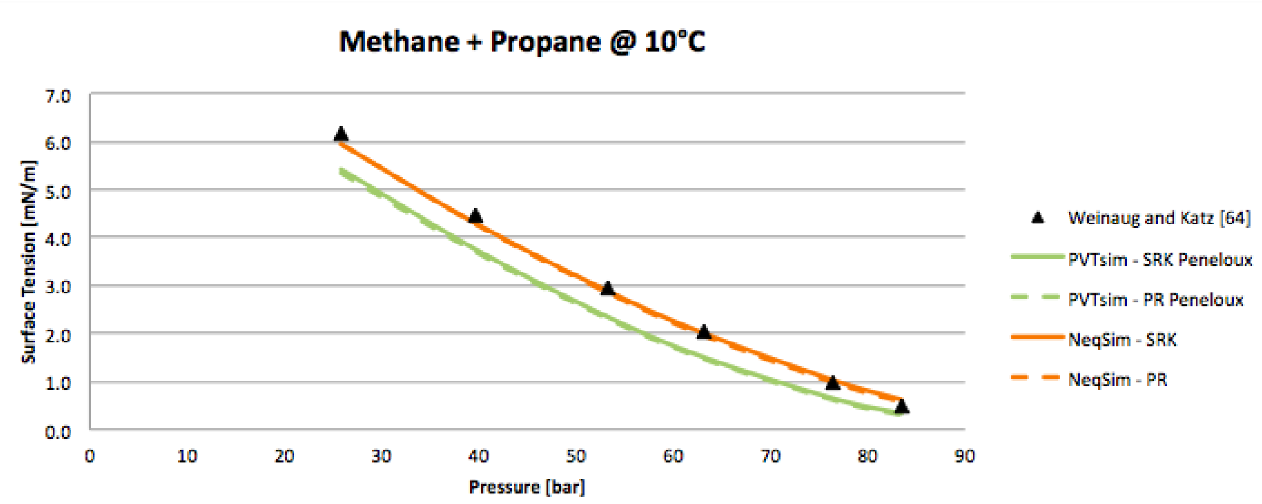

Figure 8.2: Methane + Propane

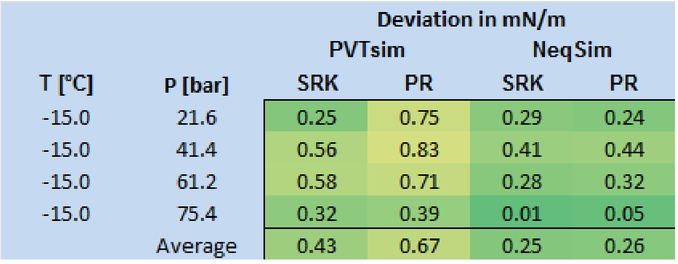

		Deviation in mN/m			
		PVTsim		NeqSim	
T [°C]	P [bar]	SRK	PR	SRK	PR
-15.0	21.6	0.25	0.75	0.29	0.24
-15.0	41.4	0.56	0.83	0.41	0.44
-15.0	61.2	0.58	0.71	0.28	0.32
-15.0	75.4	0.32	0.39	0.01	0.05
	Average	0.43	0.67	0.25	0.26

Table 8.1: Deviation in mN/m to Experimental Data

With regards to the performances of the two equations of states, there is not much separating them. Generally, PR is producing results slightly lower than those of SRK. Again, referring to table 8.1, the differences are negligible.

Furthermore, what is particularly interesting about the methane/propane mixture is that several experimental works have been conducted, applying different measurement methods. This provides a chance to see how well these methods coincides with software measured results.

The figures 8.4 - 8.6 show the results of the three different methods, taken at 30°C (or as close as possible). Notice that figure 8.4 has an x-axis starting at 70 bar, given that measurement was only done at high pressure for this experiment.

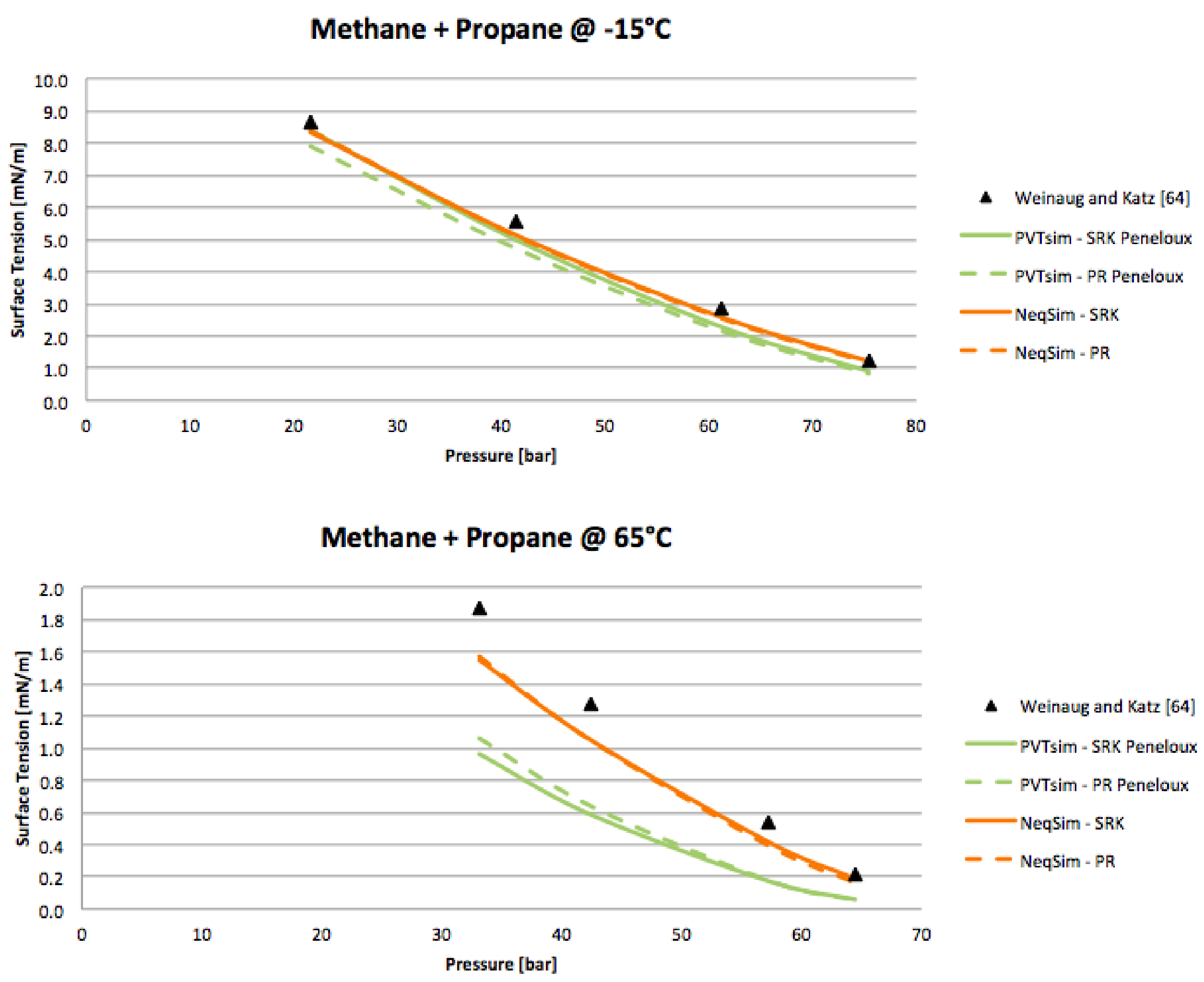

Figure 8.3: Methane + Propane

The two reports from Weinaug and Katz, using the capillary rise method and the drop volume method, are covering the same pressure range from 21.4 bar and up to about 55.0 bar. The report, where the capillary rise method was applied, is

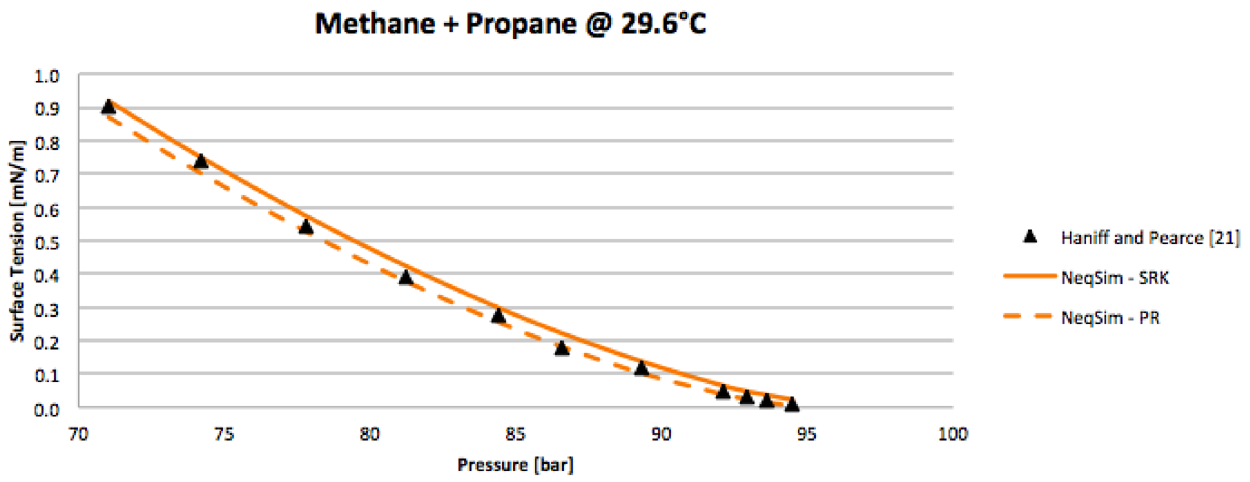

Figure 8.4: Methane + Propane Using Laser Light Scattering Method

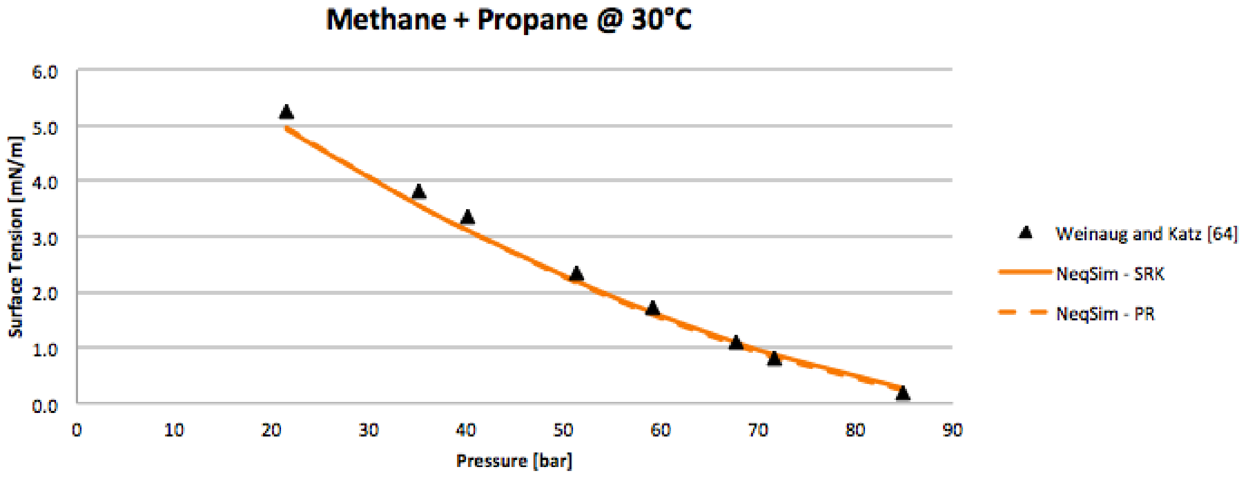

Figure 8.5: Methane + Propane Using Capillary Rise Method

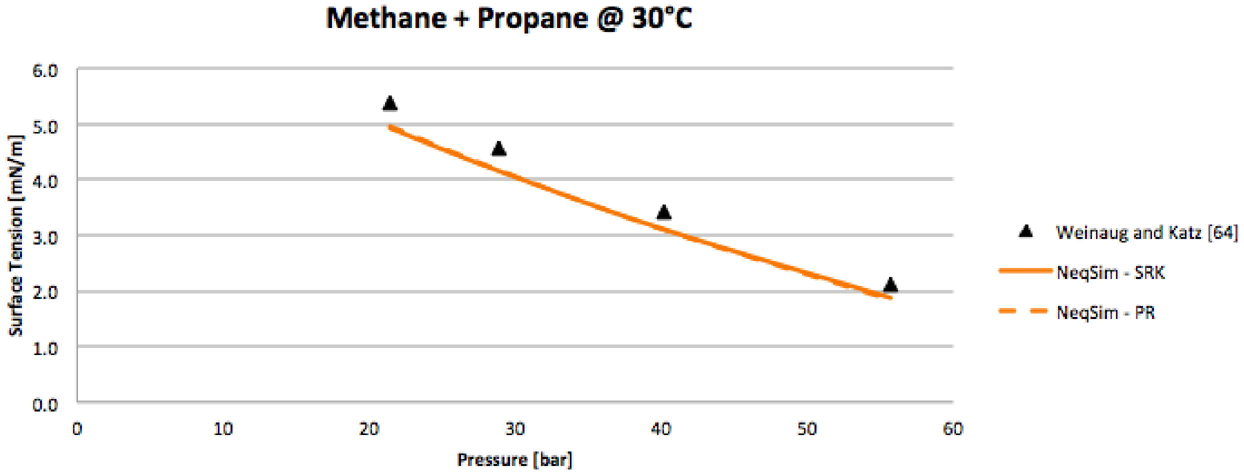

Figure 8.6: Methane + Propane Using Drop Volume Method

extending the pressure range up to 84.8 bar. However, if the coinciding pressures are compared it may seem that by using the capillary rise method, surface tensions are predicted to be somewhat lower than those found by using the drop volume method. Looking at table 8.3 and 8.4 it is recognized that 21.4 bar and 40.2 bar are pressure levels found in both reports. For 21.4 bar, the capillary rise method is giving an experimental surface tension of 5.25 mN/m, which is 0.15 mN/m lower than what produced by using the drop volume method, which is 5.40 mN/m. The same result is found for 40.2 bar. The capillary rise method gives a surface tension of 3.37 mN/m and the drop volume method a surface tension of 3.44 mN/m, a deviation of 0.07 mN/m. Of course, the simulated surface tensions are the same in both cases, and thus using capillary rise method seems to be yielding better results.

As the pressure range used with the capillary rise method stretches to 84.8 bar, it can be compared to the results from the report of Haniff and Pearce [21]. This experiment was performed within a pressure range of 69.1 - 94.5 bar. In this range, the Weinaug and Katz report using the capillary rise method has got two pressure levels coinciding pretty well with those of Haniff and Pearce. At 71.0

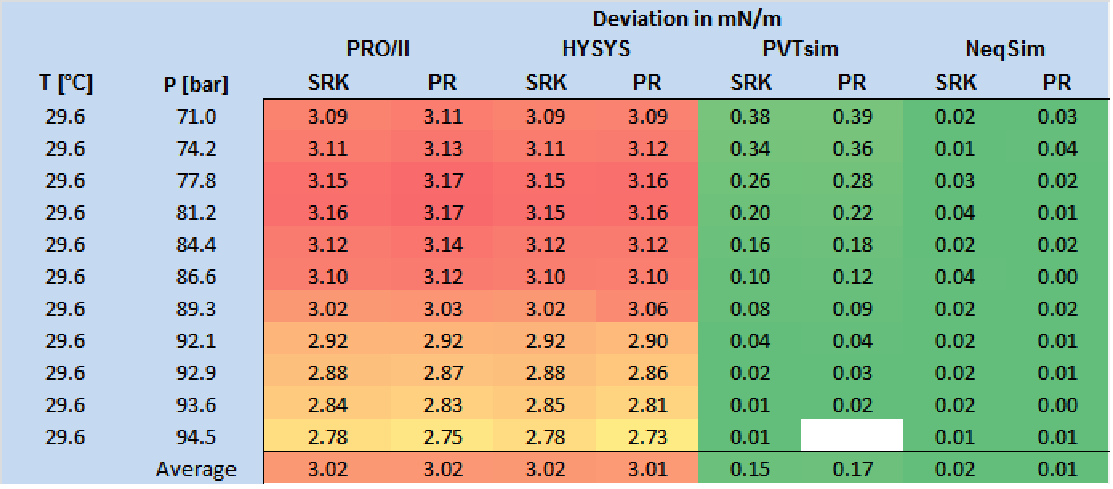

		Deviation in mN/m							
		PRO/II		HYSYS		PVTsim		NeqSim	
T [°C]	P [bar]	SRK	PR	SRK	PR	SRK	PR	SRK	PR
29.6	71.0	3.09	3.11	3.09	3.09	0.38	0.39	0.02	0.03
29.6	74.2	3.11	3.13	3.11	3.12	0.34	0.36	0.01	0.04
29.6	77.8	3.15	3.17	3.15	3.16	0.26	0.28	0.03	0.02
29.6	81.2	3.16	3.17	3.15	3.16	0.20	0.22	0.04	0.01
29.6	84.4	3.12	3.14	3.12	3.12	0.16	0.18	0.02	0.02
29.6	86.6	3.10	3.12	3.10	3.10	0.10	0.12	0.04	0.00
29.6	89.3	3.02	3.03	3.02	3.06	0.08	0.09	0.02	0.02
29.6	92.1	2.92	2.92	2.92	2.90	0.04	0.04	0.02	0.01
29.6	92.9	2.88	2.87	2.88	2.86	0.02	0.03	0.02	0.01
29.6	93.6	2.84	2.83	2.85	2.81	0.01	0.02	0.02	0.00
29.6	94.5	2.78	2.75	2.78	2.73	0.01		0.01	0.01
	Average	3.02	3.02	3.02	3.01	0.15	0.17	0.02	0.01

Table 8.2: Results Using Laser Light Scattering Method versus Software

bar, and 29.6°C, the laser light method gives a surface tension of 0.90 mN/m (table 8.2). In comparison, at 71.6 bar the capillary rise method gives a surface tension of 0.82 mN/m. This seems natural, as a slightly higher pressure would slightly decrease the surface tension. Again, at 84.4 bar, the laser light scattering method yields a surface tension of 0.27 mN/m, whereas the capillary rise method at 84.8 bar yields 0.19 mN/m. As previously mentioned, with an increased pressure the surface tension decreases. Both methods appear to give good results. Even though the coinciding points are few, it would seem the method is not drastically changing the output of the experiments, and thus the whole range of data obtained and simulated on methane/propane mixtures can be evaluated against each other without much error.

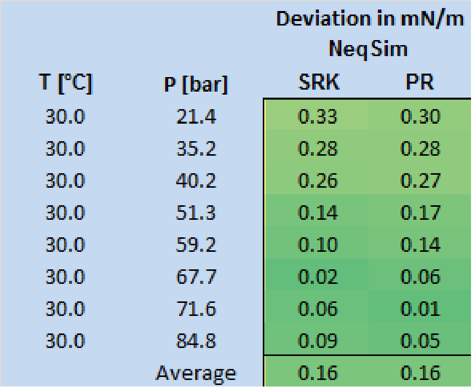

		Deviation in mN/m	
		NeqSim	
T [°C]	P [bar]	SRK	PR
30.0	21.4	0.33	0.30
30.0	35.2	0.28	0.28
30.0	40.2	0.26	0.27
30.0	51.3	0.14	0.17
30.0	59.2	0.10	0.14
30.0	67.7	0.02	0.06
30.0	71.6	0.06	0.01
30.0	84.8	0.09	0.05
	Average	0.16	0.16

Table 8.3: Results Using Capillary Rise Method versus Software

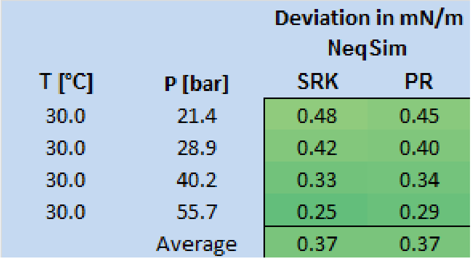

		Deviation in mN/m	
		NeqSim	
T [°C]	P [bar]	SRK	PR
30.0	21.4	0.48	0.45
30.0	28.9	0.42	0.40
30.0	40.2	0.33	0.34
30.0	55.7	0.25	0.29
	Average	0.37	0.37

Table 8.4: Results Using Drop Volume Method versus Software

Methane + n-butane/n-pentane/n-hexane/n-heptane Contrary to the availability of experimental data on methane/propane systems, the scope is somewhat limited when analyzing heavier mixtures including methane. Thus, this section comprises the ”intermediate level” mixtures. This merge is also justified through the fact that the temperature and pressure ranges and general behavior are comparable.

Experimental data for these mixtures is collected from five various reports. The first one, on methane/n-butane, was carried out by Pennington and Hough [41]. The report does not mention which measurement technique was used. However, previous works by Pennington and Hough [56][24] supports the assumption that pendant drop is applied as measurement method. Nevertheless, the data set comprises six different temperatures, ranging from 37.8°C to 87.8°C. The pressure is consistently high, starting from 89.6 bar at all temperatures and ranging to 131.0 bar at the lowest temperature and up to 106.9 bar at the highest temperature.

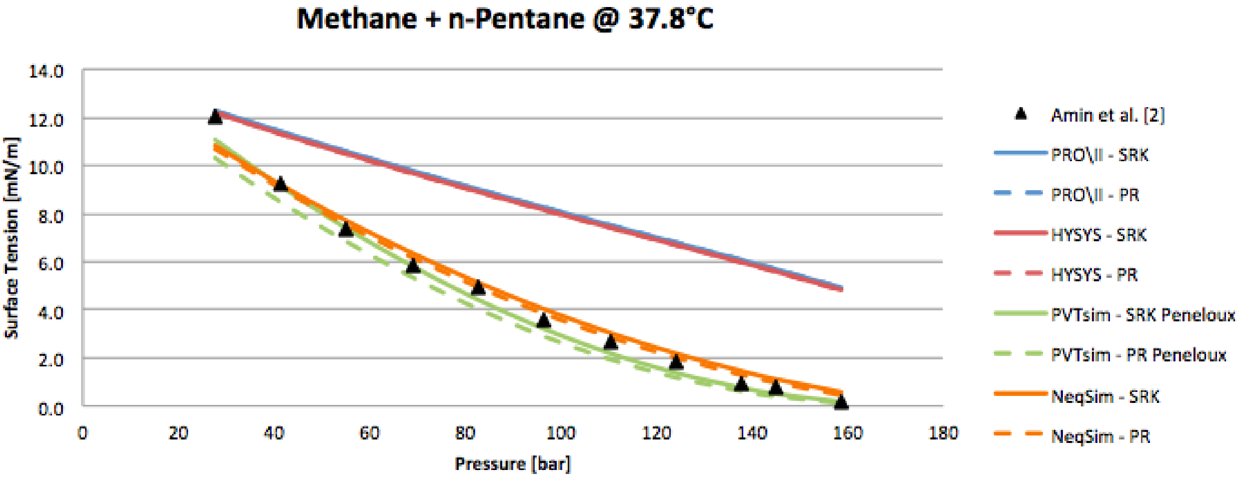

Figure 8.7: Methane + n-Pentane

The second report is on a methane/n-pentane mixture, and the work was conducted by Amin et al. [2]. Amin et al. applied the pendant drop method when performing the experimental measurement. There are only three unique temperatures, but they span from 37.8°C to 137.8°C, also examining 93.3°C in between. The pressure ranges from 27.9 bar to about 150.0 bar for the two lowest temperatures, whereas the highest temperature only comprises three pressure levels, peaking at 55.2 bar. Given the large span in both temperature and pressure, the range of surface tension is correspondingly large. At 37.8°C the surface tension ranges from 0.21 mN/m at the highest pressure to 12.03 mN/m at the lowest. 93.3°C yields surface tension ranging from 0.14 mN/m to 10.61 mN/m. Ultimately, 137.8°C gives surface tensions from 4.60 mN/ to 7.89 mN/m.

The third report comprises of work done on a methane/n-hexane mixture, and was done by Nino-Amezquita et al. [37], using the pendant drop method. The experimental data is collected using two temperatures, 26.9°C and 76.9°C, with four and five measured surface tensions on the respective temperatures. Spanning over a pressure range of 80 bar, from 20 bar to 100 bar, giving surface tensions in the region of 4.0 to 14.2 mN/m, this experiment reveals much of the same features as seen in the other binary systems evaluated in this section, despite the relatively sparse number of data points.

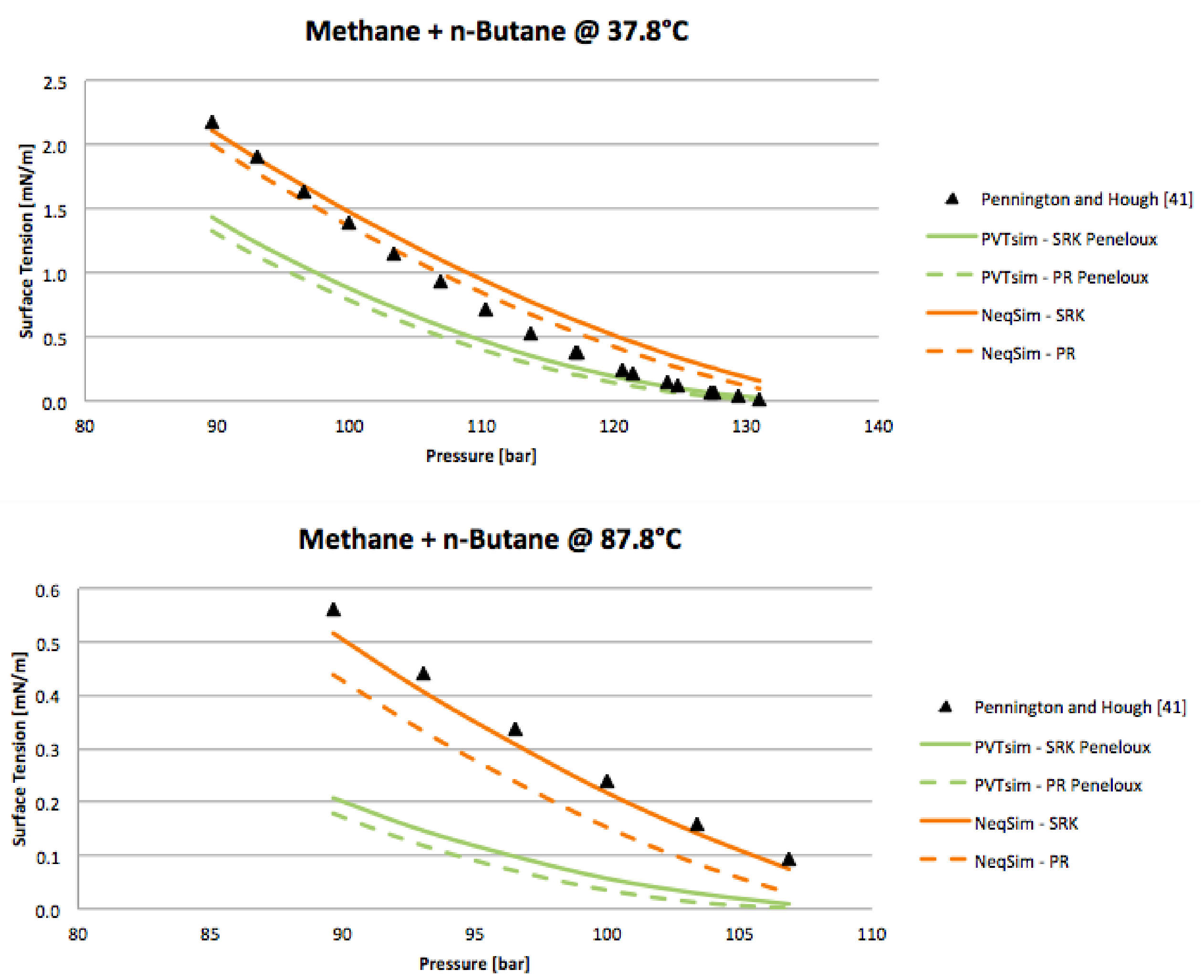

Figure 8.8: Methane + n-Butane

Lastly, there are two separate works done on methane/n-heptane systems. The two papers are similar on many aspects. The first is done by Amin et al. [2], and comprises of 20 data points spread over a temperature range of 37.8°C to 121.1°C and a pressure range of 37 - 151 bar. Surface tensions are obtained from 1.8 - 14.0 mN/m. Both experiments are performed using the pendant drop method. The second report is from Warren [63]. This report expands to a higher pressure and temperature level, giving 42 data points. The temperature starts at 37.8°C again, but now reaches 137.8°C at the most. Likewise, the pressure starts at 28 bar and now reaches 214 bar. Surface tension stretches from 0.2 - 14.9 mN/m.

Figure 8.7 is used to illustrate the general outlook and properties of the binary mixtures discussed in this section. The software performance trends are representative of what has been found, giving PRO/II and HYSYS performances much closer to the experimental data than what was found for the methane/propane systems in the previous section. This figure also shows the typical pressure and surface tension range. The method used is pendant drop method, which is used in the vast majority of the reports examined.

As figure 8.7 shows, PRO/II and HYSYS do increase their discrepancy to the experimental data with increasing pressure. At the lowest pressures and thus the

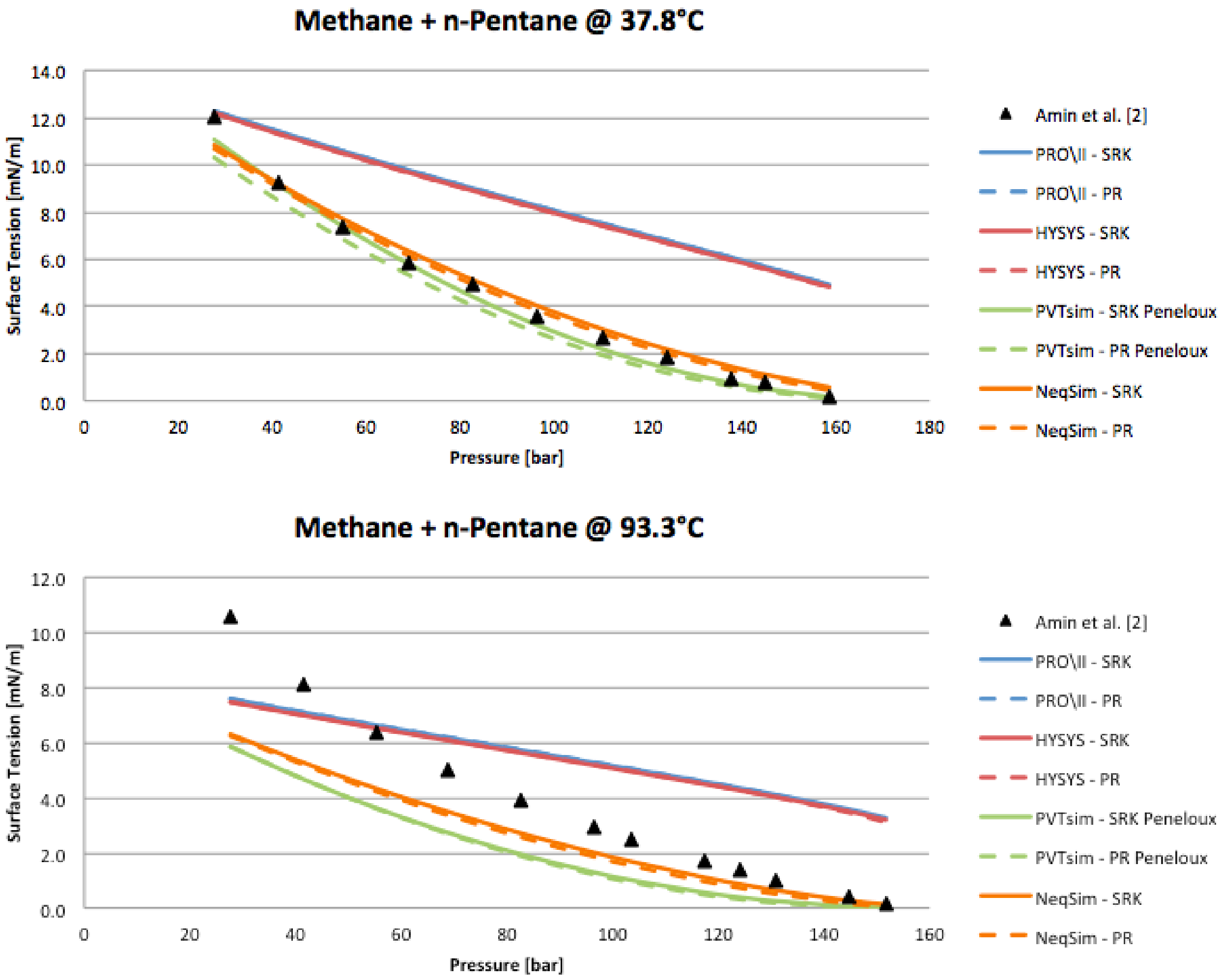

Figure 8.9: Methane + n-Pentane

highest surface tensions, they actually outperform PVTsim and NeqSim simulations. However, and again due to the simplified weighted average pure-component model, the overall performance of PRO/II and HYSYS are not satisfactory compared to those of PVTsim and NeqSim. Hence, even though all four software perform, and even to a higher standard, the norm will again be to analyze the results from PVTsim and NeqSim.

PVTsim and NeqSim do follow the curvature of the experimental data. Figure 8.7 shows that PVTsim is producing results slightly below that of NeqSim, with an exception at the lowest pressure, and the deviation is only increasing with the raising pressure until they tend towards each other again at the highest pressure. As will be shown, this is indeed the general trend when comparing the two software.

Figure 8.8 shows the performance of PVTsim and NeqSim on the methane/n-butane systems lowest and highest temperature. Notice that the values of the ordinate are not the same and the deviation between the PVTsim simulations and the experimental data is in fact decreasing as the temperature increases. For instance, the PVTsim SRK results deviate by 0.75 mN/m from the experimental data at 90 bar and 37.8°C whereas the discrepancy is reduced to 0.35 mN/m at 90 bar and 87.8°C. More details can be found in the appendix. This trend of a decrease in deviation between PVTsim and experimental data is something that can be recognized from the methane/propane section (see figure 8.3).

Another noteworthy feature is NeqSims incapability of dropping to a low surface tension quick enough to correlate with the experimental data at the lowest temperature. Above 110 bar PVTsim is actually following the experimental results better than NeqSim. At this range the surface tension drops to a low of 0.01 mN/m, which PVTsim matches well. NeqSim lowest estimation is 0.1 mN/m, which is ten times the experimental value. On the other hand, this is the extreme end of the scale, and for all practical purposes, NeqSim has a lower average deviation to the experimental data than PVTsim.

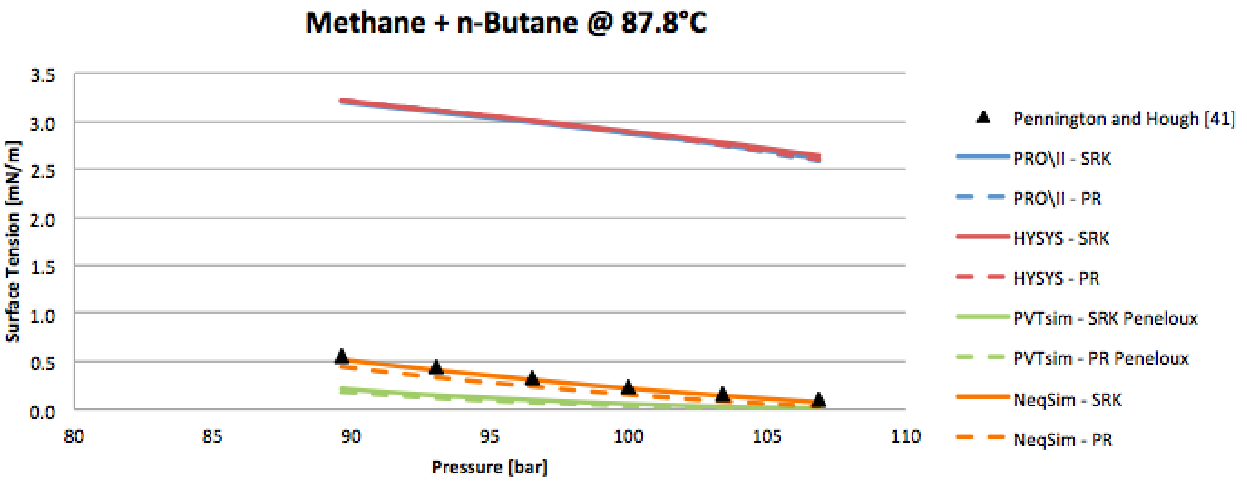

Figure 8.10: Surface Tensions at High Temperatures

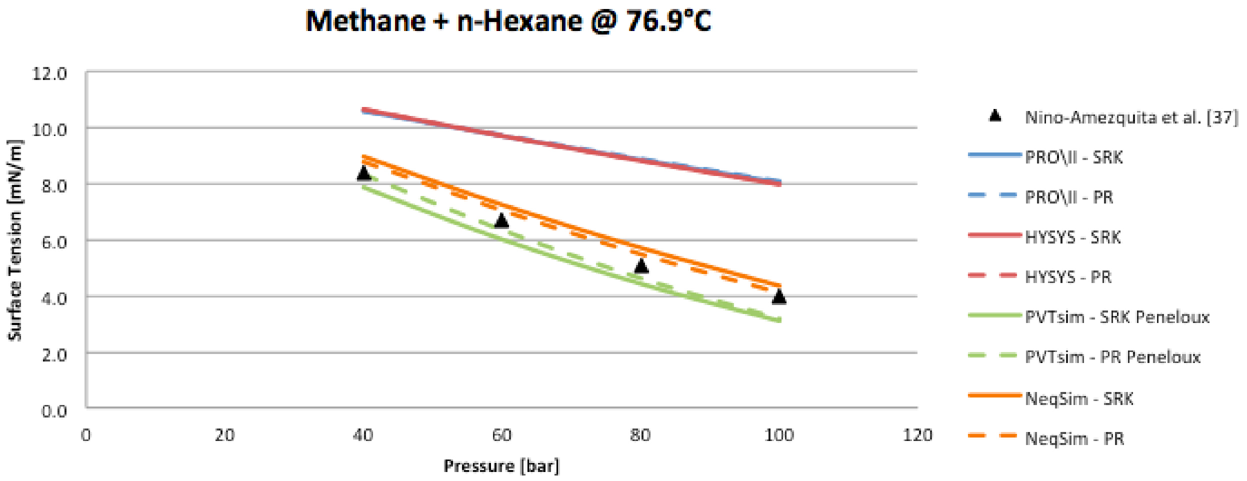

Figure 8.11: Surface Tensions at High Temperatures

Figure 8.9 shows the results from analysing software performance on the methane/n-pentane system. Experiments are performed on 137.8°C as well, but this only comprises three data points so 93.3°C provides a more interesting comparison. This mixture is interesting in a particular aspect, and that is the behavior of the experimental data at low pressure. As seen in figure 8.9, PRO/II and HYSYS performances are included in the graphics, and this is because PVTsim and NeqSim greatly underestimate the surface tension. In fact, even PRO/II and HYSYS underestimates at the highest surface tensions. However, there might be reasons to question these experimental results. Figures 8.10 and 8.11 show work done by others, on slightly different mixtures but approximately the same temperature and pressure level. Interestingly, NeqSim and PVTsim coincide with the experimental data in the lowest pressure region in all cases, contrary to what is the case for the methane/n-pentane mixture of Amin et al. [2]. As all works have been carried out using the pendant drop method, there is no explanation in the use of technique. In addition, as can be seen in figure 8.13, other works by Amin et al. show the same tendency. In other aspects, the methane/n-pentane mixture shows the same attributes as the other mixtures in this section, and hence will not be discussed any further.

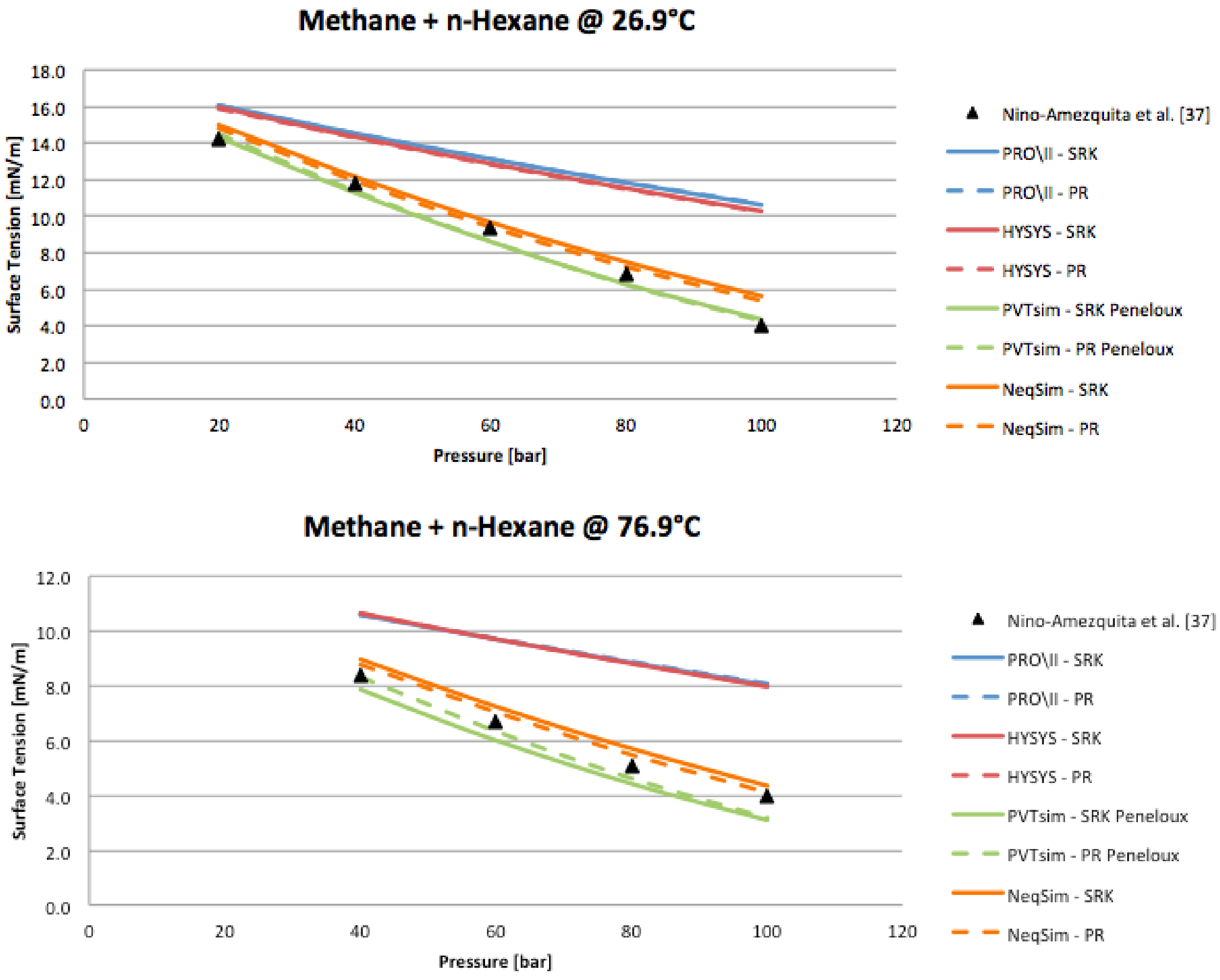

Figure 8.12: Methane + n-Hexane

As mentioned in the previous paragraph, the results from analyzing the Nino-Amezquita et al. work [37] are more coincident with the general tendencies of binary systems. This is visualized in figure 8.12, displaying the only two temperatures that was evaluated in the paper [37].

The general tendency, with respect to how PVTsim and NeqSim are far superior to the other software, may be restored. However, there is a deviation to the general hierarchy of performance as PVTsim over large ranges outperforms NeqSim. This is best seen by looking at the table of deviation from the experimental data, table 8.5. Knowing that the largest deviations are marked by the deepest red and at the other

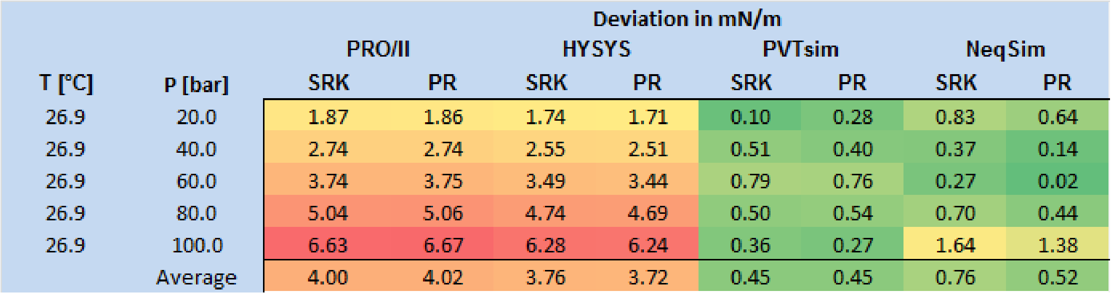

		Deviation in mN/m							
		PRO/II		HYSYS		PVTsim		NeqSim	
T [°C]	P [bar]	SRK	PR	SRK	PR	SRK	PR	SRK	PR
26.9	20.0	1.87	1.86	1.74	1.71	0.10	0.28	0.83	0.64
26.9	40.0	2.74	2.74	2.55	2.51	0.51	0.40	0.37	0.14
26.9	60.0	3.74	3.75	3.49	3.44	0.79	0.76	0.27	0.02
26.9	80.0	5.04	5.06	4.74	4.69	0.50	0.54	0.70	0.44
26.9	100.0	6.63	6.67	6.28	6.24	0.36	0.27	1.64	1.38
	Average	4.00	4.02	3.76	3.72	0.45	0.45	0.76	0.52

Table 8.5: Deviation from Experimental Data on Methane/n-Hexane at 26.9°C

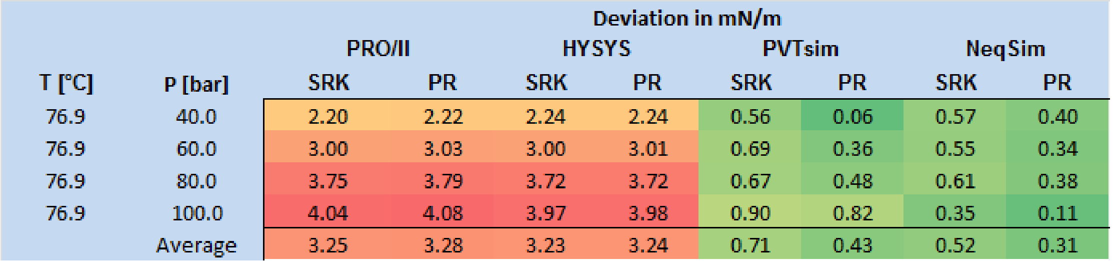

		Deviation in mN/m							
		PRO/II		HYSYS		PVTsim		NeqSim	
T [°C]	P [bar]	SRK	PR	SRK	PR	SRK	PR	SRK	PR
76.9	40.0	2.20	2.22	2.24	2.24	0.56	0.06	0.57	0.40
76.9	60.0	3.00	3.03	3.00	3.01	0.69	0.36	0.55	0.34
76.9	80.0	3.75	3.79	3.72	3.72	0.67	0.48	0.61	0.38
76.9	100.0	4.04	4.08	3.97	3.98	0.90	0.82	0.35	0.11
	Average	3.25	3.28	3.23	3.24	0.71	0.43	0.52	0.31

Table 8.6: Deviation from Experimental Data on Methane/n-Hexane at 76.9°C

end the smallest deviations are toned deep green, there is a shift in performance with regard to which software is performing best along the pressure range. The trend of the experimental data is curved opposite of what is expected, and one may speculate in the extreme points being strays, especially when observing that the mixture at 76.9°C in figure 8.12 is again following the normal curvature. This is also reflected in table 8.6, showing that NeqSim again is providing results closer to the experimental data. Nevertheless, it is clear that both NeqSim and PVTsim are producing satisfactory simulations.

Finally, the methane/n-heptane mixture concludes this section. The evaluation of this binary system comprises two works, as previously stated, by Amin et al. [2] and Warren [63], respectively. These reports represent a broad database, and as figure 8.13 shows, the results are matching really well with regards to surface tension and performance of the software. As the work of Warren comprises a larger pressure span, the results of these experimental data will be evaluated

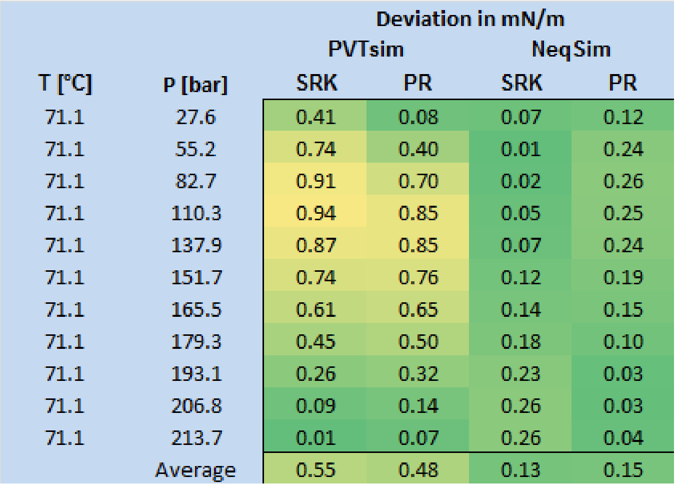

		Deviation in mN/m			
		PVTsim		NeqSim	
T [°C]	P [bar]	SRK	PR	SRK	PR
71.1	27.6	0.41	0.08	0.07	0.12
71.1	55.2	0.74	0.40	0.01	0.24
71.1	82.7	0.91	0.70	0.02	0.26
71.1	110.3	0.94	0.85	0.05	0.25
71.1	137.9	0.87	0.85	0.07	0.24
71.1	151.7	0.74	0.76	0.12	0.19
71.1	165.5	0.61	0.65	0.14	0.15
71.1	179.3	0.45	0.50	0.18	0.10
71.1	193.1	0.26	0.32	0.23	0.03
71.1	206.8	0.09	0.14	0.26	0.03
71.1	213.7	0.01	0.07	0.26	0.04
	Average	0.55	0.48	0.13	0.15

Table 8.7: Deviation from Experimental Data on Methane/n-Heptane at 71.1°C

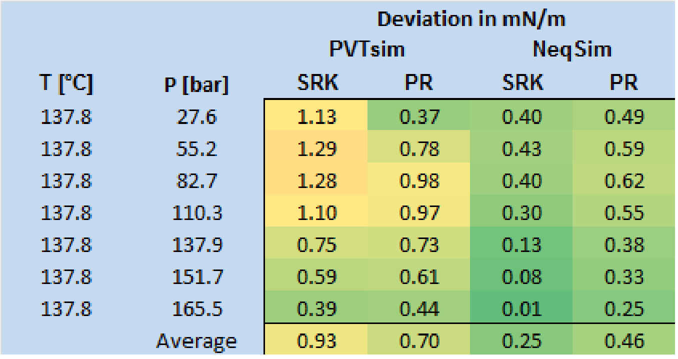

		Deviation in mN/m			
		PVTsim		NeqSim	
T [°C]	P [bar]	SRK	PR	SRK	PR
137.8	27.6	1.13	0.37	0.40	0.49
137.8	55.2	1.29	0.78	0.43	0.59
137.8	82.7	1.28	0.98	0.40	0.62
137.8	110.3	1.10	0.97	0.30	0.55
137.8	137.9	0.75	0.73	0.13	0.38
137.8	151.7	0.59	0.61	0.08	0.33
137.8	165.5	0.39	0.44	0.01	0.25
	Average	0.93	0.70	0.25	0.46

Table 8.8: Deviation from Experimental Data on Methane/n-Heptane at 137.8°C

further.

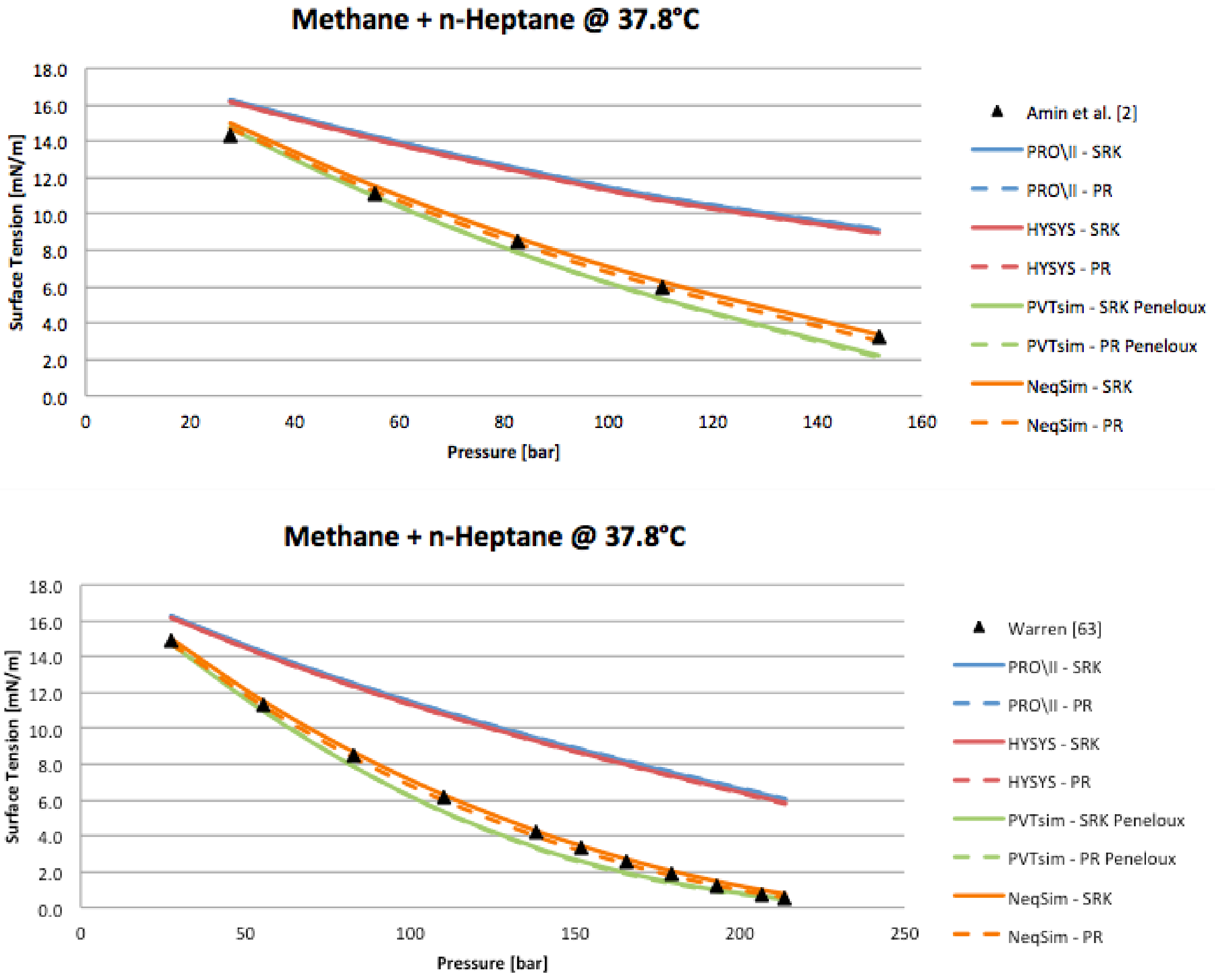

Figure 8.13: Methane + n-Heptane: Comparison of Two Works

As seen in figure 8.13, PRO/II and HYSYS are again grossly overestimating the surface tension, and will therefore not be discussed further. Now, figure 8.14 shows the development of PVTsim and NeqSim as the temperature is increased. The same trend as previously mentioned can be observed with regards to how PVTsim starts off well, then deviates more and more before again closing in on the experimental data as the surface tension drops towards 0 mN/m. Table 8.7 and

8.8 show the deviations for the two temperatures shown in figure 8.14 in detail. As a general observation it is however safe to say that NeqSim is overall outperforming PVTsim.

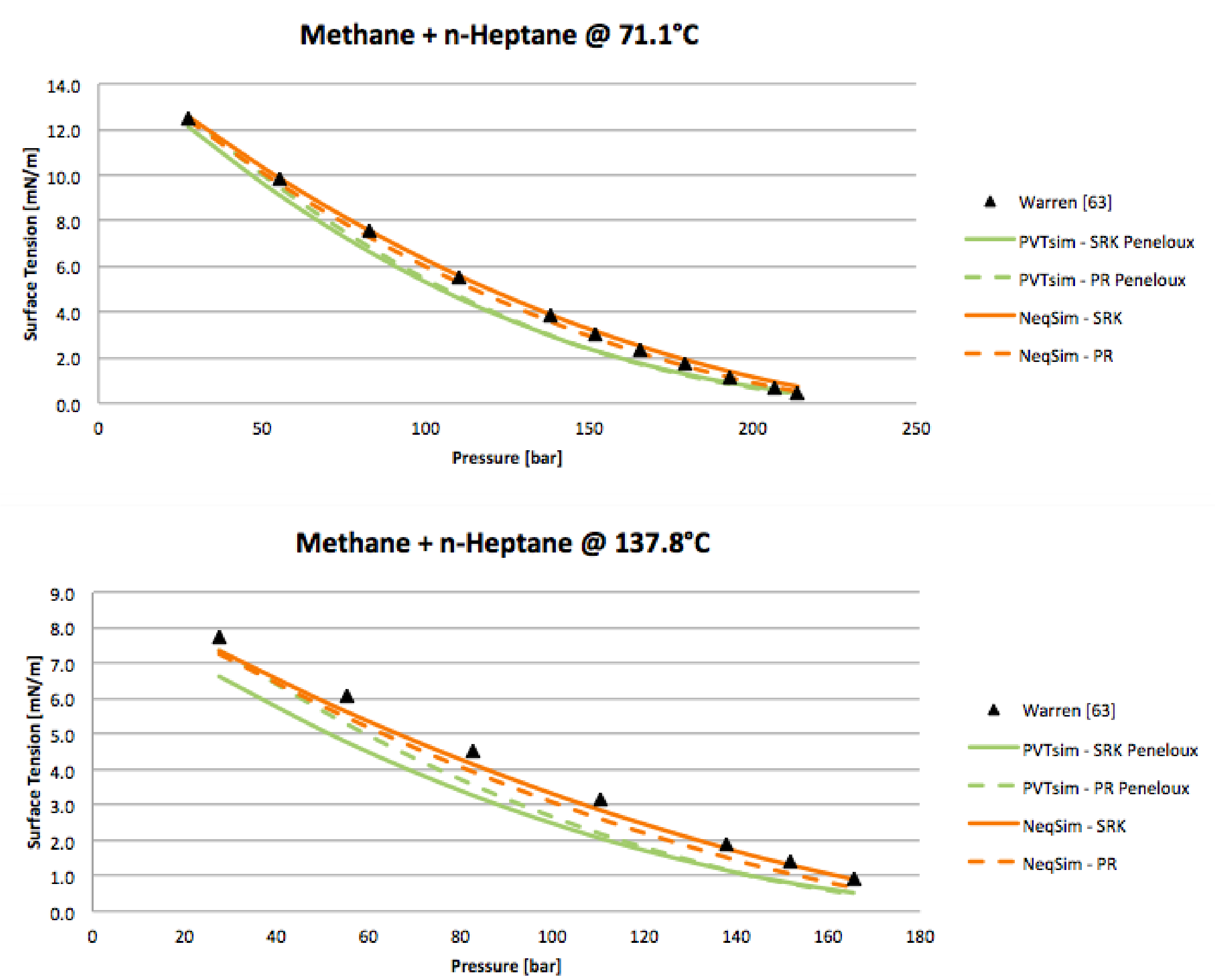

Figure 8.14: Methane + n-Heptane

Methane + n-Nonane This section only comprises one work on the binary system of methane/n-nonane. The experimental work was carried out by Deam and Maddox [13], using the Pendant Drop Method. What makes this report stand out is the fact that experiments was partly performed on sub-zero temperature. However, there are only two temperatures, -1.1°C and 24.4°C. Pressures are ranging from 20 - 100 bar, giving surface tensions in the range of 8.3 - 25.3 mN/m.

An experimental surface tension of 25.3 mN/m is the highest surface tension evaluated on hydrocarbon systems in this thesis. This surface tension is obtained at -1.1°C. Even though this is not the lowest temperature evaluated, the low pressure combined with the relatively heavy binary system that methane/n-nonane represents makes for a very high surface tension. The results of the software simulation are shown in figure 8.15.

With surface tensions reaching 25 mN/m, PRO/II and HYSYS are producing good results at the lowest pressures. However, as the pressure increases, those two software do not follow the same trendline as the experimental data and they actually deviate by more than 6 mN/m at 102 bar. With that clarified, figure 8.16

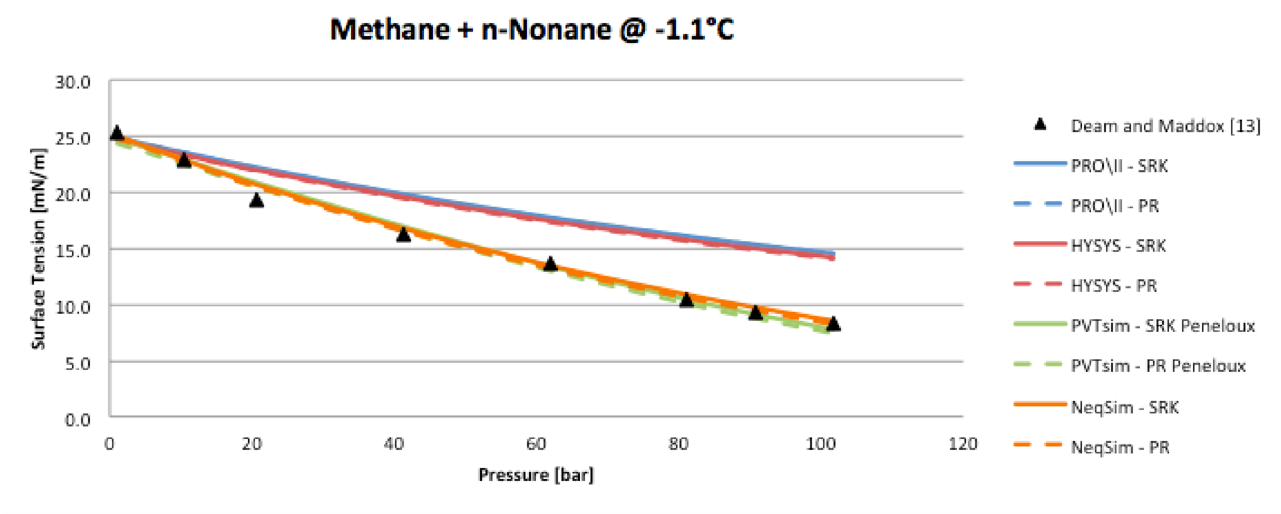

Figure 8.15: Methane + n-Nonane

shows the performance of PVTsim and NeqSim exclusively. In addition, it shows, from previously, how PVTsim and NeqSim performed on the methane/propane system evaluated by Weinaug and Katz [64]. These are the only observations done on sub-zero temperatures. Table 8.9 and 8.10 show the deviation of PVTsim and NeqSim from the experimental data on the two binary systems. Obviously, both software are performing to a high standard over the whole range on both mixtures.

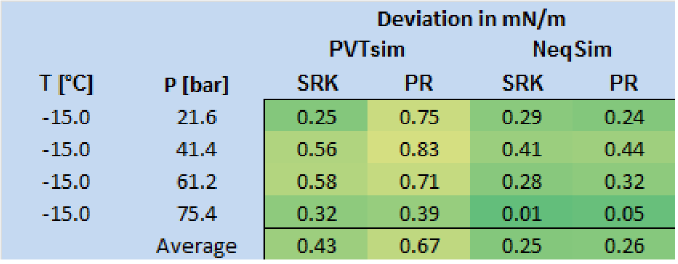

		Deviation in mN/m			
		PVTsim		NeqSim	
T [°C]	P [bar]	SRK	PR	SRK	PR
-15.0	21.6	0.25	0.75	0.29	0.24
-15.0	41.4	0.56	0.83	0.41	0.44
-15.0	61.2	0.58	0.71	0.28	0.32
-15.0	75.4	0.32	0.39	0.01	0.05
	Average	0.43	0.67	0.25	0.26

Table 8.9: Deviation from Experimental Data on Methane/Propane at -15°C

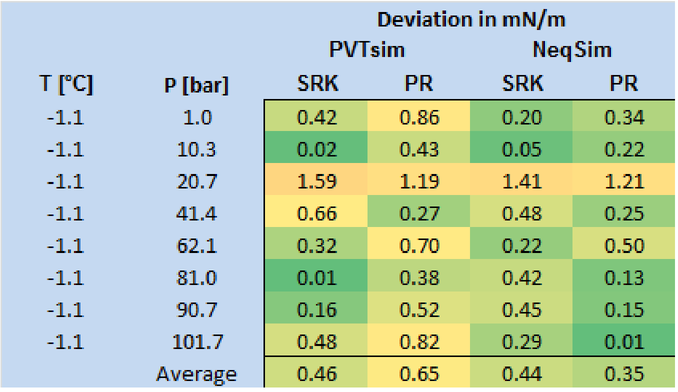

		Deviation in mN/m			
		PVTsim		NeqSim	
T [°C]	P [bar]	SRK	PR	SRK	PR
-1.1	1.0	0.42	0.86	0.20	0.34
-1.1	10.3	0.02	0.43	0.05	0.22
-1.1	20.7	1.59	1.19	1.41	1.21
-1.1	41.4	0.66	0.27	0.48	0.25
-1.1	62.1	0.32	0.70	0.22	0.50
-1.1	81.0	0.01	0.38	0.42	0.13
-1.1	90.7	0.16	0.52	0.45	0.15
-1.1	101.7	0.48	0.82	0.29	0.01
	Average	0.46	0.65	0.44	0.35

Table 8.10: Deviation from Experimental Data on Methane/n-Nonane at -1.1°C

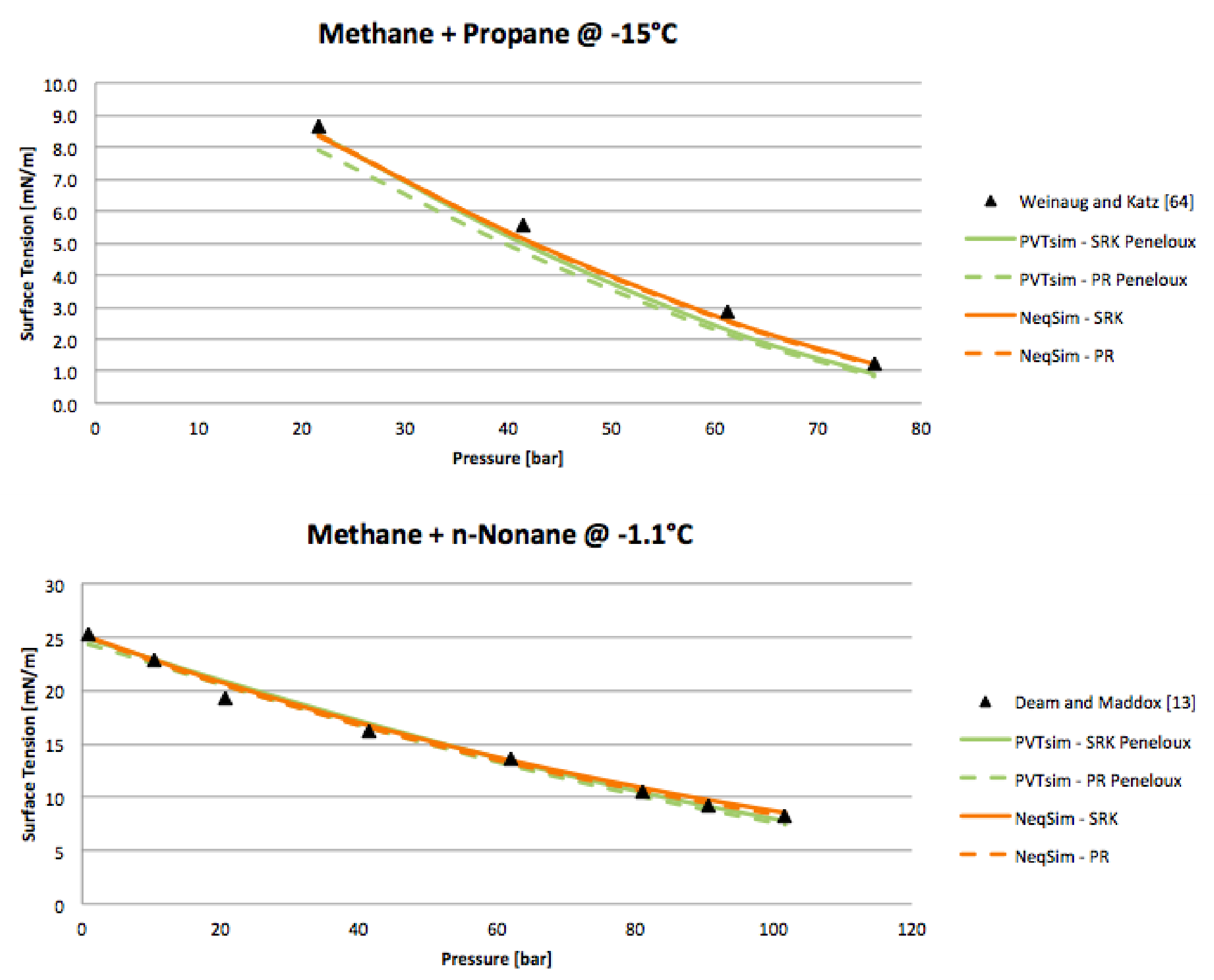

Figure 8.16: Sub-zero Temperature Surface Tension Comparison

Methane + n-Decane There are two works done on methane/n-decane, one by Amin et al. [2] and the other by Stegemeier [56]. Both experimental works are carried out by using the pendant drop technique. The two works are quite similar in that they span over wide ranges of pressure and temperature. Amin et al. did examine surface tension at 37.8°C, 93.3°C and 137.8°C, whereas Stegemeier only worked at 37.8°C and 71.1°C. Furthermore, Stegemeiers experiments were conducted at very high pressure, ranging from 103 - 321 bar. Amin et al. used lower pressures, 28 bar, but through quite extensive data quantity, pressures ultimately reached 276 bar. The surface tensions from the Stegemeier report ranges from 0.5 mN/m to 9.8 mN/m. The wider temperature and pressure span implies a wider surface tension span as wall, ranging from 0.7 mN/m to 20.5 mN/m.

Figure 8.17 shows the two works' experimental data and the software performance on the lowest temperatures, 37.8°C. It shows that NeqSim is consistently producing better results. That being mentioned, table 8.11 and 8.12 show that both NeqSim and PVTsim are providing good results, NeqSim being a bit more accurate. Also worth mentioning, as discussed for the methane/n-pentane system, is how data from Amin et al. somehow overshoots all software at relatively low pressure.

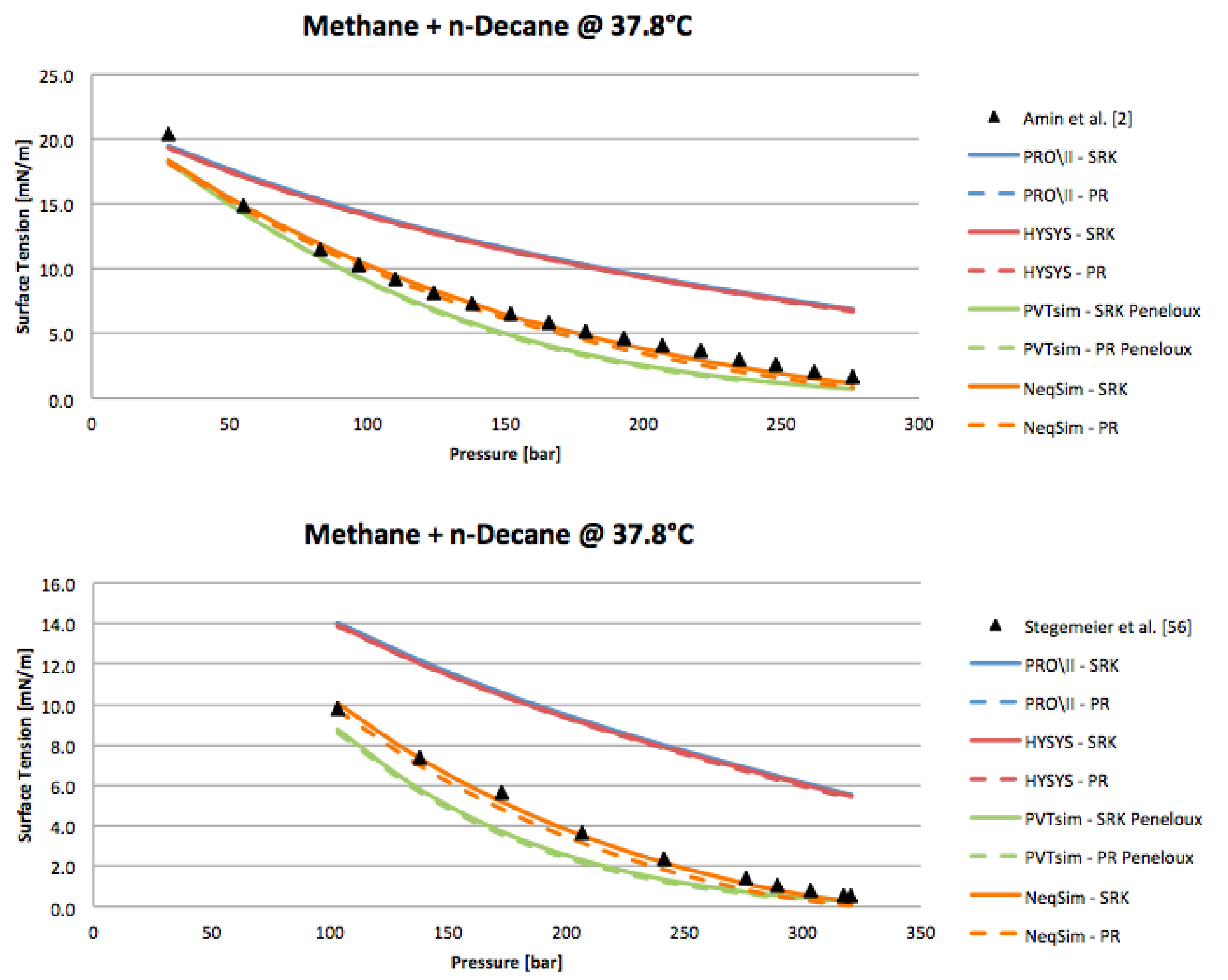

Figure 8.17: Methane + n-Decane

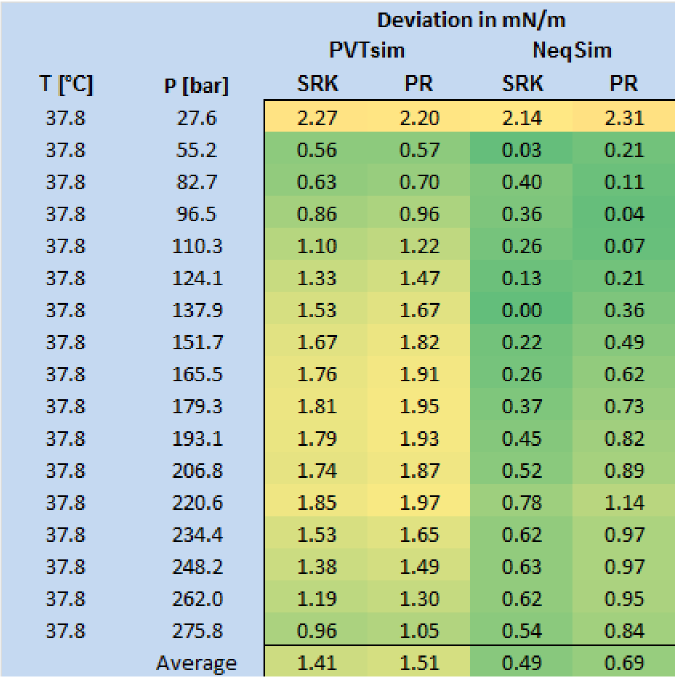

		Deviation in mN/m			
		PVTsim		NeqSim	
T [°C]	P [bar]	SRK	PR	SRK	PR
37.8	27.6	2.27	2.20	2.14	2.31
37.8	55.2	0.56	0.57	0.03	0.21
37.8	82.7	0.63	0.70	0.40	0.11
37.8	96.5	0.86	0.96	0.36	0.04
37.8	110.3	1.10	1.22	0.26	0.07
37.8	124.1	1.33	1.47	0.13	0.21
37.8	137.9	1.53	1.67	0.00	0.36
37.8	151.7	1.67	1.82	0.22	0.49
37.8	165.5	1.76	1.91	0.26	0.62
37.8	179.3	1.81	1.95	0.37	0.73
37.8	193.1	1.79	1.93	0.45	0.82
37.8	206.8	1.74	1.87	0.52	0.89
37.8	220.6	1.85	1.97	0.78	1.14
37.8	234.4	1.53	1.65	0.62	0.97
37.8	248.2	1.38	1.49	0.63	0.97
37.8	262.0	1.19	1.30	0.62	0.95
37.8	275.8	0.96	1.05	0.54	0.84
	Average	1.41	1.51	0.49	0.69

Table 8.11: Deviation from Experimental Data on Methane/n-Decane

Ethane + n-Pentane Last of the binary hydrocarbon systems to be evaluated is the mixture obtained from the work of Nilssen et al. [34] on ethane/n-pentane. The amount of experimental data done on binary hydrocarbon systems not containing methane is scarce, this being the only one analyzed in this thesis. In addition, the work done by Nilssen et al. only comprises one temperature, $21°C$. Admittedly, there are some interesting features in this ethane/n-pentane mixture. PRO/II and HYSYS are arguably producing much better results, as table 8.13 shows. In addition to the small amount of data available, the pressure range evaluated only spans from 6 to 30 bar. In total, this work provides an interesting indication on how software performs on binary systems not containing methane, but hardly a platform to draw any conclusive from.

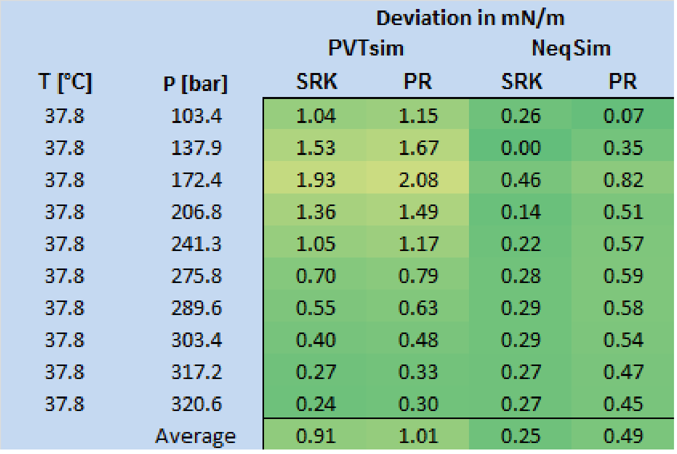

		Deviation in mN/m			
		PVTsim		NeqSim	
T [°C]	P [bar]	SRK	PR	SRK	PR
37.8	103.4	1.04	1.15	0.26	0.07
37.8	137.9	1.53	1.67	0.00	0.35
37.8	172.4	1.93	2.08	0.46	0.82
37.8	206.8	1.36	1.49	0.14	0.51
37.8	241.3	1.05	1.17	0.22	0.57
37.8	275.8	0.70	0.79	0.28	0.59
37.8	289.6	0.55	0.63	0.29	0.58
37.8	303.4	0.40	0.48	0.29	0.54
37.8	317.2	0.27	0.33	0.27	0.47
37.8	320.6	0.24	0.30	0.27	0.45
	Average	0.91	1.01	0.25	0.49

Table 8.12: Deviation from Experimental Data on Methane/n-Decane

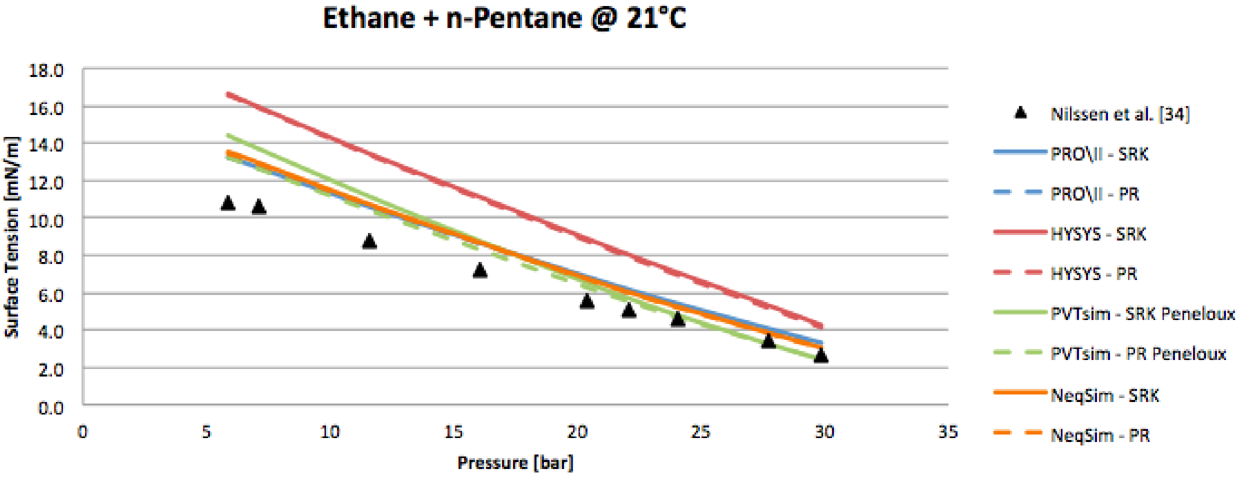

Figure 8.18: Ethane + n-Pentane

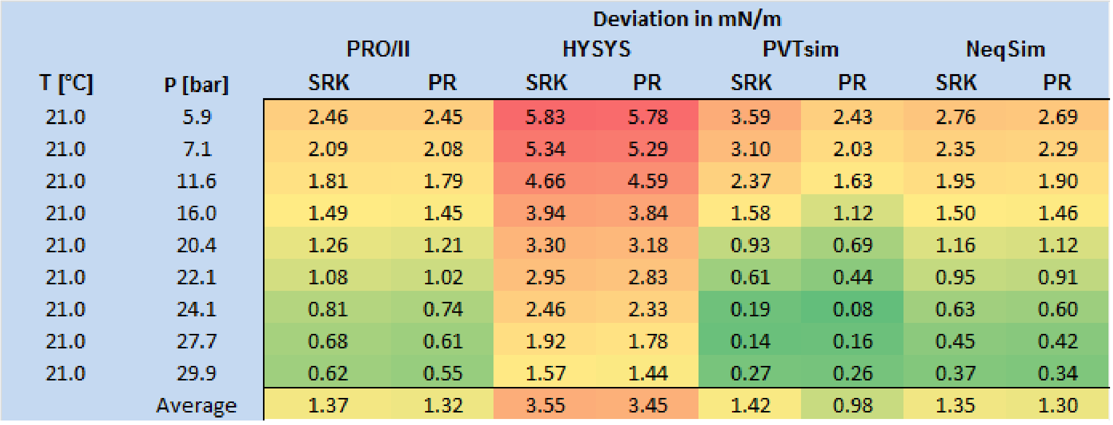

		Deviation in mN/m							
		PRO/II		HYSYS		PVTsim		NeqSim	
T [°C]	P [bar]	SRK	PR	SRK	PR	SRK	PR	SRK	PR
21.0	5.9	2.46	2.45	5.83	5.78	3.59	2.43	2.76	2.69
21.0	7.1	2.09	2.08	5.34	5.29	3.10	2.03	2.35	2.29
21.0	11.6	1.81	1.79	4.66	4.59	2.37	1.63	1.95	1.90
21.0	16.0	1.49	1.45	3.94	3.84	1.58	1.12	1.50	1.46
21.0	20.4	1.26	1.21	3.30	3.18	0.93	0.69	1.16	1.12
21.0	22.1	1.08	1.02	2.95	2.83	0.61	0.44	0.95	0.91
21.0	24.1	0.81	0.74	2.46	2.33	0.19	0.08	0.63	0.60
21.0	27.7	0.68	0.61	1.92	1.78	0.14	0.16	0.45	0.42
21.0	29.9	0.62	0.55	1.57	1.44	0.27	0.26	0.37	0.34
	Average	1.37	1.32	3.55	3.45	1.42	0.98	1.35	1.30

Table 8.13: Deviation from Experimental Data on Ethane/n-Pentane

Ternary Systems

Contrary to the situation on binary systems, there are few available works done evaluating surface tension on ternary hydrocarbon systems. In this thesis, only two different systems will be analyzed, one containing methane, ethane and n-pentane, the other methane, propane and n-decane. Contrary to analyzing binary systems, composition now affects the surface tension, and therefore works done on the same system may differ with regards to the composition.

Methane + Ethane + n-Pentane The first report, on methane, ethane and propane, has been taken from the works of Nilssen et al. [35]. As for the experiment on the binary system of ethane and propane performed by Nilssen et al., this work examines one temperature, 21°C, as well. This work has been divided into three, separated by different compositions. Figure 8.19 shows the three compositions in one graph. Composition 1, as numerated in the graph, contains 17.46mol% methane, 3.08mol% ethane and 79.40mol% n-pentane. Composition 2 contains 34.20mol% methane, 6.04mol% ethane and 59.76mol% n-pentane. Finally, composition 3 contains 50.61mol% methane, 8.93mol% ethane and 40.46mol% n-pentane. Each composition has been evaluated within a small pressure range, which in total spans from 16 to 78 bar. These parameters produces surface tensions from 4.3 to 12.8 mN/m.

The immediate difference to binary systems is that PVTsim is now producing as good results as NeqSim, if not better. The details are shown in table 8.14. Looking at the deviations of PVTsim and NeqSim to the experimental data, it is clear that overall PVTsim PR is performing better. NeqSim PR is not much off though, and on the second composition it actually performs better. It appears there is a shift in performance around this pressure, which might be attributed to the pressure rather than composition. According to calculations, the surface tension would alter by only 2.2-3.6% if one used composition 1 over the whole pressure range, compared to changing the composition.

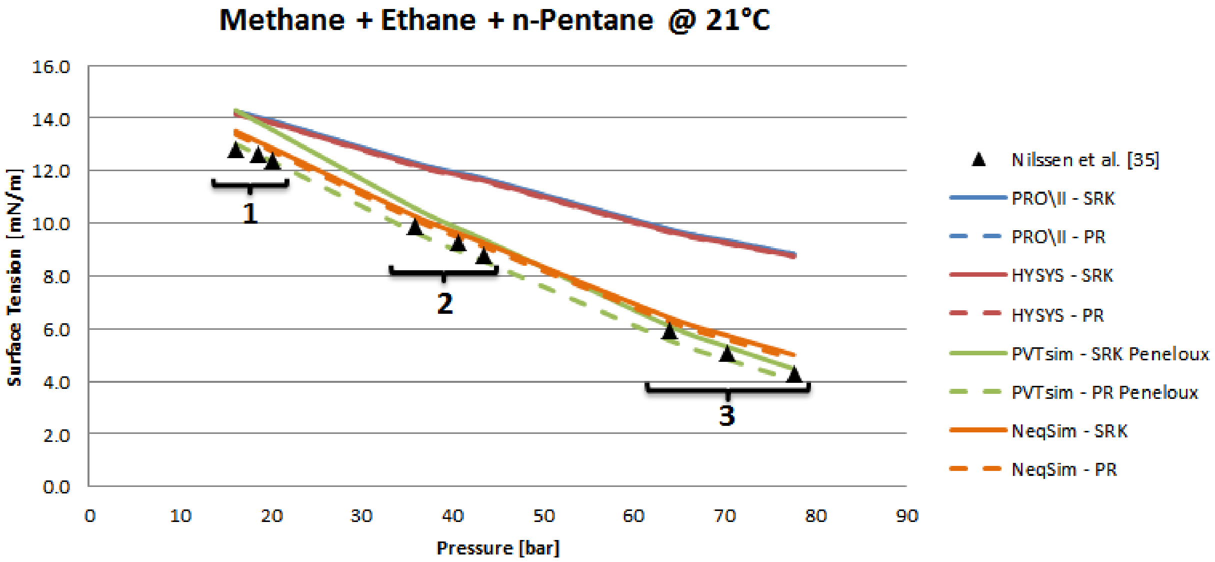

Figure 8.19: Methane + Ethane + n-Pentane

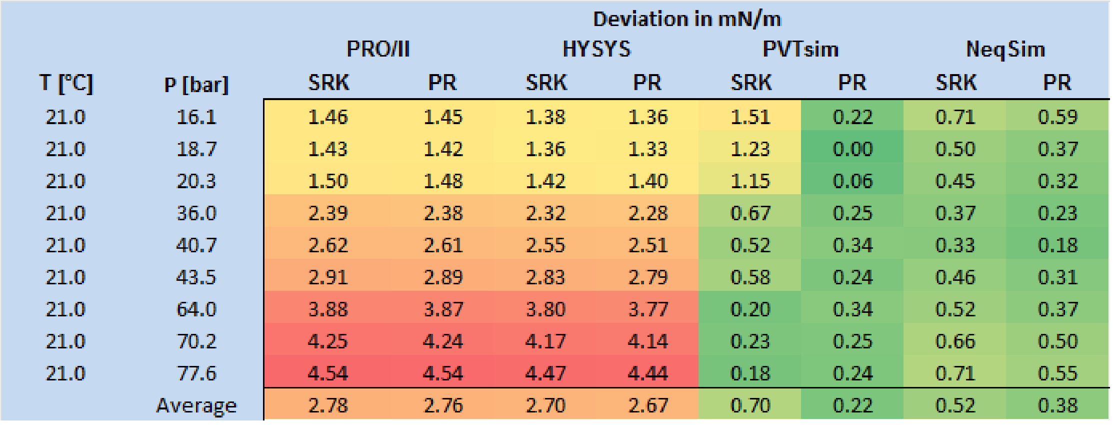

		Deviation in mN/m							
		PRO/II		HYSYS		PVTsim		NeqSim	
T [°C]	P [bar]	SRK	PR	SRK	PR	SRK	PR	SRK	PR
21.0	16.1	1.46	1.45	1.38	1.36	1.51	0.22	0.71	0.59
21.0	18.7	1.43	1.42	1.36	1.33	1.23	0.00	0.50	0.37
21.0	20.3	1.50	1.48	1.42	1.40	1.15	0.06	0.45	0.32
21.0	36.0	2.39	2.38	2.32	2.28	0.67	0.25	0.37	0.23
21.0	40.7	2.62	2.61	2.55	2.51	0.52	0.34	0.33	0.18
21.0	43.5	2.91	2.89	2.83	2.79	0.58	0.24	0.46	0.31
21.0	64.0	3.88	3.87	3.80	3.77	0.20	0.34	0.52	0.37
21.0	70.2	4.25	4.24	4.17	4.14	0.23	0.25	0.66	0.50
21.0	77.6	4.54	4.54	4.47	4.44	0.18	0.24	0.71	0.55
	Average	2.78	2.76	2.70	2.67	0.70	0.22	0.52	0.38

Table 8.14: Deviation from Experimental Data on Methane/Ethane/n-Pentane

Methane + Propane + n-Decane The second and last ternary system consists of methane, propane and n-decane. The work was carried out by Fotland and Bjørlykke [18], and consists of experiments performed on two different samples of composition, shown in table 8.15. The work done on this report is rather extensive regarding data points, counting 91 unique conditions, and the temperature ranges from $20°C$ to $97°C$. However, the pressure used in the experimental work is relatively high, ranging from 105.9 to 272.6 bar. The high pressure is because the scope of this work was to test out the laser light scattering method, which was new in the late 80's and enabled scientists to work at a higher pressure than normal. In turn, this results in low surface tensions, ranging from 0.001 - 1.6 mN/m.

Component	Sample 1	Sample 2
Methane	0.815	0.717
Propane	0.111	0.209
n-Decane	0.074	0.074

Table 8.15: Composition of the Two Samples Given in Mole Fractions

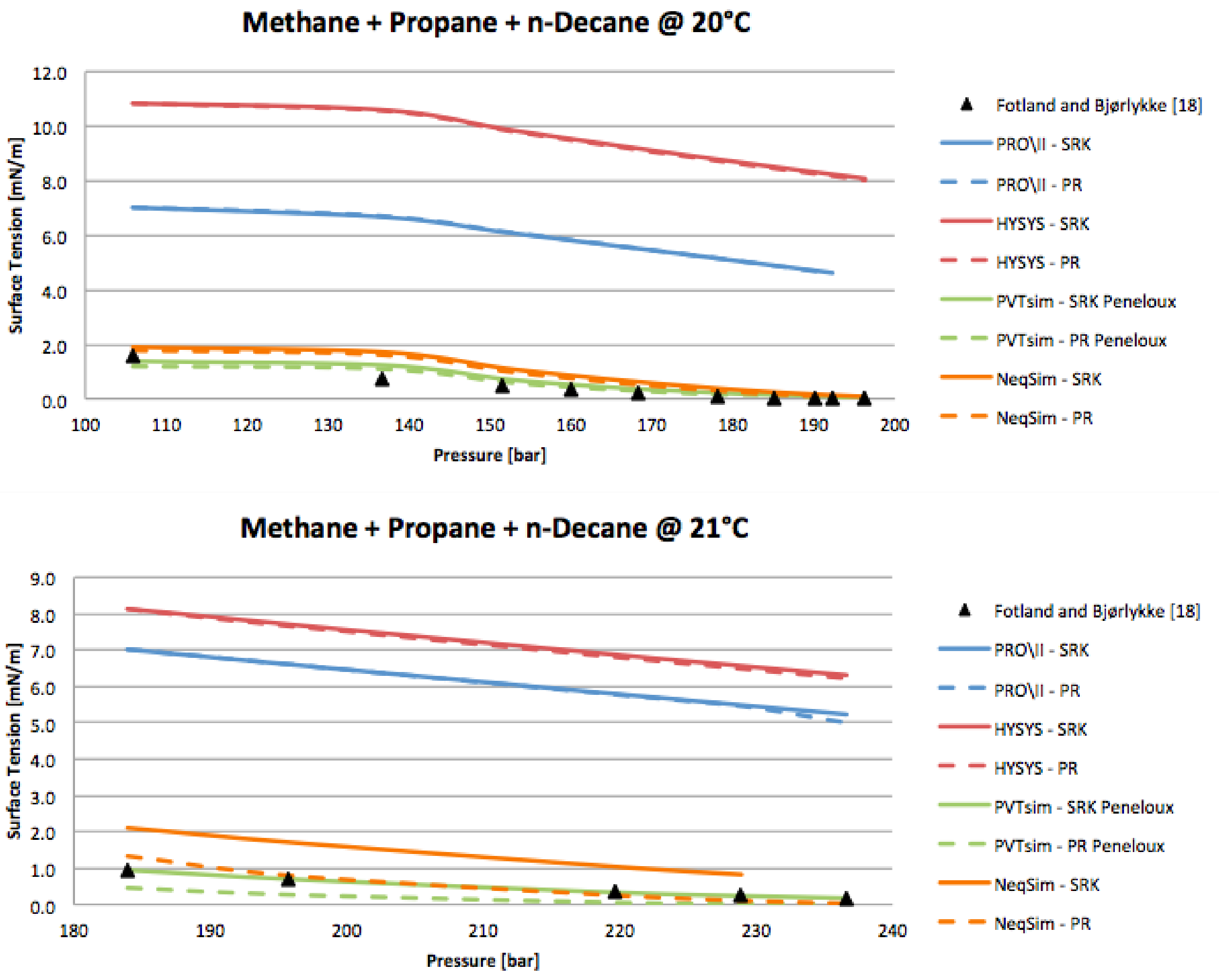

Figure 8.20: Methane + Propane + n-Decane

Figure 8.20 shows the two samples at their lowest temperatures, 20°C and 21°C, respectively. Note that the abscissas are not equal, given that the pressure range is shifted. Nevertheless, the same trends are present as what was observed for the methane/ethane/n-pentane mix. PVTsim and NeqSim are providing good results, whereas PRO/II and HYSYS are overestimating the surface tension. Details are given in tables 8.16 and 8.17.

		Deviation in mN/m							
		PRO/II		HYSYS		PVTsim		NeqSim	
T [°C]	P [bar]	SRK	PR	SRK	PR	SRK	PR	SRK	PR
21.0	183.9	6.10	6.11	7.23	7.19	0.04	0.46	1.19	0.24
21.0	195.7	5.92	5.92	7.02	6.98	0.01	0.42	1.03	0.11
21.0	219.7	5.42	5.40	6.50	6.43	0.05	0.32	0.66	0.13
21.0	228.9	5.24	5.21	6.31	6.24	0.02	0.24	0.57	0.14
21.0	236.6	5.07		6.15	6.06	0.01	0.16		0.14
	Average	5.55	5.66	6.64	6.58	0.02	0.32	0.86	0.15

Table 8.16: Deviation of Methane + Propane + n-Decane Sample 2 to Experimental Data @ 21°C

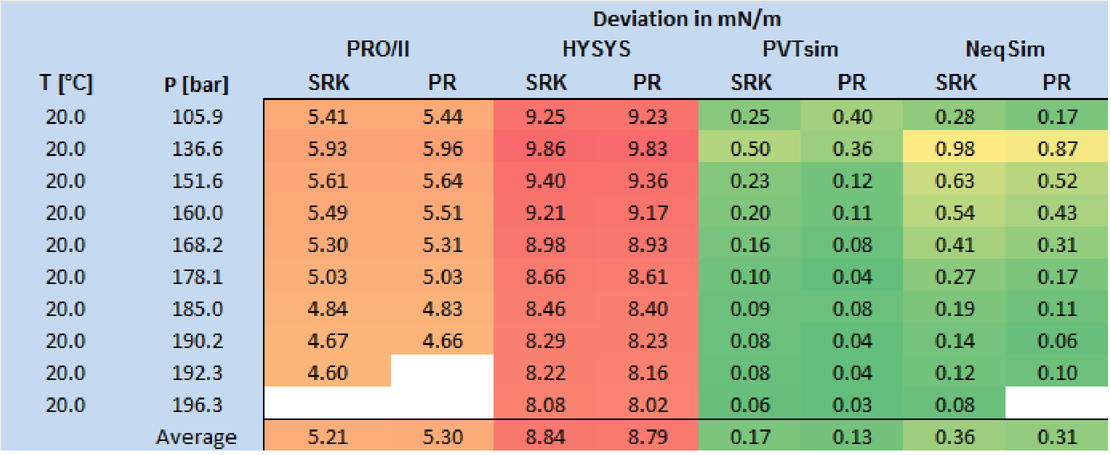

		Deviation in mN/m							
		PRO/II		HYSYS		PVTsim		NeqSim	
T [°C]	P [bar]	SRK	PR	SRK	PR	SRK	PR	SRK	PR
20.0	105.9	5.41	5.44	9.25	9.23	0.25	0.40	0.28	0.17
20.0	136.6	5.93	5.96	9.86	9.83	0.50	0.36	0.98	0.87
20.0	151.6	5.61	5.64	9.40	9.36	0.23	0.12	0.63	0.52
20.0	160.0	5.49	5.51	9.21	9.17	0.20	0.11	0.54	0.43
20.0	168.2	5.30	5.31	8.98	8.93	0.16	0.08	0.41	0.31
20.0	178.1	5.03	5.03	8.66	8.61	0.10	0.04	0.27	0.17
20.0	185.0	4.84	4.83	8.46	8.40	0.09	0.08	0.19	0.11
20.0	190.2	4.67	4.66	8.29	8.23	0.08	0.04	0.14	0.06
20.0	192.3	4.60		8.22	8.16	0.08	0.04	0.12	0.10
20.0	196.3			8.08	8.02	0.06	0.03	0.08	
	Average	5.21	5.30	8.84	8.79	0.17	0.13	0.36	0.31

Table 8.17: Deviation of Methane + Propane + n-Decane Sample 1 to Experimental Data @ 20°C

Gas Condensate Systems

Similar to the situation on ternary systems, data on more complex gas condensate systems are limited compared to binary hydrocarbon systems. In this thesis, the experimental data of two reports have been evaluated, namely Danesh et al. [12] and Heng et al. [22].

Danesh et al. The report by Danesh et al. [12] targeted to improve the prediction of surface tension of gas condensate systems by using a modified scaling law and parachor method. In doing so, five and twenty-component mixtures were selected and prepared to model real gas condensate fluids. The compositions of the tested fluids are given in table 8.18 and 8.19. The surface tension was determined by measuring the gas condensate interface curvature in an equilibrium cell. The two five-component mixtures A and B had similar components and were tested at 40°C and 80°C, and 30°C and 35°C, respectively. Pressures are ranging from 125.0 bar to 304.2 bar. Fluid C is measured at 65.5°C, 93.3°C and 121.1°C, using pressures all above 330 bar. Given the high pressures and temperatures, surface tensions are relatively low, ranging from a low of 0.1 mN/m to 4.2 mN/m at the most.

Component	Fluid A Mole(%)	Fluid B Mole(%)
C1	82.05	82.32
C3	8.95	8.71
nC5	5.00	5.05
nC10	1.99	1.98
nC16	2.01	1.94

Table 8.18: Composition of Fluid A and B

Figures 8.21, 8.22 and 8.24 show the surface tension of three compositions at 40°C, 35°C and 65.5°C, respectively. Again, take note of the abscissas, as they are unequal due to the high pressures.

Component	Mole(%)	Component	Mole(%)
C1	80.11	nC11	0.45
C2	8.23	nC12	0.44
C3	2.11	nC13	0.44
nC4	1.07	nC14	0.41
nC5	0.80	nC15	0.41
nC6	1.20	nC16	0.39
nC7	0.96	nC17	0.38
nC8	0.55	nC18	0.37
nC9	0.49	nC19	0.36
nC10	0.48	nC20	0.35

Table 8.19: Composition of Fluid C

Figure 8.21 shows the five-component fluid A. This is the fluid used at the lowest pressures, ranging from 125 to 276.6 bar. Additionally, it is the experimental setup that yielded the most data points. Interestingly, a lot of the same features as were observed for binary hydrocarbon systems again manifest themselves. PRO/II and HYSYS are overestimating, HYSYS even more than PRO/II, whereas PVTsim and NeqSim are again providing good results, with NeqSim providing results just above PVTsim. This is normal, however, contrary to what was observed for ternary hydrocarbon systems, where NeqSim and PVTsim both were overestimating, PVTsim are now underestimating. NeqSim are providing results missing by only 0.32 mN/m and 0.21 mN/m on average for SRK and PR, respectively. Details are shown in table 8.20.

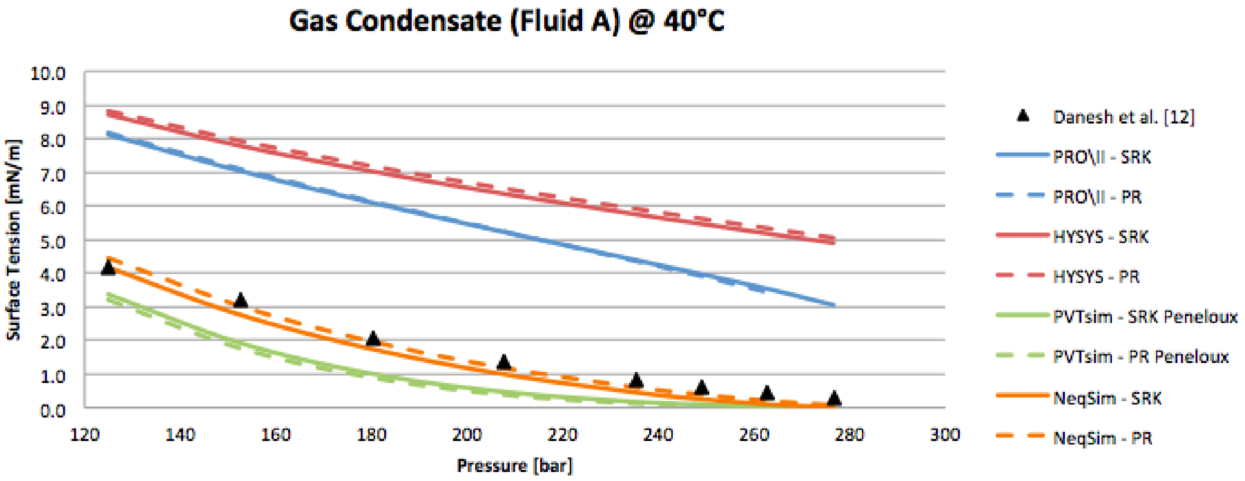

Figure 8.21: Surface Tension for Danesh Fluid A @ 40°C

Figure 8.22 shows the other five-component fluid, fluid B. As table 8.18 reveals, the fluids are very similar in composition, however only the higher specter of pressure is tested compared to experiments done on fluid A. Hence, there are fewer data points. Worth noticing is that PRO/II PR is unable to produce results under these conditions. In addition, PVTsim PR and NeqSim SRK fail to give results at the highest pressure. Figure 8.23 shows the phase envelope for fluid B at 35°C and

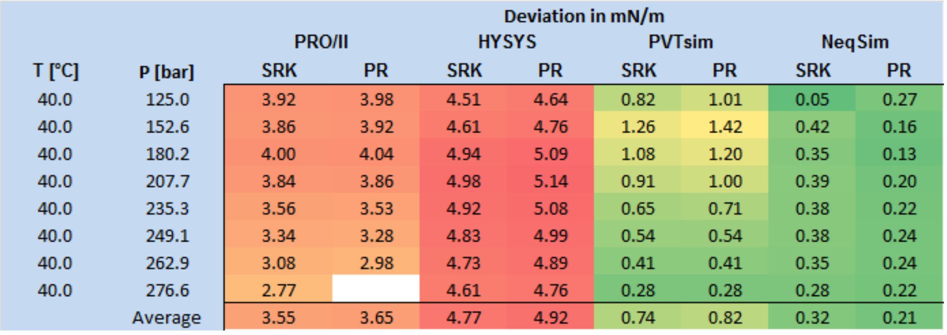

		Deviation in mN/m							
		PRO/II		HYSYS		PVTsim		NeqSim	
T [°C]	P [bar]	SRK	PR	SRK	PR	SRK	PR	SRK	PR
40.0	125.0	3.92	3.98	4.51	4.64	0.82	1.01	0.05	0.27
40.0	152.6	3.86	3.92	4.61	4.76	1.26	1.42	0.42	0.16
40.0	180.2	4.00	4.04	4.94	5.09	1.08	1.20	0.35	0.13
40.0	207.7	3.84	3.86	4.98	5.14	0.91	1.00	0.39	0.20
40.0	235.3	3.56	3.53	4.92	5.08	0.65	0.71	0.38	0.22
40.0	249.1	3.34	3.28	4.83	4.99	0.54	0.54	0.38	0.24
40.0	262.9	3.08	2.98	4.73	4.89	0.41	0.41	0.35	0.24
40.0	276.6	2.77		4.61	4.76	0.28	0.28	0.28	0.22
	Average	3.55	3.65	4.77	4.92	0.74	0.82	0.32	0.21

Table 8.20: Deviation to Experimental Surface Tension for Danesh Fluid A @ 40°C

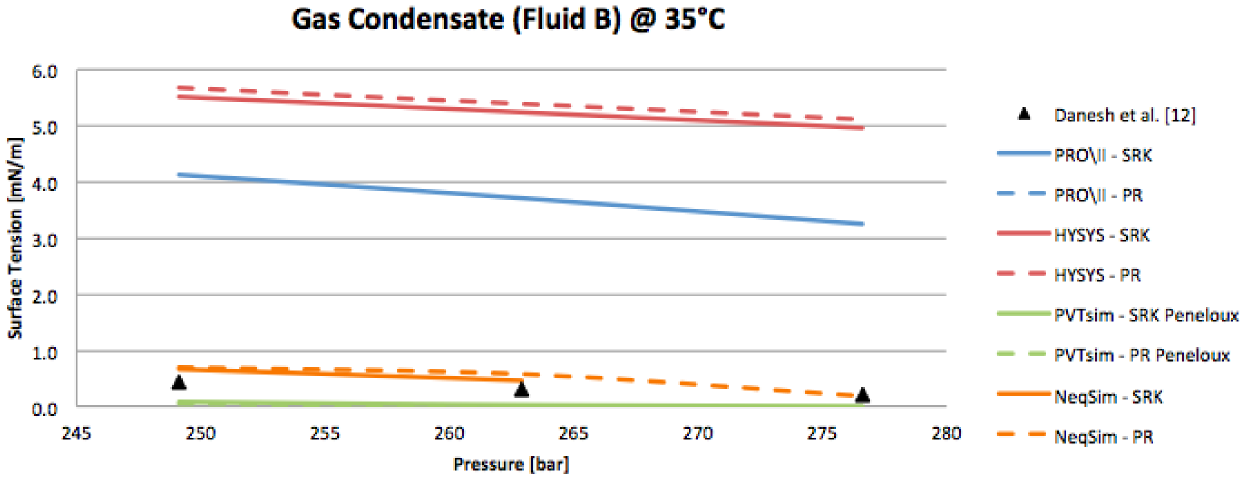

Figure 8.22: Surface Tension for Danesh Fluid B @ 35°C

276.6 bar using NeqSim SRK. As experimental conditions are approaching critical conditions, as in this case, not all software are able to produce results. This explains the blanks in table 8.21. Otherwise, the rest of the results, comparing table 8.21 to table 8.20, coincide with fluid A.

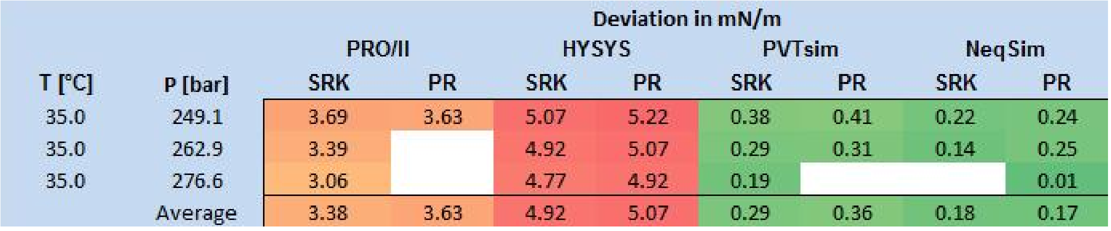

		Deviation in mN/m							
		PRO/II		HYSYS		PVTsim		NeqSim	
T [°C]	P [bar]	SRK	PR	SRK	PR	SRK	PR	SRK	PR
35.0	249.1	3.69	3.63	5.07	5.22	0.38	0.41	0.22	0.24
35.0	262.9	3.39		4.92	5.07	0.29	0.31	0.14	0.25
35.0	276.6	3.06		4.77	4.92	0.19			0.01
	Average	3.38	3.63	4.92	5.07	0.29	0.36	0.18	0.17

Table 8.21: Deviation to Experimental Surface Tension for Danesh Fluid B @ 35°C

Figure 8.24 shows the twenty-component fluid, fluid C. As stated above, the pressure applied on fluid C is exclusively above 330 bar. Again, this implies extremely low surface tension, which in the critical area means that some software do not produce results.

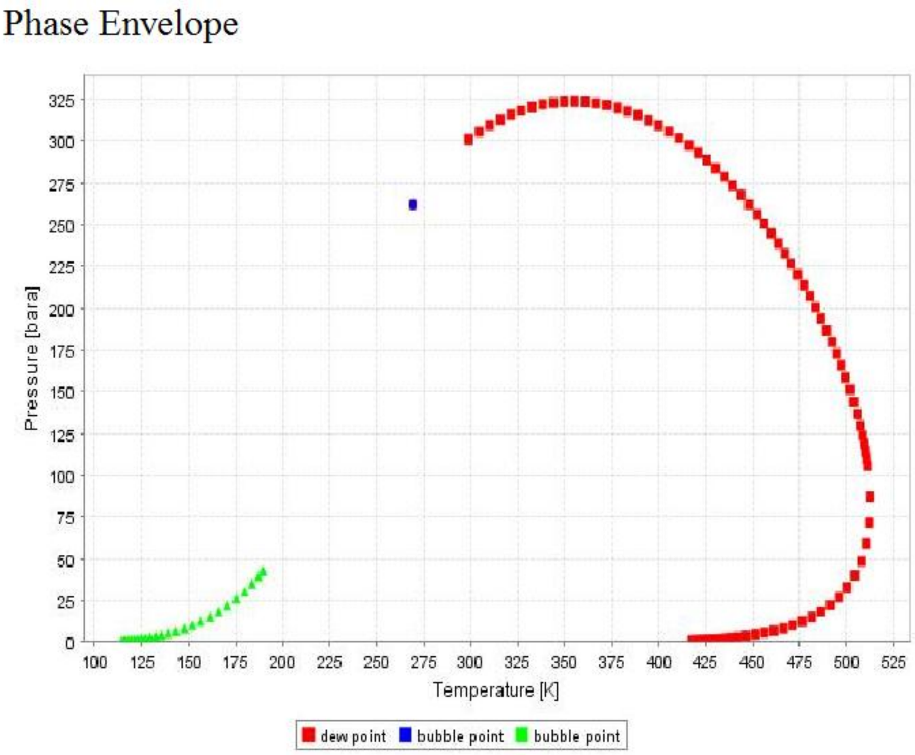

Figure 8.23: NeqSim Phase Envelope for Fluid B @ 35°C and 276.6 bar

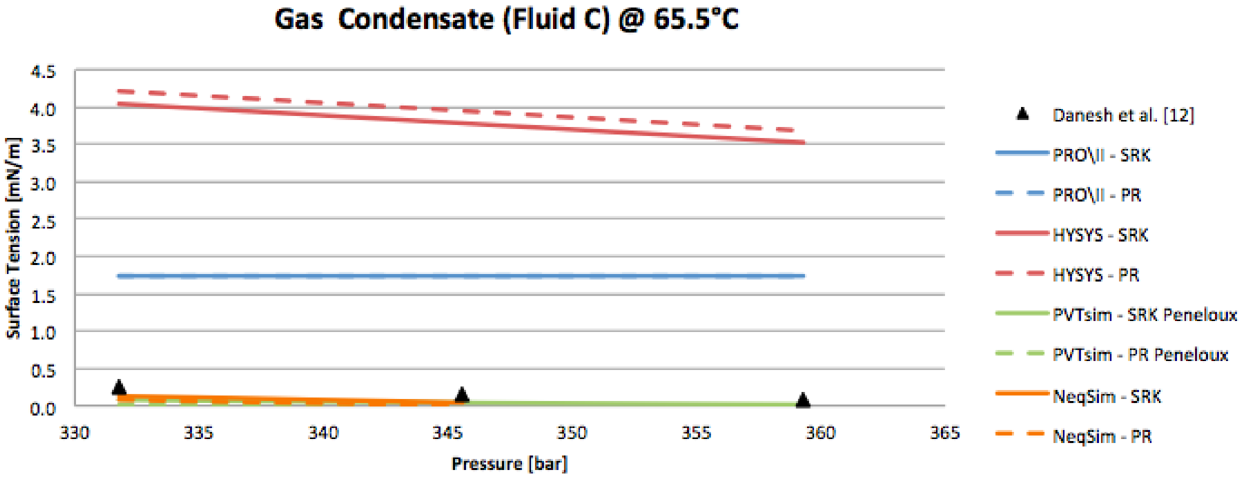

Figure 8.24: Surface Tension for Danesh Fluid C @ 65.5°C

Heng et al. The two last systems evaluated on gas condensate were taken from the report of Heng et al. [22], in co-operation with Oilphase-DBR Schlumberger. From this report it is deducted two hydrocarbon systems named Wet Gas and Associate Gas, whose composition are given in table 8.22. The two gas compositions were meant to represent a somewhat rich natural gas, and an associate gas (GOR about 1700). The measurement method used was the capillary rise method.

The wet gas surface tension was evaluated at four temperatures: -45.6°C, -17.8°C, 10°C and 37.8°C. Pressures ranging from 13.8 - 103.4 bar. This span of temperature and pressure results in surface tensions ranging from 0.2 - 13.6 mN/m. There are few data points and at 37.8°C, there is only one. However, at 10°C four measurements are done. Consequently, this represents the largest span in both pressure and surface tension, and is thus well suited for analysis. It is shown in figure 8.25.

Component	Wet Gas mole(%)	Ass. Gas mole(%)
C1	67.67	58.68
C2	19.17	4.98
C3	7.68	1.94
nC4	3.88	0.98
nC7	0.53	4.49
Mcyclo-C6	0.53	4.42
Toluene	0.53	4.74
n-C10		5.09
3-Methylnonane		5.16
Butylcyclo-C6		5.00
1,3-Diethylbenzene		5.00

Table 8.22: Composition of Wet and Associate Gas

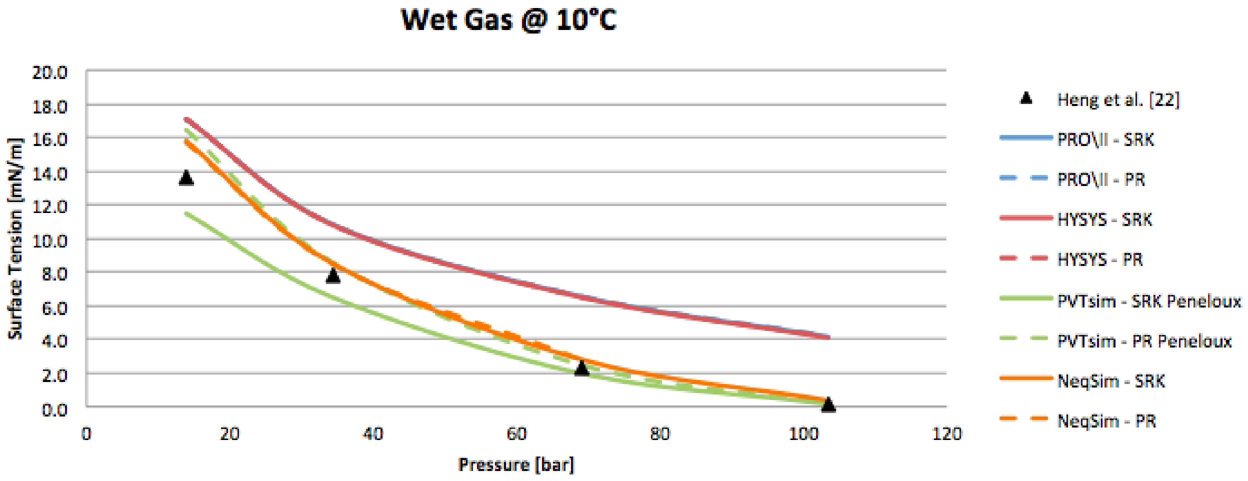

Figure 8.25: Surface Tension for GPA Wet Gas @ 10°C

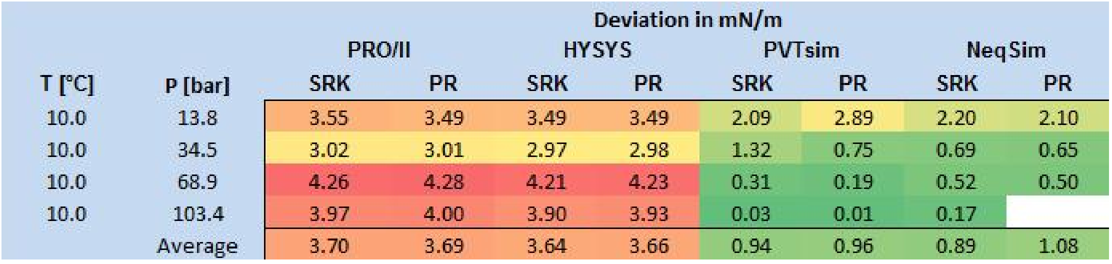

		Deviation in mN/m							
		PRO/II		HYSYS		PVTsim		NeqSim	
T [°C]	P [bar]	SRK	PR	SRK	PR	SRK	PR	SRK	PR
10.0	13.8	3.55	3.49	3.49	3.49	2.09	2.89	2.20	2.10
10.0	34.5	3.02	3.01	2.97	2.98	1.32	0.75	0.69	0.65
10.0	68.9	4.26	4.28	4.21	4.23	0.31	0.19	0.52	0.50
10.0	103.4	3.97	4.00	3.90	3.93	0.03	0.01	0.17	
	Average	3.70	3.69	3.64	3.66	0.94	0.96	0.89	1.08

Table 8.23: Deviation to Experimental Surface Tension for GPA Wet Gas @ 10°C

Still, even though they might appear to be improving, PRO/II and HYSYS are overestimating by about 3.6 - 3.7 mN/m (see table 8.23). Again, on average, NeqSim just outperform PVTsim, except for at the lowest surface tension.

Lastly, the associate gas is analyzed. There is somewhat more consistency in the experiments carried out on the associate gas. There are three temperatures. 10°C, which coincides with the temperature evaluated for wet gas, 37.8°C and 93.3°C. In addition, the pressures applied are equal, ranging from 13.8 bar in all three cases and up to 137.9 bar for 10°C and 172.4 bar for the last two. Surface tensions range from 2.3 - 18.1 mN/m.

Figure 8.26 shows the experimental data along with the software results for the associate gas at 10°C, to be able to compare with the wet gas. Interestingly, there is now an overestimation of the surface tension from both PVTsim and NeqSim to start off with. It appears that the heavier components added to the associate gas represents a problem for the ability to calculate accurate surface tensions. Figure 8.27 shows how this overestimation decays and disappears as temperature is increased. Table 8.24 and 8.25 show the deviations. On average, NeqSim PR is now the best performer throughout.

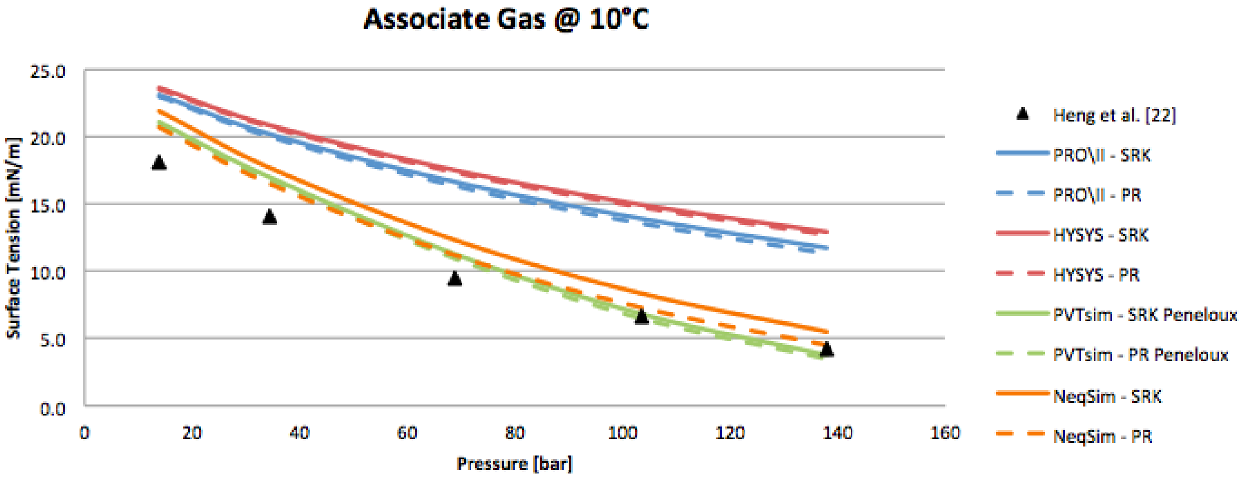

Figure 8.26: Surface Tension for GPA Associate Gas @ 10°C

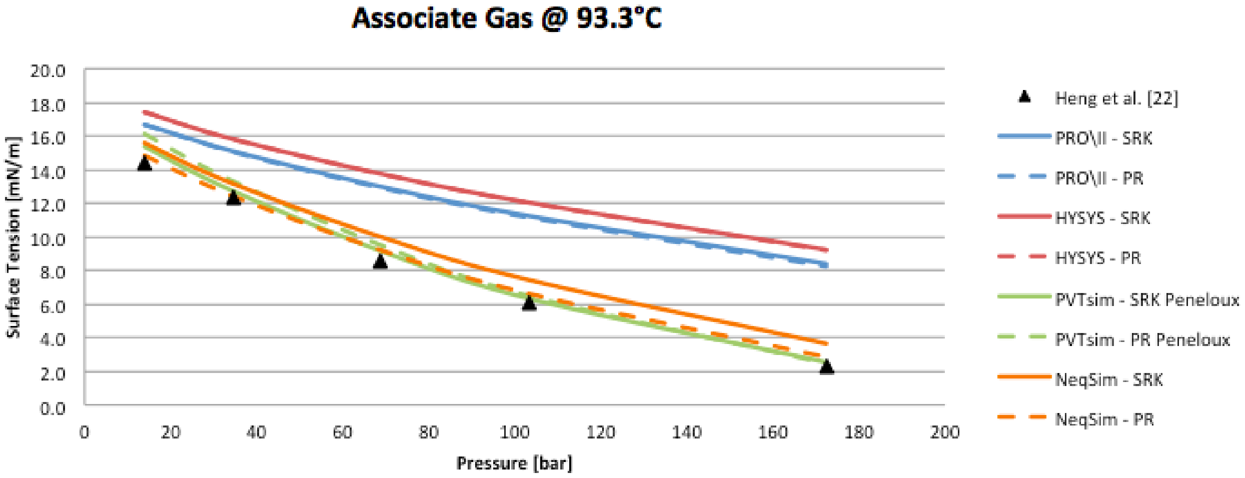

Figure 8.27: Surface Tension for GPA Associate Gas 93.3°C

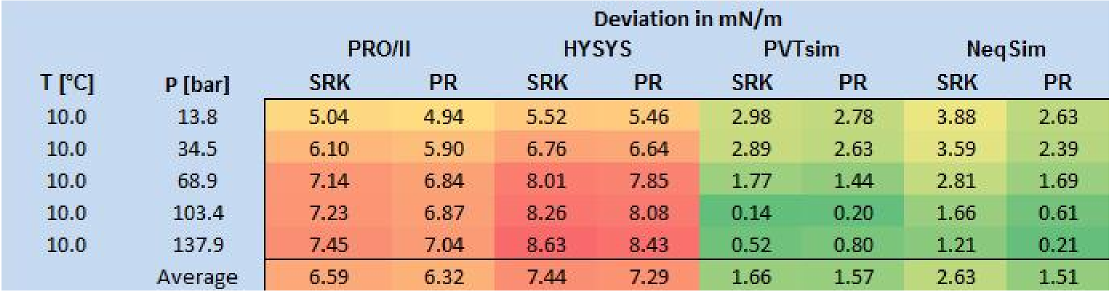

		Deviation in mN/m							
		PRO/II		HYSYS		PVTsim		NeqSim	
T [°C]	P [bar]	SRK	PR	SRK	PR	SRK	PR	SRK	PR
10.0	13.8	5.04	4.94	5.52	5.46	2.98	2.78	3.88	2.63
10.0	34.5	6.10	5.90	6.76	6.64	2.89	2.63	3.59	2.39
10.0	68.9	7.14	6.84	8.01	7.85	1.77	1.44	2.81	1.69
10.0	103.4	7.23	6.87	8.26	8.08	0.14	0.20	1.66	0.61
10.0	137.9	7.45	7.04	8.63	8.43	0.52	0.80	1.21	0.21
	Average	6.59	6.32	7.44	7.29	1.66	1.57	2.63	1.51

Table 8.24: Deviation to Experimental Surface Tension for GPA Associate Gas @ $10°C$

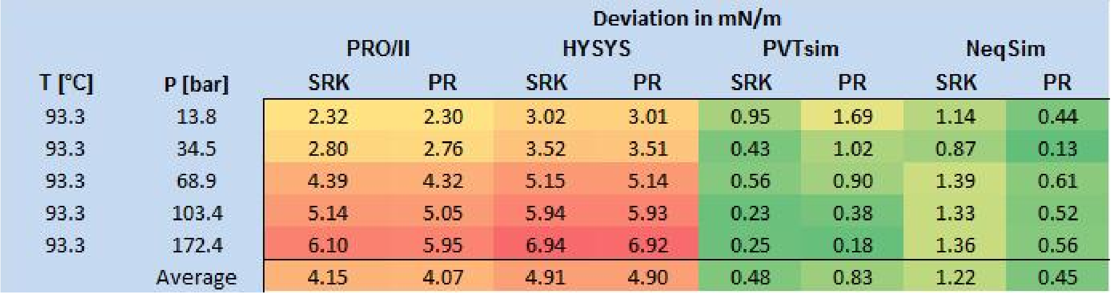

		Deviation in mN/m							
		PRO/II		HYSYS		PVTsim		NeqSim	
T [°C]	P [bar]	SRK	PR	SRK	PR	SRK	PR	SRK	PR
93.3	13.8	2.32	2.30	3.02	3.01	0.95	1.69	1.14	0.44
93.3	34.5	2.80	2.76	3.52	3.51	0.43	1.02	0.87	0.13
93.3	68.9	4.39	4.32	5.15	5.14	0.56	0.90	1.39	0.61
93.3	103.4	5.14	5.05	5.94	5.93	0.23	0.38	1.33	0.52
93.3	172.4	6.10	5.95	6.94	6.92	0.25	0.18	1.36	0.56
	Average	4.15	4.07	4.91	4.90	0.48	0.83	1.22	0.45

Table 8.25: Deviation to Experimental Surface Tension for GPA Associate Gas @ $93.3°C$

8.1.2 Glycol systems

This section is divided into three parts: 100wt% MEG, 80wt% MEG/20wt% water and 50wt% MEG/50wt% water. Each part containing a comparison between the two gas mixtures used with the MEG mixtures, namely 100mol% methane and 85mol% methane/15 mol% ethane. The experimental matrices are shown in table 7.2 and 7.3, and the reader is referred to chapter 7 for a more thorough description of the mixtures. When analyzing the software performance on glycol systems, some specific points of interest are weighted:

- How does NeqSim perform compared to the other software?
- Internally in NeqSim, which of the Equations of State (CPA, SRK and PR) gives the best results?
- General tendencies with change in temperature and pressure?
- How does the introduction of ethane in the mixture affect the result?
- How does the quantity of water in the mixture affect the result?

Some specific points regarding glycol systems must be explained before the discussion part can begin. First of all it is not possible to simulate a glycol mixture with SRK in HYSYS. Aspen HYSYS wants you to simulate glycol systems with PR. Additionally, in NeqSim the CPA EoS is used in addition to SRK and PR. This is because CPA EoS is regarded as most accurate when simulating glycol mixtures. Lastly, the Peneloux volume correction in PVTsim is not used when simulating glycol mixtures. This is due to the fact that regular SRK and PR performs better.

100wt% MEG

Figures 8.28 and 8.29 are used to illustrate the general tendencies of how the software perform on the 100wt% MEG liquid mixture. For more data describing this mixture the reader is referenced to appendix A.2. It is evident from these figures that all the software overestimate the surface tension, but PVTsim clearly has the highest discrepancy from the experimental data. This is because the model implemented in PVTsim is for simulation of water and hydrocarbons and not for MEG, hence it has very poor performance when only MEG is present in the aqueous phase. Therefore PVTsim will perform better when the system contains more water. The reader is referred to section 3.2.1 for a review of the model.

PRO/II and HYSYS are performing well at the lowest pressures, but as the pressure is increasing the discrepancy is also increasing. The absolute deviation of the different software from the 100wt% MEG + methane and 100wt% MEG + methane/ethane mixtures at 20°C are given in tables 8.26 and 8.27. When studying PRO/II and HYSYS the tables clearly shows that the deviation is larger at high pressures. Looking at table 8.26 the deviation for PRO/II PR at 22.3 bar is 4.43 mN/m, while at 131.4 bar the deviation is as high as 16.33 mN/m. This is almost a quadrupling of the deviation. The experimental data has a declining trend with increasing pressure, while PRO/II and HYSYS produce data that is almost constant with increasing pressure. This is due to fairly simple weighted average pure-component models, which are explained in section 3.2 and chapter 4. This will be the case for all mixtures in this section.

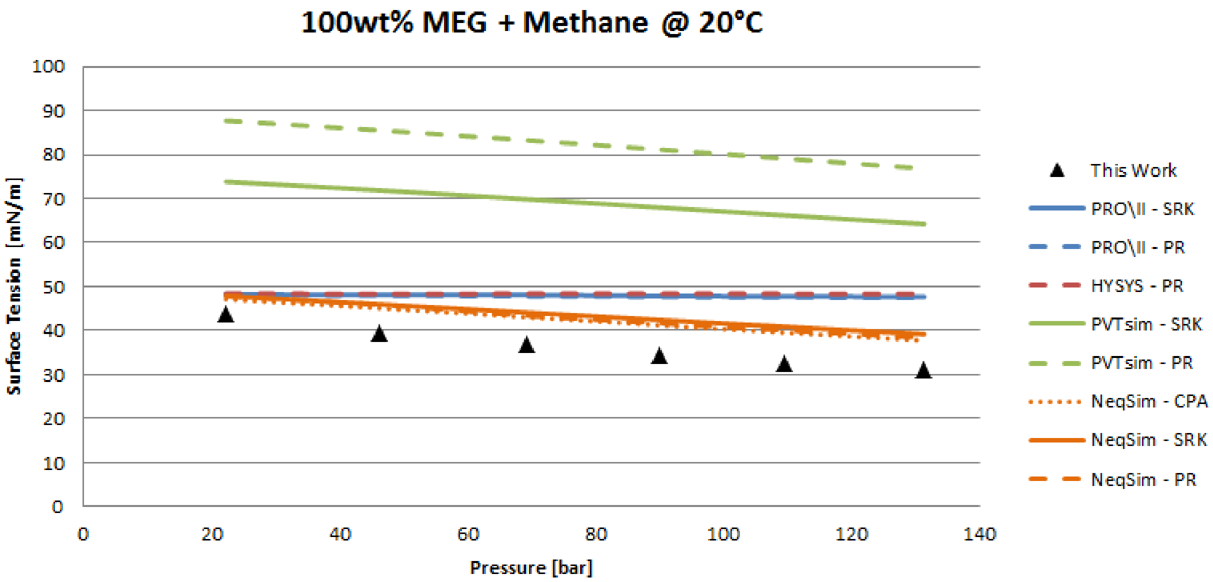

Figure 8.28: 100wt% MEG + Methane

NeqSim is the software with the best performance over the entire pressure range, but NeqSim is also overestimating the surface tension and has its largest discrepancy at the highest pressure. How the different EoS performs internally in NeqSim are shown in figures 8.30 and 8.31. These are the same graphs as in figures 8.28 and 8.29, but now showing only NeqSim. The different EoS follow the same trend and are quite consistent. Looking at tables 8.26 and 8.27 we can do a comparison between the three EoS in NeqSim. The CPA model performs better than PR and

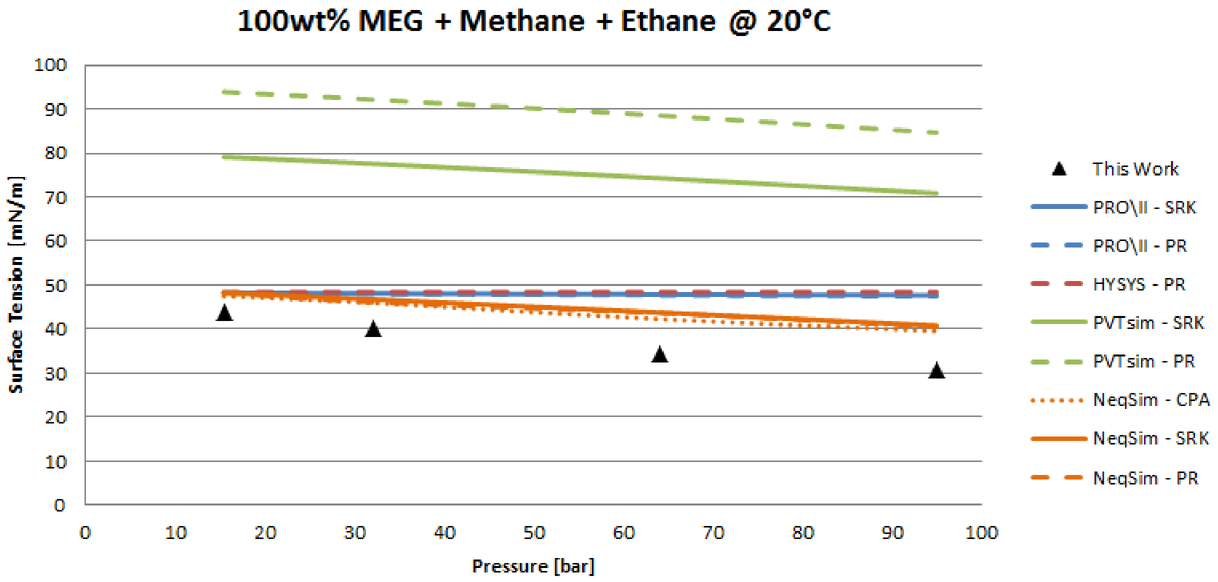

Figure 8.29: 100wt% MEG + Methane/Ethane

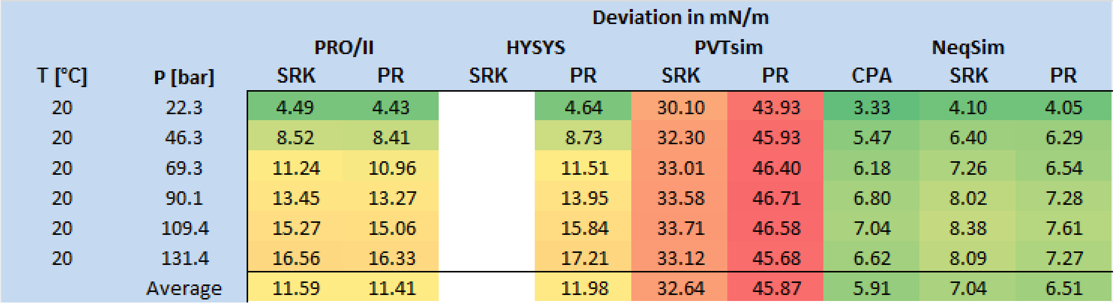

		Deviation in mN/m								
		PRO/II		HYSYS		PVTsim			NeqSim	
T [°C]	P [bar]	SRK	PR	SRK	PR	SRK	PR	CPA	SRK	PR
20	22.3	4.49	4.43		4.64	30.10	43.93	3.33	4.10	4.05
20	46.3	8.52	8.41		8.73	32.30	45.93	5.47	6.40	6.29
20	69.3	11.24	10.96		11.51	33.01	46.40	6.18	7.26	6.54
20	90.1	13.45	13.27		13.95	33.58	46.71	6.80	8.02	7.28
20	109.4	15.27	15.06		15.84	33.71	46.58	7.04	8.38	7.61
20	131.4	16.56	16.33		17.21	33.12	45.68	6.62	8.09	7.27
	Average	11.59	11.41		11.98	32.64	45.87	5.91	7.04	6.51

Table 8.26: Deviation of the 100wt% MEG + Methane Mixture

SRK at all pressure points, and the average deviations for the 100wt% MEG + methane mixture are 5.91, 7.04 and 6.51 mN/m for respectively CPA, SRK and PR. It is clear that the discrepancy is increasing when ethane is used in the mixture. The average deviation for the CPA increases from 5.91 mN/m to 6.64 mN/m because of the introduction of ethane. This relationship applies to all of the EoS. At 90.09 bar the deviation for the 100wt% MEG + methane mixture is 6.80, 8.02 and 7.28 mN/m for respectively CPA, SRK and PR. At 95.01 bar the deviation for the 100wt% MEG + methane/ethane mixture is 8.94, 10.13 and 9.90 mN/m.

The figure 8.32 show how the software perform at 5°C, and the table 8.28 display the deviation. We now compare the 100wt% MEG + methane/ethane mixture at

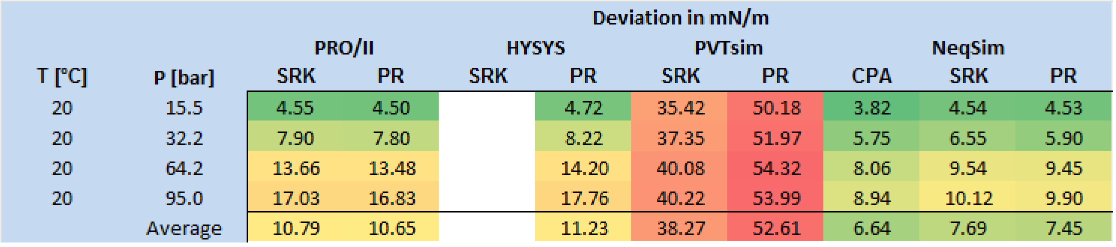

		Deviation in mN/m								
		PRO/II		HYSYS		PVTsim			NeqSim	
T [°C]	P [bar]	SRK	PR	SRK	PR	SRK	PR	CPA	SRK	PR
20	15.5	4.55	4.50		4.72	35.42	50.18	3.82	4.54	4.53
20	32.2	7.90	7.80		8.22	37.35	51.97	5.75	6.55	5.90
20	64.2	13.66	13.48		14.20	40.08	54.32	8.06	9.54	9.45
20	95.0	17.03	16.83		17.76	40.22	53.99	8.94	10.12	9.90
	Average	10.79	10.65		11.23	38.27	52.61	6.64	7.69	7.45

Table 8.27: Deviation of the 100wt% MEG + Methane/Ethane Mixture

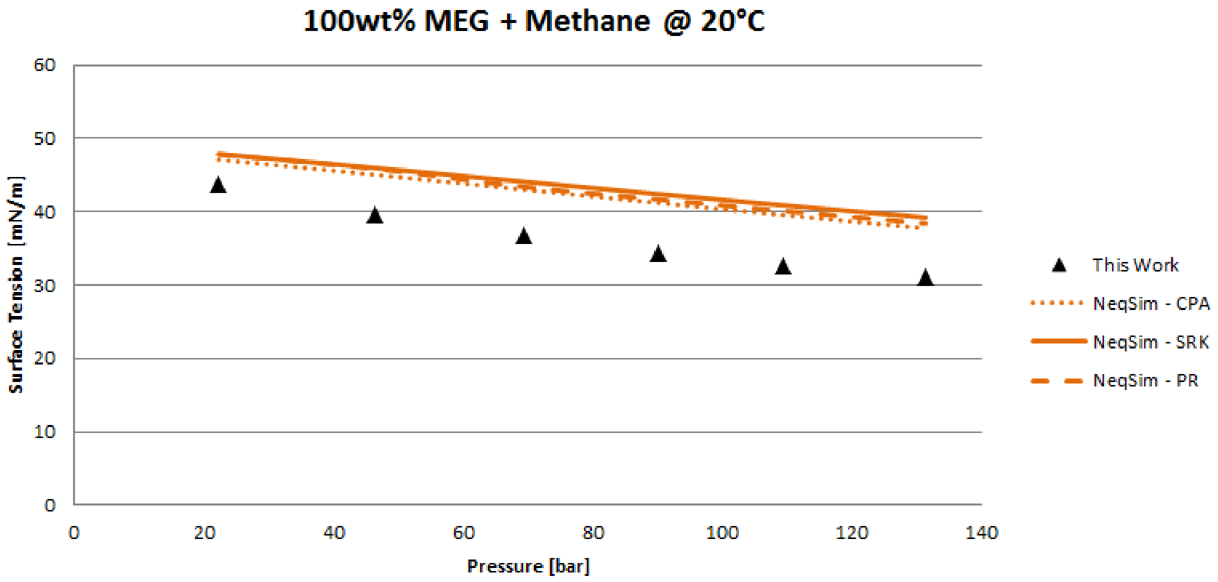

Figure 8.30: 100wt% MEG + Methane

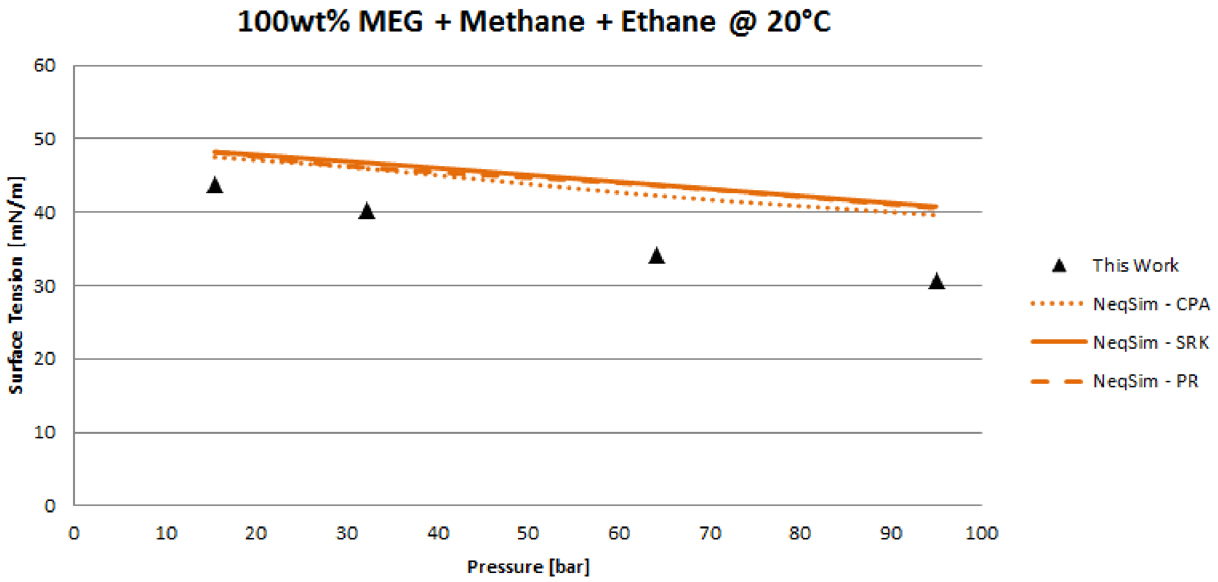

Figure 8.31: 100wt% MEG + Methane/Ethane

the two different temperatures. At 20°C the average deviation is 6.64, 7.69 and 7.45 mN/m for respectively CPA, SRK and PR. At 5°C the average deviation is 9.25, 11.11 and 10.97 mN/m. This clearly shows that the deviation of NeqSim from experimental data is higher at low temperatures. This relationship is valid for all software. Also the performance internally in NeqSim is equal to that of 20°C with CPA being the most accurate model.

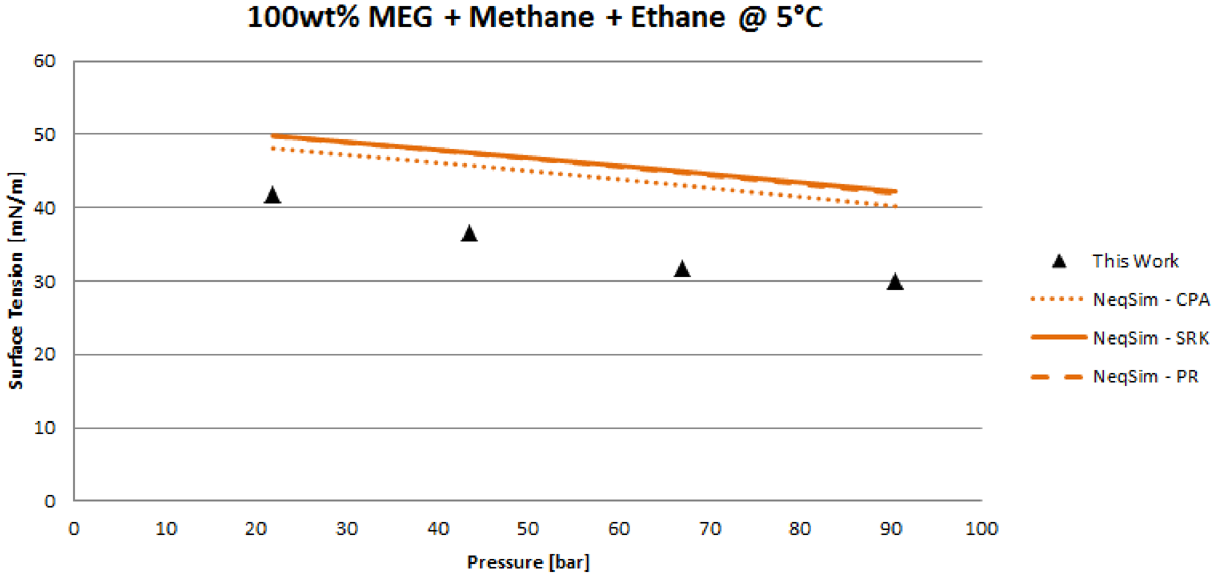

Figure 8.32: 100wt% MEG + Methane/Ethane

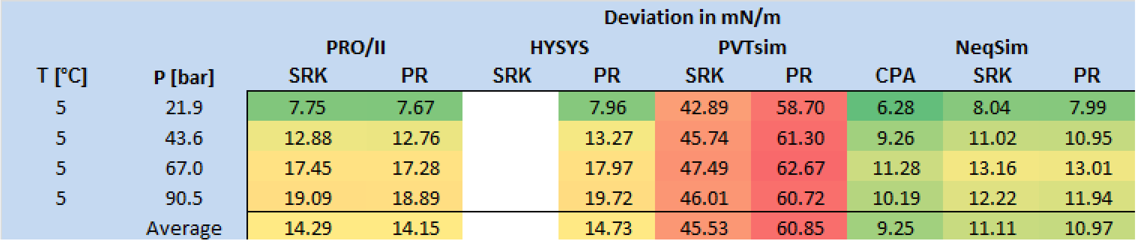

		Deviation in mN/m								
		PRO/II		HYSYS		PVTsim		NeqSim		
T [°C]	P [bar]	SRK	PR	SRK	PR	SRK	PR	CPA	SRK	PR
5	21.9	7.75	7.67		7.96	42.89	58.70	6.28	8.04	7.99
5	43.6	12.88	12.76		13.27	45.74	61.30	9.26	11.02	10.95
5	67.0	17.45	17.28		17.97	47.49	62.67	11.28	13.16	13.01
5	90.5	19.09	18.89		19.72	46.01	60.72	10.19	12.22	11.94
	Average	14.29	14.15		14.73	45.53	60.85	9.25	11.11	10.97

Table 8.28: Deviation of the 100wt% MEG + Methane/Ethane Mixture

80wt% MEG/20wt% Water

Figures 8.33 and 8.34 are used to illustrate the general tendencies of how the software perform for the 80wt% MEG/20wt% water liquid mixture. The absolute deviations of the different software at 20°C are given in tables 8.29 and 8.30. The software are overestimating the surface tension compared to the experimental value, as was the case for the 100wt% MEG mixture. It is still PVTsim that has the largest average discrepancy, but it is much lower than in the 100wt% MEG mixture. When comparing tables 8.26 and 8.29, it is seen that the average deviation has decreased with about 10mN/m for both PR and SRK. This is also the case for the mixture containing ethane. The model in PVTsim performs better when water is present compared to the 100wt% MEG, as was explained in section 8.1.2. The 80wt% MEG/20wt% water mixture contains approximately 40 mol% water.

For PRO/II and HYSYS the case is different from PVTsim, with an increase in discrepancy compared to the 100wt% MEG mixture. However, the increase for HYSYS is quite small while the increase for PRO/II is large, leading to HYSYS performing better than PRO/II for this mixture. Looking at table 8.30 the average deviations for HYSYS PR and PRO/II PR are 11.98 mN/m and 18.35mN/m. For the 100wt% MEG mixture (see table 8.27) the average deviations are 11.23 mN/m and 10.65mN/m. The trend for the software is similar to the 100wt% MEG mixture where the discrepancy is much larger at elevated pressures.

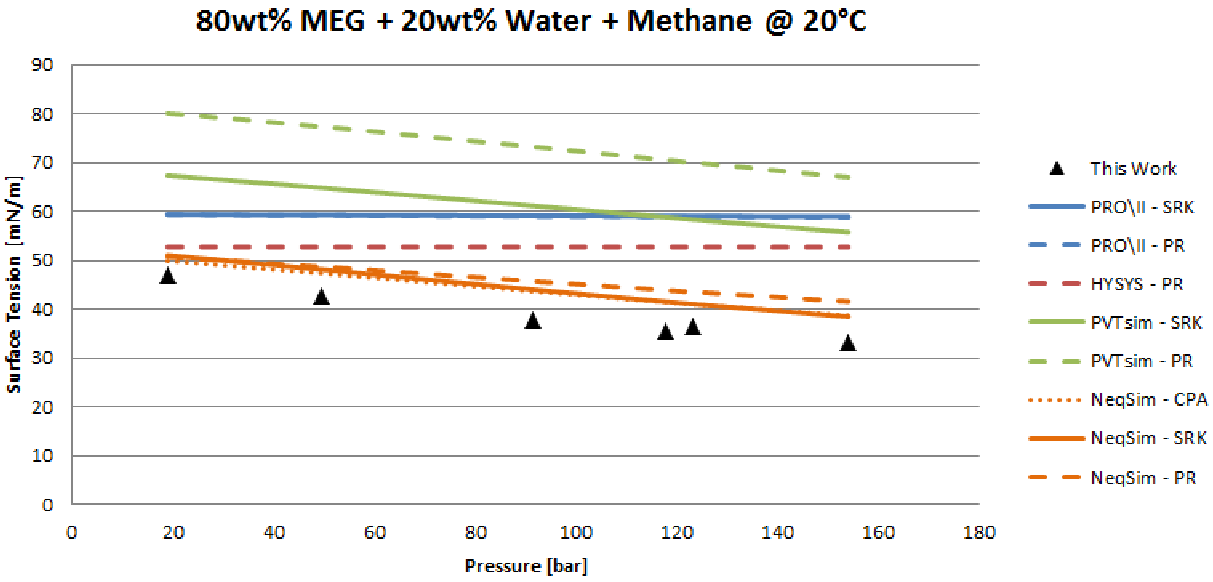

Figure 8.33: 80wt% MEG/20wt% Water + Methane

		Deviation in mN/m								
		PRO/II		HYSYS		PVTsim		NeqSim		
T [°C]	P [bar]	SRK	PR	SRK	PR	SRK	PR	CPA	SRK	PR
20	18.9	12.45	12.42		5.79	20.42	33.17	2.99	4.15	3.82
20	49.6	16.55	16.48		10.03	22.12	34.64	4.63	5.43	6.00
20	91.5	21.25	21.13		14.86	23.30	35.37	5.84	6.18	7.89
20	117.7	23.68	23.54		17.37	23.48	35.21	6.14	6.22	8.58
20	123.1	22.62	22.48		16.33	21.95	33.62	4.66	4.69	7.17
20	154.1	25.73	25.56		19.50	22.52	33.79	5.49	5.26	8.38
	Average	20.38	20.27		13.98	22.30	34.30	4.96	5.32	6.97

Table 8.29: Deviation of the 80wt% MEG/20wt% Water + Methane Mixture

How the different EoS performs internally in NeqSim are shown in figure 8.35 and 8.36. These are the same graphs as in figures 8.33 and 8.34, but now showing only NeqSim. The CPA EoS is once again the model with the lowest average deviation, and it also performs better compared to the 100wt% MEG mixture. The average deviations for the 80wt% MEG/20wt% water + methane mixture are 4.96, 5.32 and 6.97 mN/m for respectively CPA, SRK and PR, whilst for the 100wt% MEG mixture + methane (see table 8.26) the deviations are 5.91, 7.04 and 6.51 mN/m. One point worth mentioning is that SRK performs better than in the 100wt% MEG mixture, while PR produce worse results. SRK actually has a lower discrepancy

		Deviation in mN/m								
		PRO/II		HYSYS		PVTsim		NeqSim		
T [°C]	P [bar]	SRK	PR	SRK	PR	SRK	PR	CPA	SRK	PR
20	16.4	12.31	12.27		5.68	24.73	38.33	2.94	4.09	3.74
20	30.0	16.35	16.29		9.80	27.59	41.09	5.79	6.76	6.86
20	43.2	17.76	17.68		11.28	27.79	41.16	6.00	6.79	7.32
20	64.0	20.61	20.50		14.22	28.60	41.72	6.87	7.37	8.58
20	105.1	25.17	25.02		18.92	28.87	41.37	7.43	7.38	9.84
	Average	18.44	18.35		11.98	27.52	40.73	5.80	6.48	7.27

Table 8.30: Deviation of the 80wt% MEG/20wt% Water + Methane/Ethane Mixture

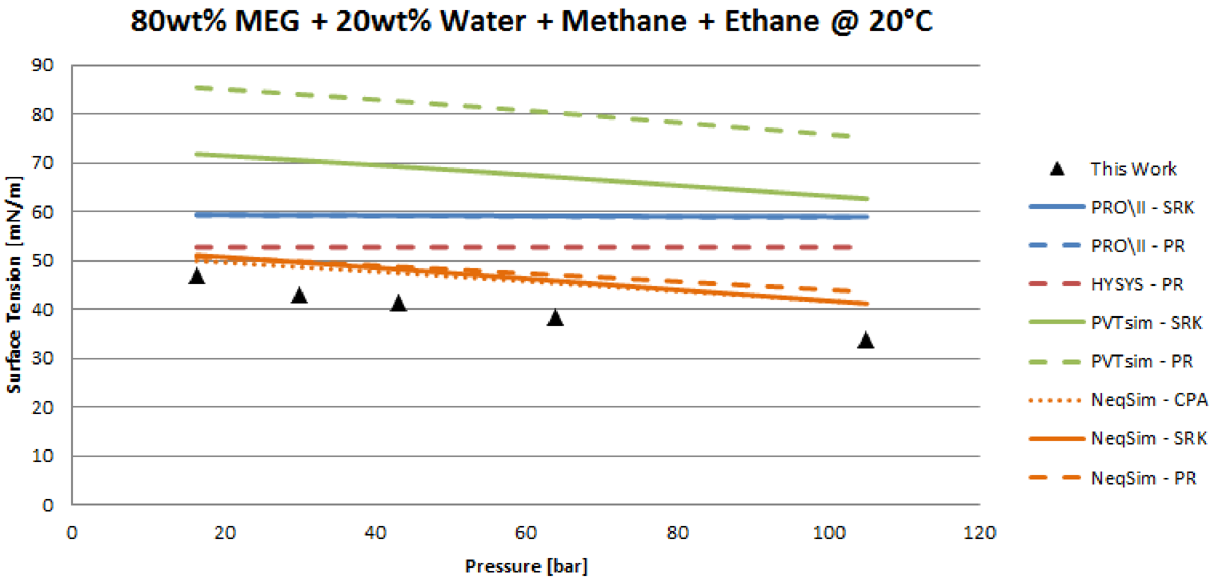

Figure 8.34: 80wt% MEG/20wt% Water + Methane/Ethane

than CPA at the highest pressure. Referring to table 8.29 the deviation for CPA and SRK EoS at 154.1 bar is 5.49 and 5.26 mN/m. The general trend regarding the use of ethane in the mixture is similar to that of the100wt% MEG mixture, meaning the discrepancy is larger with the use of ethane.

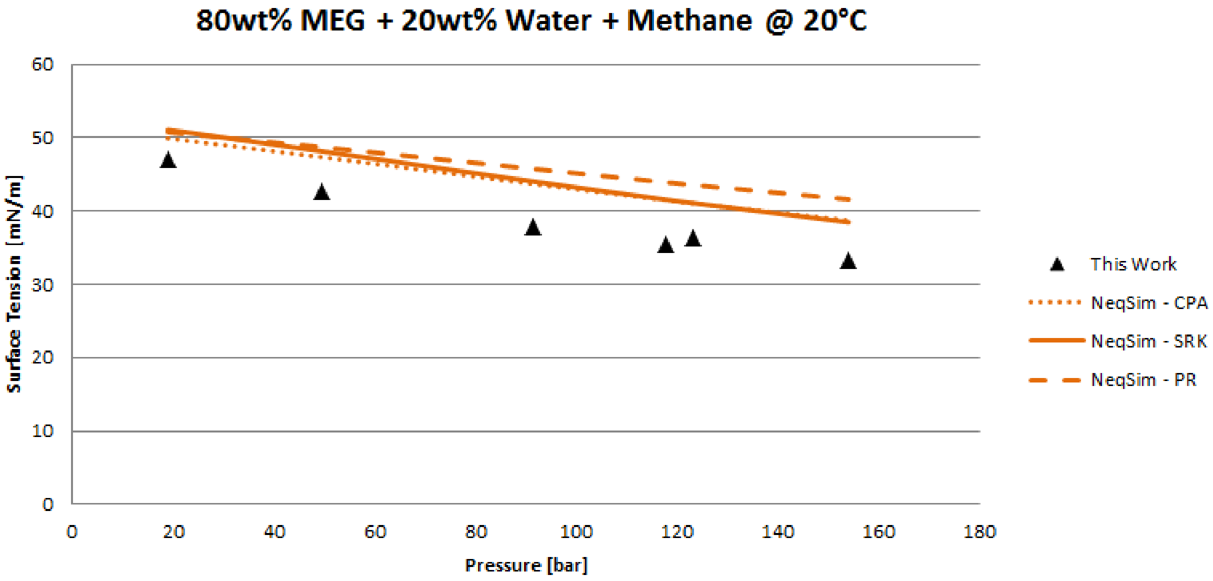

Figure 8.35: 80wt% MEG/20wt% Water + Methane

The figure 8.37 show the same mixture, but now at 5°C. The tendency is identical to that of the 100wt% MEG mixture, meaning the discrepancy is larger at 5°C compared to 20°C. The CPA EoS also performs better internally at 5°C compared to 20°C. This relationship is given by comparing tables 8.30 and 8.31. The deviation of the CPA model is increasing from 5.80 to 7.86 mN/m which is an increase of 2.06 mN/m. The increase for SRK and PR are 2.84 and 2.78 mN/m.

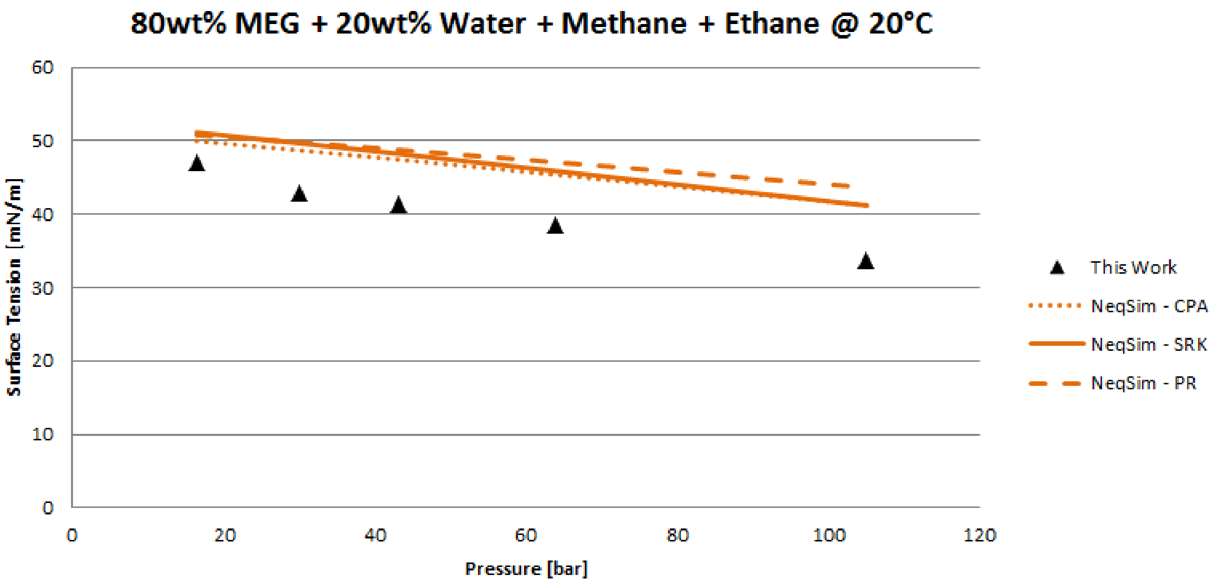

Figure 8.36: 80wt% MEG/20wt% Water + Methane/Ethane

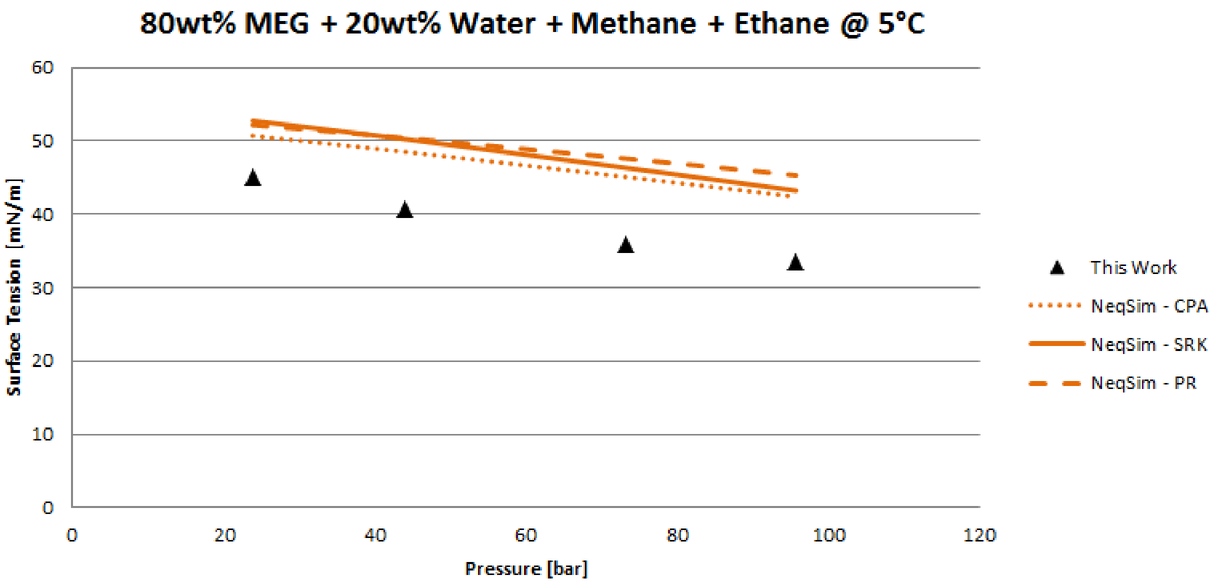

Figure 8.37: 80wt% MEG/20wt% Water + Methane/Ethane

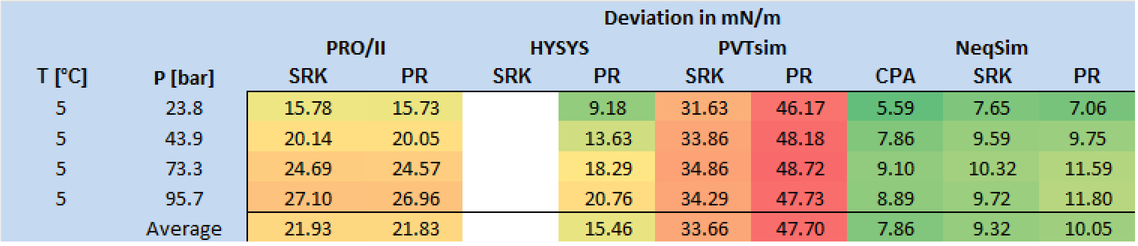

		Deviation in mN/m								
		PRO/II		HYSYS		PVTsim		NeqSim		
T [°C]	P [bar]	SRK	PR	SRK	PR	SRK	PR	CPA	SRK	PR
5	23.8	15.78	15.73		9.18	31.63	46.17	5.59	7.65	7.06
5	43.9	20.14	20.05		13.63	33.86	48.18	7.86	9.59	9.75
5	73.3	24.69	24.57		18.29	34.86	48.72	9.10	10.32	11.59
5	95.7	27.10	26.96		20.76	34.29	47.73	8.89	9.72	11.80
	Average	21.93	21.83		15.46	33.66	47.70	7.86	9.32	10.05

Table 8.31: Deviation of the 80wt% MEG/20wt% Water + Methane/Ethane Mixture

50wt% MEG/50wt% Water

Figures 8.38 and 8.39 are used to illustrate the general tendencies of how the software perform on the 50wt% MEG/50wt% water mixture. Looking at the graphs, it is observed that PVTsim no longer is the software with the largest deviation. PVTsim PR still has a large discrepancy, but PVTsim SRK provides accurate results. The average deviations for the 50wt% MEG/50wt% water + methane and 50wt% MEG/50wt% water + methane/ethane mixtures are given in tables 8.32 and 8.33. Looking at table 8.32 it is observed that PVTsim SRK has an average deviation of 8.24 mN/m, which is better than PRO/II and HYSYS, and almost as good as NeqSim PR. When comparing tables 8.29 and 8.32, it is observed that the average deviation for the 50wt% MEG/50wt% water mixture is a lot smaller than for the 80wt% MEG/20wt% water mixture. The 50wt% MEG/50wt% water mixture contains approximately 70 mol% water.

PRO/II and HYSYS continue the trend of increasing deviation with increasing amount of water present in the system, but it is still HYSYS that has the lowest discrepancy. The average deviations for the 50wt% MEG/50wt% water + methane/ethane mixture are 20.60, 20.56 and 13.54 mN/m for respectively PRO/II SRK, PRO/II PR and HYSYS PR. Looking at table 8.30 the average deviations for the 80wt% MEG/20wt% water + methane/ethane mixture are 18.44, 18.35 and 11.98 mN/m. The same relationship applies to the mixture without ethane, but to a lesser degree. This is due to higher pressures used in the 80wt% MEG/20wt% water mixture, which have a large contribution to the average deviation.

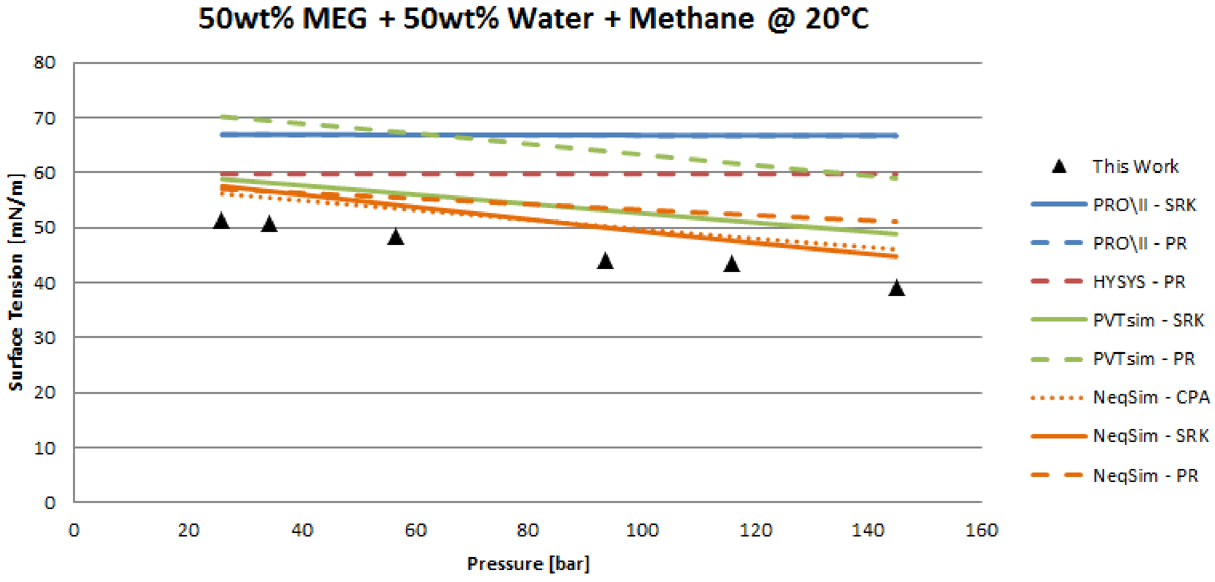

Figure 8.38: 50wt% MEG/50wt% Water + Methane

The figures 8.40 and 8.41 show how NeqSim performs at this mixture, and it is still the CPA EoS that is most accurate. However, CPA produces worse results than for the 80wt% MEG/20wt% water mixture. The average deviation taken from table 8.32 is 5.43 mN/m. For the 80wt% MEG/20wt% water + methane mixture given in table 8.29 the deviation is 4.96 mN/m. This is even more obvious in the mixtures containing ethane, namely tables 8.33 and 8.30. The general observation is that the 50wt% MEG/50wt% water mixtures have much higher deviations at

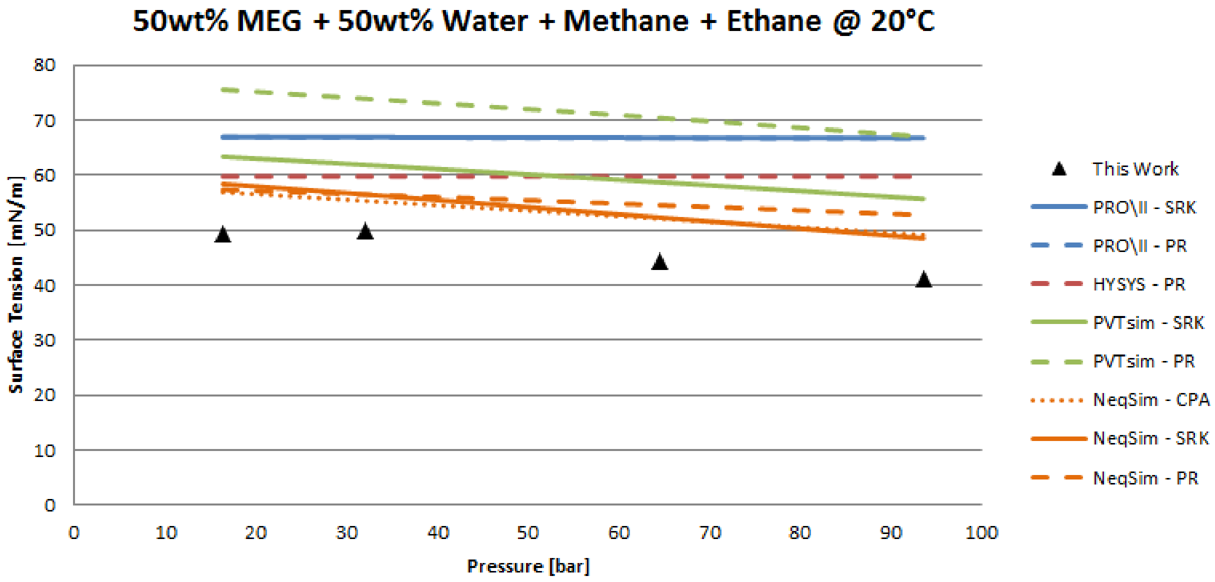

Figure 8.39: 50wt% MEG/50wt% Water + Methane/Ethane

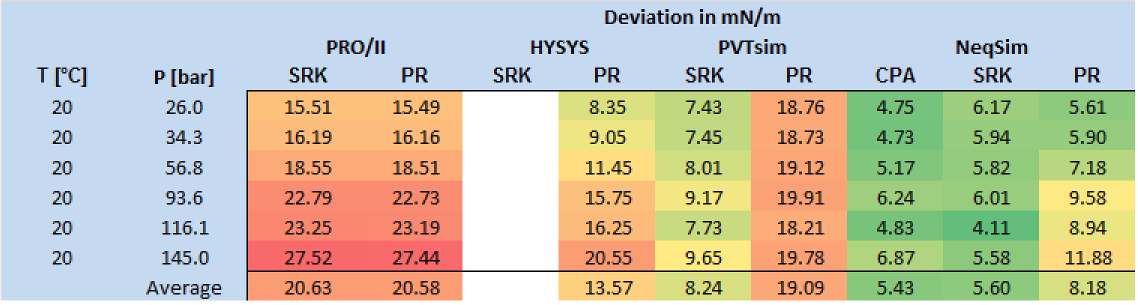

		Deviation in mN/m								
		PRO/II		HYSYS		PVTsim		NeqSim		
T [°C]	P [bar]	SRK	PR	SRK	PR	SRK	PR	CPA	SRK	PR
20	26.0	15.51	15.49		8.35	7.43	18.76	4.75	6.17	5.61
20	34.3	16.19	16.16		9.05	7.45	18.73	4.73	5.94	5.90
20	56.8	18.55	18.51		11.45	8.01	19.12	5.17	5.82	7.18
20	93.6	22.79	22.73		15.75	9.17	19.91	6.24	6.01	9.58
20	116.1	23.25	23.19		16.25	7.73	18.21	4.83	4.11	8.94
20	145.0	27.52	27.44		20.55	9.65	19.78	6.87	5.58	11.88
	Average	20.63	20.58		13.57	8.24	19.09	5.43	5.60	8.18

Table 8.32: Deviation of the 50wt% MEG/50wt% Water + Methane Mixture

the lowest pressures than the 80wt% MEG/20wt% water mixtures. At the highest pressures it is the SRK EoS that is most accurate, as was the case for the 80wt% MEG/20wt% water mixture. However this trend is more visible in the 50wt% MEG/50wt% water mixture. Considering table 8.32 the deviations at 145.0 bar are 6.87 and 5.58 mN/m for CPA and SRK, while at the 80wt% MEG/20wt% water + methane mixture the deviations at 154.1 bar are 5.49 and 5.26 mN/m. The PR EoS continues the poor development and produces even worse results than in the 80wt% MEG/20wt% water mixture. The largest deviation for the 50wt% MEG/50wt% water + methane/ethane mixture is 11.52 mN/m at 93.6 bar and for the 50wt% MEG/50wt% water + methane it is 11.88 mN/m at 145.0 bar.

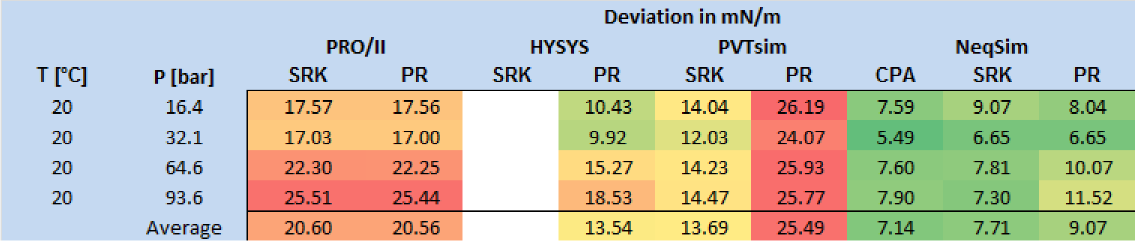

		Deviation in mN/m								
		PRO/II		HYSYS		PVTsim		NeqSim		
T [°C]	P [bar]	SRK	PR	SRK	PR	SRK	PR	CPA	SRK	PR
20	16.4	17.57	17.56		10.43	14.04	26.19	7.59	9.07	8.04
20	32.1	17.03	17.00		9.92	12.03	24.07	5.49	6.65	6.65
20	64.6	22.30	22.25		15.27	14.23	25.93	7.60	7.81	10.07
20	93.6	25.51	25.44		18.53	14.47	25.77	7.90	7.30	11.52
	Average	20.60	20.56		13.54	13.69	25.49	7.14	7.71	9.07

Table 8.33: Deviation of the 50wt% MEG/50wt% Water + Methane/Ethane Mixture

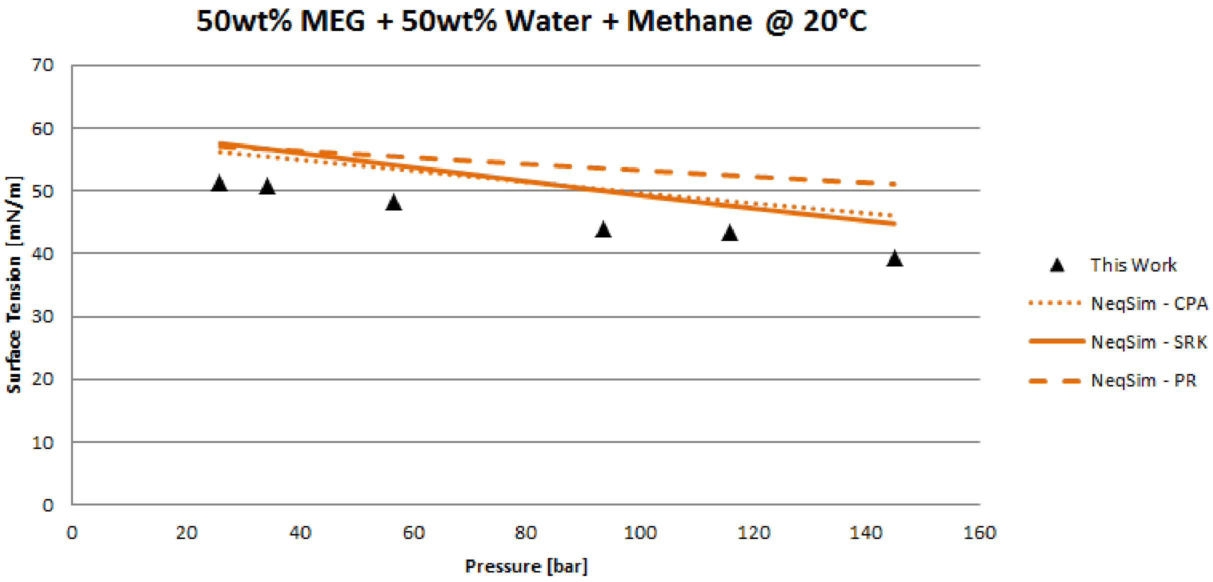

Figure 8.40: 50wt% MEG/50wt% Water + Methane

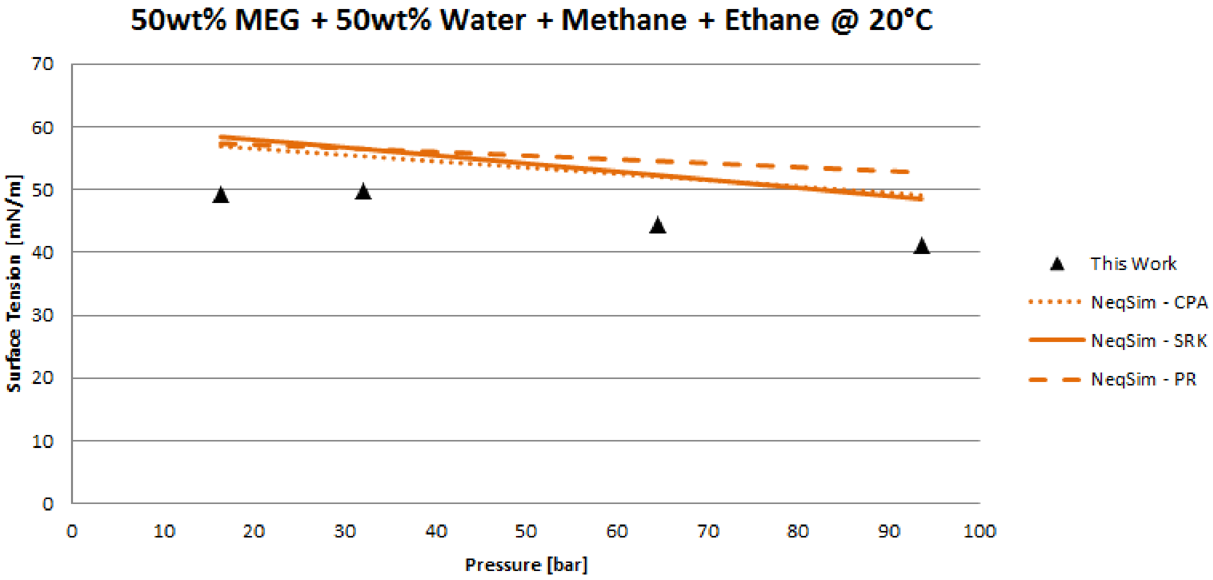

Figure 8.41: 50wt% MEG/50wt% Water + Methane/Ethane

The figures 8.42 and 8.43 show the same mixtures, but now at 5°C. The deviation is once more larger than at 20°C, and the trends are equal to that discussed in earlier sections.

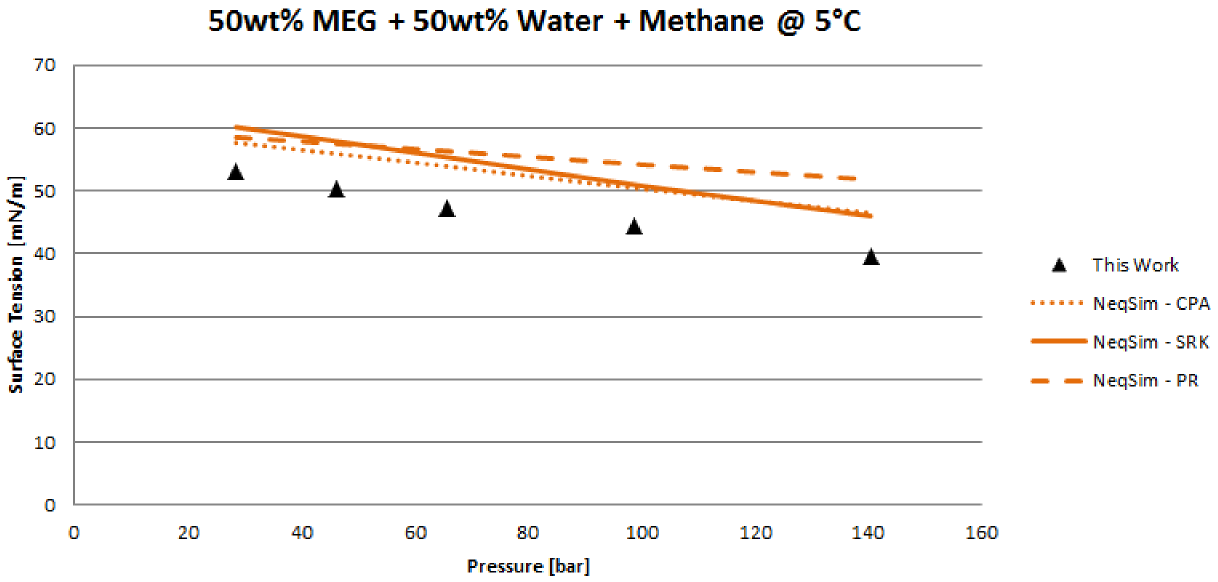

Figure 8.42: 50wt% MEG/50wt% Water + Methane

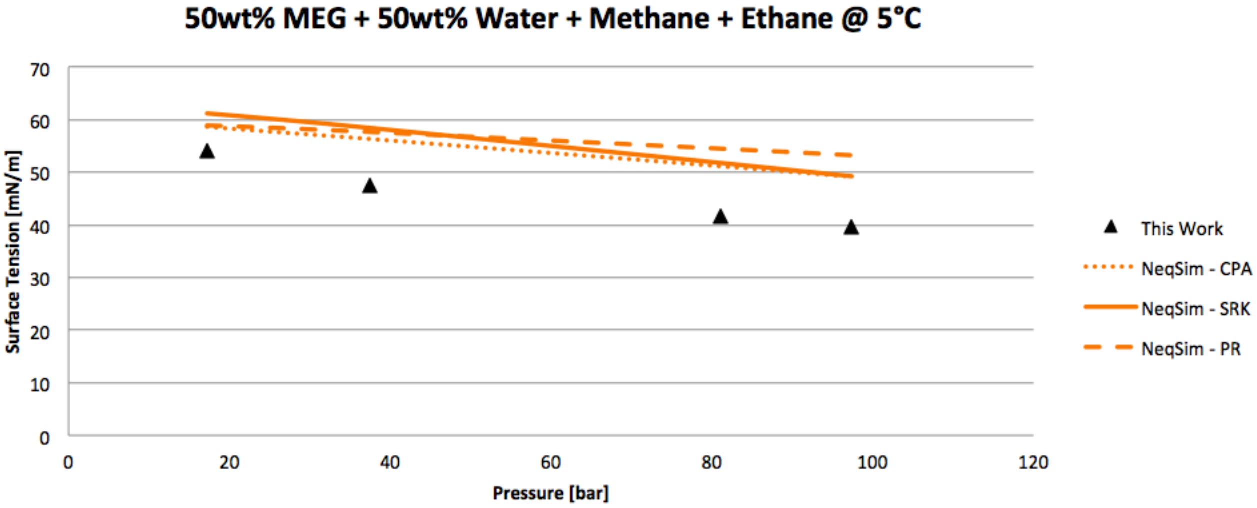

Figure 8.43: 50wt% MEG/50wt% Water + Methane/Ethane

8.1.3 Comparison of Models

In this section the various possibilities of models in each software are compared. In PRO/II and HYSYS it is possible to choose amongst different models to calculate surface tension as explained in chapter 4, while in NeqSim and PVTsim it is only one possibility. However, in HYSYS there is only one possibility for calculation of glycol mixtures, hence only PRO/II will be discussed in the paragraph regarding glycol mixtures. The discussion will be based on graphs from selected mixtures shown in sections 8.1.1 and 8.1.2. Only PR EoS will be shown for both PRO/II and HYSYS. This is because PR and SRK provide equal values for all mixtures.

Hydrocarbon mixtures

PRO/II has three options to choose amongst: weighted average pure-component model, API procedure 10A3.1 and parachor method. The Parachor method is equal to the one implemented in PVTsim, thus it will not be discussed here. The comparison will be between the API method and the pure component method. HYSYS has two models to choose amongst: the weighted average pure-component and API procedure 10A3.2.

Figures 8.44 and 8.45 shows how the different models perform compared to each other in light hydrocarbon systems. The API methods clearly perform better than the default models, and they follow the trend of the experimental data much better. They tend to underestimate the surface tension, while the default models overestimate it as discussed in section 8.1.1. The biggest difference between the models is at the highest pressures where the surface tension values are low. The problem for the API models is that they tend to produce a value of zero when the experimental surface tension is below 1 mN/m. This is a bigger issue in PRO/II than in HYSYS as seen in figure 8.45.

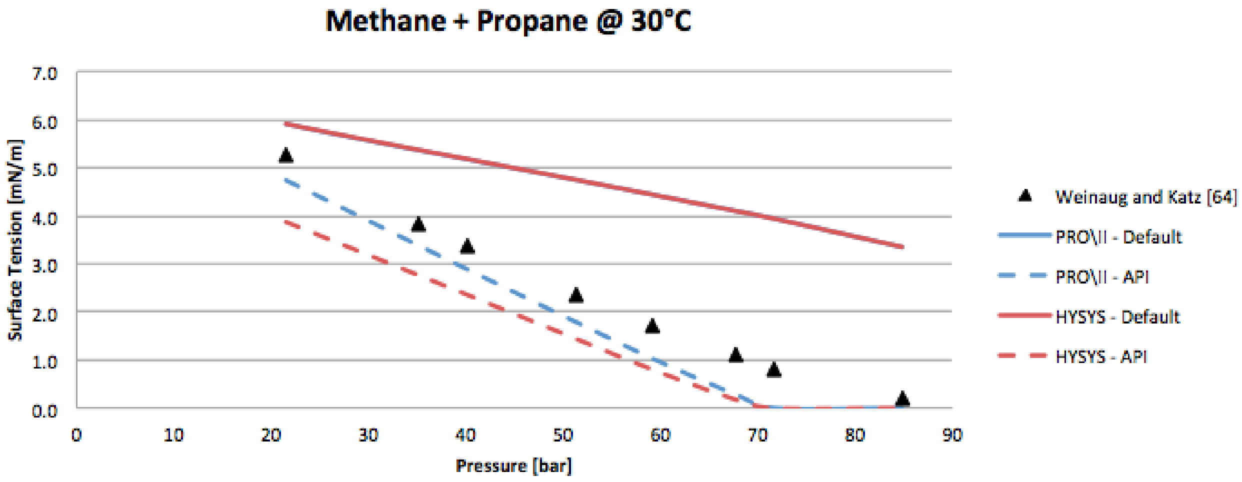

Figure 8.44: Methane + Propane

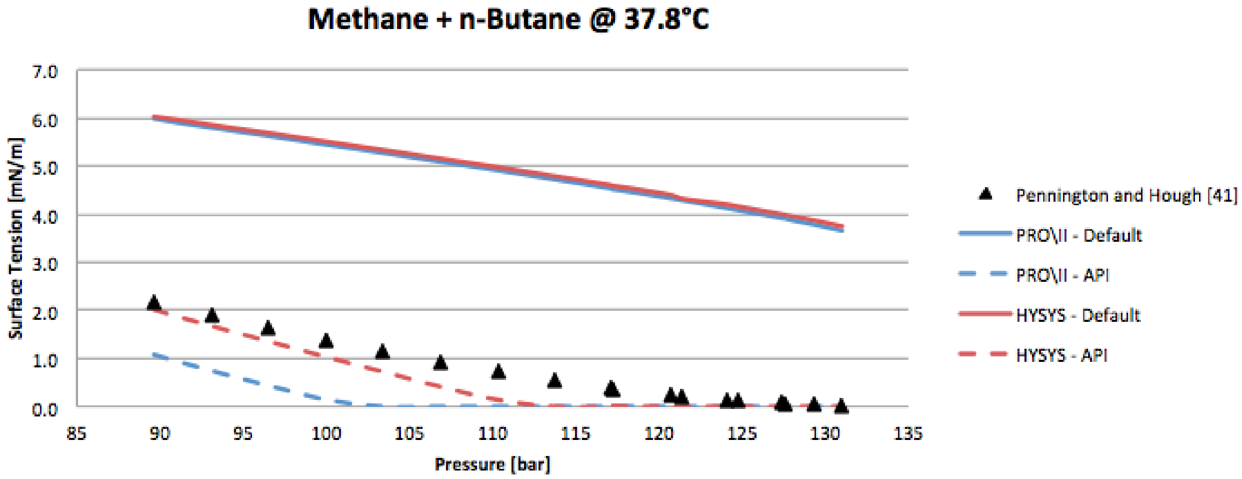

Figure 8.45: Methane + n-Butane

Figure 8.46 shows the performance of the models for the methane + n-heptane system at two different temperatures. At the lowest temperature it is the PRO/II API model that has the best performance, while the HYSYS API model now has a poorer performance than the default models. Both of the API models now overestimate the surface tension. However at the highest temperature the PRO/II API model shifts to underestimating the surface tension again, and at the highest pressure it produces a value of zero when the actual value is 1.82 mN/m. At this temperature HYSYS API is the model with the best performance. It still overestimates the surface tension but now to a lesser degree. However, at the highest pressure the model shifts to underestimate the surface tension as PRO/II does. It seems that when the experimental value is high the API models overestimate the surface tension as the default models do.

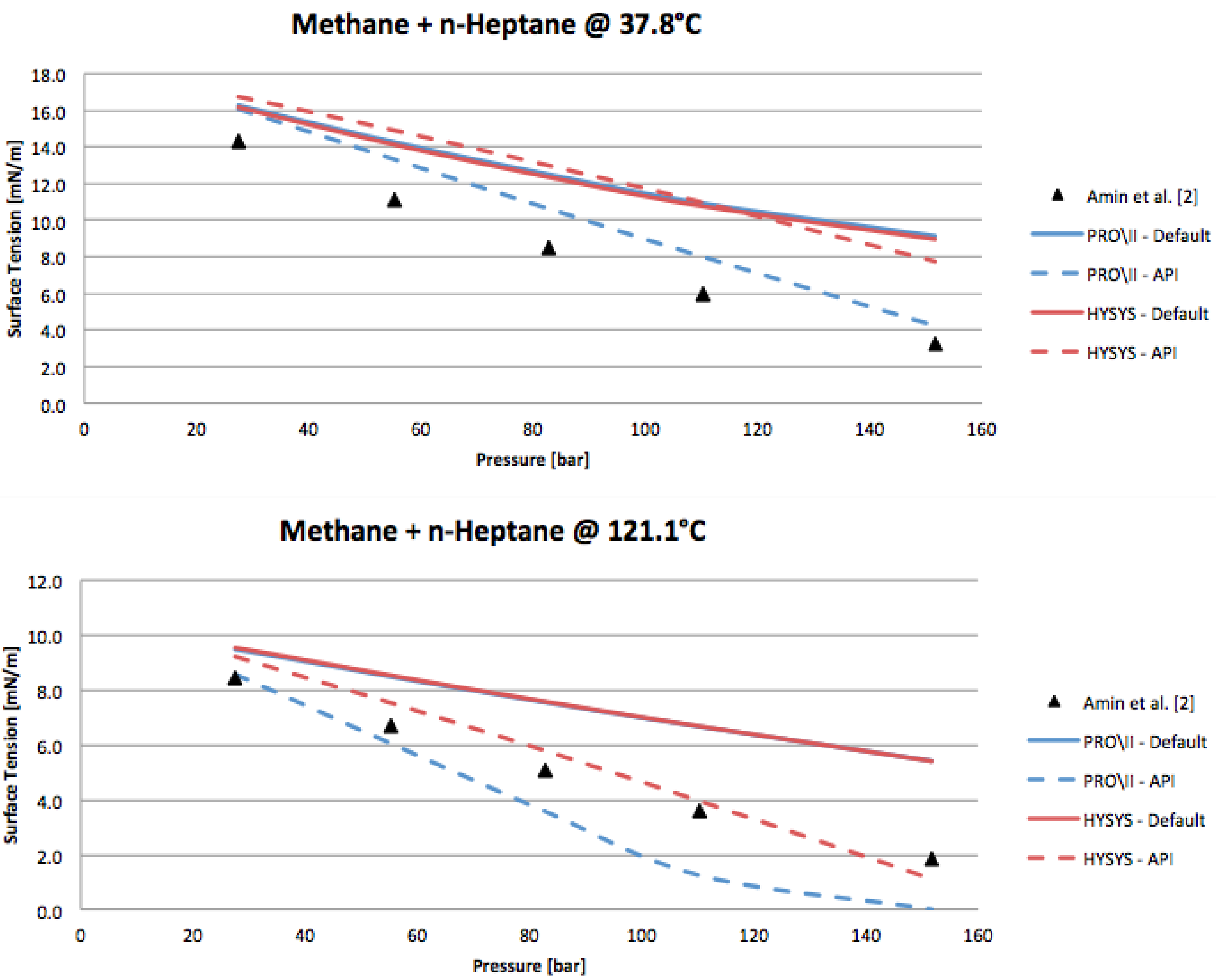

Figure 8.46: Methane + n-Heptane

Finally, figure 8.47 shows how the models perform against a more complex fluid. The API models follow the trend of the experimental data very satisfactory. The trends are as discussed earlier in this section. At large experimental values the models overestimate, while at the lowest values the models underestimate.

From these graphs it is clear that the API models have a much smaller discrepancy than the default models in PRO/II and HYSYS. The API models have problems simulating mixtures where the surface tension value is close to zero, but it is still better than the default models, which overestimates the surface tension at

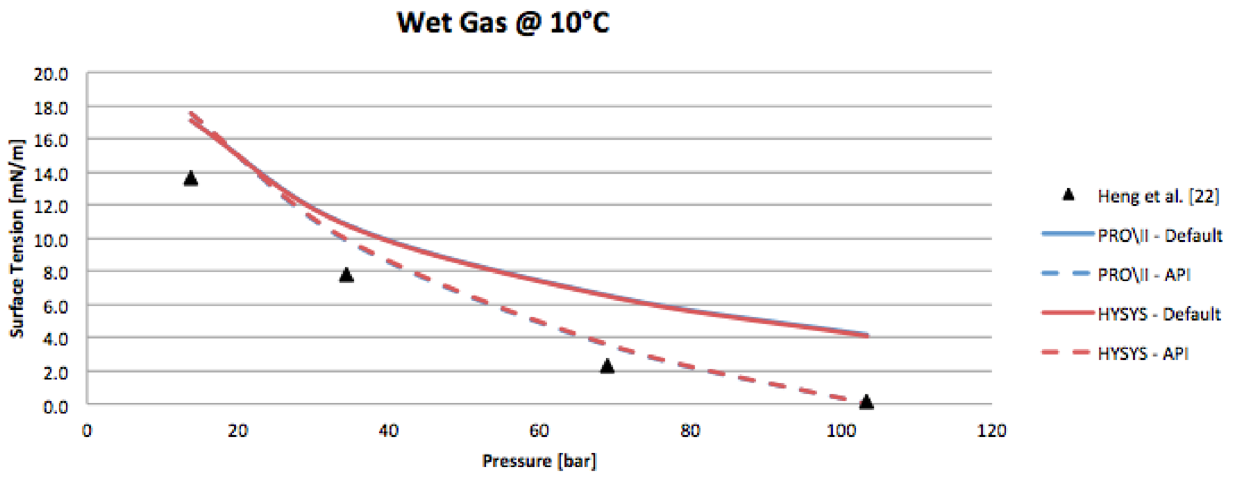

Figure 8.47: Wet Gas

all conditions. For HYSYS it is therefore recommended to use the API model when calculating surface tension. For PRO/II it is however recommended to use the parachor method instead of the API model, because it has a much better performance when the surface tension is close to zero. The performance of the parachor model is thoroughly discussed in section 8.1.1.

Glycol mixtures

PRO/II has two options to choose amongst: weighted average pure-component model and a ”wet” surface tension model. Figure 8.48 shows how the models perform on the 100wt% MEG mixture. The ”wet” model has a smaller deviation than the default model but it has the same trend as the default one. The ”wet” model is fairly accurate at the lowest pressures, but as the pressure is increased it overestimates the surface tension to a great extent. Similar results are seen in the mixtures not containing ethane.

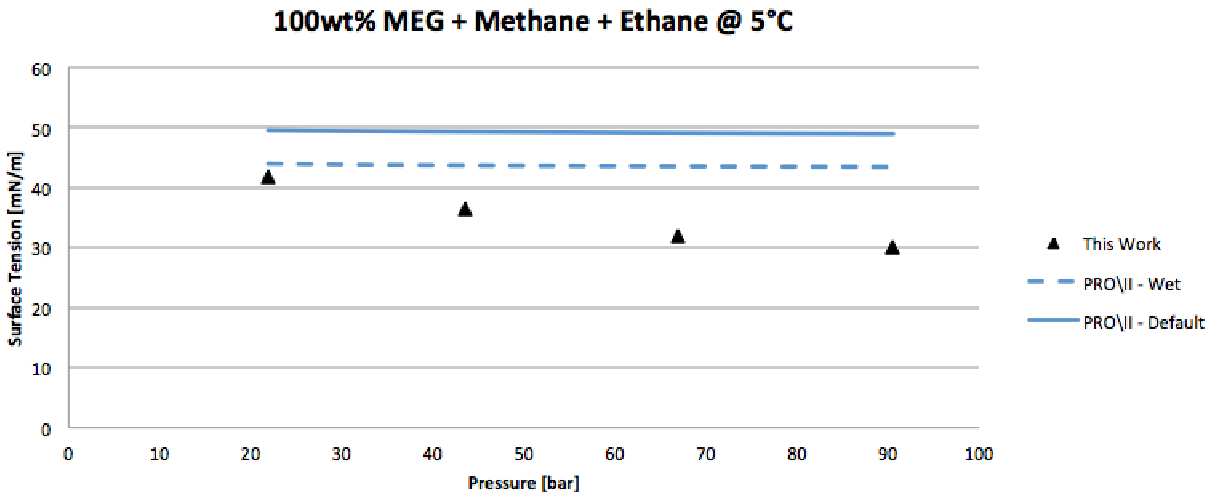

Figure 8.48: 100wt% MEG + Methane/Ethane

Figures 8.49 and 8.50 shows the 80wt% MEG + 20wt% water and 50wt% MEG + 50wt% water mixtures. The trend for both models is that the discrepancy to experimental data is increasing with increasing amount of water in the system. The ”wet” model is better than the default model at all mixtures, but at the 50wt% MEG + 50wt% water mixture the difference is as small as 1.36 mN/m. The difference between the two models is decreasing with a larger portion of water in the system.

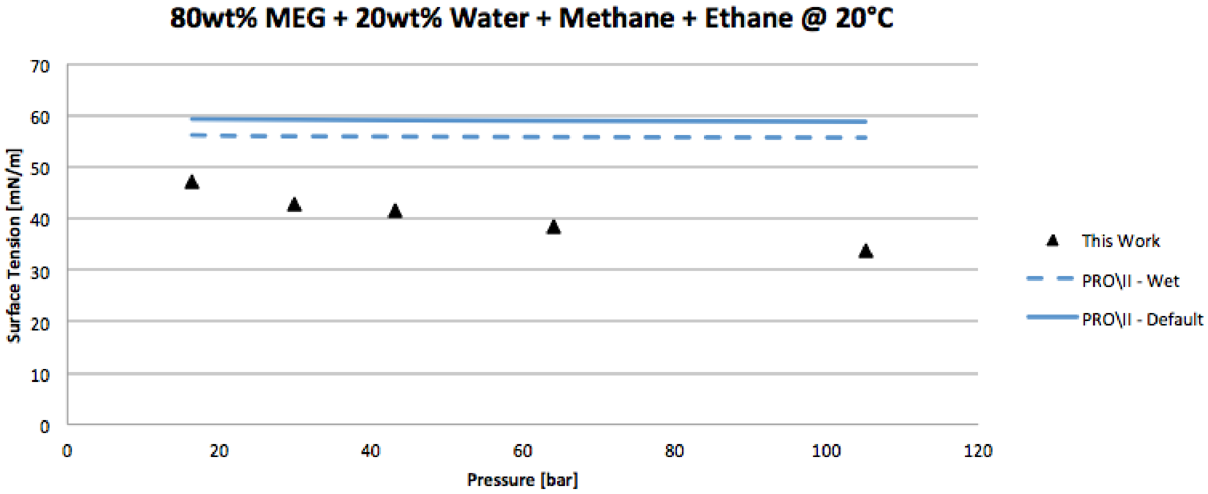

Figure 8.49: 80wt% MEG/20wt% Water + Methane/Ethane

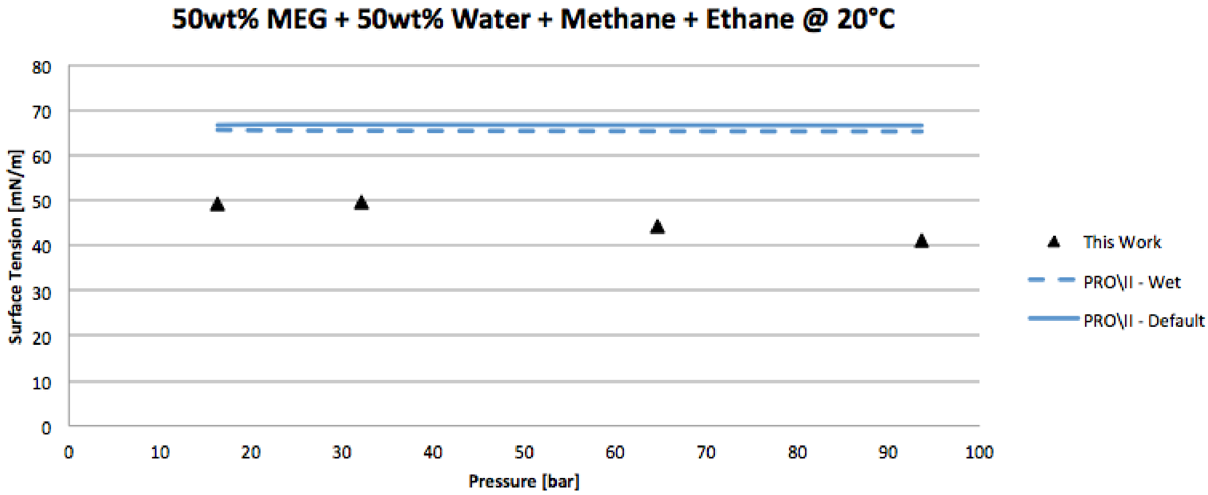

Figure 8.50: 50wt% MEG/50wt% Water + Methane/Ethane

From these graphs we can conclude that the ”wet” model has a smaller discrepancy than the default model, although either of them can be said to give satisfactory results. The issue with the models is the large discrepancy at the largest pressures. If a glycol mixture containing less than 50wt% water is simulated the ”wet” model should be used. However, if the amount of water is increased above 50wt% the default model will be the preferred choice.

8.1.4 Importance of Surface Tension

As described in chapter 2 the surface tension is important for the design of separators. It is therefore important that the software, which are used in the simulation process, can give an accurate estimate of the surface tension. As shown in this discussion there are several software that have a high discrepancy from experimental data, and thus will give an inaccurate estimation of the separators design. First of all HYSYS and PRO/II have an unacceptable large discrepancy for hydrocarbon mixtures at high pressures. The surface tension can in some cases be close to zero. However, in real fluid cases the surface tension is considered low when it is 1 mN/m. Looking at experimental values above 1 mN/m the discrepancy for HYSYS and PRO/II can be four times as large as the experimental value. This can lead to very wrong conclusions regarding sizing of equipment. For PVTsim and NeqSim the case is quite different. The software are seldom off with more than 1 mN/m on average for complex fluids, which is very satisfactory for a preliminary design.

For the case of glycol mixtures the surface tensions are much higher than that of hydrocarbons meaning it is easier to separate the different phases. PRO/II and HYSYS perform better at these mixtures, but the discrepancy is still large. The deviation for PRO/II can be up to twice as large as the experimental value, while the deviation for HYSYS is at maximum 50% larger. This is still very large and will lead to incorrectly design of equipment. This is also the case for PVTsim, which has a large discrepancy, when MEG is the dominating fluid in the mixture. It is therefore only NeqSim that can be trusted to give adequate results. However, the discrepancy for NeqSim is also quite large and is at worst case 10% off compared to the experimental data.

8.2 Density and Solubility

When performing experiments on surface tension, other properties of interest were recorded as well. Liquid and vapor density and the liquid phase solubility was recorded and analyzed in the same way as the surface tension, using software to evaluate their performance. Density is used in calculating surface tension and is an important property in designing gas liquid separators. Liquid phase solubility describes how much gas is dissolved in the liquid. It is important to avoid gas in the liquid phase as this decrease pump efficiency and can cause damage to downstream equipment. Separators need to be large enough to facilitate sufficient retention time for bubbles to coalesce and separate.

Only data obtained in this work is used when looking at the software performance for calculating density and solubility, as this actually is outside the scope of work.

8.2.1 Density

Density varies with temperature and pressure. This variation is rather small for liquids but much greater for gases.

Liquid Density

The change in liquid density is largely attributed to the composition. Figure 8.51 shows that, in general, all software predict liquid density with high accuracy. However, this figure shows the density for the quadnary mixture of MEG, water, methane and ethane. The corresponding conditions and weight percentage between MEG, water and methane without ethane (figure 8.52), shows that PVTsim

PR and SRK are underestimating the density by 0.11 and 0.21 g/cm^3, respectively. Table 8.34 shows the deviation for all the software to experimental data on all experiments performed for this thesis. For mixtures not including ethane, PVTsim SRK and PR are off the score and deviation increases with decreasing MEG content, while NeqSim CPA performs better than both NeqSim SRK and PR. Noteworthy, NeqSim deviation, contrary to PVTsim, decrease with decreasing MEG content. PRO/II and HYSYS are providing excellent results throughout. As ethane is added to the system, there is a significant change to how PVTsim calculates the liquid density. Table 8.35 illustrates how the software performances change with the addition of ethane. In general, ethane does not affect the liquid density, except for PVTsim, which eliminates almost the entire deviation to the experimental data. In conclusion, all software are providing good results on liquid density.

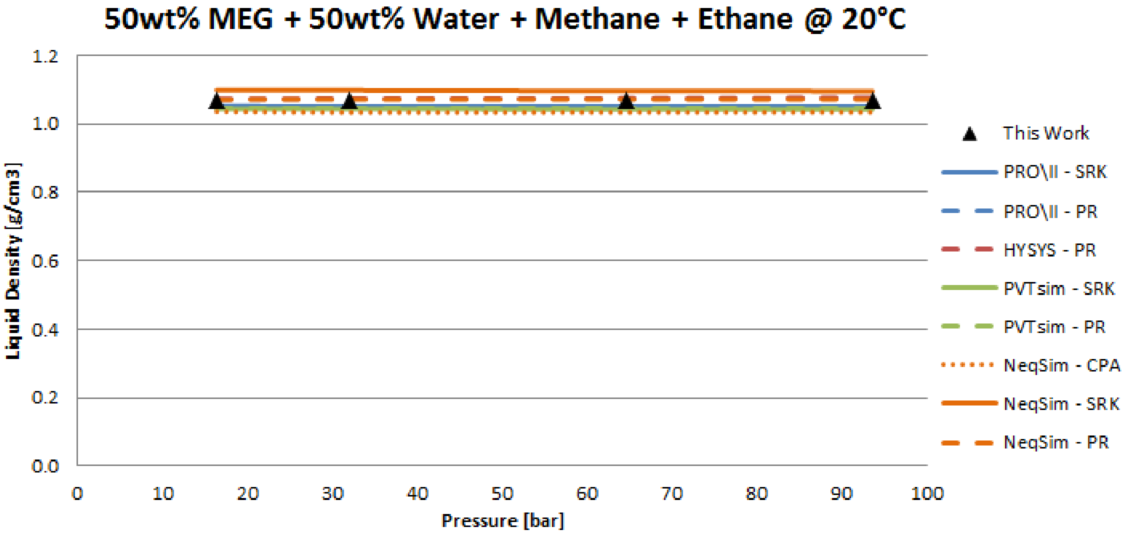

Figure 8.51: Liquid Density of 50wt% MEG/50 wt% Water + Methane/Ethane @ 20°C

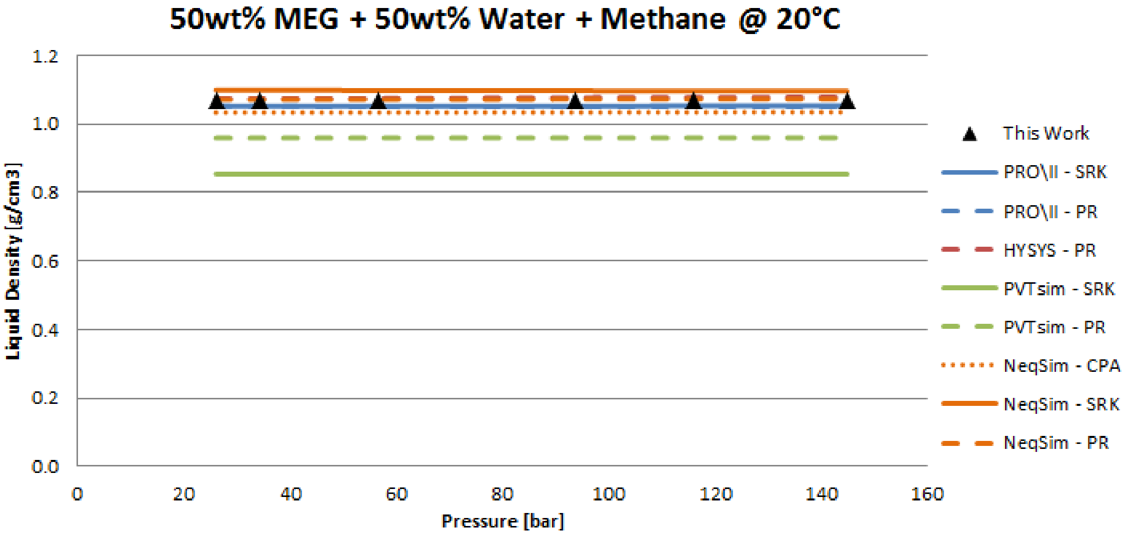

Figure 8.52: Liquid Density of 50wt% MEG/50 wt% Water + Methane @ 20°C

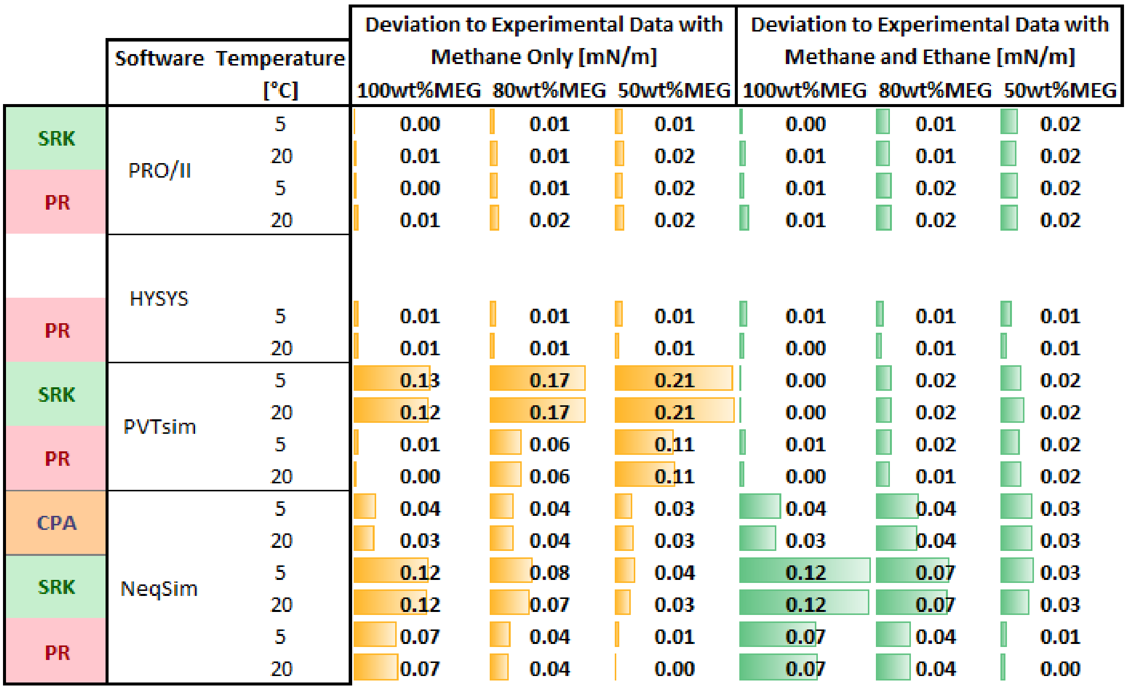

	Software	Temperature [°C]	Deviation to Experimental Data with Methane Only [mN/m]			Deviation to Experimental Data with Methane and Ethane [mN/m]		
			100wt%MEG	80wt%MEG	50wt%MEG	100wt%MEG	80wt%MEG	50wt%MEG
SRK	PRO/II	5	0.00	0.01	0.01	0.00	0.01	0.02
		20	0.01	0.01	0.02	0.01	0.01	0.02
PR		5	0.00	0.01	0.02	0.01	0.02	0.02
		20	0.01	0.02	0.02	0.01	0.02	0.02
	HYSYS							
PR		5	0.01	0.01	0.01	0.01	0.01	0.01
		20	0.01	0.01	0.01	0.00	0.01	0.01
SRK	PVTsim	5	0.13	0.17	0.21	0.00	0.02	0.02
		20	0.12	0.17	0.21	0.00	0.02	0.02
PR		5	0.01	0.06	0.11	0.01	0.02	0.02
		20	0.00	0.06	0.11	0.00	0.01	0.02
CPA	NeqSim	5	0.04	0.04	0.03	0.04	0.04	0.03
		20	0.03	0.04	0.03	0.03	0.04	0.03
SRK		5	0.12	0.08	0.04	0.12	0.07	0.03
		20	0.12	0.07	0.03	0.12	0.07	0.03
PR		5	0.07	0.04	0.01	0.07	0.04	0.01
		20	0.07	0.04	0.00	0.07	0.04	0.00

Table 8.34: Deviation to Experimental Data for Liquid Density

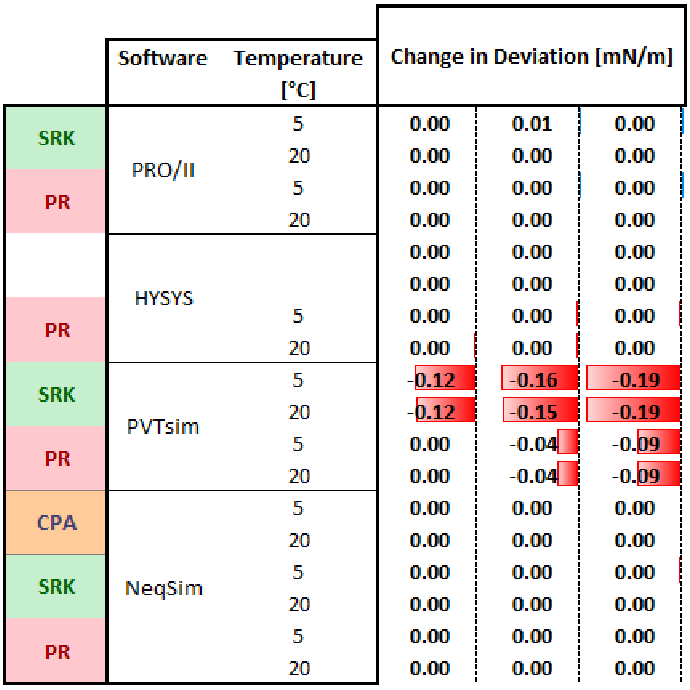

	Software	Temperature [°C]	Change in Deviation [mN/m]		
SRK	PRO/II	5	0.00	0.01	0.00
		20	0.00	0.00	0.00
PR		5	0.00	0.00	0.00
		20	0.00	0.00	0.00
	HYSYS		0.00	0.00	0.00
			0.00	0.00	0.00
PR		5	0.00	0.00	0.00
		20	0.00	0.00	0.00
SRK	PVTsim	5	-0.12	-0.16	-0.19
		20	-0.12	-0.15	-0.19
PR		5	0.00	-0.04	-0.09
		20	0.00	-0.04	-0.09
CPA	NeqSim	5	0.00	0.00	0.00
		20	0.00	0.00	0.00
SRK		5	0.00	0.00	0.00
		20	0.00	0.00	0.00
PR		5	0.00	0.00	0.00
		20	0.00	0.00	0.00

Table 8.35: Change in Deviation to Experimental Data as Ethane is Added

Vapor Density

The vapor density is more affected by the change in temperature and pressure than what the case is for liquid density. This is shown in figure 8.53, which shows the vapor density changing with the pressure for the 50wt% MEG and 50wt% water mixture containing methane and ethane. This is the same mixture as the liquid density shown in figure 8.51. Contrary to the liquid density, where PVTsim in particular was off bounds, all software produce results within a small error of the experimental data. The same applies to the mixtures not containing ethane, figure 8.54. Overall, there is very little deviation to the experimental data for all software. Details are shown in table 8.36.

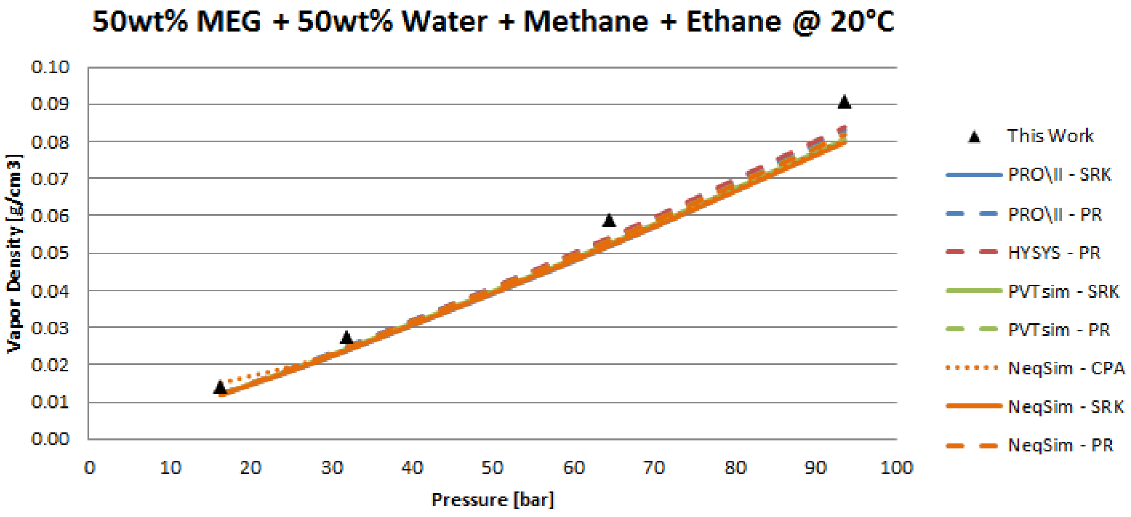

Figure 8.53: Vapor Density of 50wt% MEG/50 wt% water + Methane/Ethane @ 20°C

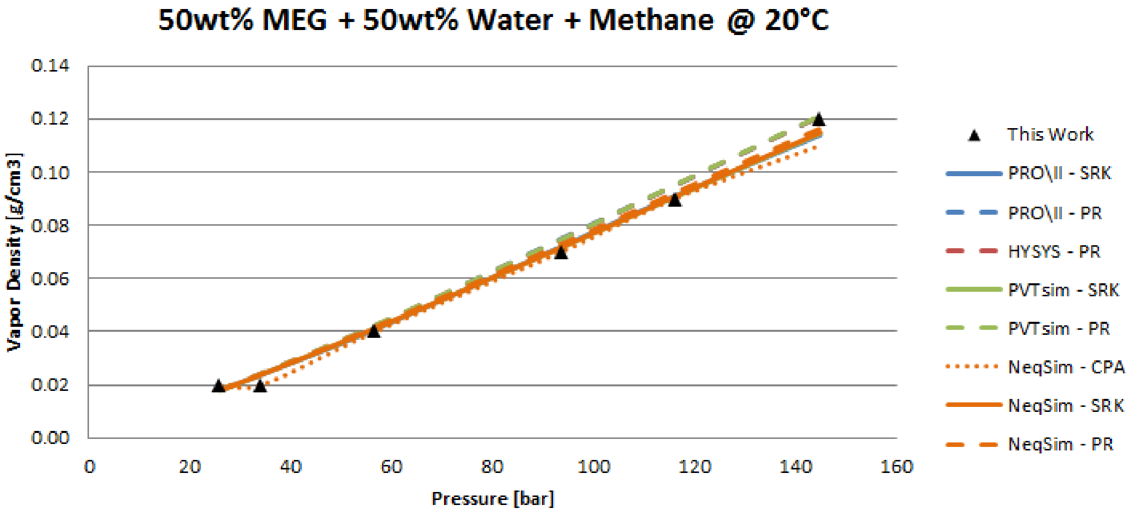

Figure 8.54: Vapor Density of 50wt% MEG/50 wt% Water + Methane @ 20°C

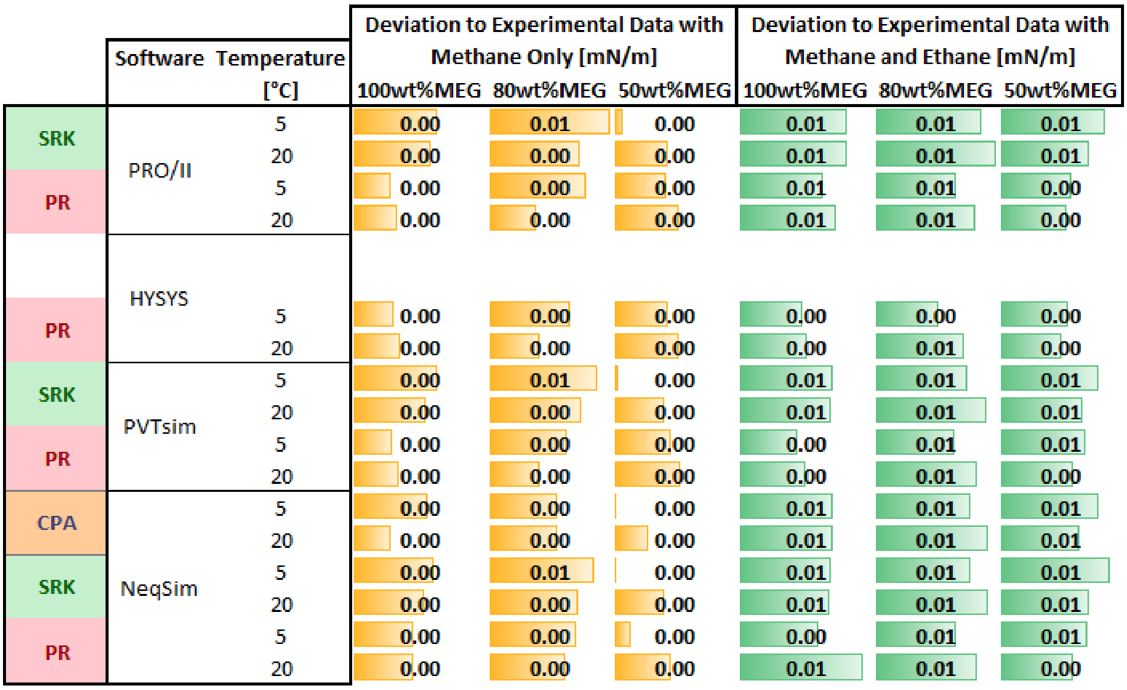

	Software	Temperature [°C]	Deviation to Experimental Data with Methane Only [mN/m]			Deviation to Experimental Data with Methane and Ethane [mN/m]		
			100wt%MEG	80wt%MEG	50wt%MEG	100wt%MEG	80wt%MEG	50wt%MEG
SRK	PRO/II	5	0.00	0.01	0.00	0.01	0.01	0.01
		20	0.00	0.00	0.00	0.01	0.01	0.01
PR		5	0.00	0.00	0.00	0.01	0.01	0.00
		20	0.00	0.00	0.00	0.01	0.01	0.00
	HYSYS							
PR		5	0.00	0.00	0.00	0.00	0.00	0.00
		20	0.00	0.00	0.00	0.00	0.01	0.00
SRK	PVTsim	5	0.00	0.01	0.00	0.01	0.01	0.01
		20	0.00	0.00	0.00	0.01	0.01	0.01
PR		5	0.00	0.00	0.00	0.00	0.01	0.01
		20	0.00	0.00	0.00	0.00	0.01	0.00
CPA	NeqSim	5	0.00	0.00	0.00	0.01	0.01	0.01
		20	0.00	0.00	0.00	0.01	0.01	0.01
SRK		5	0.00	0.01	0.00	0.01	0.01	0.01
		20	0.00	0.00	0.00	0.01	0.01	0.01
PR		5	0.00	0.00	0.00	0.00	0.01	0.01
		20	0.00	0.00	0.00	0.01	0.01	0.00

Table 8.36: Deviation to Experimental Data for Vapor Density

8.2.2 Solubility

Solubility is the property of a solid, liquid or gaseous chemical substance called solute to dissolve in a solid, liquid, or gaseous solvent to form a homogeneous solution of the solute in the solvent. When solubility is discussed in this thesis, it is understood as the percentage of moles of the given component in the liquid phase. The solubility is not recorded for every mixture due to various reasons, which is discussed in section 7.3.

Methane Liquid Phase Composition

The methane liquid phase composition is low, as expected. It varies from 0.04 mol% at the lowest pressure for the 50wt% MEG/50wt% water + methane/ethane mixture at 5°C to 0.83 mol% at the highest pressure for the 100wt% MEG + methane/ethane mixture at 20°C.

As the temperature increases the solubility of a gas decreases. Increased temperature causes an increase in kinetic energy. The higher kinetic energy causes more motion in molecules, which breaks intermolecular bonds and migrates from the solution.

In addition, the solubility of gases depends on the varying change of pressure, therefore an increase in pressure would equal higher solubility. This statement can be proven by Henry's Law, which states that the solubility of a gas in a liquid is directly proportional to the pressure of that gas above the surface of the solution. This can be expressed as:

$$C = k * P_{gas} \tag{8.1}$$

C = the solubility of a gas in solvent

k = the proportionality constant

P_{gas} = the partial pressure of the gas above the solution

Figure 8.55 and 8.56 shows how the value of the experimental data decrease as the temperature is increased from 5°C to 20°C, as well as the increase of methane composition due to the raising pressure. Interestingly, PRO/II SRK produces the best results, whereas NeqSim SRK and PVTsim SRK are overestimating. NeqSim CPA, PRO/II PR and PVTsim PR are also providing satisfactory results. HYSYS PR and NeqSim PR are producing results so close to zero that they do not appear in the graph.

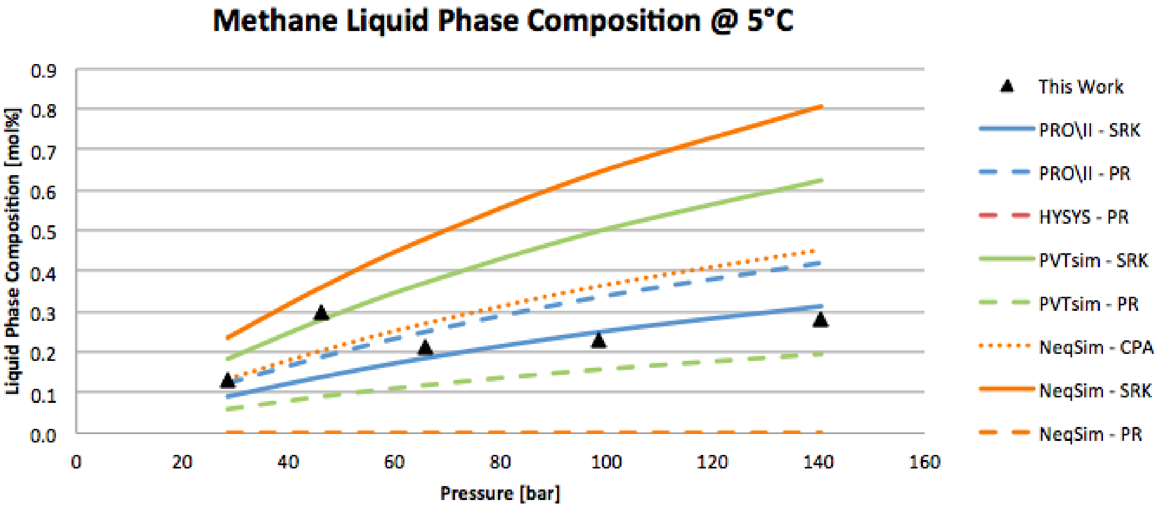

Figure 8.55: Methane Liquid Phase Composition of 50wt% MEG/50wt% Water + Methane @ 5°C

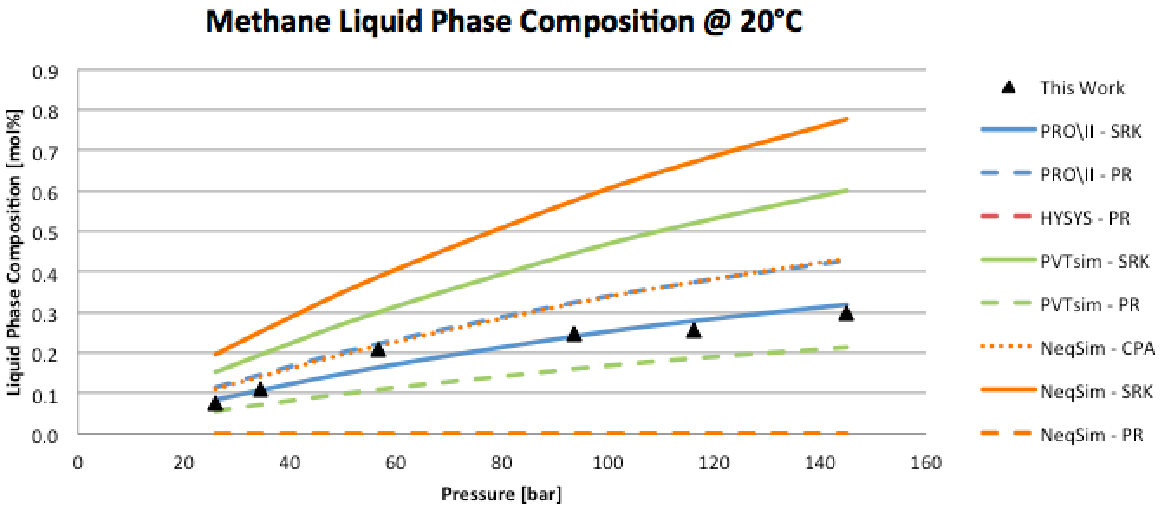

Figure 8.56: Methane Liquid Phase Composition of 50wt% MEG/50wt% Water + Methane @ 20°C

Table 8.37 shows the details of how the software deviate from the experimental data for all the mixtures. Obviously, the margins of error are small, and it is hard to read much out of the numbers. It appears the general trend is that the deviation decreases as the wt% of water is increased in the mixture, the only exception for mixtures only containing methane being for NeqSim SRK. As ethane is introduced the trends are more unclear. These results were obtained after the capillary tube was replaced, and this caused some more uncertainty in the methane and ethane composition reading.

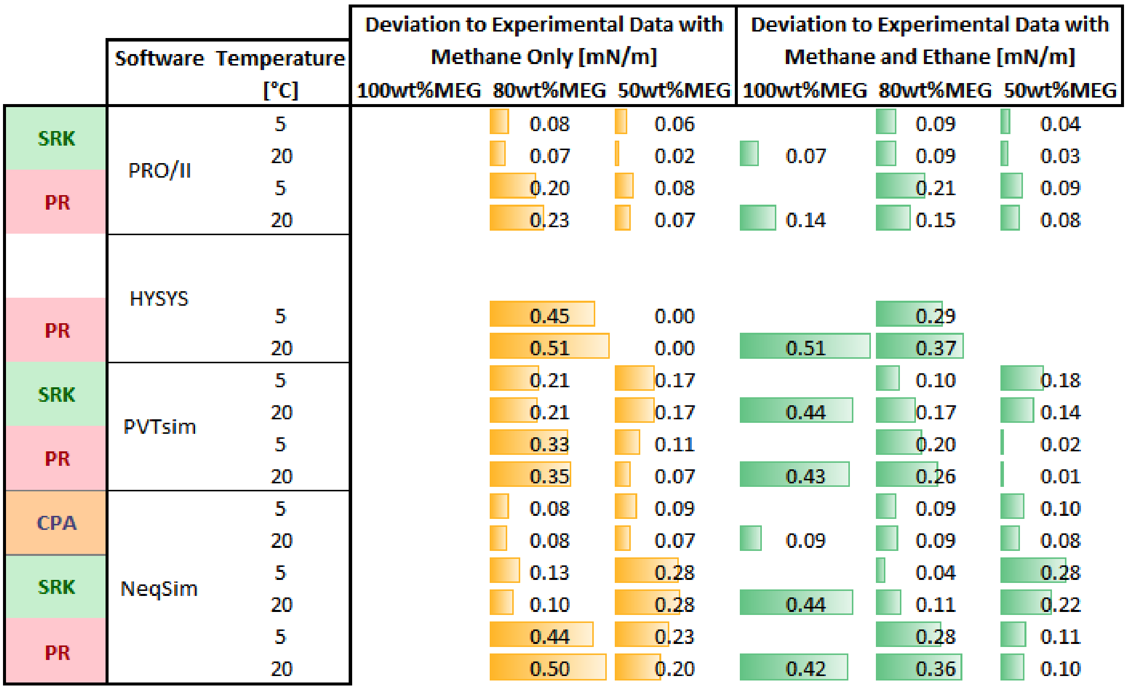

	Software	Temperature [°C]	Deviation to Experimental Data with Methane Only [mN/m]			Deviation to Experimental Data with Methane and Ethane [mN/m]		
			100wt%MEG	80wt%MEG	50wt%MEG	100wt%MEG	80wt%MEG	50wt%MEG
SRK	PRO/II	5		0.08	0.06		0.09	0.04
		20		0.07	0.02	0.07	0.09	0.03
PR		5		0.20	0.08		0.21	0.09
		20		0.23	0.07	0.14	0.15	0.08
	HYSYS							
PR		5		0.45	0.00		0.29	
		20		0.51	0.00	0.51	0.37	
SRK	PVTsim	5		0.21	0.17		0.10	0.18
		20		0.21	0.17	0.44	0.17	0.14
PR		5		0.33	0.11		0.20	0.02
		20		0.35	0.07	0.43	0.26	0.01
CPA	NeqSim	5		0.08	0.09		0.09	0.10
		20		0.08	0.07	0.09	0.09	0.08
SRK		5		0.13	0.28		0.04	0.28
		20		0.10	0.28	0.44	0.11	0.22
PR		5		0.44	0.23		0.28	0.11
		20		0.50	0.20	0.42	0.36	0.10

Table 8.37: Deviation to Experimental Data for Methane Liquid Phase Composition

Figure 8.57 shows the software predictions after ethane was added to the mixture. How the software perform relative to the others is the same as before, however the experimental data are now lowered compared to before. This means most software are overestimating. Again, HYSYS PR and NeqSim PR gave results approximately equal to zero.

Comparing figure 8.57 to 8.58 show how the software estimation changes with wt% MEG, as figure 8.58 shows the results for the 80wt% MEG/20wt% water mixture. PRO/II PR now estimates the highest mol% methane. The increase in methane mol% as pressure is increased is slower than predicted, but both NeqSim CPA and SRK as well as PRO/II SRK provides good results.

Ethane Liquid Phase Composition

Similar to methane, the ethane liquid phase composition is low. It varies from 0.01 mol% or less at several points to a maximum of 0.39 mol% at the highest pressure for the 100wt% MEG + methane/ethane mixture at 20°C. This is the same mixture at which the maximum methane mol% was found, which may suggest there was too much gas in that sample, as this ethane content is 13 times bigger than at 50wt% MEG/50wt% water + methane/ethane and 39 times bigger than for the 80wt% MEG/20wt% water + methane/ethane mixture. Seeing this as a deviation in the measurement, ethane mol% is generally less than 0.1.

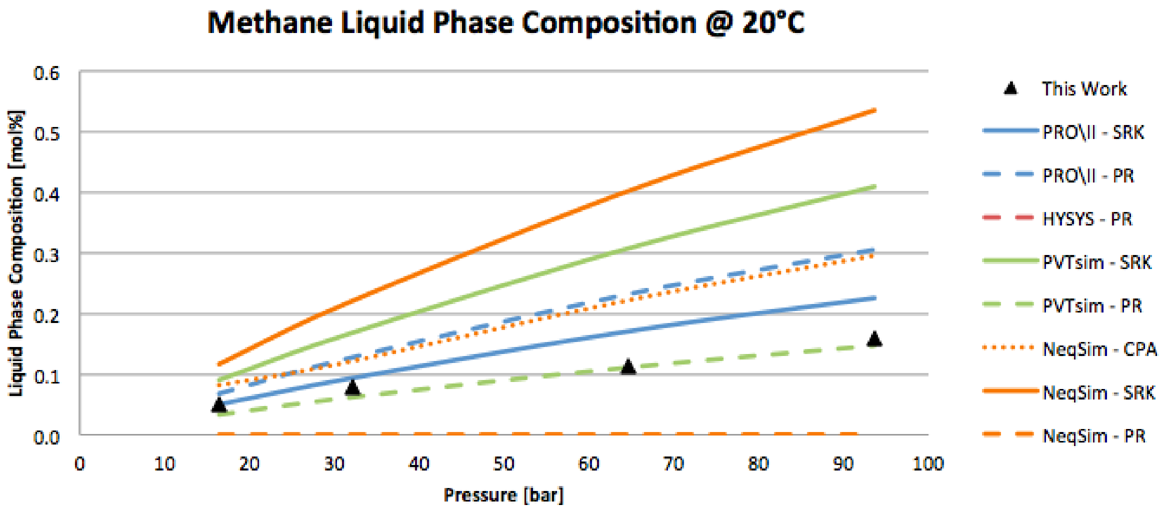

Figure 8.57: Methane Liquid Phase Composition of 50wt% MEG/50wt% Water + Methane/Ethane @ 20°C

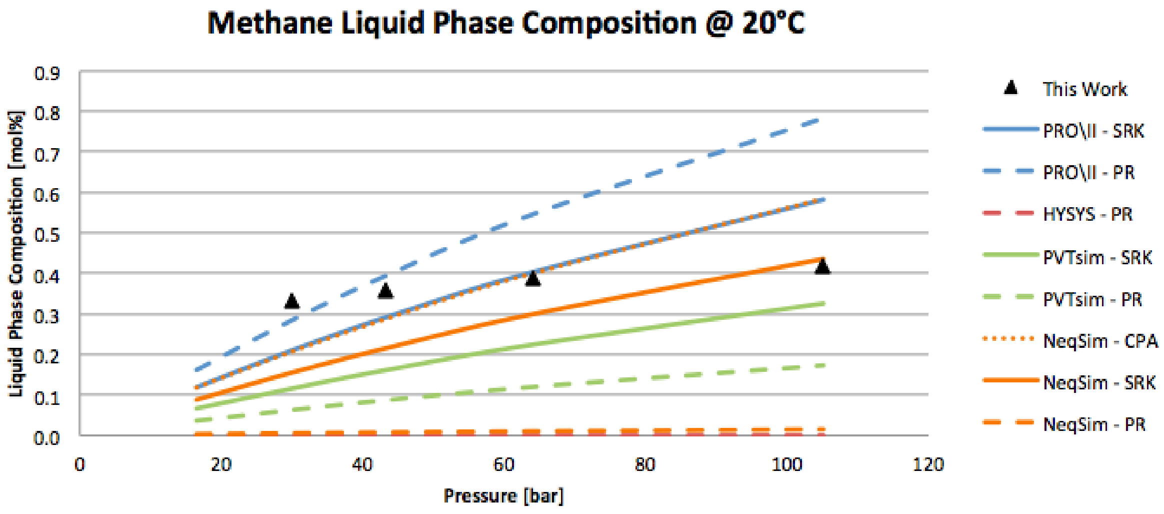

Figure 8.58: Methane Liquid Phase Composition of 80wt% MEG/20wt% Water + Methane/Ethane @ 20°C

As the GC did not respond for the 100wt% MEG + methane/ethane mixture at 5°C, as previously discussed, there are only compositional data on 20°C for this mixture. In addition, HYSYS now produce results too small to take into consideration, and is therefore taken out of the graphs.

Figure 8.59 show the ethane liquid phase composition at 20°C. As stated earlier, there is a chance that these samples contained too much gas, as there were some troubles running the GC in this period. In particular, the point at 64.2 bar appears to be too high. However, PRO/II PR and SRK provide a good estimation of the solubility. NeqSim CPA estimates values just below PRO/II, while both NeqSim and PVTsim SRK and PR give very low values.

As water is added to the mixture (80wt% MEG and 20wt% water), the ethane liquid phase composition falls below 0.10 mol% (figure 8.60). Still, PRO/II is estimating the highest values, and because the experimental data has decreased, NeqSim CPA is now providing the best results. There has also been a significant

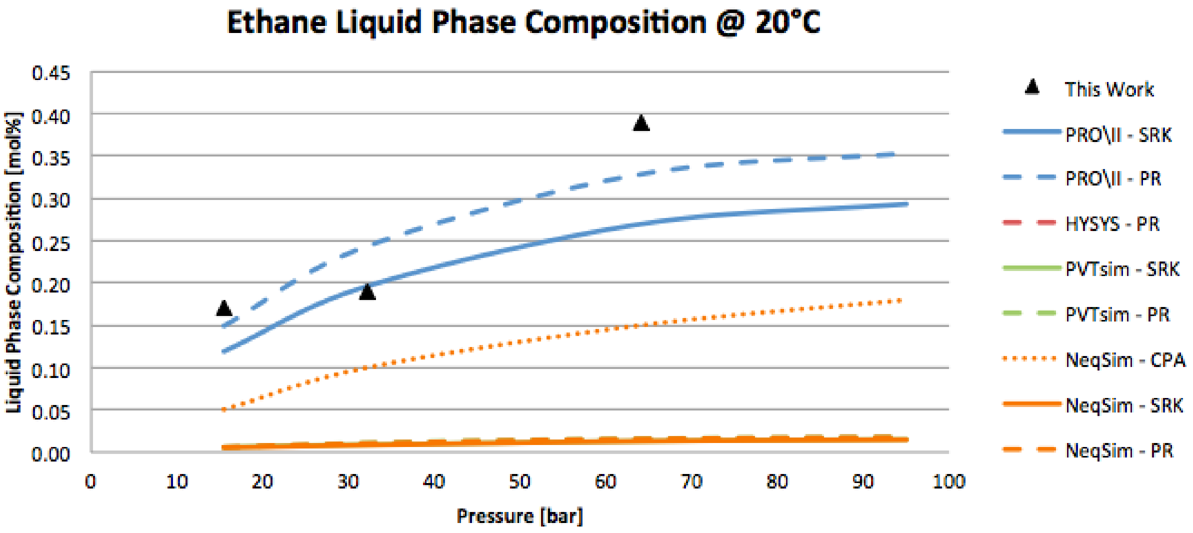

Figure 8.59: Ethane Liquid Phase Composition of 100wt% MEG + Methane/Ethane @ 20°C

increase in the estimation of ethane liquid phase composition of NeqSim SRK. PVTsim SRK and PR are also improving, whereas NeqSim PR is still producing very low results.

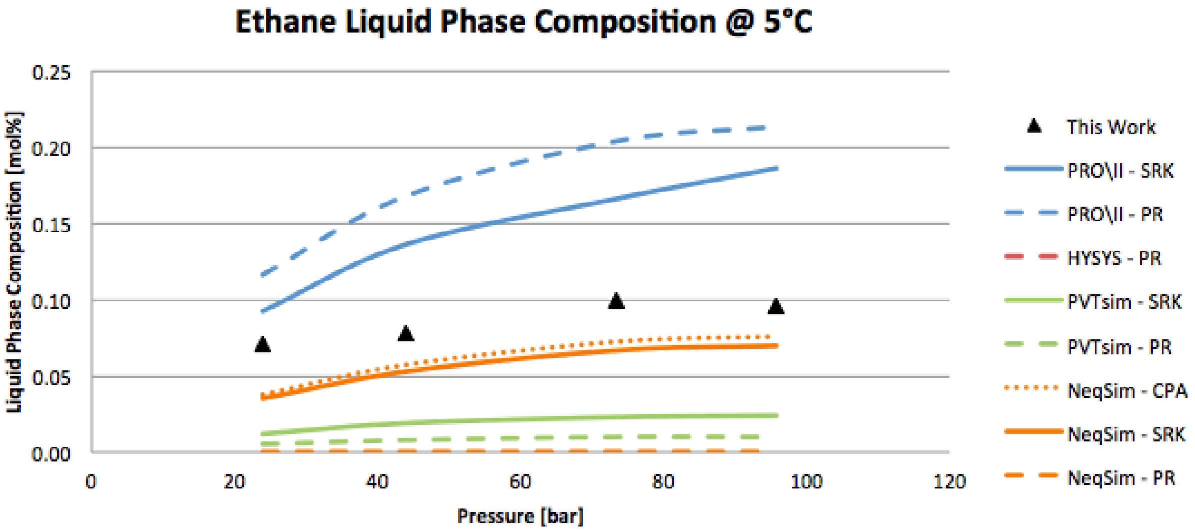

Figure 8.60: Ethane Liquid Phase Composition of 80wt% MEG/20wt% Water + Methane/Ethane @ 5°C

Finally, figure 8.61 shows the ethane liquid phase composition as the weight percent of water is increased to 50. NeqSim SRK keeps increasing its estimate and giving the highest results. Then PRO/II SRK and PR follow somewhat above the experimental data. NeqSim CPA is again providing the results closest to the experimental data, but now PVTsim SRK is slightly overestimating the ethane liquid phase composition. PVTsim PR, however, is underestimating some, as is NeqSim PR.

Table 8.38 shows how the different software deviate to the experimental data. Obviously, there is a lot of inconsistencies, and even though the deviations appear small it must be taken into consideration that the mol% of ethane in the liquid

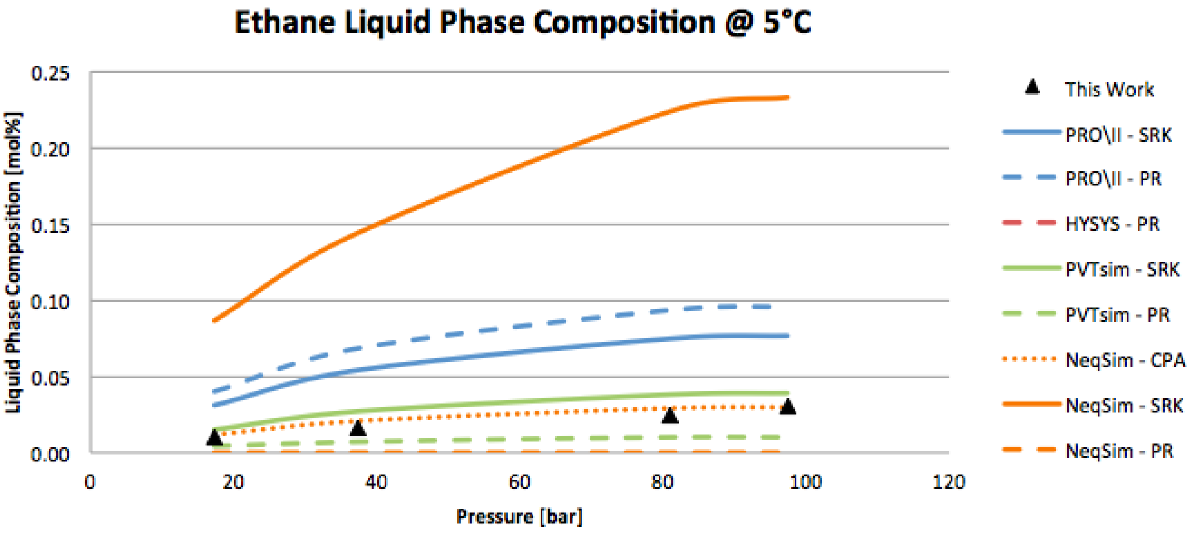

Figure 8.61: Ethane Liquid Phase Composition of 50wt% MEG/50wt% Water + Methane/Ethane @ 5°C

phase generally is below 0.10. The performances are only satisfying as water weight percent is increased to 50, however not for NeqSim SRK.

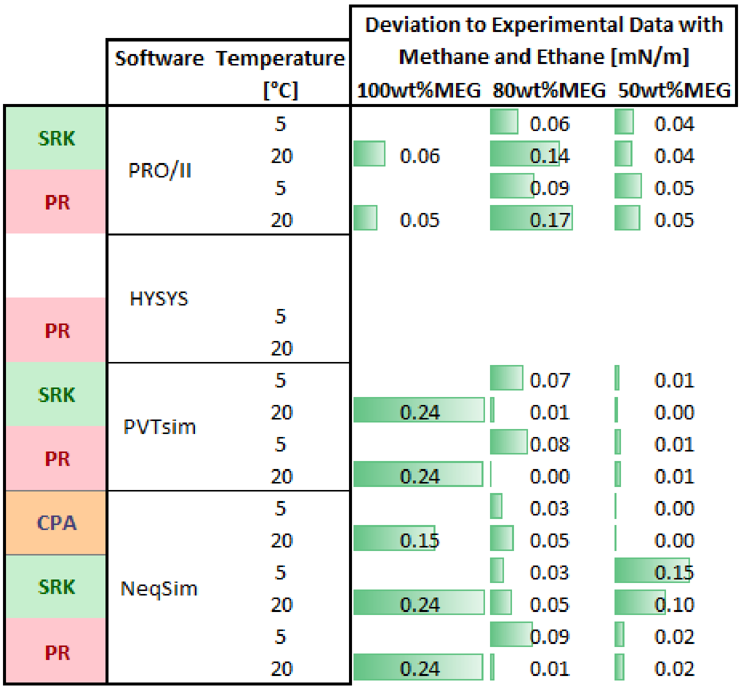

	Software	Temperature [°C]	Deviation to Experimental Data with Methane and Ethane [mN/m] 100wt%MEG	80wt%MEG	50wt%MEG
SRK	PRO/II	5		0.06	0.04
		20	0.06	0.14	0.04
PR		5		0.09	0.05
		20	0.05	0.17	0.05
	HYSYS				
PR		5			
		20			
SRK	PVTsim	5		0.07	0.01
		20	0.24	0.01	0.00
PR		5		0.08	0.01
		20	0.24	0.00	0.01
CPA	NeqSim	5		0.03	0.00
		20	0.15	0.05	0.00
SRK		5		0.03	0.15
		20	0.24	0.05	0.10
PR		5		0.09	0.02
		20	0.24	0.01	0.02

Table 8.38: Deviation to Experimental Data for Ethane Liquid Phase Composition

MEG and Water Liquid Phase Composition

Naturally, MEG and water are the dominating components in the liquid phase. In general, as figures 8.62 and 8.63 show, the software estimate MEG and water liquid phase composition for the 80wt% MEG/20wt% water + methane/ethane mixture at 20°C. Obviously, all software produce almost the same results, and the accuracy is also quite good with respect to the experimental data. The tables 8.39

and 8.40 show the deviations for the software to the experimental data of MEG and water, respectively. In general, the deviations are larger than what was the case for methane and ethane, but the molecular amount of MEG and water is so large that the percentage deviation is small.

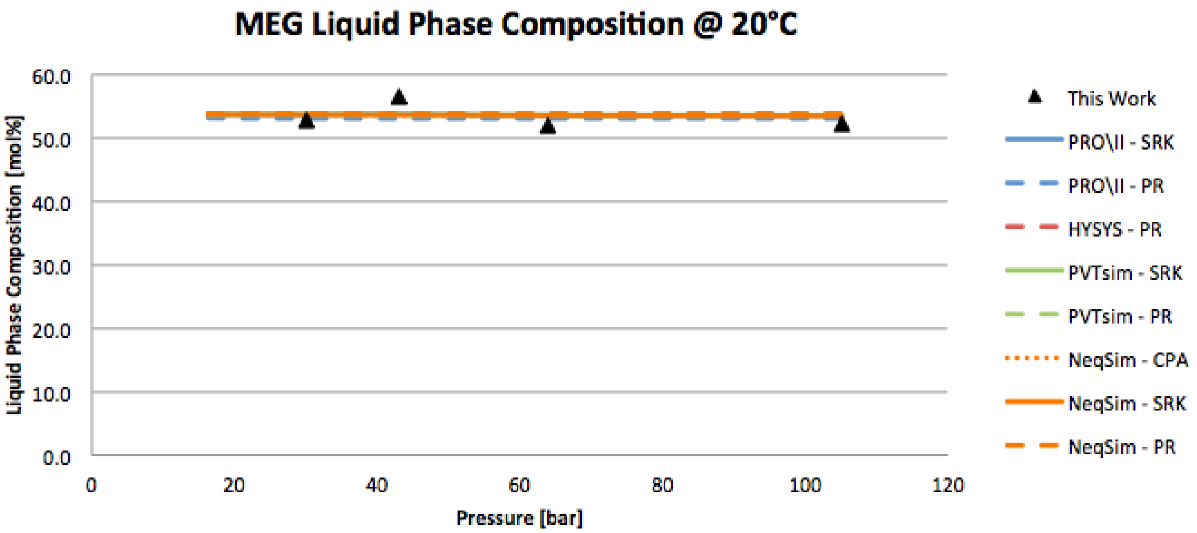

Figure 8.62: MEG Liquid Phase Composition of 80wt% MEG/20wt% Water + Methane/Ethane @ 20°C

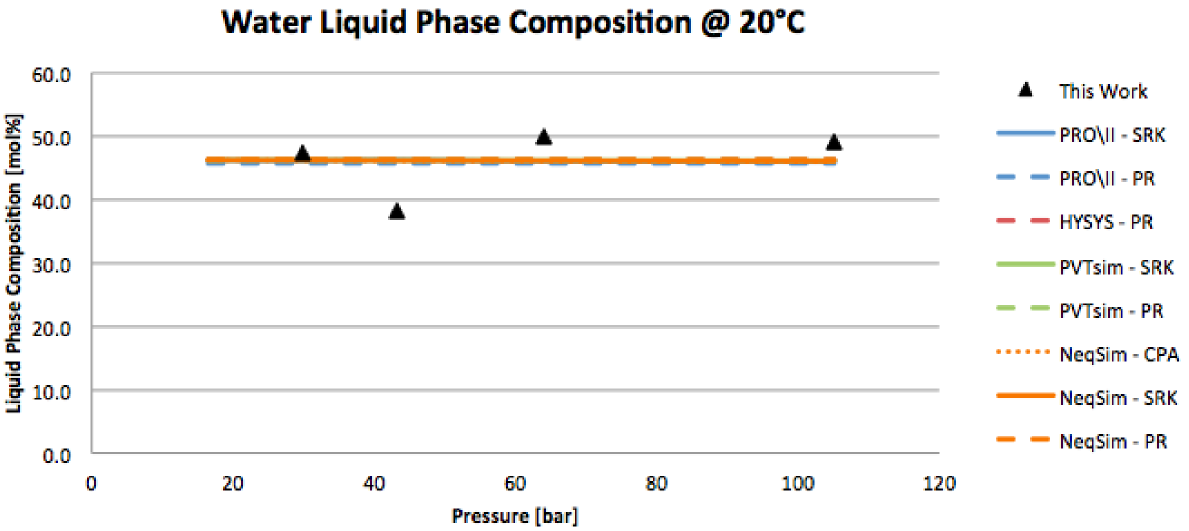

Figure 8.63: Water Liquid Phase Composition of 80wt% MEG/20wt% Water + Methane/Ethane @ 20°C

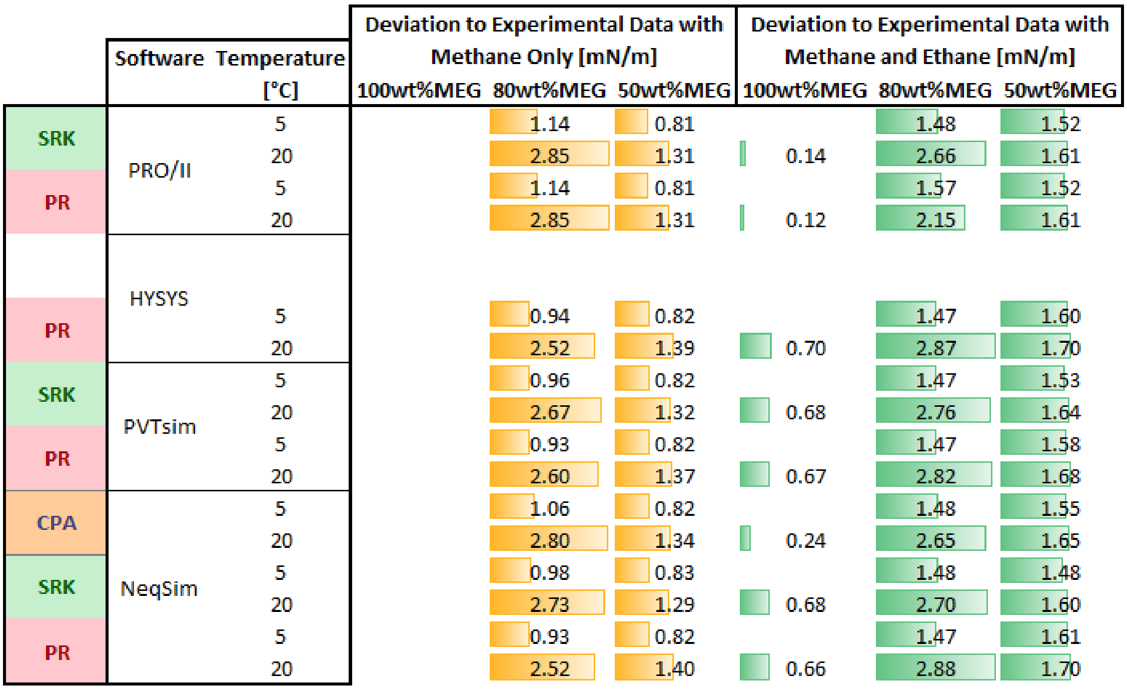

	Software	Temperature [°C]	Deviation to Experimental Data with Methane Only [mN/m]			Deviation to Experimental Data with Methane and Ethane [mN/m]		
			100wt%MEG	80wt%MEG	50wt%MEG	100wt%MEG	80wt%MEG	50wt%MEG
SRK	PRO/II	5		1.14	0.81		1.48	1.52
		20		2.85	1.31	0.14	2.66	1.61
PR		5		1.14	0.81		1.57	1.52
		20		2.85	1.31	0.12	2.15	1.61
	HYSYS							
PR		5		0.94	0.82		1.47	1.60
		20		2.52	1.39	0.70	2.87	1.70
SRK	PVTsim	5		0.96	0.82		1.47	1.53
		20		2.67	1.32	0.68	2.76	1.64
PR		5		0.93	0.82		1.47	1.58
		20		2.60	1.37	0.67	2.82	1.68
CPA	NeqSim	5		1.06	0.82		1.48	1.55
		20		2.80	1.34	0.24	2.65	1.65
SRK		5		0.98	0.83		1.48	1.48
		20		2.73	1.29	0.68	2.70	1.60
PR		5		0.93	0.82		1.47	1.61
		20		2.52	1.40	0.66	2.88	1.70

Table 8.39: Deviation to Experimental Data for MEG Liquid Phase Composition

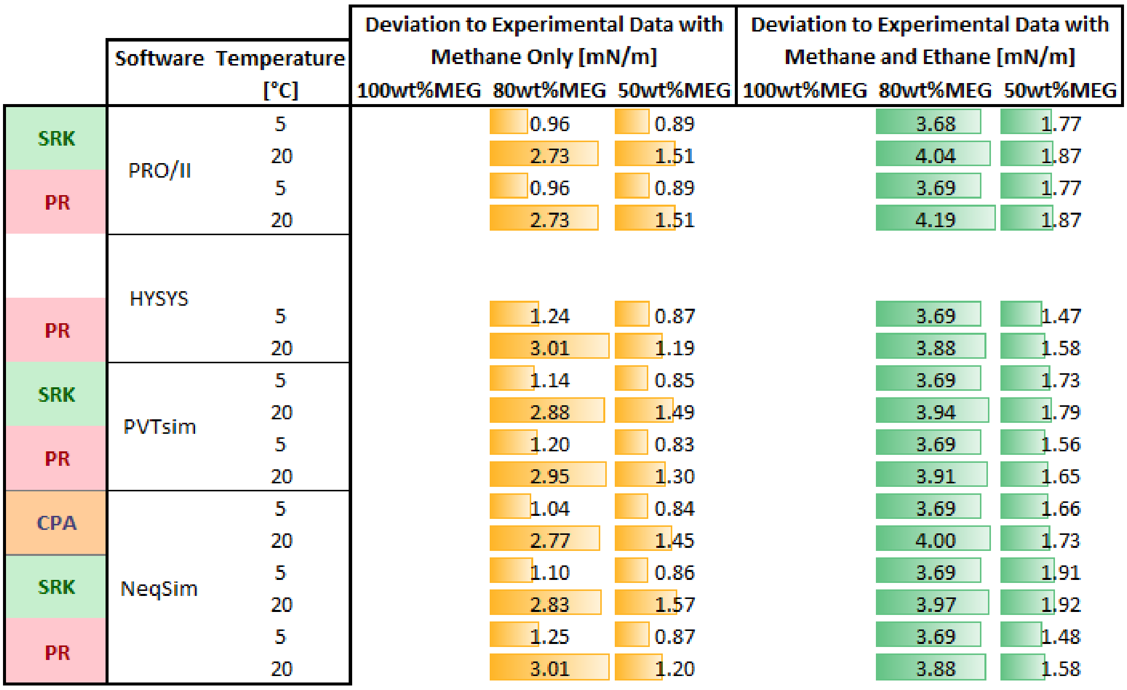

	Software	Temperature [°C]	Deviation to Experimental Data with Methane Only [mN/m]			Deviation to Experimental Data with Methane and Ethane [mN/m]		
			100wt%MEG	80wt%MEG	50wt%MEG	100wt%MEG	80wt%MEG	50wt%MEG
SRK	PRO/II	5		0.96	0.89		3.68	1.77
		20		2.73	1.51		4.04	1.87
PR		5		0.96	0.89		3.69	1.77
		20		2.73	1.51		4.19	1.87
	HYSYS							
PR		5		1.24	0.87		3.69	1.47
		20		3.01	1.19		3.88	1.58
SRK	PVTsim	5		1.14	0.85		3.69	1.73
		20		2.88	1.49		3.94	1.79
PR		5		1.20	0.83		3.69	1.56
		20		2.95	1.30		3.91	1.65
CPA	NeqSim	5		1.04	0.84		3.69	1.66
		20		2.77	1.45		4.00	1.73
SRK		5		1.10	0.86		3.69	1.91
		20		2.83	1.57		3.97	1.92
PR		5		1.25	0.87		3.69	1.48
		20		3.01	1.20		3.88	1.58

Table 8.40: Deviation to Experimental Data for Water Liquid Phase Composition

Chapter 9

Conclusion

The target of this thesis was to review how surface tension impact on separation design. Experimental work has been conducted to determine the surface tension in MEG/water mixtures. It is sought to evaluate the accuracy of NeqSim to other simulation software when calculating surface tension. This was done by comparison to experimental data from the experimental work and from literature.

Quality design of separation equipment was found to be of utmost importance as failing to do so could lead to premature demand of replacement of expensive equipment, costs regarding cleaning at high frequency and not being able to meet pollution standards. Even though geometry is ultimately the factor demanding the main focus when it comes to design, parameters like surface tension is also important. Surface tension is important when calculating droplet size and thus the settling section area of the separator. Also, it could tell something about whether break up liquid films already formed in the separator could be an issue.

The experimental work consists of measurement of surface tension, density and phase composition, where surface tension was the main task. The experimental setup has functioned over the entire timespan, and the results, with the exception of a few data points, have been very satisfactory. The deviation of the surface tension measurements was calculated on the basis of recommendations from ISO. The total average deviation for all mixtures was stated to be 2.00%. However, there are two interesting trends in the uncertainty analysis. The first is that adding ethane to the mixture reduces the deviation compared to when using pure methane gas. The second is that the deviation increases with higher amount of water present in the system.

The results of the comparison of the software against experimental data regarding hydrocarbon mixtures show two clear tendencies. Firstly, the performance of PRO/II and HYSYS throughout the whole range of experimental data is not adequate. They both are, with a few exceptions, overestimating the surface tension for all mixtures due to their simple weighted average pure component models. Second, even though the performance of both PVTsim and NeqSim could be termed satisfactory, NeqSim is superior to the estimations of PVTsim throughout most of the experimental data. The only exception is for the ternary systems, where both software overestimate the surface tension, but PVTsim slightly less than NeqSim. The data base on both ternary systems and more complex simulations of real gases, or indeed real gases, are however sparse and could favorably be further extended.

The results from the comparison of glycol mixtures show that all software overestimate the surface tension. NeqSim is once again the software with the best accuracy for all mixtures, and the CPA EoS is the overall preferred choice. In contrast to hydrocarbon mixtures PVTsim now has a large discrepancy throughout. However, the accuracy is a lot better when the amount of water in the system is increased. PRO/II and HYSYS performs better than for the hydrocarbon mixtures. The deviation for PRO/II is however drastically increasing when water is the dominating component in the system.

Chapter 10

Further Work

This thesis focuses on mixtures containing hydrocarbon and MEG/water relations. It is desirable to test the software against more systems, such as TEG/water, amines and other hydrocarbon relations to get an even better basis for comparison. It is also desirable to test more reservoir fluid systems regarding hydrocarbons, which is limited due to low availability in the literature.

In this study the experimental work consists of 100 wt% MEG, 80 wt% MEG/20 wt% water and 50 wt% MEG/50 wt% water mixtures. The experimental work of MEG/water mixtures should be continued with focus on mixtures dominated by water (e.g 5 wt% MEG/95 wt% water). In addition, reservoir fluid systems regarding hydrocarbons should be examined in the lab to extend the data base. Due to lack of time this was not possible in this thesis.

The discussion in this thesis is based on the default models implemented in each software. The different models are investigated and a brief comparison has been conducted. It is however desirable to get a better comparison between the various possibilities in the software.

When simulating glycol mixtures in NeqSim the linear gradient theory is used because the full gradient theory is not yet fully implemented. It is desirable to simulate the glycol mixtures with the gradient theory as this is expected to give more accurate results. The experimental data produced in this work will contribute to the implementation of the gradient theory for glycol systems in NeqSim.

Bibliography

[1] M. L. Alexander and M. J. Matteson. "The Automation of an Interfacial Tensiometer". In: *Colloids Surf.* (1987), pp. 201–217.

[2] R. Amin and T.N. Smith. "Interfacial tension and spreading coefficient under reservoir conditions". In: *Fluid Phase Equilibria* 142 (1997), pp. 231–241.

[3] *Aspen HYSYS Physical Property System V7.1.* 2009.

[4] T. Austrheim. "Experimental Characterization of High Pressure Natural Gas Scrubbers". PhD thesis. Universitetet i Bergen, 2006.

[5] *Azarenergy Co.* (Retrived 03/03-2014). URL: `http://www.azarenergy.com/index.php?option=com_content&task=view&id=87&Itemid=168`.

[6] A. I. Bailey. *Surface and Interfacial tension.* (Retrived 14/01-2014). Sept. 2010. URL: `http://www.thermopedia.com/content/30/`.

[7] V. Bongiono, L. E. Scriven, and H. T. Davis. "Molecular theory of fluid interfaces". In: *J. colloid and interface Sci.* (1976), pp. 462–475.

[8] J. W. Cahn and J. E. Hiliard. "Free Energy of a Nonuniform System. I. Interfacial Free Energy". In: *J. Chem. Phys.* 28 (1958), p. 258.

[9] *Calsep PVTsim V20.1.0 Method Documentation.*

[10] John M. Campbell and Robert A. Hubbard. *Gas Conditioning and Processing.* 8th. Vol. 2. Campbell Petroleum Series, 2004.

[11] Z. Chen, S Xia, and P. Ma. "Measuring Surface Tension of Liquids at High Temperature and Elevated Pressure". In: *J. Chem. Eng. Data* 53 (2008), pp. 742–744.

[12] A.S. Danesh et al. "A Modified Scaling Law and Parachor Method Approach for Improved Prediction of Interracial Tension of Gas-Condensate Systems". In: *Soc. Petr. Engrs.* (1991), pp. 515–523.

[13] J. R. Deam and R. N. Maddox. "Interfacial Tension in Hydrocarbon System". In: *J. Chem. and Eng. Data* (1970), pp. 216–222.

[14] R. B. Dorshow. "The Simultaneous Measurement of Interfacial Tension and Oil Viscosity at Reservoir Conditions for Prudhoe Bay Fluids by Surface Laser Light Scattering Spectroscopy". In: *Soc. Petr. Eng.* (1995), pp. 120–128.

[15] M. J. Fawcett. "Evaluation of Correlation and Parachors To Predict Low Interfacial Tensions in Condensate Systems". In: *Soc. Petr. Eng.* (1994), pp. 1–22.

[16] A. Firoozabadi and H. J. Ramney. "Surface Tension of Water-Hydrocarbon Systems at Reservoir Conditions". In: *J. of Can. Petr. Tech* (1988), pp. 41–48.

[17] A. Firoozabadi et al. "Surface Tension of Reservoir Crude-Oil/Gas Systems Recognizing the Asphalt in the Heavy Fraction". In: *Soc. Petr. Eng.* (1988), pp. 265–272.

[18] P. Fotland and O. P. Bjørlykke. “Phase Behavior and Interfacial Tension as a Function of Pressure and Temperature in a Ternary Alkane System”. In: *J. Phys. Chem* 93 (1989), pp. 6407–6413.

[19] F. Gozalpour et al. “Viscosity, density, interfacial tension and compositional data for near critical mixtures of methane + butane and methane + decane systems at 310.95 K”. In: *Fluid Phase Equilibria* 233 (2005), pp. 144–150.

[20] D. I. Hakim, D. Steinberg, and L.I. Stiel. “Generalized Relationship for the Surface Tension of Polar Fluids”. In: *Ind. Eng. Chem. Fundamen.* 10 (1971), pp. 174–175.

[21] M. S. Haniff and A. J. Pearce. “Measuring Interfacial Tensions in a Gas-Condensate System With a Laser-Light-Scattering Technique”. In: *Soc. Petr. Engrs.* (1990), pp. 589–594.

[22] J.N. Heng et al. “High Pressure Gas Separation and Conditioning”. In: *Gas Proc. Assoc.* (2008).

[23] J. O. Hinze. “Fundamentals of the Hydrodynamic Mechanism of Splitting in Dispersion Processes”. In: *AIChE Journal* (1955), pp. 289–295.

[24] E. W. Hough and H. G. Warren. “Correlation of Interfacial Tension of Hydrocarbons”. In: *Soc. Petr. Eng.* (1966), pp. 345–349.

[25] S. H. Huang and M. Radosz. “Equation of state for small, large, polydisperse and associating molecules”. In: *Eng. Chem. Res.* (1990), p. 2284.

[26] American Petroleum Institute. *Technical Data Book - Petroleum Refining.* 3rd. Vol. 2. American Petroleum Institute, 1977.

[27] American Petroleum Institute. *Technical Data Book - Petroleum Refining.* 4th. Vol. 2. American Petroleum Institute, 1983.

[28] M. Ishii and M. A. Grolmes. “Inception Criteria for Droplet Entrainment in Two-Phase Concurrent Film Flow”. In: *AIChE Journal* (1975), pp. 308–318.

[29] H. Kahl, T. Wadewitz, and J. Winkelmann. “Surface Tension and Interfacial Tension of Binary Organic Liquid Mixtures”. In: *J. Chem. Eng. Data* 48 (2003), pp. 1500–1507.

[30] G. M. Kontogeorgis et al. “An Equation of State for Associating Fluid”. In: *Ind. Eng. Chem. Res.* (1996), pp. 4310–4318.

[31] D. Lee. “Snøhvit Gas Condensate-SFW IFT Final Report”. In: (2007).

[32] E. G. B. Lindeberg, B. J. A. Bjørkvik, and K. A. Strand. “Interface Light Scattering Measurment og Low Interfacial Tension on a Gas Condensate System at High Pressure and Temperature”. In: *Soc. Petr. Eng.* (1996), pp. 265–272.

[33] C. Miqueu et al. “Petroleum mixtures: An efficient predictive method for surface tension estimations at reservoir conditions”. In: (2007).

[34] H. N. Nilssen et al. “Equilibrium Phase Densities, Interfacial Tensions for the Ethane + n-Pentane System at 294.15 K”. In: *J. Chem. Eng. Data* 56 (2011), pp. 2128–2132.

[35] H. N. Nilssen et al. “Equilibrium Phase Densities, Vapor Phase Compositions, and Interfacial Tensions for the Methane + Ethane + n-Pentane System at 294.15 K”. In: *J. Chem. Eng. Data* 56 (2011), pp. 4006–4011.

[36] H.N. Nilssen. “Experimental Characterization of Interfacial Behaviours of Hydrocarbon Mixtures in High Pressure Systems”. PhD thesis. Norwegian University of Science and Technology, 2011.

[37] O. G. Nino-Amezquita et al. “Measurement and Prediction of Interfacial Tension of Binary Mixtures”. In: *Ind. Eng. Chem. Res.* (2010), pp. 592–601.

[38] *NORSOK STANDARD P-100 - Process Systems.* Standard Norge. 2001.

[39] A. Peneloux and E. Rauzy. “A CONSISTENT CORRECTION FOR REDLICH-KWONG-SOAVE VOLUMES”. In: *Fluid Phase Equilibria* 8 (1982), pp. 7–23.

[40] Ding-Yu. Peng and D. B. Robinson. “A New Two-Constant Equation of State”. In: *Ind. Eng. Chem.* 15 (1976), pp. 59–64.

[41] B.F. Pennington and E.W. Hough. “Interfacial Tension of the Methane-Normal Butane System”. In: *Producers Monthly* (1965).

[42] B.E. Poling, J.M. Prausnitz, and J.P. O‘Connel. *The properties of gases and liquids.* 5th. McGRAW-HILL, 2001.

[43] A. Putnam. “Integratable Form of Droplet Drag Coefficient”. In: *ARS Journal* (1961).

[44] A. J. Queimeda et al. “Measurement and modeling of surface tensions of asymmetric systems: heptane, eicosane, docosane, tetracosane and their mixtures”. In: *Fluid Phase Equilibria* 214 (2003), pp. 211–221.

[45] D. N. Rao and J. I. Lee. “Determination of gas–oil miscibility conditions by interfacial tension measurements”. In: *Journal of Colloid and Interface Science* 262 (2003), pp. 474–482.

[46] O. Redlich and J.N.S Kwong. In: *Chem. Rev.* 44 (1949), p. 233.

[47] J.S. Rowlinson. “Translation of J.D. van der Waals The thermodynamic theory of capillarity under the hypothesis of a continuous variation of density”. In: *J. Stat. Phys.* 20 (1979), p. 197.

[48] *Separation technology products - Koch-Glitsch.* (Retrived 09/05-2014). URL: `http://www.koch-glitsch.com/mistelimination/default.aspx`.

[49] D. S. Sequeira, S. C. Ayirala, and D. N. Rao. “Reservoir Condition Measurements of Compositional Effects on Gas-Oil Interfacial Tension and Miscibility”. In: *Soc. Petr. Eng.* (2008), pp. 1–24.

[50] R. D. Shaver, R. L. Robinson Jr, and K. A. M. Gasem. “Equilibrium phase compositions, densities, and interfacial tensions for ethane + 1-methylnaphthalene at 344.3 K”. In: *Fluid Phase Equilibria* (2001), pp. 141–153.

[51] *SIMSCI PRO/II V9.1 Interactive Reference Help.*

[52] J. C. Slattery and J. Chen. “Alternative Solution for Spinning Drop Interfacial Tensiometer”. In: *J. Colloid Interface Sci.* (1978), pp. 371–373.

[53] G. Soave. “Equilibrium constants from a modified Redlich-Kwong equation of state”. In: *Chem. Eng. Sci.* 27 (1972), pp. 1197–1203.

[54] *Statoil/NTNU NeqSim Documentation.*

[55] G. L. Stegemeier and E. W. Hough. “Interfacial Tension of the Methane-Normal Pentane System”. In: *Prod. Monthly* (Nov. 1961), p. 6.

[56] G. L. Stegemeier et al. “Interfacial Tension of the Methane-Normal Decane System”. In: *Soc. Petr. Eng.* (1962), pp. 257–260.

[57] D. B. Thiessen and K. F. Man. *The Measurement, Instrumentation and Sensors Handbook on CD-ROM.* Print ISBN: 978-0-8493-8347-2, eBook ISBN: 978-0-415-87617-9, DOI: 10.1201/9780415876179.ch31. CRC Press Llc, 1999.

[58] M. Tun. “Using Light Scattering Method to Find the Surface Tension of Water”. In: (2006).

[59] *Uncertainty of measurement-part 3: Guide to the expression of uncertainty in measurement (GUM: 1995).* ISO/IEC Guide 98-3:2008.

[60] J.C. Viles. “Predicting Liquid Re-Entrainment in Horizontal Separators”. In: *SPE, Paragon Engineering Service* (1993), pp. 405–409.

[61] *Vötsch Industrietechnik.* (Retrived 05/02-2014). URL: `http://www.v-it.com/en/home/schunk01.c.59546.en`.

[62] O. R. Wagner and R.O. Leach. “Effect of Interfacial Tension on the Displacement Efficiency”. In: *Soc. Petr. Eng.* (1966), pp. 335–344.

[63] H. G. Warren. “Interfacial Tension Measurements of Methane-Normal Heptane and Ethylene-Normal Heptane Systems by the Pendant Drop Method””. PhD thesis. Mississippi State U., 1965.

[64] C. F. Weinaug and D. L. Katz. “Surface Tensions of Methane - Propane Mixtures”. In: *Ind. Eng. Chem.* 35 (1943), pp. 239–246.

[65] D. Yang and Y. Gu. “A New Experimental Technique for Studying Gas Mass Transfer in the Crude Oil by Analysis of the Measured Dynamic and Equilibrium Interfacial Tensions”. In: *Soc. Petr. Eng.* (2006), pp. 1–14.

[66] D. Yang and Y. Gu. “Determination of Diffusion Coefficients and Interface Mass-Transfer Coefficients of the Crude Oil-CO2 System by Analysis of the Dynamic and Equilibrium Interfacial Tensions”. In: *Ind. Eng Chem.* 47 (2008), pp. 5447–5455.

[67] H. R. Zhang, B. J. A. Bjørkvik, and B. J. Moffatt. “Determination of Low Interfacial Tension with a Laser Light Scattering Technique and a Comparative Analysis with Drop Shape Methods”. In: *Journal of Colloid and Interface Science* (2001), pp. 11–20.

[68] Y. X. Zuo and E. H. Stenby. “A Linear Gradient Theory Model for Calculating Interfacial Tensions of Mixtures”. In: *J. Colloid Interface Sci.* (1996), pp. 126–132.

Appendix A

Appendix

A.1 Experimental Data

This appendix gives a complete overview of collected experimental data.

Mixture	Data points	Temperature range ($^\circ C$)	Pressure range (bar)	Surface tension (mN/m)	Reference	Technique
Hydrocarbon systems						
methane + propane	51	29 - 39	69 - 94	0 - 0.93	Haniff and Pearce [21]	Laser Light Scattering
methane + propane	46	-15 - 65	3 - 85	0.2 - 12	Weinaug and Katz [64]	Capillary Rise
methane + propane	14	10 - 45	6 - 63	2.1 - 9.1	Weinaug and Katz [64]	Drop Volume
methane + n-butane	6	35	100 - 127	0 - 0.85	Gozalpour et al. [19]	Meniscus Height
methane + n-butane	80	37 - 88	89 - 132	0 - 2	Pennington and Hough [41]	
methane + n-pentane					Stegemeier and Hough [55]	
methane + n-pentane	36	38	82 - 167	0 - 5	Wagner et al. [62]	
methane + n-pentane	43	37 - 138	27 - 160	0.1 - 12	Amin et al. [2]	Pendant Drop
methane + n-hexane	9	27 - 77	20 - 100	4 - 14.2	Nino-Amezquita et al. [37]	Pendant Drop
methane + n-heptane	3	25	20 - 50	13 - 16.6	Nino-Amezquita et al. [37]	Pendant Drop
methane + n-heptane	20	37 - 121	37 - 151	1.8 - 14	Amin et al. [2]	Pendant Drop
methane + n-heptane	42	38 - 138	28 - 214	0.2 - 14.9	Warren [63]	Pendent Drop
methane + n-nonane	6	-1	20 - 100	8.3 - 19.3	Deam and Maddox [13]	Pendant Drop
methane + n-decane	53	37 - 138	27 - 310	0.4 - 20	Amin et al. [2]	Pendant Drop
methane + n-decane	37	38 - 88	97 - 352	0.1 - 10	Stegemeier et al. [56]	Pendant Drop
ethane + n-pentane	9	21	7 - 30	2.7 - 11	Nilssen et al. [34]	Pendant Drop
ethane + 1-methylnaphthalene	9	71	83 - 138	0.3 - 3.6	Shaver et al. [50]	
ethylene + n-heptane	51	38 - 154	14 - 97	0.3 - 13.9	Warren et al. [63]	Pendant Drop
heptane + eicosane	12	40 - 70	1	18.6 - 25.8	Queimeda et al. [44]	Wilhelmy Plate
heptane + docosane	12	40 - 70	1	19.1 - 25.9	Queimeda et al. [44]	Wilhelmy Plate
heptane + tetracosane	10	40 - 70	1	19.6 - 26	Queimeda et al. [44]	Wilhelmy Plate
cyclohexane + heptane	11	15 - 45	1	16.7 - 25.3	Kahl et al. [29]	Pendant Drop
cyclohexane + propanone	11	15 - 45	1	19.6 - 25.3	Kahl et al. [29]	Pendant Drop
benzene + p-xylene	35	80 - 200	1	8.3 - 20.3	Chen et al. [11]	Maximum Bubble Pressure
toluene + propanone	11	15 - 45	1	19.0 - 28.9	Kahl et al. [29]	Pendant Drop
methane + propane + n-decane	91	20 - 97	105 - 272	0 - 1.6	Fotland and Bjørlykke [18]	Laser Light Scattering
methane + ethane + n-pentane	9	21	16 - 77	4 - 12	Nilssen et al. [35]	Pendant Drop
heptane + eicosane + tetracosane	25	40 - 70	1	18.5 - 27.3	Queimeda et al. [44]	Wilhelmy Plate

Table A.1: Experimental Data on Binary and Ternary Systems

Mixture	Data points	Temperature range ($^\circ C$)	Pressure range (bar)	Surface tension (mN/m)	Reference	Technique
Reservoir fluid systems						
Terra Nova live oil		96	200 - 640	0.1 - 4.5	Rao and Lee [45]	
Petroleum mixtures					Miqueu et al. [33]	
Weyburn crude oil					Yang and Gu [66]	Pendant Drop
Weyburn crude oil					Yang and Gu [65]	Pendant Drop
Prudhoe bay oil	40				Dorshow [14]	Laser Light Scattering
Gas + crude oil					Firoozabadi et al. [17]	Pendant Drop
Gas + oil	16	114	103 - 413	0 - 7	Sequeira et al. [49]	Capillary Rise
Associate gas	15	10 - 93	10 - 172	0.2 - 14	Heng et al. [22]	Capillary Rise
Wet gas	10	-46 - 38	14 - 103	0.2 - 14	Heng et al. [22]	Capillary Rise
Gas condensate	15	124	300 - 413	0 - 0.7	Lindeberg [32]	Laser Light Scattering
Gas condensate	21	76	240 - 500	0 - 2	Zhang et al. [67]	Laser Light Scattering
Gas condensate	20		172 - 420	0 - 2.8	Fawcett [15]	Laser Light Scattering
Gas condensate	40	30 -12	249 - 359	0 - 0.74	Danesh et al. [12]	
Gas condensate	1	92	267	42.1	Lee [31]	Pendant Drop

Table A.2: Experimental Data on Reservoir Fluids

A.2 Tables

This section shows the complete set of data regarding surface tension in this thesis. The tables shows the experimental value and the simulated values for every software. They also show an absolute average deviation for each mixture.

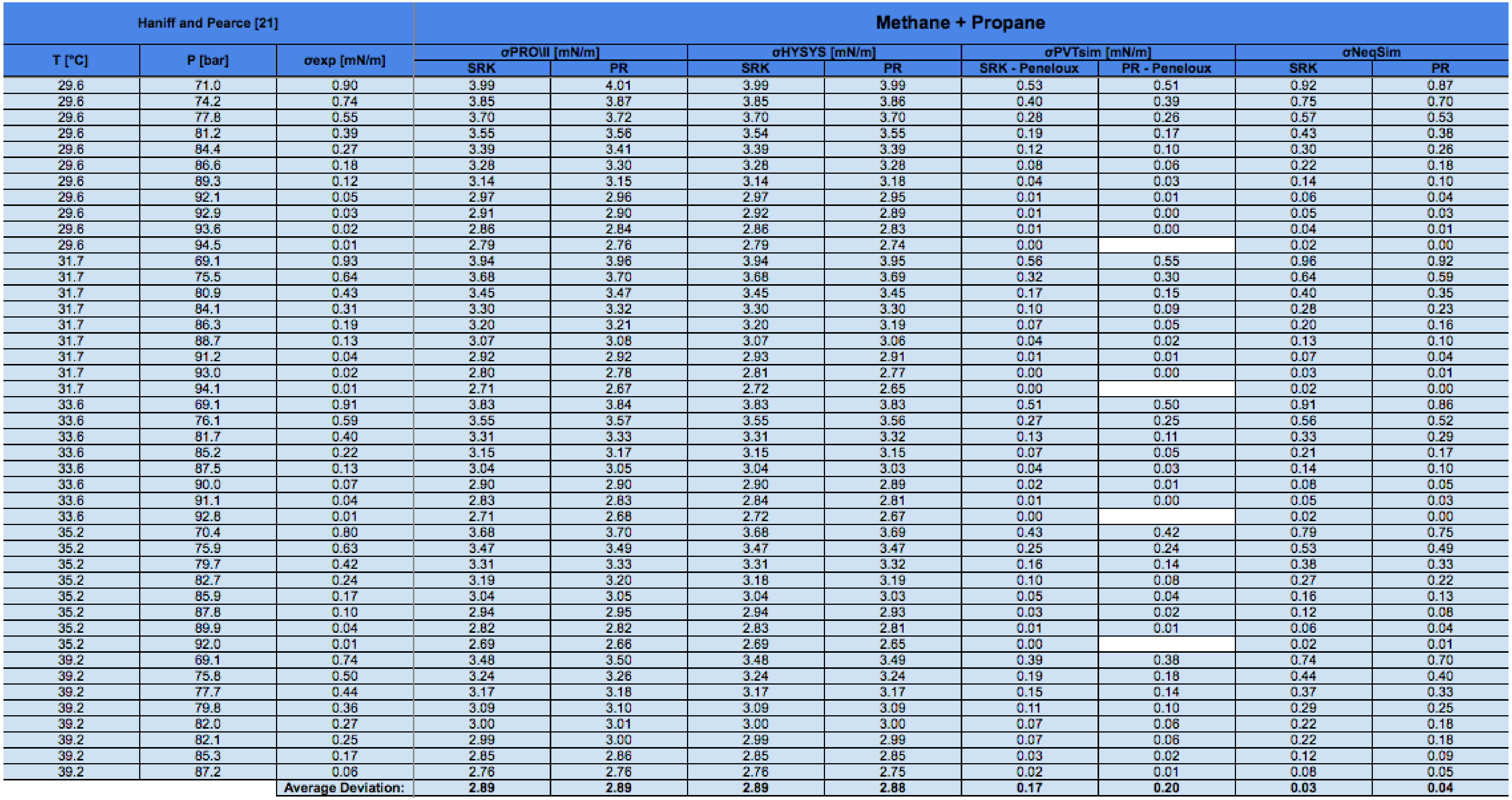

Haniff and Pearce [21]			Methane + Propane							
T [°C]	P [bar]	σexp [mN/m]	σPRO\II [mN/m]		σHYSYS [mN/m]		σPVTsim [mN/m]		σNeqSim	
			SRK	PR	SRK	PR	SRK - Peneloux	PR - Peneloux	SRK	PR
29.6	71.0	0.90	3.99	4.01	3.99	3.99	0.53	0.51	0.92	0.87
29.6	74.2	0.74	3.85	3.87	3.85	3.86	0.40	0.39	0.75	0.70
29.6	77.8	0.55	3.70	3.72	3.70	3.70	0.28	0.26	0.57	0.53
29.6	81.2	0.39	3.55	3.56	3.54	3.55	0.19	0.17	0.43	0.38
29.6	84.4	0.27	3.39	3.41	3.39	3.39	0.12	0.10	0.30	0.26
29.6	86.6	0.18	3.28	3.30	3.28	3.28	0.08	0.06	0.22	0.18
29.6	89.3	0.12	3.14	3.15	3.14	3.18	0.04	0.03	0.14	0.10
29.6	92.1	0.05	2.97	2.96	2.97	2.95	0.01	0.01	0.06	0.04
29.6	92.9	0.03	2.91	2.90	2.92	2.89	0.01	0.00	0.05	0.03
29.6	93.6	0.02	2.86	2.84	2.86	2.83	0.01	0.00	0.04	0.01
29.6	94.5	0.01	2.79	2.76	2.79	2.74	0.00		0.02	0.00
31.7	69.1	0.93	3.94	3.96	3.94	3.95	0.56	0.55	0.96	0.92
31.7	75.5	0.64	3.68	3.70	3.68	3.69	0.32	0.30	0.64	0.59
31.7	80.9	0.43	3.45	3.47	3.45	3.45	0.17	0.15	0.40	0.35
31.7	84.1	0.31	3.30	3.32	3.30	3.30	0.10	0.09	0.28	0.23
31.7	86.3	0.19	3.20	3.21	3.20	3.19	0.07	0.05	0.20	0.16
31.7	88.7	0.13	3.07	3.08	3.07	3.06	0.04	0.02	0.13	0.10
31.7	91.2	0.04	2.92	2.92	2.93	2.91	0.01	0.01	0.07	0.04
31.7	93.0	0.02	2.80	2.78	2.81	2.77	0.00	0.00	0.03	0.01
31.7	94.1	0.01	2.71	2.67	2.72	2.65	0.00		0.02	0.00
33.6	69.1	0.91	3.83	3.84	3.83	3.83	0.51	0.50	0.91	0.86
33.6	76.1	0.59	3.55	3.57	3.55	3.56	0.27	0.25	0.56	0.52
33.6	81.7	0.40	3.31	3.33	3.31	3.32	0.13	0.11	0.33	0.29
33.6	85.2	0.22	3.15	3.17	3.15	3.15	0.07	0.05	0.21	0.17
33.6	87.5	0.13	3.04	3.05	3.04	3.03	0.04	0.03	0.14	0.10
33.6	90.0	0.07	2.90	2.90	2.90	2.89	0.02	0.01	0.08	0.05
33.6	91.1	0.04	2.83	2.83	2.84	2.81	0.01	0.00	0.05	0.03
33.6	92.8	0.01	2.71	2.68	2.72	2.67	0.00		0.02	0.00
35.2	70.4	0.80	3.68	3.70	3.68	3.69	0.43	0.42	0.79	0.75
35.2	75.9	0.63	3.47	3.49	3.47	3.47	0.25	0.24	0.53	0.49
35.2	79.7	0.42	3.31	3.33	3.31	3.32	0.16	0.14	0.38	0.33
35.2	82.7	0.24	3.19	3.20	3.18	3.19	0.10	0.08	0.27	0.22
35.2	85.9	0.17	3.04	3.05	3.04	3.03	0.05	0.04	0.16	0.13
35.2	87.8	0.10	2.94	2.95	2.94	2.93	0.03	0.02	0.12	0.08
35.2	89.9	0.04	2.82	2.82	2.83	2.81	0.01	0.01	0.06	0.04
35.2	92.0	0.01	2.69	2.66	2.69	2.65	0.00		0.02	0.01
39.2	69.1	0.74	3.48	3.50	3.48	3.49	0.39	0.38	0.74	0.70
39.2	75.8	0.50	3.24	3.26	3.24	3.24	0.19	0.18	0.44	0.40
39.2	77.7	0.44	3.17	3.18	3.17	3.17	0.15	0.14	0.37	0.33
39.2	79.8	0.36	3.09	3.10	3.09	3.09	0.11	0.10	0.29	0.25
39.2	82.0	0.27	3.00	3.01	3.00	3.00	0.07	0.06	0.22	0.18
39.2	82.1	0.25	2.99	3.00	2.99	2.99	0.07	0.06	0.22	0.18
39.2	85.3	0.17	2.85	2.86	2.85	2.85	0.03	0.02	0.12	0.09
39.2	87.2	0.06	2.76	2.76	2.76	2.75	0.02	0.01	0.08	0.05
		Average Deviation:	**2.89**	**2.89**	**2.89**	**2.88**	**0.17**	**0.20**	**0.03**	**0.04**

Table A.3: Methane + Propane

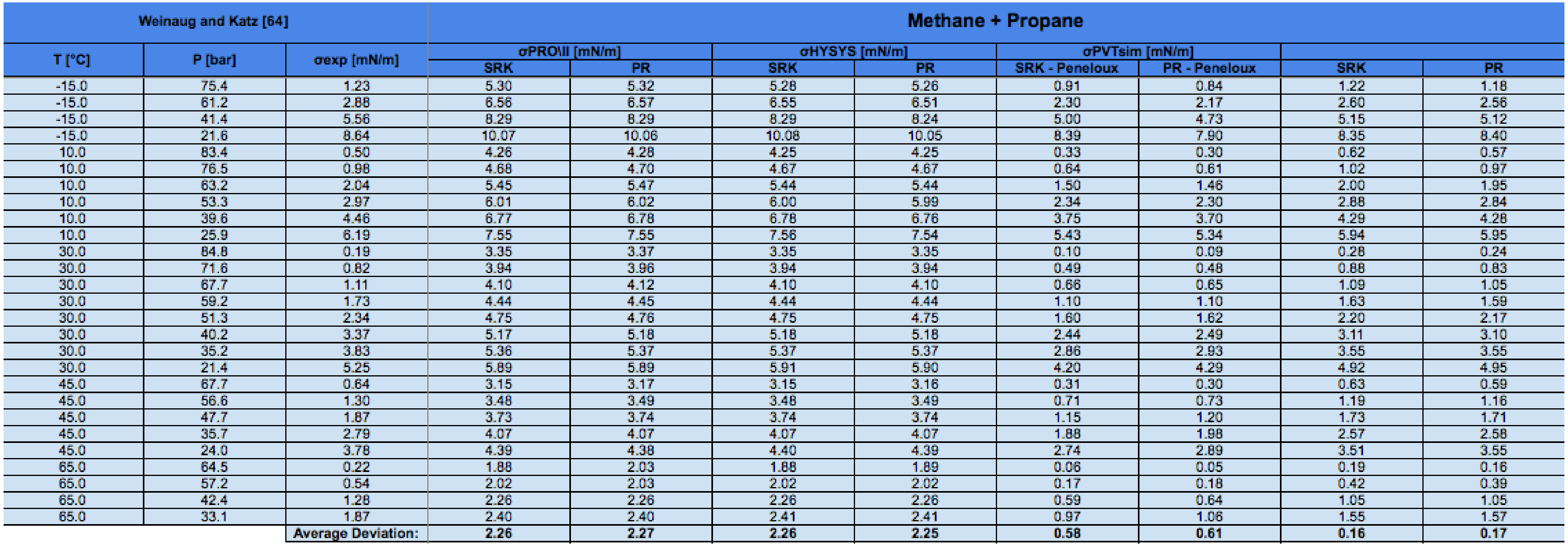

Weinaug and Katz [64]			Methane + Propane							
T [°C]	P [bar]	σexp [mN/m]	σPRO\II [mN/m]		σHYSYS [mN/m]		σPVTsim [mN/m]			
			SRK	PR	SRK	PR	SRK - Peneloux	PR - Peneloux	SRK	PR
-15.0	75.4	1.23	5.30	5.32	5.28	5.26	0.91	0.84	1.22	1.18
-15.0	61.2	2.88	6.56	6.57	6.55	6.51	2.30	2.17	2.60	2.56
-15.0	41.4	5.56	8.29	8.29	8.29	8.24	5.00	4.73	5.15	5.12
-15.0	21.6	8.64	10.07	10.06	10.08	10.05	8.39	7.90	8.35	8.40
10.0	83.4	0.50	4.26	4.28	4.25	4.25	0.33	0.30	0.62	0.57
10.0	76.5	0.98	4.68	4.70	4.67	4.67	0.64	0.61	1.02	0.97
10.0	63.2	2.04	5.45	5.47	5.44	5.44	1.50	1.46	2.00	1.95
10.0	53.3	2.97	6.01	6.02	6.00	5.99	2.34	2.30	2.88	2.84
10.0	39.6	4.46	6.77	6.78	6.78	6.76	3.75	3.70	4.29	4.28
10.0	25.9	6.19	7.55	7.55	7.56	7.54	5.43	5.34	5.94	5.95
30.0	84.8	0.19	3.35	3.37	3.35	3.35	0.10	0.09	0.28	0.24
30.0	71.6	0.82	3.94	3.96	3.94	3.94	0.49	0.48	0.88	0.83
30.0	67.7	1.11	4.10	4.12	4.10	4.10	0.66	0.65	1.09	1.05
30.0	59.2	1.73	4.44	4.45	4.44	4.44	1.10	1.10	1.63	1.59
30.0	51.3	2.34	4.75	4.76	4.75	4.75	1.60	1.62	2.20	2.17
30.0	40.2	3.37	5.17	5.18	5.18	5.18	2.44	2.49	3.11	3.10
30.0	35.2	3.83	5.36	5.37	5.37	5.37	2.86	2.93	3.55	3.55
30.0	21.4	5.25	5.89	5.89	5.91	5.90	4.20	4.29	4.92	4.95
45.0	67.7	0.64	3.15	3.17	3.15	3.16	0.31	0.30	0.63	0.59
45.0	56.6	1.30	3.48	3.49	3.48	3.49	0.71	0.73	1.19	1.16
45.0	47.7	1.87	3.73	3.74	3.74	3.74	1.15	1.20	1.73	1.71
45.0	35.7	2.79	4.07	4.07	4.07	4.07	1.88	1.98	2.57	2.58
45.0	24.0	3.78	4.39	4.38	4.40	4.39	2.74	2.89	3.51	3.55
65.0	64.5	0.22	1.88	2.03	1.88	1.89	0.06	0.05	0.19	0.16
65.0	57.2	0.54	2.02	2.03	2.02	2.02	0.17	0.18	0.42	0.39
65.0	42.4	1.28	2.26	2.26	2.26	2.26	0.59	0.64	1.05	1.05
65.0	33.1	1.87	2.40	2.40	2.41	2.41	0.97	1.06	1.55	1.57
		Average Deviation:	**2.26**	**2.27**	**2.26**	**2.25**	**0.58**	**0.61**	**0.16**	**0.17**

Table A.4: Methane + Propane

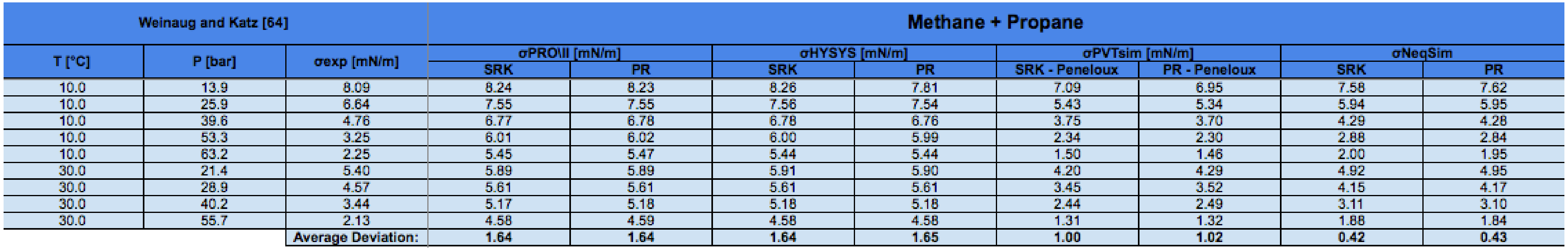

Weinaug and Katz [64]			Methane + Propane							
T [°C]	P [bar]	σexp [mN/m]	σPRO\II [mN/m]		σHYSYS [mN/m]		σPVTsim [mN/m]		σNeqSim	
			SRK	PR	SRK	PR	SRK - Peneloux	PR - Peneloux	SRK	PR
10.0	13.9	8.09	8.24	8.23	8.26	7.81	7.09	6.95	7.58	7.62
10.0	25.9	6.64	7.55	7.55	7.56	7.54	5.43	5.34	5.94	5.95
10.0	39.6	4.76	6.77	6.78	6.78	6.76	3.75	3.70	4.29	4.28
10.0	53.3	3.25	6.01	6.02	6.00	5.99	2.34	2.30	2.88	2.84
10.0	63.2	2.25	5.45	5.47	5.44	5.44	1.50	1.46	2.00	1.95
30.0	21.4	5.40	5.89	5.89	5.91	5.90	4.20	4.29	4.92	4.95
30.0	28.9	4.57	5.61	5.61	5.61	5.61	3.45	3.52	4.15	4.17
30.0	40.2	3.44	5.17	5.18	5.18	5.18	2.44	2.49	3.11	3.10
30.0	55.7	2.13	4.58	4.59	4.58	4.58	1.31	1.32	1.88	1.84
		Average Deviation:	**1.64**	**1.64**	**1.64**	**1.65**	**1.00**	**1.02**	**0.42**	**0.43**

Table A.5: Methane + Propane

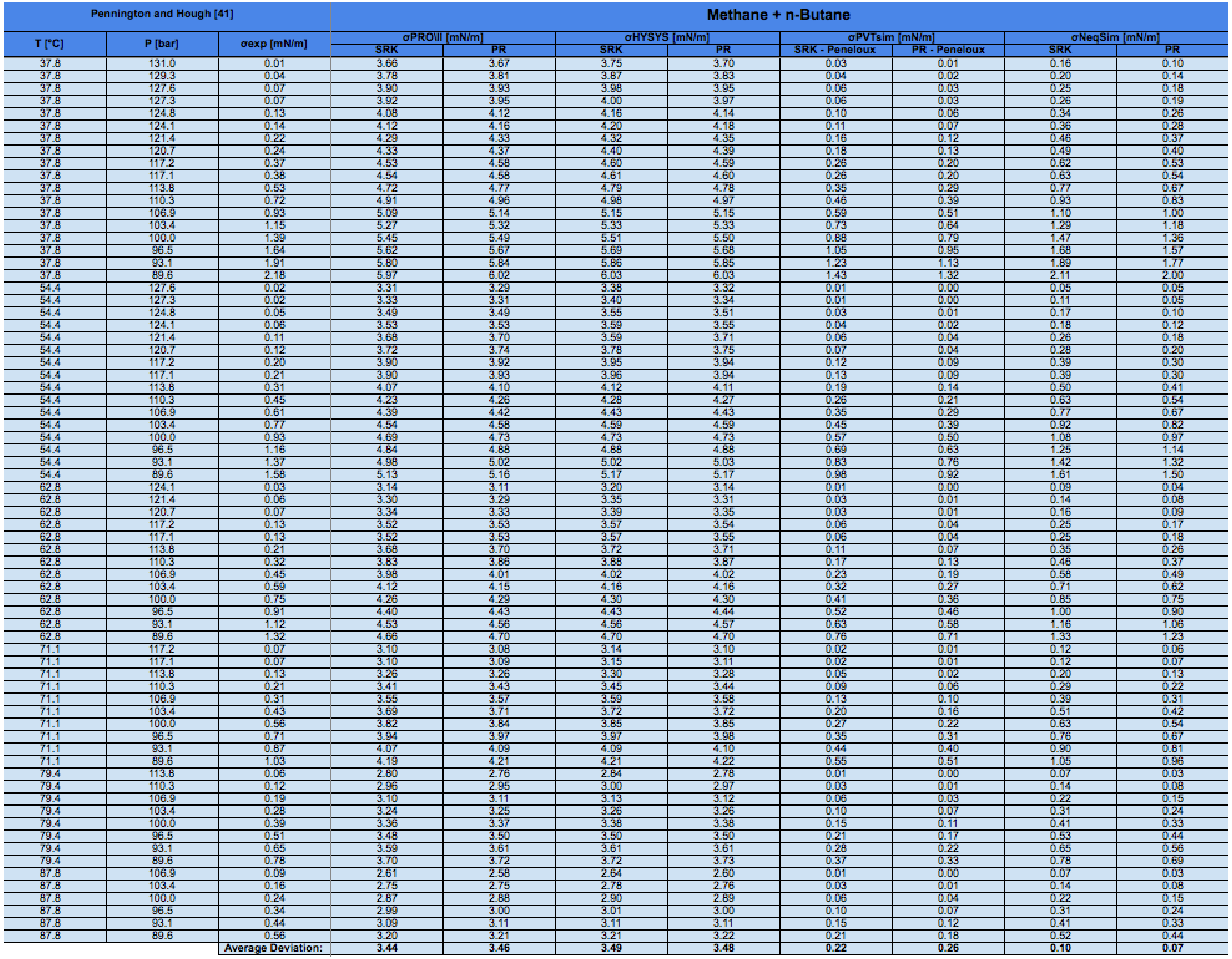

Pennington and Hough [41]			Methane + n-Butane							
T [°C]	P [bar]	σexp [mN/m]	σPRO\II [mN/m]		σHYSYS [mN/m]		σPVTsim [mN/m]		σNeqSim [mN/m]	
			SRK	PR	SRK	PR	SRK - Peneloux	PR - Peneloux	SRK	PR
37.8	131.0	0.01	3.66	3.67	3.75	3.70	0.03	0.01	0.16	0.10
37.8	129.3	0.04	3.78	3.81	3.87	3.83	0.04	0.02	0.20	0.14
37.8	127.6	0.07	3.90	3.93	3.98	3.95	0.06	0.03	0.25	0.18
37.8	127.3	0.07	3.92	3.95	4.00	3.97	0.06	0.03	0.26	0.19
37.8	124.8	0.13	4.08	4.12	4.16	4.14	0.10	0.06	0.34	0.26
37.8	124.1	0.14	4.12	4.16	4.20	4.18	0.11	0.07	0.36	0.28
37.8	121.4	0.22	4.29	4.33	4.32	4.35	0.16	0.12	0.46	0.37
37.8	120.7	0.24	4.33	4.37	4.40	4.39	0.18	0.13	0.49	0.40
37.8	117.2	0.37	4.53	4.58	4.60	4.59	0.26	0.20	0.62	0.53
37.8	117.1	0.38	4.54	4.58	4.61	4.60	0.26	0.20	0.63	0.54
37.8	113.8	0.53	4.72	4.77	4.79	4.78	0.35	0.29	0.77	0.67
37.8	110.3	0.72	4.91	4.96	4.98	4.97	0.46	0.39	0.93	0.83
37.8	106.9	0.93	5.09	5.14	5.15	5.15	0.59	0.51	1.10	1.00
37.8	103.4	1.15	5.27	5.32	5.33	5.33	0.73	0.64	1.29	1.18
37.8	100.0	1.39	5.45	5.49	5.51	5.50	0.88	0.79	1.47	1.36
37.8	96.5	1.64	5.62	5.67	5.69	5.68	1.05	0.95	1.68	1.57
37.8	93.1	1.91	5.80	5.84	5.86	5.85	1.23	1.13	1.89	1.77
37.8	89.6	2.18	5.97	6.02	6.03	6.03	1.43	1.32	2.11	2.00
54.4	127.6	0.02	3.31	3.29	3.38	3.32	0.01	0.00	0.05	0.05
54.4	127.3	0.02	3.33	3.31	3.40	3.34	0.01	0.00	0.11	0.05
54.4	124.8	0.05	3.49	3.49	3.55	3.51	0.03	0.01	0.17	0.10
54.4	124.1	0.06	3.53	3.53	3.59	3.55	0.04	0.02	0.18	0.12
54.4	121.4	0.11	3.68	3.70	3.59	3.71	0.06	0.04	0.26	0.18
54.4	120.7	0.12	3.72	3.74	3.78	3.75	0.07	0.04	0.28	0.20
54.4	117.2	0.20	3.90	3.92	3.95	3.94	0.12	0.09	0.39	0.30
54.4	117.1	0.21	3.90	3.93	3.96	3.94	0.13	0.09	0.39	0.30
54.4	113.8	0.31	4.07	4.10	4.12	4.11	0.19	0.14	0.50	0.41
54.4	110.3	0.45	4.23	4.26	4.28	4.27	0.26	0.21	0.63	0.54
54.4	106.9	0.61	4.39	4.42	4.43	4.43	0.35	0.29	0.77	0.67
54.4	103.4	0.77	4.54	4.58	4.59	4.59	0.45	0.39	0.92	0.82
54.4	100.0	0.93	4.69	4.73	4.73	4.73	0.57	0.50	1.08	0.97
54.4	96.5	1.16	4.84	4.88	4.88	4.88	0.69	0.63	1.25	1.14
54.4	93.1	1.37	4.98	5.02	5.02	5.03	0.83	0.76	1.42	1.32
54.4	89.6	1.58	5.13	5.16	5.17	5.17	0.98	0.92	1.61	1.50
62.8	124.1	0.03	3.14	3.11	3.20	3.14	0.01	0.00	0.09	0.04
62.8	121.4	0.06	3.30	3.29	3.35	3.31	0.03	0.01	0.14	0.08
62.8	120.7	0.07	3.34	3.33	3.39	3.35	0.03	0.01	0.16	0.09
62.8	117.2	0.13	3.52	3.53	3.57	3.54	0.06	0.04	0.25	0.17
62.8	117.1	0.13	3.52	3.53	3.57	3.55	0.06	0.04	0.25	0.18
62.8	113.8	0.21	3.68	3.70	3.72	3.71	0.11	0.07	0.35	0.26
62.8	110.3	0.32	3.83	3.86	3.88	3.87	0.17	0.13	0.46	0.37
62.8	106.9	0.45	3.98	4.01	4.02	4.02	0.23	0.19	0.58	0.49
62.8	103.4	0.59	4.12	4.15	4.16	4.16	0.32	0.27	0.71	0.62
62.8	100.0	0.75	4.26	4.29	4.30	4.30	0.41	0.36	0.85	0.75
62.8	96.5	0.91	4.40	4.43	4.43	4.44	0.52	0.46	1.00	0.90
62.8	93.1	1.12	4.53	4.56	4.56	4.57	0.63	0.58	1.16	1.06
62.8	89.6	1.32	4.66	4.70	4.70	4.70	0.76	0.71	1.33	1.23
71.1	117.2	0.07	3.10	3.08	3.14	3.10	0.02	0.01	0.12	0.06
71.1	117.1	0.07	3.10	3.09	3.15	3.11	0.02	0.01	0.12	0.07
71.1	113.8	0.13	3.26	3.26	3.30	3.28	0.05	0.02	0.20	0.13
71.1	110.3	0.21	3.41	3.43	3.45	3.44	0.09	0.06	0.29	0.22
71.1	106.9	0.31	3.55	3.57	3.59	3.58	0.13	0.10	0.39	0.31
71.1	103.4	0.43	3.69	3.71	3.72	3.72	0.20	0.16	0.51	0.42
71.1	100.0	0.56	3.82	3.84	3.85	3.85	0.27	0.22	0.63	0.54
71.1	96.5	0.71	3.94	3.97	3.97	3.98	0.35	0.31	0.76	0.67
71.1	93.1	0.87	4.07	4.09	4.09	4.10	0.44	0.40	0.90	0.81
71.1	89.6	1.03	4.19	4.21	4.21	4.22	0.55	0.51	1.05	0.96
79.4	113.8	0.06	2.80	2.76	2.84	2.78	0.01	0.00	0.07	0.03
79.4	110.3	0.12	2.96	2.95	3.00	2.97	0.03	0.01	0.14	0.08
79.4	106.9	0.19	3.10	3.11	3.13	3.12	0.06	0.03	0.22	0.15
79.4	103.4	0.28	3.24	3.25	3.26	3.26	0.10	0.07	0.31	0.24
79.4	100.0	0.39	3.36	3.37	3.38	3.38	0.15	0.11	0.41	0.33
79.4	96.5	0.51	3.48	3.50	3.50	3.50	0.21	0.17	0.53	0.44
79.4	93.1	0.65	3.59	3.61	3.61	3.61	0.28	0.22	0.65	0.56
79.4	89.6	0.78	3.70	3.72	3.72	3.73	0.37	0.33	0.78	0.69
87.8	106.9	0.09	2.61	2.58	2.64	2.60	0.01	0.00	0.07	0.03
87.8	103.4	0.16	2.75	2.75	2.78	2.76	0.03	0.01	0.14	0.08
87.8	100.0	0.24	2.87	2.88	2.90	2.89	0.06	0.04	0.22	0.15
87.8	96.5	0.34	2.99	3.00	3.01	3.00	0.10	0.07	0.31	0.24
87.8	93.1	0.44	3.09	3.11	3.11	3.11	0.15	0.12	0.41	0.33
87.8	89.6	0.56	3.20	3.21	3.21	3.22	0.21	0.18	0.52	0.44
		Average Deviation:	**3.44**	**3.46**	**3.49**	**3.48**	**0.22**	**0.26**	**0.10**	**0.07**

Table A.6: Methane + n-Butane

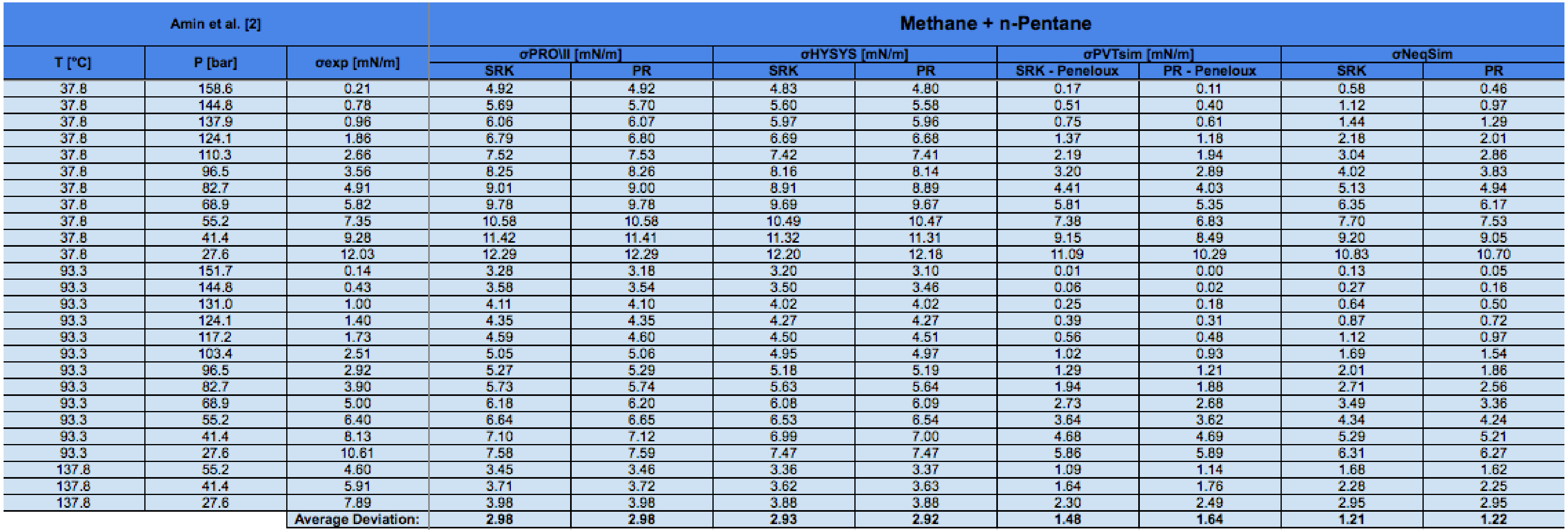

Amin et al. [2]			Methane + n-Pentane							
T [°C]	P [bar]	σexp [mN/m]	σPRO\II [mN/m]		σHYSYS [mN/m]		σPVTsim [mN/m]		σNeqSim	
			SRK	PR	SRK	PR	SRK - Peneloux	PR - Peneloux	SRK	PR
37.8	158.6	0.21	4.92	4.92	4.83	4.80	0.17	0.11	0.58	0.46
37.8	144.8	0.78	5.69	5.70	5.60	5.58	0.51	0.40	1.12	0.97
37.8	137.9	0.96	6.06	6.07	5.97	5.96	0.75	0.61	1.44	1.29
37.8	124.1	1.86	6.79	6.80	6.69	6.68	1.37	1.18	2.18	2.01
37.8	110.3	2.66	7.52	7.53	7.42	7.41	2.19	1.94	3.04	2.86
37.8	96.5	3.56	8.25	8.26	8.16	8.14	3.20	2.89	4.02	3.83
37.8	82.7	4.91	9.01	9.00	8.91	8.89	4.41	4.03	5.13	4.94
37.8	68.9	5.82	9.78	9.78	9.69	9.67	5.81	5.35	6.35	6.17
37.8	55.2	7.35	10.58	10.58	10.49	10.47	7.38	6.83	7.70	7.53
37.8	41.4	9.28	11.42	11.41	11.32	11.31	9.15	8.49	9.20	9.05
37.8	27.6	12.03	12.29	12.29	12.20	12.18	11.09	10.29	10.83	10.70
93.3	151.7	0.14	3.28	3.18	3.20	3.10	0.01	0.00	0.13	0.05
93.3	144.8	0.43	3.58	3.54	3.50	3.46	0.06	0.02	0.27	0.16
93.3	131.0	1.00	4.11	4.10	4.02	4.02	0.25	0.18	0.64	0.50
93.3	124.1	1.40	4.35	4.35	4.27	4.27	0.39	0.31	0.87	0.72
93.3	117.2	1.73	4.59	4.60	4.50	4.51	0.56	0.48	1.12	0.97
93.3	103.4	2.51	5.05	5.06	4.95	4.97	1.02	0.93	1.69	1.54
93.3	96.5	2.92	5.27	5.29	5.18	5.19	1.29	1.21	2.01	1.86
93.3	82.7	3.90	5.73	5.74	5.63	5.64	1.94	1.88	2.71	2.56
93.3	68.9	5.00	6.18	6.20	6.08	6.09	2.73	2.68	3.49	3.36
93.3	55.2	6.40	6.64	6.65	6.53	6.54	3.64	3.62	4.34	4.24
93.3	41.4	8.13	7.10	7.12	6.99	7.00	4.68	4.69	5.29	5.21
93.3	27.6	10.61	7.58	7.59	7.47	7.47	5.86	5.89	6.31	6.27
137.8	55.2	4.60	3.45	3.46	3.36	3.37	1.09	1.14	1.68	1.62
137.8	41.4	5.91	3.71	3.72	3.62	3.63	1.64	1.76	2.28	2.25
137.8	27.6	7.89	3.98	3.98	3.88	3.88	2.30	2.49	2.95	2.95
		Average Deviation:	**2.98**	**2.98**	**2.93**	**2.92**	**1.48**	**1.64**	**1.21**	**1.22**

Table A.7: Methane + n-Pentane

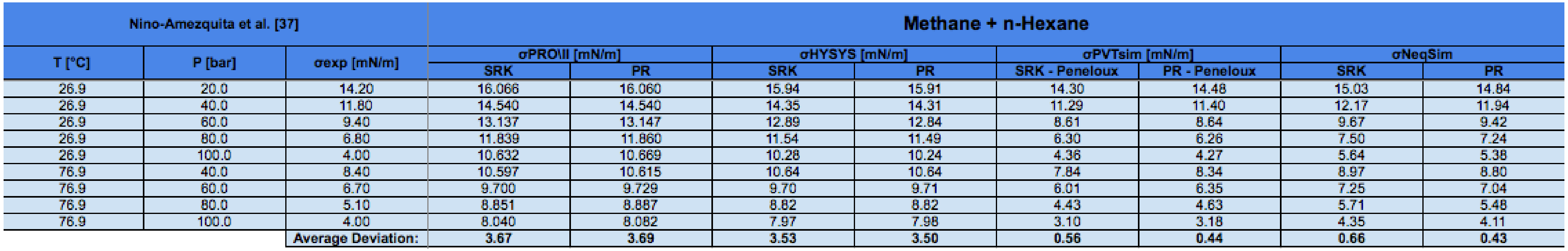

Nino-Amezquita et al. [37]			Methane + n-Hexane							
T [°C]	P [bar]	σexp [mN/m]	σPRO\II [mN/m]		σHYSYS [mN/m]		σPVTsim [mN/m]		σNeqSim	
			SRK	PR	SRK	PR	SRK - Peneloux	PR - Peneloux	SRK	PR
26.9	20.0	14.20	16.066	16.060	15.94	15.91	14.30	14.48	15.03	14.84
26.9	40.0	11.80	14.540	14.540	14.35	14.31	11.29	11.40	12.17	11.94
26.9	60.0	9.40	13.137	13.147	12.89	12.84	8.61	8.64	9.67	9.42
26.9	80.0	6.80	11.839	11.860	11.54	11.49	6.30	6.26	7.50	7.24
26.9	100.0	4.00	10.632	10.669	10.28	10.24	4.36	4.27	5.64	5.38
76.9	40.0	8.40	10.597	10.615	10.64	10.64	7.84	8.34	8.97	8.80
76.9	60.0	6.70	9.700	9.729	9.70	9.71	6.01	6.35	7.25	7.04
76.9	80.0	5.10	8.851	8.887	8.82	8.82	4.43	4.63	5.71	5.48
76.9	100.0	4.00	8.040	8.082	7.97	7.98	3.10	3.18	4.35	4.11
		Average Deviation:	**3.67**	**3.69**	**3.53**	**3.50**	**0.56**	**0.44**	**0.66**	**0.43**

Table A.8: Methane + n-Hexane

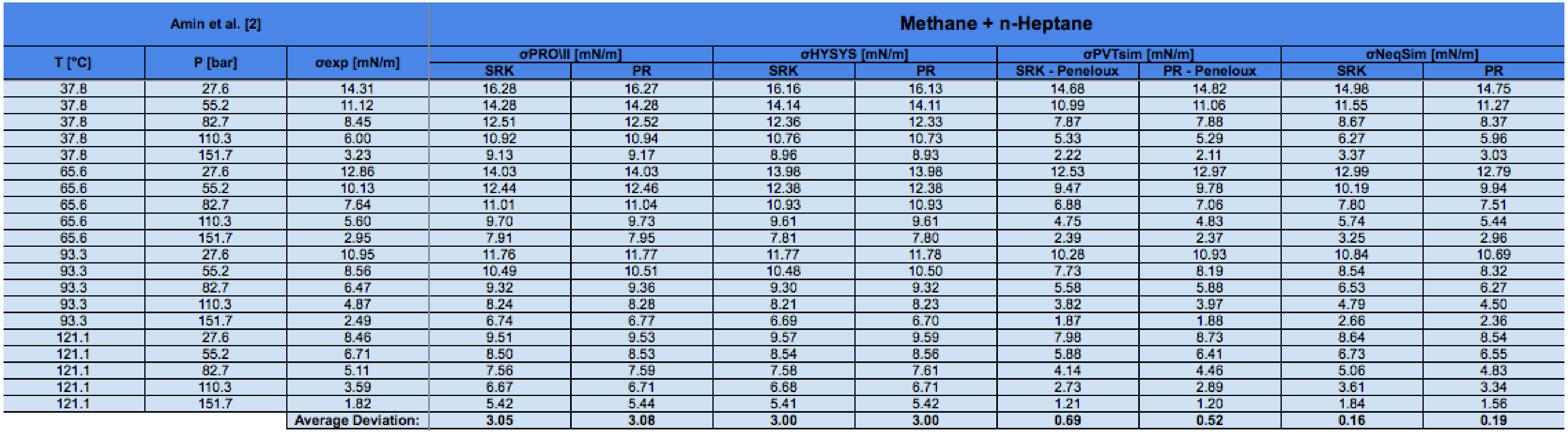

Amin et al. [2]			Methane + n-Heptane							
T [°C]	P [bar]	σexp [mN/m]	σPRO\II [mN/m]		σHYSYS [mN/m]		σPVTsim [mN/m]		σNeqSim [mN/m]	
			SRK	PR	SRK	PR	SRK - Peneloux	PR - Peneloux	SRK	PR
37.8	27.6	14.31	16.28	16.27	16.16	16.13	14.68	14.82	14.98	14.75
37.8	55.2	11.12	14.28	14.28	14.14	14.11	10.99	11.06	11.55	11.27
37.8	82.7	8.45	12.51	12.52	12.36	12.33	7.87	7.88	8.67	8.37
37.8	110.3	6.00	10.92	10.94	10.76	10.73	5.33	5.29	6.27	5.96
37.8	151.7	3.23	9.13	9.17	8.96	8.93	2.22	2.11	3.37	3.03
65.6	27.6	12.86	14.03	14.03	13.98	13.98	12.53	12.97	12.99	12.79
65.6	55.2	10.13	12.44	12.46	12.38	12.38	9.47	9.78	10.19	9.94
65.6	82.7	7.64	11.01	11.04	10.93	10.93	6.88	7.06	7.80	7.51
65.6	110.3	5.60	9.70	9.73	9.61	9.61	4.75	4.83	5.74	5.44
65.6	151.7	2.95	7.91	7.95	7.81	7.80	2.39	2.37	3.25	2.96
93.3	27.6	10.95	11.76	11.77	11.77	11.78	10.28	10.93	10.84	10.69
93.3	55.2	8.56	10.49	10.51	10.48	10.50	7.73	8.19	8.54	8.32
93.3	82.7	6.47	9.32	9.36	9.30	9.32	5.58	5.88	6.53	6.27
93.3	110.3	4.87	8.24	8.28	8.21	8.23	3.82	3.97	4.79	4.50
93.3	151.7	2.49	6.74	6.77	6.69	6.70	1.87	1.88	2.66	2.36
121.1	27.6	8.46	9.51	9.53	9.57	9.59	7.98	8.73	8.64	8.54
121.1	55.2	6.71	8.50	8.53	8.54	8.56	5.88	6.41	6.73	6.55
121.1	82.7	5.11	7.56	7.59	7.58	7.61	4.14	4.46	5.06	4.83
121.1	110.3	3.59	6.67	6.71	6.68	6.71	2.73	2.89	3.61	3.34
121.1	151.7	1.82	5.42	5.44	5.41	5.42	1.21	1.20	1.84	1.56
		Average Deviation:	**3.05**	**3.08**	**3.00**	**3.00**	**0.69**	**0.52**	**0.16**	**0.19**

Table A.9: Methane + n-Heptane

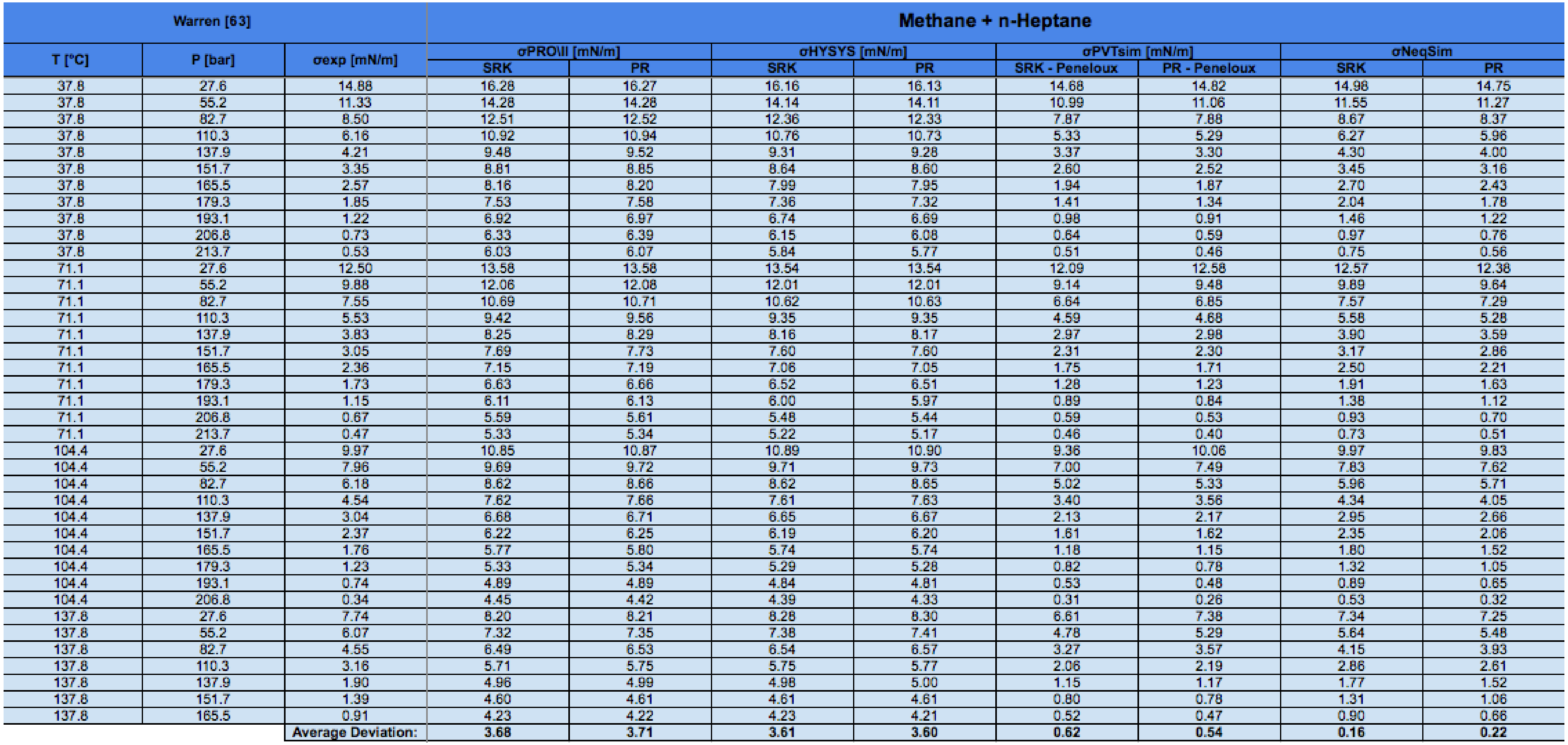

Warren [63]			Methane + n-Heptane							
T [°C]	P [bar]	σexp [mN/m]	σPRO\II [mN/m]		σHYSYS [mN/m]		σPVTsim [mN/m]		σNeqSim	
			SRK	PR	SRK	PR	SRK - Peneloux	PR - Peneloux	SRK	PR
37.8	27.6	14.88	16.28	16.27	16.16	16.13	14.68	14.82	14.98	14.75
37.8	55.2	11.33	14.28	14.28	14.14	14.11	10.99	11.06	11.55	11.27
37.8	82.7	8.50	12.51	12.52	12.36	12.33	7.87	7.88	8.67	8.37
37.8	110.3	6.16	10.92	10.94	10.76	10.73	5.33	5.29	6.27	5.96
37.8	137.9	4.21	9.48	9.52	9.31	9.28	3.37	3.30	4.30	4.00
37.8	151.7	3.35	8.81	8.85	8.64	8.60	2.60	2.52	3.45	3.16
37.8	165.5	2.57	8.16	8.20	7.99	7.95	1.94	1.87	2.70	2.43
37.8	179.3	1.85	7.53	7.58	7.36	7.32	1.41	1.34	2.04	1.78
37.8	193.1	1.22	6.92	6.97	6.74	6.69	0.98	0.91	1.46	1.22
37.8	206.8	0.73	6.33	6.39	6.15	6.08	0.64	0.59	0.97	0.76
37.8	213.7	0.53	6.03	6.07	5.84	5.77	0.51	0.46	0.75	0.56
71.1	27.6	12.50	13.58	13.58	13.54	13.54	12.09	12.58	12.57	12.38
71.1	55.2	9.88	12.06	12.08	12.01	12.01	9.14	9.48	9.89	9.64
71.1	82.7	7.55	10.69	10.71	10.62	10.63	6.64	6.85	7.57	7.29
71.1	110.3	5.53	9.42	9.56	9.35	9.35	4.59	4.68	5.58	5.28
71.1	137.9	3.83	8.25	8.29	8.16	8.17	2.97	2.98	3.90	3.59
71.1	151.7	3.05	7.69	7.73	7.60	7.60	2.31	2.30	3.17	2.86
71.1	165.5	2.36	7.15	7.19	7.06	7.05	1.75	1.71	2.50	2.21
71.1	179.3	1.73	6.63	6.66	6.52	6.51	1.28	1.23	1.91	1.63
71.1	193.1	1.15	6.11	6.13	6.00	5.97	0.89	0.84	1.38	1.12
71.1	206.8	0.67	5.59	5.61	5.48	5.44	0.59	0.53	0.93	0.70
71.1	213.7	0.47	5.33	5.34	5.22	5.17	0.46	0.40	0.73	0.51
104.4	27.6	9.97	10.85	10.87	10.89	10.90	9.36	10.06	9.97	9.83
104.4	55.2	7.96	9.69	9.72	9.71	9.73	7.00	7.49	7.83	7.62
104.4	82.7	6.18	8.62	8.66	8.62	8.65	5.02	5.33	5.96	5.71
104.4	110.3	4.54	7.62	7.66	7.61	7.63	3.40	3.56	4.34	4.05
104.4	137.9	3.04	6.68	6.71	6.65	6.67	2.13	2.17	2.95	2.66
104.4	151.7	2.37	6.22	6.25	6.19	6.20	1.61	1.62	2.35	2.06
104.4	165.5	1.76	5.77	5.80	5.74	5.74	1.18	1.15	1.80	1.52
104.4	179.3	1.23	5.33	5.34	5.29	5.28	0.82	0.78	1.32	1.05
104.4	193.1	0.74	4.89	4.89	4.84	4.81	0.53	0.48	0.89	0.65
104.4	206.8	0.34	4.45	4.42	4.39	4.33	0.31	0.26	0.53	0.32
137.8	27.6	7.74	8.20	8.21	8.28	8.30	6.61	7.38	7.34	7.25
137.8	55.2	6.07	7.32	7.35	7.38	7.41	4.78	5.29	5.64	5.48
137.8	82.7	4.55	6.49	6.53	6.54	6.57	3.27	3.57	4.15	3.93
137.8	110.3	3.16	5.71	5.75	5.75	5.77	2.06	2.19	2.86	2.61
137.8	137.9	1.90	4.96	4.99	4.98	5.00	1.15	1.17	1.77	1.52
137.8	151.7	1.39	4.60	4.61	4.61	4.61	0.80	0.78	1.31	1.06
137.8	165.5	0.91	4.23	4.22	4.23	4.21	0.52	0.47	0.90	0.66
		Average Deviation:	**3.68**	**3.71**	**3.61**	**3.60**	**0.62**	**0.54**	**0.16**	**0.22**

Table A.10: Methane + n-Heptane

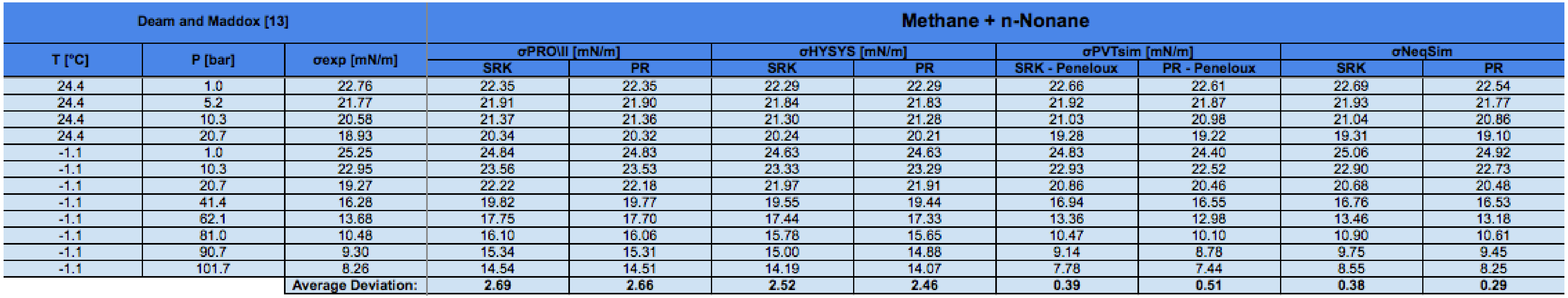

Deam and Maddox [13]			Methane + n-Nonane							
T [°C]	P [bar]	σexp [mN/m]	σPRO\II [mN/m]		σHYSYS [mN/m]		σPVTsim [mN/m]		σNeqSim	
			SRK	PR	SRK	PR	SRK - Peneloux	PR - Peneloux	SRK	PR
24.4	1.0	22.76	22.35	22.35	22.29	22.29	22.66	22.61	22.69	22.54
24.4	5.2	21.77	21.91	21.90	21.84	21.83	21.92	21.87	21.93	21.77
24.4	10.3	20.58	21.37	21.36	21.30	21.28	21.03	20.98	21.04	20.86
24.4	20.7	18.93	20.34	20.32	20.24	20.21	19.28	19.22	19.31	19.10
-1.1	1.0	25.25	24.84	24.83	24.63	24.63	24.83	24.40	25.06	24.92
-1.1	10.3	22.95	23.56	23.53	23.33	23.29	22.93	22.52	22.90	22.73
-1.1	20.7	19.27	22.22	22.18	21.97	21.91	20.86	20.46	20.68	20.48
-1.1	41.4	16.28	19.82	19.77	19.55	19.44	16.94	16.55	16.76	16.53
-1.1	62.1	13.68	17.75	17.70	17.44	17.33	13.36	12.98	13.46	13.18
-1.1	81.0	10.48	16.10	16.06	15.78	15.65	10.47	10.10	10.90	10.61
-1.1	90.7	9.30	15.34	15.31	15.00	14.88	9.14	8.78	9.75	9.45
-1.1	101.7	8.26	14.54	14.51	14.19	14.07	7.78	7.44	8.55	8.25
		Average Deviation:	**2.69**	**2.66**	**2.52**	**2.46**	**0.39**	**0.51**	**0.38**	**0.29**

Table A.11: Methane + n-Nonane

Amin et al. [2]			Methane + n-Decane							
T [°C]	P [bar]	σexp [mN/m]	σPRO\II [mN/m]		σHYSYS [mN/m]		σPVTsim [mN/m]		σNeqSim [mN/m]	
			SRK	PR	SRK	PR	SRK - Peneloux	PR - Peneloux	SRK	PR
37.8	27.6	20.50	19.55	19.52	19.35	19.32	18.23	18.30	18.36	18.19
37.8	55.2	14.84	17.29	17.26	17.11	17.08	14.28	14.28	14.87	14.63
37.8	82.7	11.52	15.35	15.33	15.19	15.15	10.89	10.82	11.92	11.63
37.8	96.5	10.27	14.48	14.46	14.32	14.29	9.41	9.31	10.63	10.31
37.8	110.3	9.17	13.67	13.65	13.51	13.48	8.07	7.95	9.43	9.10
37.8	124.1	8.21	12.91	12.89	12.76	12.73	6.88	6.74	8.34	8.00
37.8	137.9	7.35	12.20	12.18	12.05	12.02	5.82	5.68	7.35	6.99
37.8	151.7	6.57	11.53	11.51	11.39	11.36	4.90	4.75	6.35	6.08
37.8	165.5	5.86	10.90	10.88	10.77	10.73	4.10	3.95	5.60	5.24
37.8	179.3	5.21	10.30	10.28	10.18	10.14	3.40	3.26	4.84	4.48
37.8	193.1	4.60	9.75	9.73	9.62	9.60	2.81	2.67	4.15	3.78
37.8	206.8	4.04	9.22	9.20	9.09	9.10	2.30	2.17	3.52	3.15
37.8	220.6	3.72	8.71	8.69	8.59	8.55	1.87	1.75	2.94	2.58
37.8	234.4	3.04	8.23	8.20	8.12	8.06	1.51	1.39	2.42	2.07
37.8	248.2	2.58	7.77	7.73	7.66	7.59	1.20	1.09	1.95	1.61
37.8	262.0	2.14	7.32	7.27	7.22	7.14	0.95	0.85	1.52	1.19
37.8	275.8	1.69	6.89	6.83	6.80	6.70	0.73	0.64	1.15	0.85
93.3	27.6	19.40	15.36	15.37	15.46	15.48	14.61	15.23	14.80	14.65
93.3	55.2	14.80	13.82	13.84	13.91	13.93	11.74	12.21	12.41	12.18
93.3	82.7	10.80	12.45	12.48	12.53	12.56	9.27	9.59	10.30	10.00
93.3	96.5	9.60	11.82	11.84	11.89	11.92	8.18	8.43	9.34	9.02
93.3	110.3	8.50	11.22	11.24	11.28	11.31	7.17	7.36	8.43	8.09
93.3	124.1	7.60	10.64	10.67	10.70	10.73	6.25	6.39	7.58	7.22
93.3	137.9	6.80	10.09	10.12	10.14	10.17	5.42	5.51	6.78	6.41
93.3	151.7	6.01	9.57	9.59	9.62	9.64	4.67	4.72	6.04	5.65
93.3	165.5	5.36	9.07	9.09	9.11	9.14	4.00	4.01	5.34	4.94
93.3	179.3	4.74	8.60	8.61	8.63	8.65	3.39	3.37	4.69	4.28
93.3	193.1	4.15	8.14	8.15	8.17	8.18	2.86	2.81	4.08	3.67
93.3	206.8	3.66	7.70	7.70	7.73	7.73	2.39	2.32	3.52	3.10
93.3	220.6	3.07	7.28	7.27	7.30	7.30	1.97	1.89	2.99	2.58
93.3	234.4	2.60	6.87	6.86	6.89	6.87	1.61	1.52	2.51	2.10
93.3	248.2	2.15	6.47	6.45	6.50	6.46	1.29	1.20	2.06	1.66
93.3	262.0	1.72	6.09	6.05	6.10	6.06	1.02	0.92	1.65	1.27
93.3	275.8	1.34	5.72	5.67	5.73	5.67	0.79	0.69	1.28	0.92
137.8	27.6	14.65	11.96	11.98	12.25	12.28	11.36	12.26	11.61	11.49
137.8	55.2	10.45	10.81	10.84	11.06	11.10	9.12	9.81	9.77	9.57
137.8	82.7	8.00	9.76	9.80	9.98	10.03	7.20	7.69	8.12	7.85
137.8	96.5	7.05	9.27	9.31	9.45	9.53	6.34	6.74	7.36	7.06
137.8	110.3	6.24	8.80	8.84	8.99	9.04	5.55	5.87	6.64	6.31
137.8	124.1	5.53	8.34	8.38	8.53	8.58	4.83	5.08	5.95	5.60
137.8	137.9	4.89	7.91	7.95	8.08	8.13	4.17	4.35	5.30	4.93
137.8	151.7	4.31	7.50	7.53	7.66	7.70	3.57	3.69	4.69	4.31
137.8	165.5	3.70	7.10	7.12	7.23	7.28	3.04	3.10	4.12	3.72
137.8	179.3	3.31	6.71	6.73	6.85	6.88	2.55	2.57	3.58	3.18
137.8	193.1	2.85	6.34	6.35	6.47	6.49	1.85	2.12	3.08	2.67
137.8	206.8	2.43	5.98	5.98	6.10	6.11	1.50	1.75	2.61	2.20
137.8	220.6	2.03	5.64	5.62	5.75	5.74	1.18	1.41	2.18	1.76
137.8	234.4	1.66	5.30	5.27	5.40	5.38	0.91	1.12	1.77	1.37
137.8	248.2	1.32	4.97	4.92	5.06	5.02	0.68	0.87	1.41	1.02
137.8	262.0	0.99	4.64	4.58	4.73	4.67	0.49	0.65	1.12	0.70
137.8	275.8	0.68	4.33	4.24	4.40	4.32	0.33	0.48	0.77	0.43
		Average Deviation:	**3.65**	**3.64**	**3.66**	**3.65**	**1.28**	**1.18**	**0.48**	**0.64**

Table A.12: Methane + n-Decane

Stegemeier et al. [56]			Methane + n-Decane							
T [°C]	P [bar]	σexp [mN/m]	σPRO\II [mN/m]		σHYSYS [mN/m]		σPVTsim [mN/m]		σNeqSim [mN/m]	
			SRK	PR	SRK	PR	SRK - Peneloux	PR - Peneloux	SRK	PR
37.8	103.4	9.76	14.07	14.04	13.91	13.88	8.72	8.61	10.02	9.69
37.8	137.9	7.35	12.20	12.18	12.05	12.02	5.82	5.68	7.35	7.00
37.8	172.4	5.67	10.60	10.59	10.47	10.44	3.74	3.59	5.21	4.85
37.8	206.8	3.66	9.22	9.20	9.10	9.06	2.30	2.17	3.52	3.15
37.8	241.3	2.40	7.99	7.96	7.89	7.83	1.35	1.23	2.18	1.83
37.8	275.8	1.43	6.89	6.83	6.80	6.70	0.73	0.64	1.15	0.84
37.8	289.6	1.11	6.46	6.40	6.38	6.28	0.56	0.48	0.82	0.53
37.8	303.4	0.82	6.05	5.99	5.96	5.86	0.42	0.34	0.53	0.28
37.8	317.2	0.57	5.64	5.58	5.55	5.45	0.30	0.24	0.30	0.10
37.8	320.6	0.51	5.54	5.48	5.45	5.35	0.28	0.22	0.25	0.06
71.1	103.4	9.77	12.65	12.66	12.63	12.64	8.28	8.38	9.56	9.22
71.1	137.9	7.52	11.06	11.07	11.03	11.05	5.79	5.79	7.24	6.87
71.1	172.4	5.50	9.66	9.67	9.63	9.64	3.89	3.83	5.31	4.91
71.1	206.8	3.75	8.43	8.43	8.39	8.39	2.50	2.41	3.71	3.31
71.1	241.3	2.41	7.31	7.29	7.28	7.25	1.51	1.41	2.40	2.01
71.1	275.8	1.38	6.29	6.24	6.25	6.20	0.84	0.74	1.36	1.01
71.1	289.6	1.03	5.90	5.84	5.87	5.79	0.65	0.55	1.01	0.68
		Average Deviation:	**4.78**	**4.75**	**4.71**	**4.66**	**1.00**	**1.08**	**0.19**	**0.49**

Table A.13: Methane + n-Decane

Nilssen et al. [34]			Ethane + n-Pentane							
T [°C]	P [bar]	σexp [mN/m]	σPRO\II [mN/m]		σHYSYS [mN/m]		σPVTsim [mN/m]		σNeqSim [mN/m]	
			SRK	PR	SRK	PR	SRK - Peneloux	PR - Peneloux	SRK	PR
21.0	5.9	10.80	13.26	13.25	16.63	16.58	14.39	13.23	13.56	13.49
21.0	7.1	10.60	12.69	12.68	15.94	15.89	13.70	12.63	12.95	12.89
21.0	11.6	8.80	10.61	10.59	13.46	13.39	11.17	10.43	10.75	10.70
21.0	16.0	7.20	8.69	8.65	11.14	11.04	8.78	8.32	8.70	8.66
21.0	20.4	5.60	6.86	6.81	8.90	8.78	6.53	6.29	6.76	6.72
21.0	22.1	5.10	6.18	6.12	8.05	7.93	5.71	5.54	6.05	6.01
21.0	24.1	4.60	5.41	5.34	7.06	6.93	4.79	4.68	5.23	5.20
21.0	27.7	3.40	4.08	4.01	5.32	5.18	3.26	3.24	3.85	3.82
21.0	29.9	2.70	3.32	3.25	4.27	4.14	2.43	2.44	3.07	3.04
		Average Deviation:	**1.37**	**1.32**	**3.55**	**3.45**	**1.42**	**0.98**	**1.35**	**1.30**

Table A.14: Ethane + n-Pentane

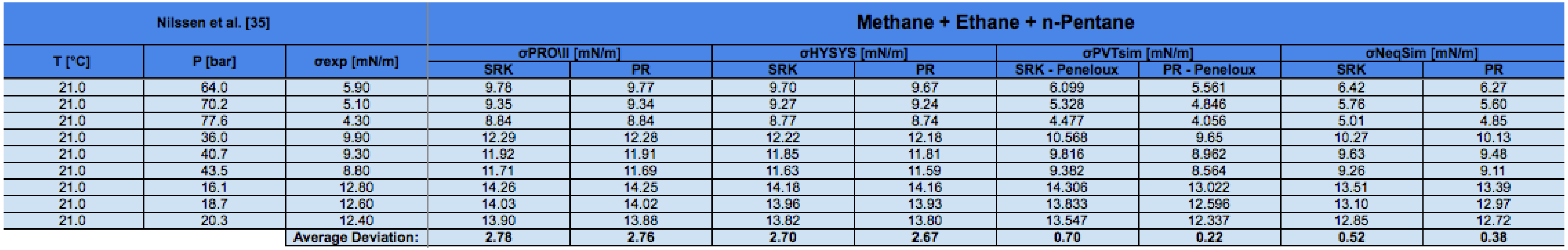

Nilssen et al. [35]			Methane + Ethane + n-Pentane							
T [°C]	P [bar]	σexp [mN/m]	σPRO\II [mN/m]		σHYSYS [mN/m]		σPVTsim [mN/m]		σNeqSim [mN/m]	
			SRK	PR	SRK	PR	SRK - Peneloux	PR - Peneloux	SRK	PR
21.0	64.0	5.90	9.78	9.77	9.70	9.67	6.099	5.561	6.42	6.27
21.0	70.2	5.10	9.35	9.34	9.27	9.24	5.328	4.846	5.76	5.60
21.0	77.6	4.30	8.84	8.84	8.77	8.74	4.477	4.056	5.01	4.85
21.0	36.0	9.90	12.29	12.28	12.22	12.18	10.568	9.65	10.27	10.13
21.0	40.7	9.30	11.92	11.91	11.85	11.81	9.816	8.962	9.63	9.48
21.0	43.5	8.80	11.71	11.69	11.63	11.59	9.382	8.564	9.26	9.11
21.0	16.1	12.80	14.26	14.25	14.18	14.16	14.306	13.022	13.51	13.39
21.0	18.7	12.60	14.03	14.02	13.96	13.93	13.833	12.596	13.10	12.97
21.0	20.3	12.40	13.90	13.88	13.82	13.80	13.547	12.337	12.85	12.72
		Average Deviation:	**2.78**	**2.76**	**2.70**	**2.67**	**0.70**	**0.22**	**0.52**	**0.38**

Table A.15: Methane + Ethane + n-Pentane

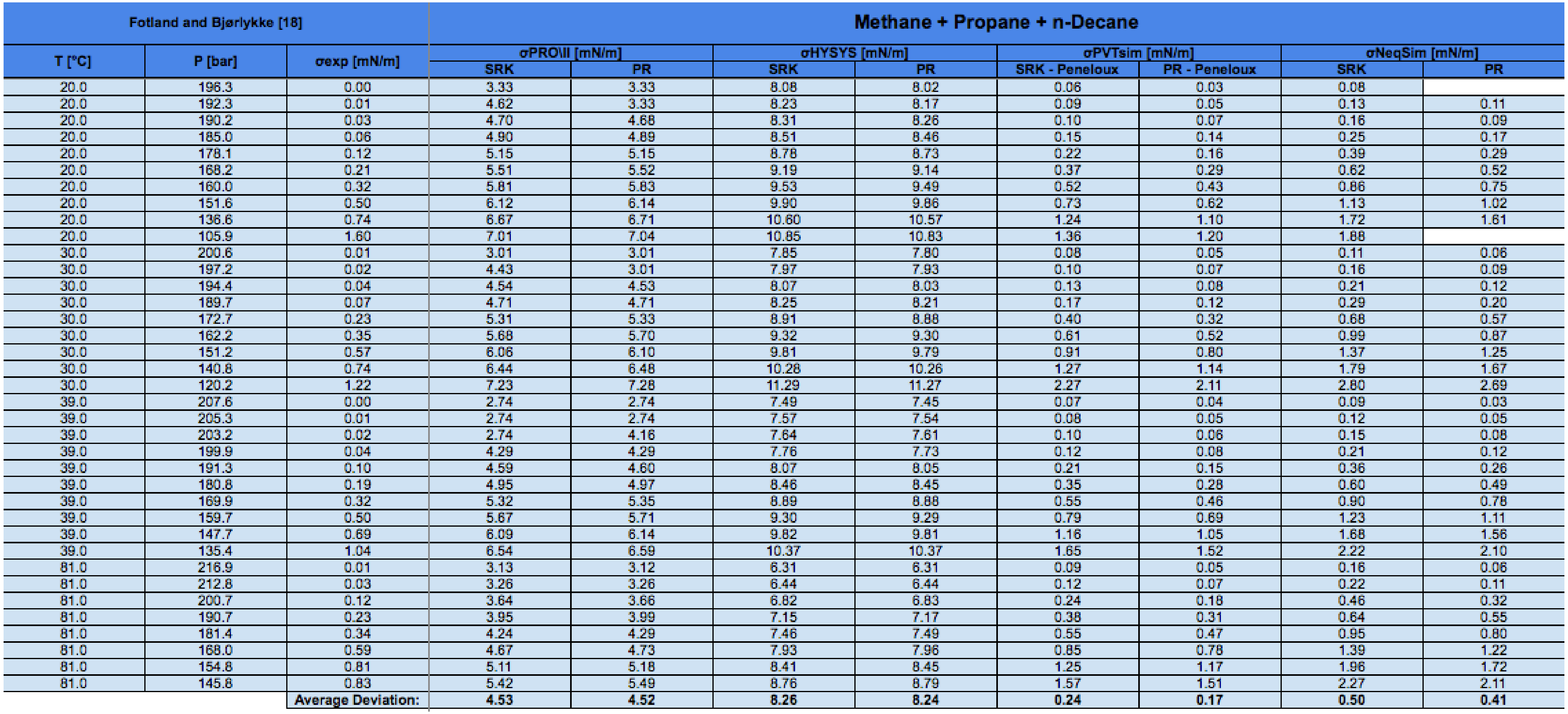

Fotland and Bjørlykke [18]			Methane + Propane + n-Decane							
T [°C]	P [bar]	σexp [mN/m]	σPRO\II [mN/m]		σHYSYS [mN/m]		σPVTsim [mN/m]		σNeqSim [mN/m]	
			SRK	PR	SRK	PR	SRK - Peneloux	PR - Peneloux	SRK	PR
20.0	196.3	0.00	3.33	3.33	8.08	8.02	0.06	0.03	0.08	
20.0	192.3	0.01	4.62	3.33	8.23	8.17	0.09	0.05	0.13	0.11
20.0	190.2	0.03	4.70	4.68	8.31	8.26	0.10	0.07	0.16	0.09
20.0	185.0	0.06	4.90	4.89	8.51	8.46	0.15	0.14	0.25	0.17
20.0	178.1	0.12	5.15	5.15	8.78	8.73	0.22	0.16	0.39	0.29
20.0	168.2	0.21	5.51	5.52	9.19	9.14	0.37	0.29	0.62	0.52
20.0	160.0	0.32	5.81	5.83	9.53	9.49	0.52	0.43	0.86	0.75
20.0	151.6	0.50	6.12	6.14	9.90	9.86	0.73	0.62	1.13	1.02
20.0	136.6	0.74	6.67	6.71	10.60	10.57	1.24	1.10	1.72	1.61
20.0	105.9	1.60	7.01	7.04	10.85	10.83	1.36	1.20	1.88	
30.0	200.6	0.01	3.01	3.01	7.85	7.80	0.08	0.05	0.11	0.06
30.0	197.2	0.02	4.43	3.01	7.97	7.93	0.10	0.07	0.16	0.09
30.0	194.4	0.04	4.54	4.53	8.07	8.03	0.13	0.08	0.21	0.12
30.0	189.7	0.07	4.71	4.71	8.25	8.21	0.17	0.12	0.29	0.20
30.0	172.7	0.23	5.31	5.33	8.91	8.88	0.40	0.32	0.68	0.57
30.0	162.2	0.35	5.68	5.70	9.32	9.30	0.61	0.52	0.99	0.87
30.0	151.2	0.57	6.06	6.10	9.81	9.79	0.91	0.80	1.37	1.25
30.0	140.8	0.74	6.44	6.48	10.28	10.26	1.27	1.14	1.79	1.67
30.0	120.2	1.22	7.23	7.28	11.29	11.27	2.27	2.11	2.80	2.69
39.0	207.6	0.00	2.74	2.74	7.49	7.45	0.07	0.04	0.09	0.03
39.0	205.3	0.01	2.74	2.74	7.57	7.54	0.08	0.05	0.12	0.05
39.0	203.2	0.02	2.74	4.16	7.64	7.61	0.10	0.06	0.15	0.08
39.0	199.9	0.04	4.29	4.29	7.76	7.73	0.12	0.08	0.21	0.12
39.0	191.3	0.10	4.59	4.60	8.07	8.05	0.21	0.15	0.36	0.26
39.0	180.8	0.19	4.95	4.97	8.46	8.45	0.35	0.28	0.60	0.49
39.0	169.9	0.32	5.32	5.35	8.89	8.88	0.55	0.46	0.90	0.78
39.0	159.7	0.50	5.67	5.71	9.30	9.29	0.79	0.69	1.23	1.11
39.0	147.7	0.69	6.09	6.14	9.82	9.81	1.16	1.05	1.68	1.56
39.0	135.4	1.04	6.54	6.59	10.37	10.37	1.65	1.52	2.22	2.10
81.0	216.9	0.01	3.13	3.12	6.31	6.31	0.09	0.05	0.16	0.06
81.0	212.8	0.03	3.26	3.26	6.44	6.44	0.12	0.07	0.22	0.11
81.0	200.7	0.12	3.64	3.66	6.82	6.83	0.24	0.18	0.46	0.32
81.0	190.7	0.23	3.95	3.99	7.15	7.17	0.38	0.31	0.64	0.55
81.0	181.4	0.34	4.24	4.29	7.46	7.49	0.55	0.47	0.95	0.80
81.0	168.0	0.59	4.67	4.73	7.93	7.96	0.85	0.78	1.39	1.22
81.0	154.8	0.81	5.11	5.18	8.41	8.45	1.25	1.17	1.96	1.72
81.0	145.8	0.83	5.42	5.49	8.76	8.79	1.57	1.51	2.27	2.11
		Average Deviation:	**4.53**	**4.52**	**8.26**	**8.24**	**0.24**	**0.17**	**0.50**	**0.41**

Table A.16: Methane + Propane + n-Decane

Fotland and Bjørlykke [18]			Methane + Propane + n-Decane (2)							
T [°C]	P [bar]	σexp [mN/m]	σPRO\II [mN/m]		σHYSYS [mN/m]		σPVTsim [mN/m]		σNeqSim [mN/m]	
			SRK	PR	SRK	PR	SRK - Peneloux	PR - Peneloux	SRK	PR
21.0	236.6	0.16	5.23	2.58	6.31	6.23	0.17	0.00		0.03
21.0	228.9	0.25	5.49	5.46	6.57	6.49	0.24	0.02	0.82	0.11
21.0	219.7	0.38	5.80	5.78	6.87	6.81	0.33	0.05	1.04	0.25
21.0	195.7	0.69	6.61	6.61	7.71	7.67	0.70	0.27	1.72	0.80
21.0	183.9	0.92	7.02	7.03	8.15	8.11	0.96	0.46	2.11	1.16
30.0	246.9	0.14	4.87	2.39	5.94	5.86	0.14	0.00	0.57	0.00
30.0	233.0	0.25	5.32	5.30	6.39	6.33	0.26	0.02	0.86	0.14
30.0	221.6	0.42	5.70	5.69	6.76	6.71	0.39	0.08	1.14	0.33
30.0	212.2	0.51	6.01	6.01	7.08	7.04	0.52	0.15	1.39	0.53
30.0	202.6	0.68	6.33	6.34	7.41	7.38	0.68	0.26	1.68	0.77
30.0	181.7	0.99	7.05	7.07	8.17	8.16	1.17	0.63	2.40	1.43
30.0	171.1	1.18	7.43	7.46	8.58	8.57	1.50	0.90	2.83	1.83
43.0	251.1	0.12	4.65	4.61	5.69	5.64	0.16	0.00	0.60	0.02
43.0	241.1	0.24	4.96	4.95	6.00	5.96	0.25	0.02	0.81	0.12
43.0	232.0	0.34	5.26	5.25	6.29	6.26	0.34	0.06	1.03	0.26
43.0	221.4	0.47	5.59	5.59	6.64	6.61	0.48	0.14	1.30	0.47
43.0	210.5	0.66	5.94	5.96	7.00	6.99	0.66	0.25	1.62	0.73
43.0	192.2	1.10	6.55	6.58	7.64	7.64	1.06	0.55	2.24	1.28
43.0	172.5	1.48	7.23	7.27	8.37	8.38	1.65	1.04	3.02	
65.0	255.8	0.13	4.22	4.19	5.23	5.19	0.17	0.00	0.60	0.03
65.0	246.4	0.24	4.50	4.49	5.51	5.49	0.26	0.03	0.80	0.13
65.0	232.1	0.40	4.93	4.94	5.95	5.94	0.43	0.11	1.15	0.37
65.0	216.6	0.61	5.41	5.43	6.43	6.44	0.67	0.26	1.59	0.73
65.0	202.1	0.89	5.86	5.90	6.91	6.92	0.97	0.49	2.06	1.14
65.0	182.6	1.23	6.50	6.55	7.58	7.61	1.50	0.93	2.80	1.82
97.0	247.9	0.21	3.85		4.80	4.78	0.23	0.02	0.67	0.10
97.0	227.1	0.44	4.44	4.45	5.39	5.40	0.48	0.15	1.16	0.45
97.0	218.4	0.60	4.69	4.71	5.65	5.66	0.62	0.25	1.40	0.64
97.0	211.4	0.86	4.89	4.92	5.86	5.88	0.75	0.35	1.61	0.82
97.0	198.5	0.94	5.28	5.32	6.25	6.29	1.03	0.57	2.02	1.19
97.0	185.4	1.20	5.68	5.73	6.67	6.71	1.38	0.87	2.49	1.62
97.0	172.8	1.53	6.09	6.15	7.09	7.14	1.77	1.23	2.99	2.09
		Average Deviation:	**4.97**	**4.86**	**6.02**	**6.00**	**0.07**	**0.32**	**0.92**	**0.18**

Table A.17: Methane + Propane + n-Decane

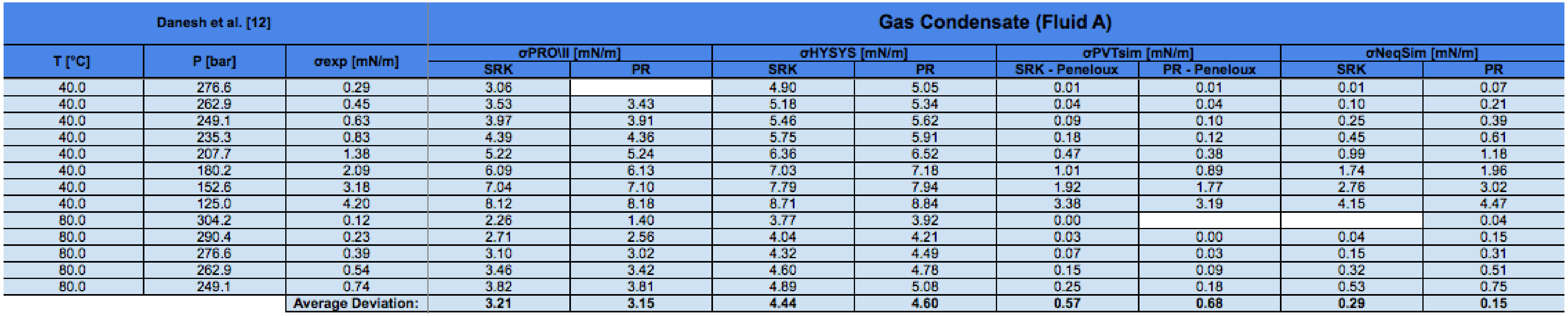

Danesh et al. [12]			Gas Condensate (Fluid A)							
T [°C]	P [bar]	σexp [mN/m]	σPRO\II [mN/m]		σHYSYS [mN/m]		σPVTsim [mN/m]		σNeqSim [mN/m]	
			SRK	PR	SRK	PR	SRK - Peneloux	PR - Peneloux	SRK	PR
40.0	276.6	0.29	3.06		4.90	5.05	0.01	0.01	0.01	0.07
40.0	262.9	0.45	3.53	3.43	5.18	5.34	0.04	0.04	0.10	0.21
40.0	249.1	0.63	3.97	3.91	5.46	5.62	0.09	0.10	0.25	0.39
40.0	235.3	0.83	4.39	4.36	5.75	5.91	0.18	0.12	0.45	0.61
40.0	207.7	1.38	5.22	5.24	6.36	6.52	0.47	0.38	0.99	1.18
40.0	180.2	2.09	6.09	6.13	7.03	7.18	1.01	0.89	1.74	1.96
40.0	152.6	3.18	7.04	7.10	7.79	7.94	1.92	1.77	2.76	3.02
40.0	125.0	4.20	8.12	8.18	8.71	8.84	3.38	3.19	4.15	4.47
80.0	304.2	0.12	2.26	1.40	3.77	3.92	0.00			0.04
80.0	290.4	0.23	2.71	2.56	4.04	4.21	0.03	0.00	0.04	0.15
80.0	276.6	0.39	3.10	3.02	4.32	4.49	0.07	0.03	0.15	0.31
80.0	262.9	0.54	3.46	3.42	4.60	4.78	0.15	0.09	0.32	0.51
80.0	249.1	0.74	3.82	3.81	4.89	5.08	0.25	0.18	0.53	0.75
		Average Deviation:	**3.21**	**3.15**	**4.44**	**4.60**	**0.57**	**0.68**	**0.29**	**0.15**

Table A.18: Gas Condensate

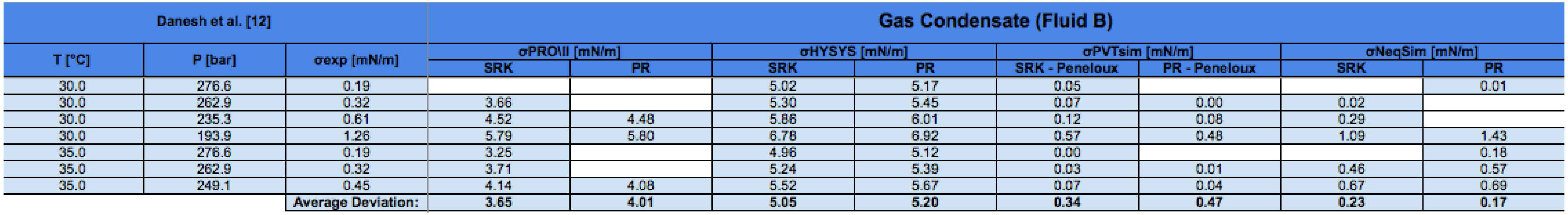

Danesh et al. [12]			Gas Condensate (Fluid B)							
T [°C]	P [bar]	σexp [mN/m]	σPRO\II [mN/m]		σHYSYS [mN/m]		σPVTsim [mN/m]		σNeqSim [mN/m]	
			SRK	PR	SRK	PR	SRK - Peneloux	PR - Peneloux	SRK	PR
30.0	276.6	0.19			5.02	5.17	0.05			0.01
30.0	262.9	0.32	3.66		5.30	5.45	0.07	0.00	0.02	
30.0	235.3	0.61	4.52	4.48	5.86	6.01	0.12	0.08	0.29	
30.0	193.9	1.26	5.79	5.80	6.78	6.92	0.57	0.48	1.09	1.43
35.0	276.6	0.19	3.25		4.96	5.12	0.00			0.18
35.0	262.9	0.32	3.71		5.24	5.39	0.03	0.01	0.46	0.57
35.0	249.1	0.45	4.14	4.08	5.52	5.67	0.07	0.04	0.67	0.69
		Average Deviation:	**3.65**	**4.01**	**5.05**	**5.20**	**0.34**	**0.47**	**0.23**	**0.17**

Table A.19: Gas Condensate

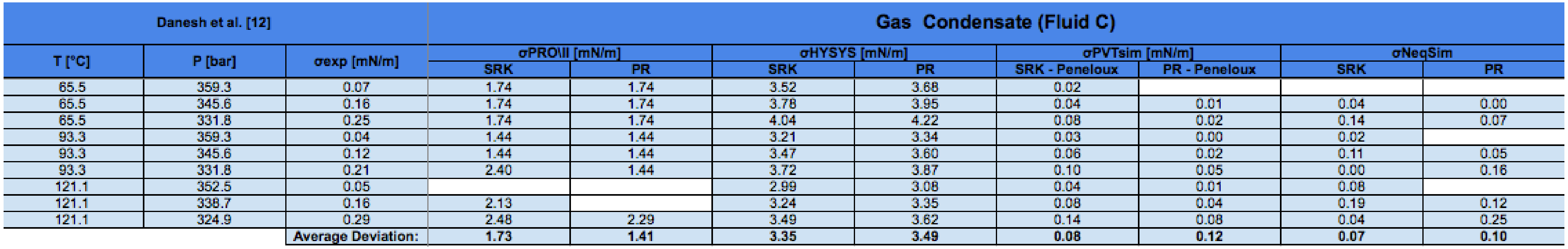

Danesh et al. [12]			Gas Condensate (Fluid C)							
T [°C]	P [bar]	σexp [mN/m]	σPRO\II [mN/m]		σHYSYS [mN/m]		σPVTsim [mN/m]		σNeqSim	
			SRK	PR	SRK	PR	SRK - Peneloux	PR - Peneloux	SRK	PR
65.5	359.3	0.07	1.74	1.74	3.52	3.68	0.02			
65.5	345.6	0.16	1.74	1.74	3.78	3.95	0.04	0.01	0.04	0.00
65.5	331.8	0.25	1.74	1.74	4.04	4.22	0.08	0.02	0.14	0.07
93.3	359.3	0.04	1.44	1.44	3.21	3.34	0.03	0.00	0.02	
93.3	345.6	0.12	1.44	1.44	3.47	3.60	0.06	0.02	0.11	0.05
93.3	331.8	0.21	2.40	1.44	3.72	3.87	0.10	0.05	0.00	0.16
121.1	352.5	0.05			2.99	3.08	0.04	0.01	0.08	
121.1	338.7	0.16	2.13		3.24	3.35	0.08	0.04	0.19	0.12
121.1	324.9	0.29	2.48	2.29	3.49	3.62	0.14	0.08	0.04	0.25
		Average Deviation:	**1.73**	**1.41**	**3.35**	**3.49**	**0.08**	**0.12**	**0.07**	**0.10**

Table A.20: Gas Condensate

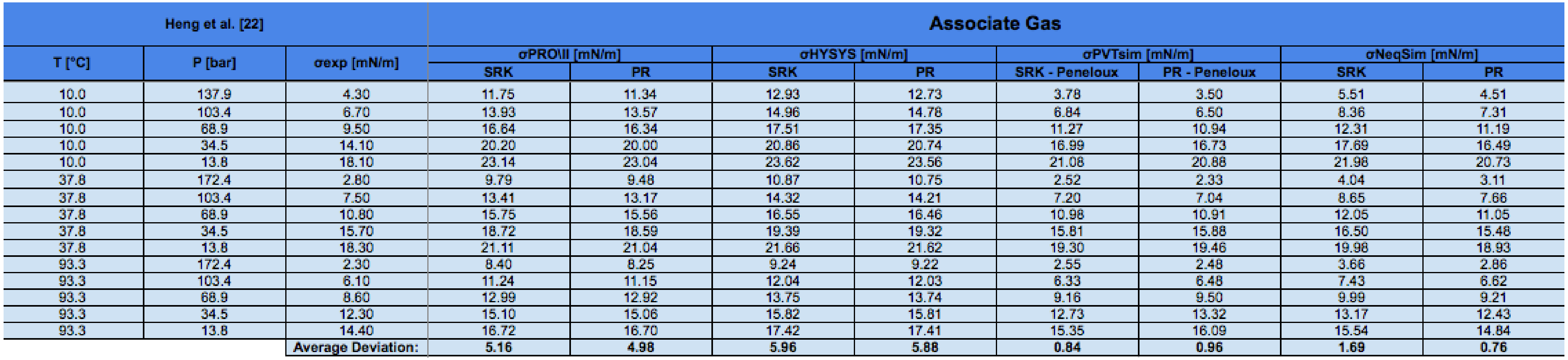

Heng et al. [22]			Associate Gas							
T [°C]	P [bar]	σexp [mN/m]	σPRO\II [mN/m]		σHYSYS [mN/m]		σPVTsim [mN/m]		σNeqSim [mN/m]	
			SRK	PR	SRK	PR	SRK - Peneloux	PR - Peneloux	SRK	PR
10.0	137.9	4.30	11.75	11.34	12.93	12.73	3.78	3.50	5.51	4.51
10.0	103.4	6.70	13.93	13.57	14.96	14.78	6.84	6.50	8.36	7.31
10.0	68.9	9.50	16.64	16.34	17.51	17.35	11.27	10.94	12.31	11.19
10.0	34.5	14.10	20.20	20.00	20.86	20.74	16.99	16.73	17.69	16.49
10.0	13.8	18.10	23.14	23.04	23.62	23.56	21.08	20.88	21.98	20.73
37.8	172.4	2.80	9.79	9.48	10.87	10.75	2.52	2.33	4.04	3.11
37.8	103.4	7.50	13.41	13.17	14.32	14.21	7.20	7.04	8.65	7.66
37.8	68.9	10.80	15.75	15.56	16.55	16.46	10.98	10.91	12.05	11.05
37.8	34.5	15.70	18.72	18.59	19.39	19.32	15.81	15.88	16.50	15.48
37.8	13.8	18.30	21.11	21.04	21.66	21.62	19.30	19.46	19.98	18.93
93.3	172.4	2.30	8.40	8.25	9.24	9.22	2.55	2.48	3.66	2.86
93.3	103.4	6.10	11.24	11.15	12.04	12.03	6.33	6.48	7.43	6.62
93.3	68.9	8.60	12.99	12.92	13.75	13.74	9.16	9.50	9.99	9.21
93.3	34.5	12.30	15.10	15.06	15.82	15.81	12.73	13.32	13.17	12.43
93.3	13.8	14.40	16.72	16.70	17.42	17.41	15.35	16.09	15.54	14.84
		Average Deviation:	**5.16**	**4.98**	**5.96**	**5.88**	**0.84**	**0.96**	**1.69**	**0.76**

Table A.21: Associate Gas

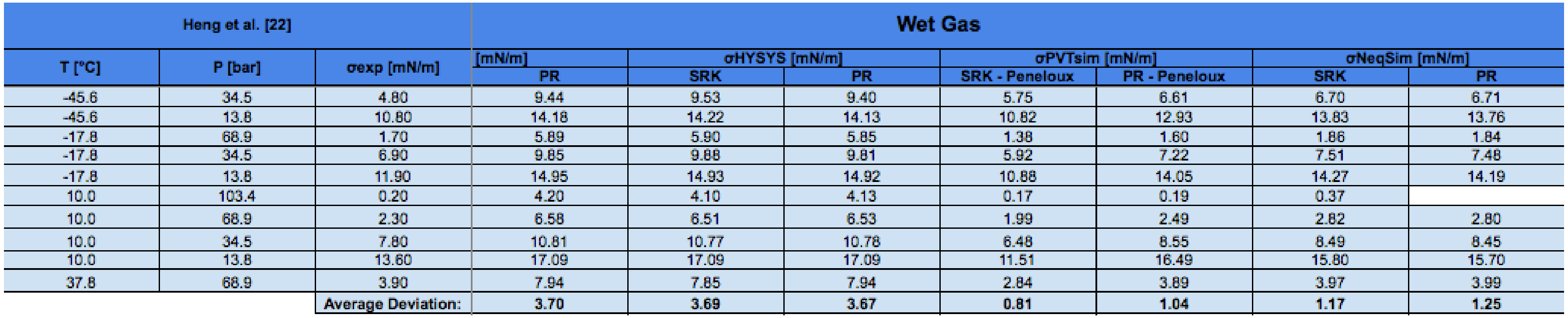

Heng et al. [22]			Wet Gas						
T [°C]	P [bar]	σexp [mN/m]	[mN/m]	σHYSYS [mN/m]		σPVTsim [mN/m]		σNeqSim [mN/m]	
			PR	SRK	PR	SRK - Peneloux	PR - Peneloux	SRK	PR
-45.6	34.5	4.80	9.44	9.53	9.40	5.75	6.61	6.70	6.71
-45.6	13.8	10.80	14.18	14.22	14.13	10.82	12.93	13.83	13.76
-17.8	68.9	1.70	5.89	5.90	5.85	1.38	1.60	1.86	1.84
-17.8	34.5	6.90	9.85	9.88	9.81	5.92	7.22	7.51	7.48
-17.8	13.8	11.90	14.95	14.93	14.92	10.88	14.05	14.27	14.19
10.0	103.4	0.20	4.20	4.10	4.13	0.17	0.19	0.37	
10.0	68.9	2.30	6.58	6.51	6.53	1.99	2.49	2.82	2.80
10.0	34.5	7.80	10.81	10.77	10.78	6.48	8.55	8.49	8.45
10.0	13.8	13.60	17.09	17.09	17.09	11.51	16.49	15.80	15.70
37.8	68.9	3.90	7.94	7.85	7.94	2.84	3.89	3.97	3.99
		Average Deviation:	**3.70**	**3.69**	**3.67**	**0.81**	**1.04**	**1.17**	**1.25**

Table A.22: Wet Gas

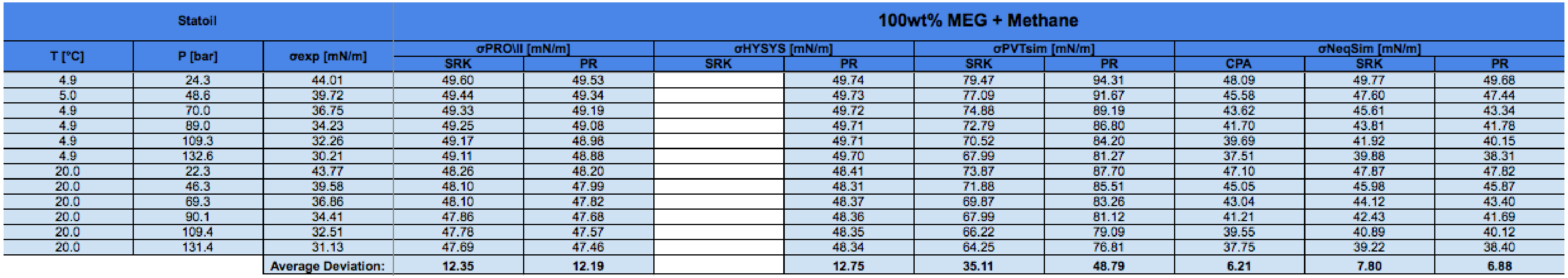

Statoil			100wt% MEG + Methane								
T [°C]	P [bar]	σexp [mN/m]	σPRO\II [mN/m]		σHYSYS [mN/m]		σPVTsim [mN/m]		σNeqSim [mN/m]		
			SRK	PR	SRK	PR	SRK	PR	CPA	SRK	PR
4.9	24.3	44.01	49.60	49.53		49.74	79.47	94.31	48.09	49.77	49.68
5.0	48.6	39.72	49.44	49.34		49.73	77.09	91.67	45.58	47.60	47.44
4.9	70.0	36.75	49.33	49.19		49.72	74.88	89.19	43.62	45.61	43.34
4.9	89.0	34.23	49.25	49.08		49.71	72.79	86.80	41.70	43.81	41.78
4.9	109.3	32.26	49.17	48.98		49.71	70.52	84.20	39.69	41.92	40.15
4.9	132.6	30.21	49.11	48.88		49.70	67.99	81.27	37.51	39.88	38.31
20.0	22.3	43.77	48.26	48.20		48.41	73.87	87.70	47.10	47.87	47.82
20.0	46.3	39.58	48.10	47.99		48.31	71.88	85.51	45.05	45.98	45.87
20.0	69.3	36.86	48.10	47.82		48.37	69.87	83.26	43.04	44.12	43.40
20.0	90.1	34.41	47.86	47.68		48.36	67.99	81.12	41.21	42.43	41.69
20.0	109.4	32.51	47.78	47.57		48.35	66.22	79.09	39.55	40.89	40.12
20.0	131.4	31.13	47.69	47.46		48.34	64.25	76.81	37.75	39.22	38.40
		Average Deviation:	**12.35**	**12.19**		**12.75**	**35.11**	**48.79**	**6.21**	**7.80**	**6.88**

Table A.23: 100wt% MEG + Methane

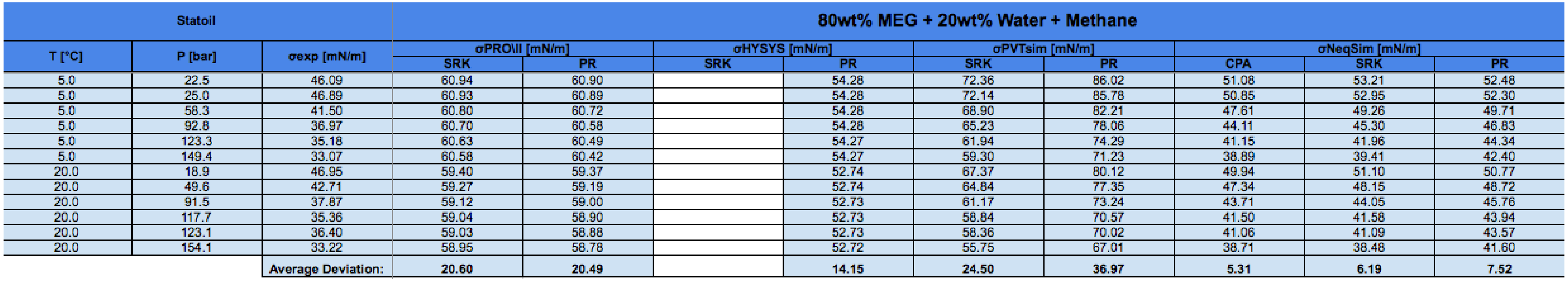

Statoil			80wt% MEG + 20wt% Water + Methane								
T [°C]	P [bar]	σexp [mN/m]	σPRO\II [mN/m]		σHYSYS [mN/m]		σPVTsim [mN/m]		σNeqSim [mN/m]		
			SRK	PR	SRK	PR	SRK	PR	CPA	SRK	PR
5.0	22.5	46.09	60.94	60.90		54.28	72.36	86.02	51.08	53.21	52.48
5.0	25.0	46.89	60.93	60.89		54.28	72.14	85.78	50.85	52.95	52.30
5.0	58.3	41.50	60.80	60.72		54.28	68.90	82.21	47.61	49.26	49.71
5.0	92.8	36.97	60.70	60.58		54.28	65.23	78.06	44.11	45.30	46.83
5.0	123.3	35.18	60.63	60.49		54.27	61.94	74.29	41.15	41.96	44.34
5.0	149.4	33.07	60.58	60.42		54.27	59.30	71.23	38.89	39.41	42.40
20.0	18.9	46.95	59.40	59.37		52.74	67.37	80.12	49.94	51.10	50.77
20.0	49.6	42.71	59.27	59.19		52.74	64.84	77.35	47.34	48.15	48.72
20.0	91.5	37.87	59.12	59.00		52.73	61.17	73.24	43.71	44.05	45.76
20.0	117.7	35.36	59.04	58.90		52.73	58.84	70.57	41.50	41.58	43.94
20.0	123.1	36.40	59.03	58.88		52.73	58.36	70.02	41.06	41.09	43.57
20.0	154.1	33.22	58.95	58.78		52.72	55.75	67.01	38.71	38.48	41.60
		Average Deviation:	**20.60**	**20.49**		**14.15**	**24.50**	**36.97**	**5.31**	**6.19**	**7.52**

Table A.24: 80wt% MEG/20wt% Water + Methane

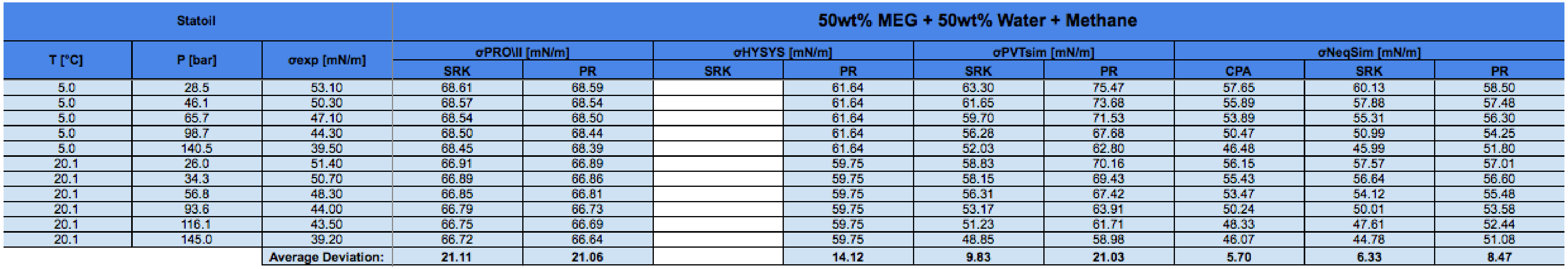

Statoil			50wt% MEG + 50wt% Water + Methane								
T [°C]	P [bar]	σexp [mN/m]	σPRO\II [mN/m]		σHYSYS [mN/m]		σPVTsim [mN/m]		σNeqSim [mN/m]		
			SRK	PR	SRK	PR	SRK	PR	CPA	SRK	PR
5.0	28.5	53.10	68.61	68.59		61.64	63.30	75.47	57.65	60.13	58.50
5.0	46.1	50.30	68.57	68.54		61.64	61.65	73.68	55.89	57.88	57.48
5.0	65.7	47.10	68.54	68.50		61.64	59.70	71.53	53.89	55.31	56.30
5.0	98.7	44.30	68.50	68.44		61.64	56.28	67.68	50.47	50.99	54.25
5.0	140.5	39.50	68.45	68.39		61.64	52.03	62.80	46.48	45.99	51.80
20.1	26.0	51.40	66.91	66.89		59.75	58.83	70.16	56.15	57.57	57.01
20.1	34.3	50.70	66.89	66.86		59.75	58.15	69.43	55.43	56.64	56.60
20.1	56.8	48.30	66.85	66.81		59.75	56.31	67.42	53.47	54.12	55.48
20.1	93.6	44.00	66.79	66.73		59.75	53.17	63.91	50.24	50.01	53.58
20.1	116.1	43.50	66.75	66.69		59.75	51.23	61.71	48.33	47.61	52.44
20.1	145.0	39.20	66.72	66.64		59.75	48.85	58.98	46.07	44.78	51.08
		Average Deviation:	**21.11**	**21.06**		**14.12**	**9.83**	**21.03**	**5.70**	**6.33**	**8.47**

Table A.25: 50wt% MEG/50wt% Water + Methane

Statoil			100wt% MEG + Methane + Ethane								
T [°C]	P [bar]	σexp [mN/m]	σPRO\II [mN/m]		σHYSYS [mN/m]		σPVTsim [mN/m]		σNeqSim [mN/m]		
			SRK	PR	SRK	PR	SRK	PR	CPA	SRK	PR
5.0	21.9	41.80	49.55	49.47		49.76	84.69	100.50	48.08	49.84	49.79
5.0	43.6	36.49	49.37	49.25		49.76	82.23	97.79	45.75	47.52	47.44
5.0	67.0	31.79	49.24	49.07		49.76	79.28	94.46	43.07	44.95	44.80
5.0	90.5	30.04	49.13	48.93		49.76	76.04	90.76	40.22	42.26	41.98
20.1	15.5	43.70	48.25	48.20		48.42	79.11	93.88	47.52	48.24	48.23
20.1	32.2	40.20	48.10	48.00		48.42	77.55	92.16	45.94	46.75	46.10
20.1	64.2	34.22	47.88	47.70		48.42	74.29	88.53	42.28	43.76	43.67
20.1	95.0	30.66	47.69	47.49		48.42	70.88	84.65	39.60	40.78	40.56
		Average Deviation:	**12.54**	**12.40**		**12.98**	**41.90**	**56.73**	**7.95**	**9.40**	**9.21**

Table A.26: 100wt% MEG + Methane/Ethane

Statoil			80wt% MEG + 20wt% Water + Methane + Ethane								
T [°C]	P [bar]	σexp [mN/m]	σPRO\II [mN/m]		σHYSYS [mN/m]		σPVTsim [mN/m]		σNeqSim [mN/m]		
			SRK	PR	SRK	PR	SRK	PR	CPA	SRK	PR
5.0	23.8	45.11	60.90	60.84		54.29	76.74	91.28	50.70	52.76	52.17
5.0	43.9	40.66	60.79	60.71		54.29	74.51	88.84	48.52	50.25	50.41
4.9	73.3	35.99	60.68	60.56		54.28	70.85	84.72	45.09	46.32	47.58
5.0	95.7	33.52	60.62	60.48		54.28	67.81	81.25	42.41	43.24	45.32
20.1	16.4	47.06	59.37	59.33		52.74	71.79	85.39	50.00	51.15	50.80
20.1	30.0	42.94	59.29	59.22		52.74	70.53	84.02	48.73	49.70	49.80
20.1	43.2	41.46	59.22	59.13		52.74	69.25	82.62	47.45	48.24	48.78
20.1	64.0	38.51	59.12	59.01		52.73	67.11	80.23	45.38	45.88	47.09
20.1	105.1	33.81	58.98	58.83		52.73	62.67	75.18	41.24	41.19	43.65
		Average Deviation:	**19.99**	**19.90**		**13.53**	**30.25**	**43.83**	**6.72**	**7.74**	**8.50**

Table A.27: 80wt% MEG/20wt% Water + Methane/Ethane

Statoil			50wt% MEG + 50wt% Water + Methane + Ethane								
T [°C]	P [bar]	σexp [mN/m]	σPRO\II [mN/m]		σHYSYS [mN/m]		σPVTsim [mN/m]		σNeqSim [mN/m]		
			SRK	PR	SRK	PR	SRK	PR	CPA	SRK	PR
5.0	17.3	54.09	68.62	68.60		61.65	68.34	81.39	58.56	61.28	58.99
5.0	37.4	47.53	68.56	68.52		61.65	66.19	79.09	56.36	58.46	57.69
4.9	81.1	41.65	68.48	68.42		61.65	60.93	73.19	51.18	51.80	54.51
5.0	97.4	39.64	68.46	68.39		61.65	58.79	70.75	49.19	49.26	53.26
20.1	16.4	49.32	66.89	66.88		59.75	63.36	75.52	56.91	58.40	57.36
20.1	32.1	49.83	66.85	66.82		59.75	61.85	73.89	55.32	56.48	56.48
20.1	64.6	44.48	66.78	66.72		59.75	58.71	70.41	52.07	52.29	54.54
20.1	93.6	41.22	66.73	66.66		59.75	55.69	67.00	49.12	48.52	52.74
		Average Deviation:	**21.70**	**21.66**		**14.73**	**15.76**	**27.93**	**7.62**	**8.59**	**9.73**

Table A.28: 50wt% MEG/50wt% Water + Methane/Ethane